Appendix F Response to Requests for Additional Information

A large number of Requests for Additional Information (RAIs) were generated during the USNRC review of MUAP-07013. Table F-1 identifies the responses to questions.

References

F-1. Letter, Y. Ogata (MHI) to J. Ciocco (USNRC), MHI's Partial Responses to the NRC's Requests for Additional Information on Topical Report MUAP-07013-P (R0) "Small Break LOCA Methodology for US-APWR", UAP-HF-09002, Mitsubishi Heavy Industries, Jan. 2009.

F-2. Letter, Y. Ogata (MHI) to J. Ciocco (USNRC), MHI's 2nd Part Responses to the NRC's Requests for Additional Information on Topical Report MUAP-07013-P (R0) "Small Break LOCA Methodology for US-APWR", UAP-HF-09041, Mitsubishi Heavy Industries, Feb. 2009.

F-3. Letter, Y. Ogata (MHI) to J. Ciocco (USNRC), MHI's 1st Response to the NRC's Request for Additional Information on Topical Report MUAP-07013-P (R0) "Small Break LOCA Methodology for US-APWR" on 06/11/2009, UAP-HF-09362, Mitsubishi Heavy Industries, Jul. 2009.

F-4. Letter, Y. Ogata (MHI) to J. Ciocco (USNRC), MHI's 2nd Response to the NRC's Request for Additional Information on Topical Report MUAP-07013-P (R0) "Small Break LOCA Methodology for US-APWR" on 06/11/2009, UAP-HF-09417, Mitsubishi Heavy Industries, Aug. 2009.

F-5. Letter, Y. Ogata (MHI) to J. Ciocco (USNRC), MHI's 1st Response to the NRC's Request for Additional Information on Topical Report MUAP-07013-P (R0) "Small Break LOCA Methodology for US-APWR" on 09/08/2009, UAP-HF-09512, Mitsubishi Heavy Industries, Oct. 2009.

F-6. Letter, Y. Ogata (MHI) to J. Ciocco (USNRC), MHI's 2nd Response to the NRC's Request for Additional Information on Topical Report MUAP-07013-P (R0) "Small Break LOCA Methodology for US-APWR" on 09/08/2009, UAP-HF-09041, Mitsubishi Heavy Industries, Nov. 2009.

F-7. Letter, Y. Ogata (MHI) to J. Ciocco (USNRC), MHI's 1st Response to the NRC's

Request for Additional Information on Topical Report MUAP-07013-P (R0) “Small Break LOCA Methodology for US-APWR” on 11/17/2009, UAP-HF-09559, Mitsubishi Heavy Industries, Dec. 2009.

F-8. Letter, Y. Ogata (MHI) to J. Ciocco (USNRC), MHI's 2nd Response to the NRC's Request for Additional Information on Topical Report MUAP-07013-P (R0) “Small Break LOCA Methodology for US-APWR” on 11/17/2009, UAP-HF-10003, Mitsubishi Heavy Industries, Jan. 2010.

F-9. Letter, Y. Ogata (MHI) to J. Ciocco (USNRC), MHI’s 1st Response to NRC's Request for Additional Information on Topical Report MUAP-07013-P (R0) “Small Break LOCA Methodology for US-APWR” on 2/16/2010, UAP-HF-10059, Mitsubishi Heavy Industries, Mar. 2010.

F-10. Letter, Y. Ogata (MHI) to J. Ciocco (USNRC), MHI's 2nd Response to the NRC's Request for Additional Information on Topical Report MUAP-07013-P (R0) “Small Break LOCA Methodology for US-APWR” on 2/16/2010, UAP-HF-10074, Mitsubishi Heavy Industries, Mar. 2010.

F-11. Letter, Y. Ogata (MHI) to J. Ciocco (USNRC), MHI's 1st Response to the NRC's Request for Additional Information on Topical Report MUAP-07013-P (R0) “Small Break LOCA Methodology for US-APWR” on 3/22/2010, UAP-HF-10113, Mitsubishi Heavy Industries, Apr. 2010.

F-12. Letter, Y. Ogata (MHI) to J. Ciocco (USNRC), MHI's 2nd Response to the NRC's Request for Additional Information on Topical Report MUAP-07013-P (R0) “Small Break LOCA Methodology for US-APWR” on 3/22/2010, UAP-HF-10137, Mitsubishi Heavy Industries, May 2010.

F-13. Letter, Y. Ogata (MHI) to J. Ciocco (USNRC), MHI's Response to the NRC's Request for Additional Information on Topical Report MUAP-07013-P (R0) “Small Break LOCA Methodology for US-APWR” on 4/15/2010 : “Scaling Analysis for US-APWR Small Break LOCA”, UAP-HF-09568, UAP-HF-10151, Mitsubishi Heavy Industries, Jun. 2010.

F-14. Letter, Y. Ogata (MHI) to J. Ciocco (USNRC), MHI's Response to the NRC's Request for Additional Information on Topical Report MUAP-07013-P (R0) “Small Break LOCA

Methodology for US-APWR” on 4/9/2010, UAP-HF-10138, Mitsubishi Heavy Industries, May 2010.

F-15. Letter, Y. Ogata (MHI) to J. Ciocco (USNRC), MHI's Response to the NRC's Request for Additional Information on Topical Report MUAP-07013-P (R1) “Small Break LOCA Methodology for US-APWR” on 09/28/2010, UAP-HF-10266, Mitsubishi Heavy Industries, Sep. 2010.

F-16. Letter, Y. Ogata (MHI) to J. Ciocco (USNRC), Revision to MHI’s RAI Responses on Topical Report MUAP-07013-P (R0) “Small Break LOCA Methodology for US-APWR”, UAP-HF-10258, Mitsubishi Heavy Industries, Sep. 2010.

Table F-1 (1/5) Requests for Additional Information

Question	Topic	Reference	Related RAI
1-1	Scalability	Ref. F-1	
1-2	Scalability	Ref. F-3	
3-1	Version information	Ref. F-5	
3-2	Output file	Ref. F-6	
3-3	Advanced Accumulator	Ref. F-5	
4-1	SBLOCA Phase change	Ref. F-1	
4-2	Relative pressure	Ref. F-1	
4-3	Loop seal clearing	Ref. F-1	
4-4	Stored energy	Ref. F-1	
4-5	Stored energy	Ref. F-1	
4-6	Energy balance	Ref. F-1	
4-7	Vapor generation in pressurizer	Ref. F-1	
4-8	Safety injection	Ref. F-1	
4-9	Uncertainty of loop seal clearing	Ref. F-1	
4-10	PIRT ranking	Ref. F-1	
4-11	PIRT ranking	Ref. F-1	
4-12	Confirmation	Ref. F-1	
4-13	SBLOCA Phase change	Ref. F-3	4-1
4-14	Vapor generation in pressurizer	Ref. F-3	4-7
4-15	PIRT ranking	Ref. F-3	4-10
4-16	PIRT ranking	Ref. F-4	4-11
4-17	Confirmation	Ref. F-4	4-12
4-18	SBLOCA Phase change	Ref. F-7	4-1, 4-13
5-1	Scaling analysis	Ref. F-1	
5-2	Scaling analysis	Ref. F-3	5-1
6-1	Code manuals	Ref. F-1	
6-2	Code assessment	Ref. F-2	
6-3	Separator component	Ref. F-1	
6-4	Code manuals	Ref. F-4	6-1
6-5	Code assessment	Ref. F-3	6-2
6-6	Code assessment	Ref. F-3	6-2
6-7	Code manuals	Ref. F-8	6-4
7-1	ECC bypass	Ref. F-1	
7-2	Refill/reflood heat transfer	Ref. F-1	
7-3	Gap conductance model	Ref. F-1	
7-4	Actinide	Ref. F-1	
7-5	Metal water reaction	Ref. F-1	
7-6	Equation in section 7	Ref. F-1	
7-8	Critical flow model	Ref. F-1	
7-9	Critical flow model	Ref. F-1	
7-10	CHF model	Ref. F-2	
7-11	CHF model	Ref. F-2	
7-12	Prevent return to nucleate boiling	Ref. F-1	
7-13	Bypass flow	Ref. F-3	7-1
7-14	Reflood	Ref. F-3	

Table F-1 (2/5) Requests for Additional Information

RAI Number	TOPIC	REFERENCE	
7-15	Reflood	Ref. F-3	7-2
7-16	FLECHT-SEASET	Ref. F-4	7-2
7-17	Reflood	Ref. F-3	7-2
7-18	CHF model	Ref. F-3	7-2, 7-10
7-19	Critical flow model	Ref. F-3	7-8
7-20	Critical flow model	Ref. F-4	7-8
7-21	Critical flow model	Ref. F-3	7-8
7-22	CHF model	Ref. F-4	7-10
7-23	Flow oscillation	Ref. F-8	7-14
8-1	Code assessment	Ref. F-1	
8-2	Code assessment	Ref. F-1	
8-3	Advanced accumulator	Ref. F-3	
8-4	Loop seal phenomena	Ref. F-4 Ref. F-16	
8-5	SG U-tube	Ref. F-4	
8-3	Error correction	Ref. F-3	8-2
8.1-1	Code assessment	Ref. F-1	
8.1-2	Decay heat	Ref. F-1	
8.1-3	Nodalization	Ref. F-1	
8.1-4	PCT	Ref. F-4	8.1-2
8.1-5	Nodalization	Ref. F-4	8.1-3
8.1.1-1	ROSA	Ref. F-1	
8.1.1-2	ROSA	Ref. F-2	
8.1.1-3	ROSA	Ref. F-1	
8.1.1-4	ROSA	Ref. F-1	
8.1.1-5	ROSA	Ref. F-1	
8.1.1-6	ROSA	Ref. F-5	
8.1.1-7	ROSA	Ref. F-5	
8.1.2-1	ORNL/THTF	Ref. F-1	
8.1.2-2	ORNL/THTF	Ref. F-1	
8.1.2-3	ORNL/THTF	Ref. F-1	
8.1.2-4	ORNL/THTF	Ref. F-1	
8.1.2-5	ORNL/THTF	Ref. F-1	
8.1.2-6	ORNL/THTF	Ref. F-1	
8.1.2-7	ORNL/THTF	Ref. F-1	
8.1.2-8	ORNL/THTF	Ref. F-2	
8.1.2-9	ORNL/THTF	Ref. F-2	
8.1.2-10	ORNL/THTF	Ref. F-2	
8.1.2-11	ORNL/THTF	Ref. F-1	
8.1.2-12	ORNL/THTF	Ref. F-1	
8.1.2-13	ORNL/THTF	Ref. F-3	8.1.2-5
8.1.2-14	ORNL/THTF	Ref. F-5	
8.1.2-14	ORNL/THTF	Ref. F-8	8.1.2-13
8.1.2-14-1	ORNL/THTF	Ref. F-10	8.1.2-14
8.1.3-1	ORNL/THTF	Ref. F-1	

Table F-1 (3/5) Requests for Additional Information

RAI Number	TOPIC	REFERENCE	
8.1.3-2	ORNL/THTF	Ref. F-1	
8.1.3-3	ORNL/THTF	Ref. F-1	
8.1.3-4	ORNL/THTF	Ref. F-1	
8.1.3-5	ORNL/THTF	Ref. F-1	
8.1.3-6	ORNL/THTF	Ref. F-1	
8.1.3-7	ORNL/THTF	Ref. F-2	
8.1.3-8	ORNL/THTF	Ref. F-1	
8.1.3-9	ORNL/THTF	Ref. F-5	
8.1.3-9-1	ORNL/THTF	Ref. F-10	8.1.3-9
8.1.3-10	ORNL/THTF	Ref. F-5	
8.1.3-11	ORNL/THTF	Ref. F-5	
8.1.4-1	UPTF	Ref. F-1	
8.1.4-2	UPTF	Ref. F-1	
8.1.4-3	UPTF	Ref. F-1	
8.1.4-4	UPTF	Ref. F-1	
8.1.4-5	UPTF	Ref. F-2	
8.1.4-6	UPTF	Ref. F-1	
8.1.4-7	UPTF	Ref. F-3	8.1.4-3
8.1.4-8	UPTF	Ref. F-4	8.1.4-4
8.1.4-9	UPTF	Ref. F-3	8.1.4-6
8.1.4-10	UPTF	Ref. F-5	
8.1.4-11	UPTF	Ref. F-6	
8.1.4-11-1	UPTF	Ref. F-10	8.1.4-11
8.1.4-10	UPTF	Ref. F-7	
8.1.5-1	Dukler	Ref. F-1	
8.1.5-2	Dukler	Ref. F-1	
8.1.5-3	Dukler	Ref. F-1	
8.1.5-4	Dukler	Ref. F-1	
8.1.5-5	Dukler	Ref. F-1	
8.1.5-6	Dukler	Ref. F-1	
8.1.5-7	Dukler	Ref. F-2	
8.1.5-9	Dukler	Ref. F-5	
8.1.5-10	Dukler	Ref. F-5	
8.2.1-1	ROSA	Ref. F-1	
8.2.1-2	ROSA	Ref. F-1	
8.2.1-3	ROSA	Ref. F-2	
8.2.1-4	ROSA	Ref. F-1	
8.2.1-5	ROSA	Ref. F-1 Ref. F-16	
8.2.1-6	ROSA	Ref. F-2	
8.2.1-7	ROSA	Ref. F-5	
8.2.1-8	ROSA	Ref. F-6	
8.2.1-8-1	ROSA	Ref. F-10	8.2.1-8
8.2.1-9	ROSA	Ref. F-6	
8.2.1-10	ROSA	Ref. F-6	

Table F-1 (4/5) Requests for Additional Information

RAI Number	TOPIC	REFERENCE	
8.2.1-11	ROSA	Ref. F-6	
8.2.1-12	ROSA	Ref. F-5 Ref. F-6	
8.2.1-12-1	ROSA	Ref. F-10	8.2.1-12
8.2.1-12-2	ROSA	Ref. F-10	8.2.1-10, 8.2.1-11, 8.2.1-12
8.2.1-13	ROSA	Ref. F-6	
8.2.1-14	ROSA	Ref. F-5	
8.2.1-14-1	ROSA	Ref. F-10	8.2.1-14
8.2.1-15	ROSA	Ref. F-5	
8.2.1-16	ROSA	Ref. F-6	8.2.1-6
8.2.1-17	ROSA	Ref. F-5	
8.2.1-18	ROSA	Ref. F-6	
8.2.1-19	ROSA	Ref. F-6	
8.2.1-20	ROSA	Ref. F-5	
8.2.1-21	ROSA	Ref. F-5	
8.2.1-22	ROSA	Ref. F-5	
8.2.1-23	ROSA	Ref. F-5	
8.2.1-23-1	ROSA	Ref. F-10	8.2.1-23
8.2.1-24	ROSA	Ref. F-5	
8.2.1-25	ROSA	Ref. F-5	
8.3.1-1	Bypass flow	Ref. F-7	
8.3.1-2	CCFL	Ref. F-8	
8.3.1-3	Counter-current flow	Ref. F-8	
8.3.1-4	Local power	Ref. F-8	
8.3.1-5	3-D flow distribution	Ref. F-7	
8.3.1-6	Mixture level in upper plenum	Ref. F-7	
8.3.1-7	Mixture level in pressurizer	Ref. F-7	
8.3.1-8	SG U-tube	Ref. F-7	
8.3.1-9	Loop seal	Ref. F-7	
8.3.1-10	Downcomer and lower plenum	Ref. F-7	
8.3.1-11	3-D flow	Ref. F-7	
8.4.1-1	Nodalization	Ref. F-8	
C-1	Critical flow model	Ref. F-1	
C-2	Critical flow model	Ref. F-1	
D-1	Advanced Accumulator	Ref. F-1	
D-2	Advanced Accumulator	Ref. F-3	D-1
E-1	Sample analysis	Ref. F-5	
CA-1	Confirmatory analysis	Ref. F-6	
CA-2	Confirmatory analysis	Ref. F-5	
CA-3	Confirmatory analysis	Ref. F-5	
CA-4	Confirmatory analysis	Ref. F-5	
CA-5	Confirmatory analysis	Ref. F-6	
CA-5-1	Confirmatory analysis	Ref. F-9	CA-5
CA-6	Confirmatory analysis	Ref. F-5	

Table F-1 (5/5) Requests for Additional Information

RAI Number	TOPIC	REFERENCE
CA-7	Confirmatory analysis	Ref. F-6
LS-1	LOFT and Semiscale	Ref. F-11
LS-2	LOFT and Semiscale	Ref. F-11
LS-3	LOFT and Semiscale	Ref. F-11
LS-4	LOFT and Semiscale	Ref. F-12
LS-5	LOFT and Semiscale	Ref. F-11
LS-6	LOFT and Semiscale	Ref. F-11
LS-7	LOFT and Semiscale	Ref. F-12
S-1	Scaling analysis	Ref. F-13
S-2	Scaling analysis	Ref. F-13
S-3	Scaling analysis	Ref. F-13
S-4	Scaling analysis	Ref. F-13
S-5	Scaling analysis	Ref. F-13
S-6	Scaling analysis	Ref. F-13
S-7	Scaling analysis	Ref. F-13
S-8	Scaling analysis	Ref. F-13
S-9	Scaling analysis	Ref. F-13
S-10	Scaling analysis	Ref. F-13
S-11	Scaling analysis	Ref. F-13
S-12	Scaling analysis	Ref. F-13
S-13	Scaling analysis	Ref. F-13
S-14	Scaling analysis	Ref. F-13
S-15	Scaling analysis	Ref. F-13
S-16	Scaling analysis	Ref. F-13
S-17	Scaling analysis	Ref. F-13
S-18	Scaling analysis	Ref. F-13
M-1	Code modification	Ref. F-14
M-2	Code modification	Ref. F-14
M-3	Code modification	Ref. F-14
M-4	Code modification	Ref. F-14
1	Code modification	Ref. F-15
2	Code modification	Ref. F-15
3	Code modification	Ref. F-15

REQUEST 1-1

Table 1.1-1
The table attempts to present the correspondence between the organization of the SBLOCA methodology topical report (MUAP-07013-P (R0)) and the roadmap identified in Regulatory Guide 1.203 for the development and assessment of the evaluation methodology. Different sections of the topical report are associated with the 20 steps identified in the Regulatory Guide. Provide a more refined association of sub-sections of the topical report to the 20 steps. For example, Section 8 is identified to address Step 15: Assess Scalability of Models. However, there is no specific section title in Section 8 that addresses the task identified in Section 15.

RESPONSE

Reviewer is correct. MHI has missed to provide an individual section for Step 15 (Assessment of Models Scalability). However, it is already implicitly discussed in Section 5 (Step 6) entitled "Perform Scaling Analysis and Identify Similarity Criteria". Therefore, MHI now summarizes the scaling analysis results from each test (IET, SET) and conclude them.

The scalability of the experimental facilities used for the validation of the code is well verified. Therefore, the physical model is also applicable for the plant analysis including for the US-APWR. To reflect the sequence of steps in EM development and assessment based on the RG 1.203, the following modification has been made:

Section 8.1: **Input Preparation and Calculations to Assess Model Fidelity or Accuracy (Step 14)** *- The content is the same.*

Section 8.2: **Models Scalability Assessment (Step 15)** → new section to be created.
- The content is the summary of those reported in Section 5 about Scaling Analysis and Similarity Criteria Identification, and the Identification of existing data of the Integral Effects Tests (IETs) and Separate Effect Tests (SETs) to complete the Database.

Section 8.3: **Determining the Capability of Field Equations to Represent Process and Phenomena and the Ability of Numeric Solutions to Approximate Equation Set (Step 16)**
- The content is the same.

Section 8.4: **Determining the Applicability of Evaluation Model to Simulate System Components (Step 17)**
- The content is the same

Section 8.5: **Input Preparation and Calculations to Assess System Interactions and Global Capability (Step 18)**
- This section was previously designated as Section 8.2, the content remains the same.

Draft of the new Section 8.2:

8.2 Models Scalability Assessment

The scalability evaluation is limited to whether the specific model or correlation is appropriate for application to the configuration and conditions of the plant and transient under evaluation. The scaling issue was basically resolved in Step 6. This section provides the summary and conclusion.

To validate the M-RELAP5 code for the high-ranking phenomena, six (6) Separate Effect Tests (SETs) and one (1) Integral Effects Test (IET) are selected as follows:

1. ROSA/LSTF Void Profile test
2. ORNL/THTF Void Profile test
3. ORNL/THTF Uncovered heat transfer test
4. ORNL/THTF Reflood test
5. UPTF SG plenum CCFL test
6. Dukler Air-Water Flooding test
7. ROSA-IV/LSTF small break (5%) LOCA test (SB-CL-18)

The scalability of the above tests to the US-APWR model is described in the following subsections:

8.2.1 Separate Effect Tests (SETs)

8.2.1.1 Scalability of the ROSA/LSTF Void Profile Test

- Elevations: preserved, i.e., one-to-one correspondence with the reference PWR. Because the LSTF hot and cold leg inner diameters (IDs) are smaller than those of the reference PWR, only the elevations of the top of the primary hot and cold legs were set equal to those of the reference PWR.
- Volumes: scaled by the facility scaling factor 1/48.
- Flow area: scaled by 1/48 in the pressure vessel and 1/24 in the steam generators. However, the hot and cold legs were scaled to conserve the ratio of the length to the square root of pipe diameter, i.e., L/sqrt(D) for the reference PWR. Such an approach was adopted to better simulate the flow regime transition in the primary loops.
- Core power: scaled by 1/48 at core powers equal to or less than 14% of the scaled reference PWR rated power. The LSTF rated and steady-state power is 10 MWt, i.e., 14% of the rated reference PWR core power scaled by 1/48. With this scaled core power, a reduced core inlet flow rate can be obtained and the condition of the steam generator secondary side is changed to accommodate the scaled power.
- Fuel assembly: dimensions, i.e., fuel rod diameter, pitch and length, guide thimble diameter pitch and length, and ratio of number of fuel rods to number of guide thimbles, designed to be the same as the 17x17 fuel assembly of the reference PWR to preserve the heat transfer characteristics of the core. The total number of rods 1064 for heated rods and 104 for unheated rods. They are scaled by 1/48.
- Design pressures: approximately the same as the reference PWR.
- Fluid flow differential pressures (ΔPs): set to be equal to the reference PWR for scaled flow rates.
- Flow capacities: scaled by the overall scaling factor where practicable.
- Core and lower plenum: in comparison with the reference PWR, the length of the heated zone, fuel rod diameter and pitch, power peaking factor and number of spacers are conserved. The core volume and the number of fuel rods are scaled at a ratio of 1/48.

8.2.1.2 Scalability of the ORNL/THTF Void Profile Test

Thermal Hydraulic Test Facility (THTF) contains a 64-rod electrically heated bundle with internal dimensions typical of a 17x17 PWR fuel assembly. The scaling of the facility is acceptable because it adopts full length and prototypical dimensions.

8.2.1.3 Scalability of the ORNL/THTF Uncovered-Bundle Heat Transfer Test

The objective of heat transfer testing was to acquire a heat transfer coefficient and fluid conditions in a partially uncovered bundle. The THTF contains a 64-rod electrically heated bundle with internal dimensions typical of a 17x17 PWR fuel assembly. The scaling of the facility is acceptable because it adopts full length and prototypical dimensions.

8.2.1.4 Scalability of the ORNL/THTF High-Pressure Reflood Test

The THTF has a 64-rod, full-length rod bundle heat transfer loop. Rod diameter and pitch are typical of a 17x17 PWR fuel assembly. The scaling of the facility is acceptable because it adopts full length and prototypical dimensions.

8.2.1.5 Scalability of the UPTF Full-scale SG Plenum CCFL Test

Since UPTF hot leg separate effect test is full scale model, scaling is not an issue.

8.2.1.6 Scalability of the Dukler Air-Water Flooding test

Verification of the experimental results was carried out using general correlation using dimensionless parameters in Reference 5.2.1.6-2. Dimensionless groups which relate momentum fluxes are shown as follows:

$$j_g^* = j_g \rho_g^{1/2}[gD(\rho_f - \rho_g)]^{-1/2} \qquad (8.2.1.6\text{-}1)$$

$$j_f^* = j_f \rho_f^{1/2}[gD(\rho_f - \rho_g)]^{-1/2} \qquad (8.2.1.6\text{-}2)$$

Correlations for flooding in vertical tubes may be expressed in the general form

$$j_g^{*1/2} + m j_f^{*1/2} = C \qquad (8.2.1.6\text{-}3)$$

For turbulent flow **m** is equal to unity. The value of **C** is found to depend on the design of the ends of the tubes and the way in which the liquid and gas are added and extracted. For tubes with sharp-edged flange, **C** = 0.725, when end effects are minimized, **C** lies between 0.88 and 1.0. Hewitt and Wallis found that for an air-water system the flooding velocities could be correlated by the equation

$$j_g^{*1/2} + j_f^{*1/2} = 0.88 \qquad (8.2.1.6\text{-}4)$$

8.2.2 Integral Effect Tests (IETs)

8.2.2.1 ROSA-IV/LSTF small break (5%) LOCA test (SB-CL-18)

The LSTF is an experimental facility designed to model a full height primary system of the reference PWR. The four primary loops of the reference PWR are represented by two equal-volume loops. The overall facility scaling factor is 1/48. The overall scaling factor was used as follows:

- Elevations: preserved, i.e., one to one correspondence with the reference PWR. Because the LSTF hot and cold leg inner diameters (IDs) are smaller than those of the reference PWR, only the elevations of the top of the primary hot and cold legs were set equal to those of the reference PWR.
- Volumes: scaled by the facility scaling factor 1/48.
- Flow area: scaled by 1/48 in the pressure vessel and 1/24 in the steam generators. However, the hot and cold legs were scaled to conserve the ratio of the length to the square root of pipe diameter, i.e., L/sqrt(D) for the reference PWR. Such an approach was taken to better simulate the flow regime transition in the primary loops. In other words, the hot and cold legs were sized to conserve the volume scaling and the ratio of the length to the square root of pipe diameter, L/sqrt(D), for the reference PWR in expectation that the flow regime transitions in the primary loops can be simulated appropriately by taking this scaling approach.

- Core power: scaled by 1/48 at core powers equal to or less than 14% of the scaled reference PWR rated power. The LSTF rated and steady-state power is 10 MWt, i.e., 14% of the rated reference PWR core power scaled by 1/48. With this scaled core power, a reduced core inlet flow rate can be obtained and the condition of the steam generator secondary side is changed to accommodate the scaled power.
- Fuel assembly: dimensions, i.e., fuel rod diameter, pitch and length, guide thimble diameter pitch and length, and ratio of number of fuel rods to number of guide thimbles, designed to be the same as the 17x17 fuel assembly of the reference PWR to preserve the heat transfer characteristics of the core. The total number of rods was scaled by 1/48 and is 1064 for heated and 104 for unheated rods.
- Design pressures: approximately the same as the reference PWR.
- Fluid flow differential pressures (ΔPs): set to be equal to the reference PWR for scaled flow rates.
- Flow capacities: scaled by the overall scaling factor where practicable.

REQUEST 1-2

(Related RAI 1-1)

Scaling of the test facility relative to the US-APWR needs to be addressed. In compliance with Step 6 of the evaluation model development and assessment process (EMDAP), as identified in Regulatory Guide 1.203, provide quantitative scaling analysis to ensure that the data from separate effects tests (SET) and integral effects tests (IET), and the models based on those data, will be applicable to the analysis of the US-APWR.

a) Identify non-dimensional groups that govern the physical phenomena to be examined by the test facilities and compare the similitude between the facilities and the US-APWR.

b) Based on the US-APWR-specific scaling analysis, address Step 8 of the EMDAP (evaluate the effects of IET distortions and SET scale up capability).

c) Assess scalability of models (Step 15 of the EMDAP) - this is to demonstrate that models and correlations implemented in M-RELAP5 for the PIRT high ranking phenomena are appropriate for the SBLOCA evaluation specific to the configuration and conditions of the US-APWR.

Examples of quantitative scaling analysis are:

a. Novak Zuber, Wolfgang Wulff, Upendra S. Rohatgi and Ivan Catton, "Application of Fractional Scaling Analysis (FSA) to Loss of Coolant Accidents (LOCA), Part 1: Methodology Development", Paper: 153, 11th International Topical Meeting on Nuclear Reactor Thermal-Hydraulics (NURETH-11), Popes’ Palace Conference Center, Avignon, France, October 2-6, 2005.

b. Wolfgang Wulff, Novak Zuber, Upendra S. Rohatgi and Ivan Catton, "Application of Fractional Scaling Analysis (FSA) to Loss of Coolant Accidents (LOCA), Part 2. System Level Scaling for System Depressurization", Paper: 111, 11th International Topical Meeting on Nuclear Reactor Thermal-Hydraulics (NURETH-11), Popes’ Palace Conference Center, Avignon, France, October 2-6, 2005.

c. Ivan Catton, Wolfgang Wulff, Novak Zuber, and Upendra S. Rohatgi, "Application of Fractional Scaling Analysis (FSA) to Loss of Coolant Accidents (LOCA), Part 3. Component Level Scaling for Peak Clad Temperature", Paper: 055, 11th International Topical Meeting on Nuclear Reactor Thermal-Hydraulics (NURETH-11), Popes’ Palace Conference Center, Avignon, France, October 2-6, 2005.

d. Wolfgang Wulff and Upendra S. Rohatgi, "System Scaling for the Westinghouse AP600 Pressurized Water Reactor and Related Test Facilities, Analysis and Results", NUREG/CR-5541, January 1998.

e. J. N. Reyes, Jr., Qiao Wu and John B. King, Jr. "Scaling Assessment for the Design of the OSU APEX-1000 Test Facility", OSU-APEX-03001 (Rev. 0), May 12, 2003.

f. Revision 1: R. E. Gamble, A. F. Fanning and V. Chandola, Revision 2: P. Saha, "ESBWR Scaling Report", NEDO-33082, Revision 1, December 2002, Revision 2, April 2008.

g. S. Banerjee, M. G. Ortiz, T. K. Larson and D. L. Reeder, "Top Down Scaling Analyses Methodology for AP600 Integral Tests", INEL-96/0040, May 1997.

RESPONSE

[

]

Appendix A

[

]

[

]

Appendix B

[

]

[

]

[

]

[

]

Appendix C

REQUEST 3-1

Contrary to the normal practice with RELAP5-3D and RELAP5/MOD3.3 code versions, there is no M-RELAP version information given in the output files. Lack of this type of information makes it impossible to confirm which version of M-RELAP is being used for the MHI analysis. Include a version identifier in the M-RELAP output for all future runs.

RESPONSE

Modified versions of Subroutine *aatl* and *gninit1* were created. For future runs, the M-RELAP5 output echo will print the version identifier at the header. The modification will be reflected in future versions of M-RELAP5.

The print out sample is shown as follows:

REQUEST 3-2

[

]

RESPONSE

[

]

[

]

REQUEST 3-3

[

]

RESPONSE

[

]

[

]

REQUEST 4-1

Section 4.2
Report identifies five phases of the SBLOCA transient. However, boundaries of these phases are not clearly defined. Provide parameters that indicate when one phase ends and other begins.

RESPONSE

In order to identify various phenomena, a small break LOCA transient can be divided into five periods: blowdown, natural circulation, loop seal clearance, boil-off, and core recovery. The duration of each period depends on the break size and the performance of the ECCS. The following discussion of these five periods assumes that the small break occurs in the cold leg, as a limiting location to the peak cladding temperature (PCT). The periods during small break LOCA are described as follows:

Blowdown period

The blowdown period starts from the initiation of the break. It ends when the primary system pressure has decreased to nearly equal the secondary system pressure.

Upon initiation of the break, the primary side of the reactor-coolant system (RCS) rapidly depressurizes until the hot coolant flashes into vapor. Reactor trip is automatically initiated on the low pressurizer pressure setpoint of 1860 psia (for the US-APWR). Then, the reactor coolant pump (RCP) will trip automatically at reactor trip. For the US-APWR LOCA analysis, the RCPs automatically trip, after 3 seconds delay following the reactor trip. The ECCS actuation signal is generated when the pressurizer pressure decreases to the low pressurizer pressure setpoint of 1760 psia (US-APWR) and the high-head safety injection initiates, after a time delay. Loss of condenser steam dump effectively isolates the steam generator (SG) secondary side, causing it to pressurize to the safety valve set point of **[ ]** psia (US-APWR), and release steam through the safety valves. During this blowdown phase, the break flow is single-phase liquid. The coolant in the RCS also remains in the liquid phase throughout most of the blowdown period, although towards the end of the blowdown period, phase separation (vapor formation) starting to occur in the upper head, upper plenum and hot legs. Finally, the rapid depressurization ends when the RCS reaches a pressure just above the steam generator secondary side pressure. This ends the blowdown period.

Natural Circulation period

The natural-circulation period starts at the end of blowdown. It ends when the liquid flow rate at the top of SG u-tubes decreases to zero.

At the end of the blowdown period, two-phase natural circulation is established when the RCS reaches a quasi-equilibrium condition with duration depending on break size. Another indication is that the RCP head pressure shall be zero to initiate natural circulation. During this period, loop seal formation occurs in the cross-over leg, the piping between the SG outlet and the inlet of RCP. The loop seals remain plugged and the system drains from the top to down with voids beginning to form at the top of the SG tubes and continuing to form in the upper head and top of the upper plenum region. The decay heat is removed by heat transfer (condensation and convection) to the SG secondary side during this time. The emergency feedwater is initiated to maintain the secondary side inventory. Vapor generated in the core is trapped within the RCS by the loop seal (liquid plug). As more low quality coolant flow exits the break, the vapor accumulates in the downhill side of the SG tubes and the crossover leg. The natural circulation will continue until driving-head on the cold leg side of the loops is no longer sufficient, due to the accumulation of steam in loops between the top of the steam generator tubes and the loop seals. In another word, the mass flowrate at the top of SG tubes shall be zero to indicate the end of natural circulation.

Loop Seal Clearance period

The loop-seal clearance period starts when natural circulation ends. The period ends when the liquid level on the downhill side of the steam generator reaches the elevation of the loop seal and steam is vented towards the break.

With the loop seals present, the break remains covered with water. The RCS coolant inventory continues to decrease and steam volume in the RCS increases. The relative pressure in the core increases, which, together with the loss of coolant inventory through the break, causes the liquid levels in the core and the SG to continue to decrease. If, during this process, the core mixture-level drops below the top of the core, a core uncovery occurs, and the cladding temperature in the upper part of the core will begin to heat up. The core uncovery can be a rapid and deep level drop but short in duration. When the liquid level of the downhill side of the SG is depressed to the elevation of the loop seals, the seals clear and steam initially trapped in the RCS can be vented through the break. The break flow changes from initially a low quality mixture to primarily steam. As the pressure imbalances throughout the RCS are restored, the back pressure in the core is relieved. Then, the core liquid level is restored to the cold leg elevation with the coolant flowing from the downcomer.

Boil-off period

The boil-off period starts after the loop seals clear and ends when the minimum RCS inventory is reached.

After the loop seal clearing, the RCS primary-side pressure continues to fall below that of the secondary-side caused by the continuous coolant outflow from the break with an increasing flow-quality. This process signifies the gradual boil-off of the liquid inventory in the reactor vessel that consequently decreases the mixture-level therein (i.e. in the core). The decreasing rate would be even higher if the RCS pressure is too high for the ECCS to compensate the boil-off rate. In some cases, the decrease in mixture level will reach a minimum value that result in a deep core uncovery. The boil-off period ends when the core collapsed liquid level reaches a minimum. At this time, the RCS has depressurized to the accumulator setpoint of 600 psia (for US-APWR). The accumulator will inject ECCS water to the RCS at a rate higher than the break flow.

Core Recovery period

The core recovery starts at the end of the boil-off period and ends when the fuel rod cladding in the entire core is quenched by a low-quality mixture.

Eventually, the combined flowrates supplied by the high-head safety injection and the accumulator exceed the break flow. The vessel mass inventory increases and the core recovery is established. The accumulator injection into the core begins before the coolant is completely discharged into the containment, and the RCS pressure is still significantly above the containment pressure. The core recovery indicates the end of small break LOCA, when all parts of the core is quenched and covered by a low quality mixture.

REQUEST 4-2

Section 4.2
Report (Page 4-4) indicated that relative pressure in the core increases. Explain what is relative pressure? How does it decrease liquid level in the core? (Loop Seal Clearance)

RESPONSE

The description of the loop seal clearance period will be clarified as follows:

The loop-seal-clearance period starts when natural circulation ends. The period ends when the liquid level on the downhill side of the steam generator reaches the elevation of the loop seal and steam is vented towards the break.

With the loop seals present, the break remains covered with water. The RCS coolant inventory continues to decrease and steam volume in the RCS increases. During loop seal formation, the hydrostatic pressure difference that develops in the SG tubes depresses the liquid level in the core. This phenomenon is due to the difference in void fraction and mixture densities on the two sides of the SG. The uphill side of the SG is in countercurrent flow, with steam flowing upwards and liquid flowing downwards. The downhill side experiences co-current flow, with both phases flowing downwards. The mixture density is higher in the uphill side compared to the downhill side, which may generate a considerable hydrostatic pressure difference due to the height of the tubes.

This pressure difference is transmitted to the two-phase level in the core through the hot leg. As a result, the core is pressurized relative to the downcomer and a considerable portion of core inventory may be forced out from the core. If, during this process, the core mixture-level drops below the top of the core, a core uncovery occurs, and the cladding temperature in the upper part of the core will begin to heat up. The core uncovery can be rapid and deep, but is short in duration. When the liquid level on the downhill side of the SG reaches the elevation of the loop seals, the seals clear and steam initially trapped in the hot portions of the RCS can be vented to the break.
The break flow changes from initially a low-quality mixture to primarily steam. As the pressure imbalances throughout the RCS are restored, the back pressure in the core is relieved. Then, the core liquid level is restored to the cold leg elevation with coolant flowing from the downcomer to the core

REQUEST 4-3

Section 4.2
What is mechanism of loop seal clearing? It is not clear from the description.

RESPONSE

The responses to REQUESTs 4-1 and 4-2 above provide an improved description of the loop seal clearing mechanism. Figures RAI-4-3.1 and RAI-4-3.2 show the mechanisms of loop-seal formation and clearance.

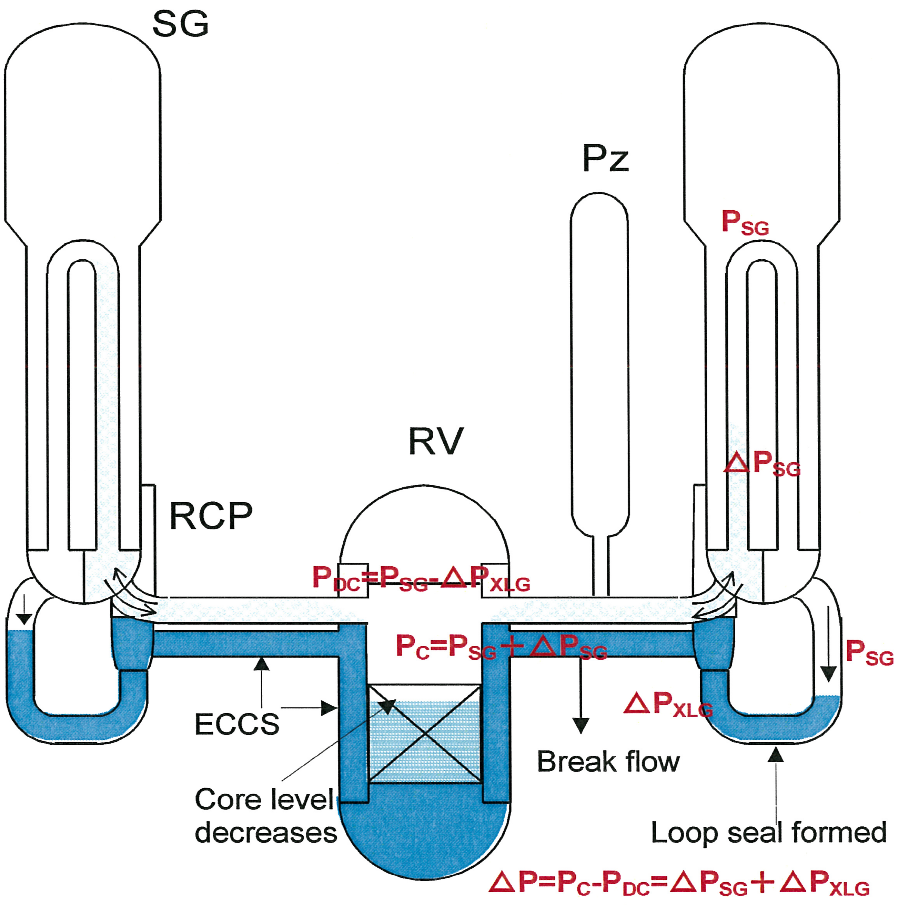
SG
Pz
P_{SG}
RV
ΔP_{SG}
RCP
$P_{DC}=P_{SG}-\Delta P_{XLG}$
$P_C=P_{SG}+\Delta P_{SG}$
P_{SG}
ΔP_{XLG}
ECCS
Break flow
Core level decreases
Loop seal formed
$\Delta P=P_C-P_{DC}=\Delta P_{SG}+\Delta P_{XLG}$

Figure RAI-4-3.1 Mechanism of loop seal formation

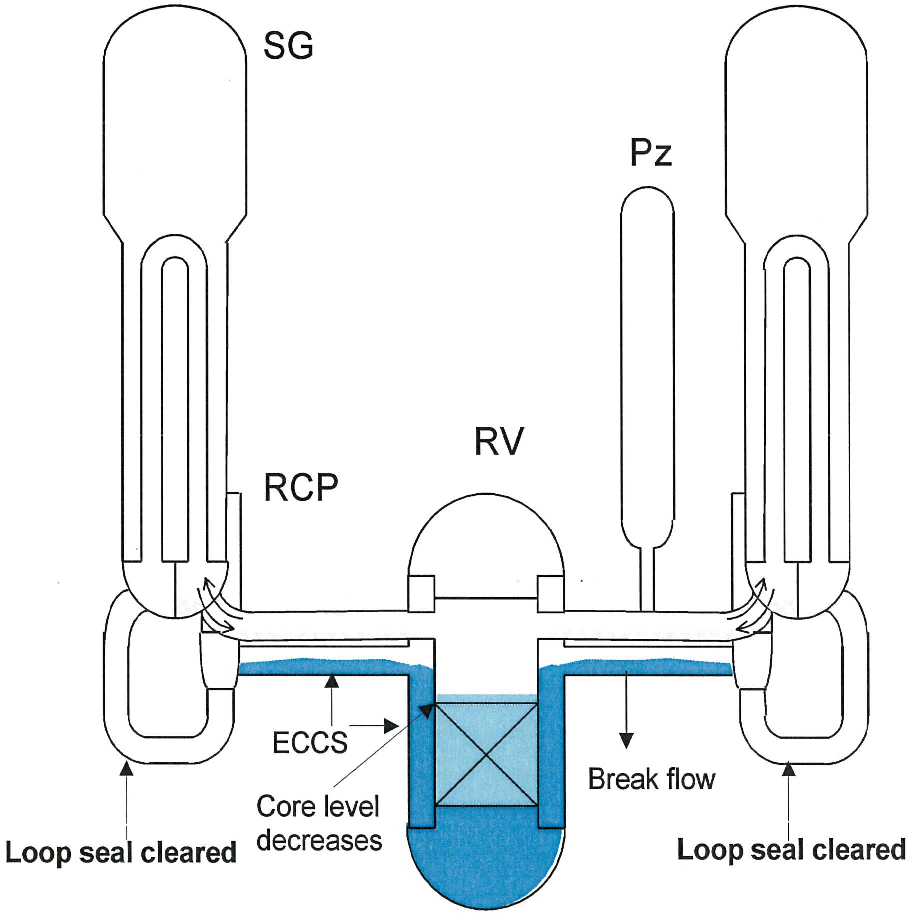
SG
Pz
RV
RCP
ECCS
Core level decreases
Break flow
Loop seal cleared
Loop seal cleared

Figure RAI-4-3.2 Mechanism of loop seal clearing

REQUEST 4-4

[

]

RESPONSE

[

]

REQUEST 4-5

[

]

RESPONSE

[

]

REQUEST 4-6

[

]

RESPONSE

[

]

REQUEST 4-7

Section 4.3.2.7
Pressurizer pressure is used as a parameter for reactor trip and safety injection signal. Vapor generation in the primary system will have strong influence on this pressure. Explain why interfacial mass transfer or flashing has not been identified as a phenomenon of interest.

RESPONSE

The interfacial mass transfer or flashing is identified as a phenomenon of interest in a postulated large-break LOCA, during the blowdown period, where depressurization rate is much higher than that of small-break LOCA. In addition, all phenomena are judged based on their impact to the PCT calculation. Although vapor generation in the primary system, especially in the uncovered core has a strong influence on pressure, its impact to PCT is relatively low. For all PWR systems and US-APWR, the reactor trip and safety injection pressure setpoints of 1860 psia and 1760 psia, respectively, are reached before bulk flashing occurs in the core. Finally, the initiation of flashing in the upper head strongly depends on the initial coolant temperature, not only pressure, and does not occur before the setpoints are reached.

REQUEST 4-8

Section 4.3.2.9
The report mentions that for smaller breaks the loop seal may not clear. During Loop Seal Clearing period, what is the status of safety injection (including accumulator flow) for various break sizes? (PIRT-45)

RESPONSE

Sensitivity studies were performed and documented in the Technical Report accompanying the DCD. The technical report cites that the loop seal may not clear for break size equal to or smaller than 1-inch.

Stabilization of the primary pressure at a relatively high level during a small-break size prevents injection of the accumulator's borated water for some time, while the boil-off process and break flow will continue to reduce the liquid inventory in the reactor vessel. The accumulator will be initiated once the RCS pressure reduces to 600 psia. Table RAI-4-8.1 provides an insight about the status of ECCS during a small-break LOCA. Once actuated, the HHIS will continue to operate. Accumulator flow was not initiated during the calculations for the smaller breaks shown in the table.

Table RAI-4-8.1 Status of ECCS during a small-break LOCA

No.	**Break Size**	**Loop Seal Status**		**Status of ECCS throughout Small-Break transient**	
		Clear	No Clear	HHIS (SI Pumps) Initiated at (s)	Advanced Accumulator Initiated at (s)
1	2-inch	X		221	Not actuated[1)]
2	3.4-inch (DVI Line)	X		153	Not actuated[1)]
3	7.5-inch	X		130	299
4	1-ft^2	X		126	90

[1)] *Not actuated in the specified duration of this transient calculation*

REQUEST 4-9

Section 4.3.2.9
There is some uncertainty as to whether loop seal clearing (PIRT #45) will occur first in the broken loop or in the lumped intact loop (3 loops combined). The effect of loop dynamics (or asymmetric effects) was not included as one of the phenomenon for consideration in the PIRT process. Please explain.

RESPONSE

The reviewer is correct that there are uncertainties on which loop would clear first in a symmetrical 4-loop PWR. However, the proximity to the break favors the broken loop. Also the break size could influence preferential loop seal clearing.

It has been shown by integral effect tests (IETs) performed in the past that normally, the loop-seal in the broken loop will clear first (allow vapor to pass through). When this happens, the stored liquid in the upper parts of the downcomer will fall and the two-phase level in the core will rise rapidly.

MHI believes that the uncertainty in the loop seal clearing process is not caused by the effect of loop dynamics (i.e. asymmetric effects), but due to the uncertainty in the flow regime and its impact on flow resistance through the loop seal. Entrainment and counter-current flow limiting (CCFL) in the uphill of RCP suction leg affects the mass retention in the loop seal piping following the venting. MHI is also in the opinion that as long as the capacity of injection flow rates of SI pumps and accumulator are more than sufficient, the effect of loop asymmetric or unbalanced can be well mitigated.

REQUEST 4-10

[

]

RESPONSE

[

]

REQUEST 4-11

Section 4.4
How are medium ranked phenomena treated in the analyses?
Are there any assessments of the medium ranked phenomena?

RESPONSE

[

]

Table RAI-4-11.1 PIRT for Small Break LOCA (Medium-ranked phenomena)

Location	Process / Phenomena	Small Break LOCA				
		Blowdown	Natural Circulation	Loop Seal Clearance	Boil-off	Recovery
Fuel Rod						
2	Core kinetics, Reactor Trip (fission power)					
3	Decay Heat					
4	Oxidation of Cladding					
5	Clad Deformation (Creep/Burst)					
Core						
8	Heat Transfer below the Mixture Level					
12	Entrainment/Deentrainment					
13	3-D Flow					
17	Top Nozzle/Tie Plate CCFL					
Neutron Reflector						
Upper Head						
22	Drainage to Core / Initial Fluid Temperature					
23	Bypass Flow between Upper Head and Downcomer (Cold Leg)					
Upper Plenum						
25	Mixture Level					
26	Drainage to Core					
27	Entrainment/Deentrainment					
28	Bypass Flow / Hot Leg - Downcomer Gap					
Hot leg						
30	Stratified Flow/Counter-flow					
31	Entrainment/Deentrainment					
Pressurizer and Surge Line						
Steam Generator						
39	Primary Side Heat Transfer					
40	Secondary Side Heat Transfer (Water Level)					
42	Multi U-Tube Behavior					
43	AFW					
Crossover Leg						
45	Loop Seal Formation and Clearance (Entrainment/Flow Regime/Interfacial Drag/Flow Resistance)					

Asterisk (*) denotes that the ranking is "break size dependent."

Table RAI-4-11.1(cont'd) PIRT for Small Break LOCA (Medium-ranked phenomena)

Location	**Process / Phenomena**	**Small Break LOCA**				
		Blowdown	**Natural Circulation**	**Loop Seal Clearance**	**Boil-off**	**Recovery**
Reactor Coolant Pump						
48	Coastdown Performance					
Cold Leg						
51	Stratified Flow					
52	Steam Condensation by ACC Water					
Accumulator						
56	Large Flow Injection/ Flow Resistance					
Downcomer/Lower Plenum						
60	Mixture Level/Void Distribution					
62	ECCS Water/Mixing					
64	DVI/SI Water/Flowrate					
65	DVI/SI Water/Condensation					
66	DVI/SI Water/ Injection Temperature					
Break						

Asterisk (*) denotes that the ranking is "break size dependent."

REQUEST 4-12

Section 4.4.2
What does confirmation mean?
What are the criteria of confirmation?

RESPONSE

Confirmation in this context means the analyses performed using M-RELAP5 to validate the important models related to high-ranking phenomena. The criterion of confirmation is that if there are phenomena, models and/or parameters that are of important interest for US-APWR SBLOCA scenario or certain test activities, then those items must be verified and validated through comparisons with experimental data or independent calculations. The objectives are (1) to judge whether a model can be categorized as best-estimate or conservative in calculating the PCT, and (2) to verify that for each H-ranked phenomenon, the Appendix-K model is conservative.

Table 4.3.2-2 is the SBLOCA PIRT showing the high-ranking phenomena. The H-ranked phenomena consist of 2 categories. The first category contains those phenomena for which M-RELAP5 is judged to have a best-estimate capability, such as models related to the core mixture level and the countercurrent flow limiting (CCFL) models. In consideration that M-RELAP5 is almost the same with RELAP5-3D, the implementation of the Appendix-K model does not cause any impact to these models. Therefore, we can expect best-estimate results. The second category contains phenomena that are directly affected by the Appendix-K model, such as decay heat and modifications to the heat transfer logic that directly affect the PCT calculation. Applying these models yields conservative results (the PCT is higher than that calculated using the BE approach).

REQUEST 4-13

(Related RAI 4-1)

The heat transfer logic at the end of blowdown must be precisely defined in the documentation so that it can be verified against the code and the analysis.

RESPONSE

The heat transfer mode selection logic to prevent the return to nucleate boiling once CHF has been predicted during the blowdown and to prevent the return to transition boiling after the cladding surface superheat exceed 300 R during the blowdown is introduced in M-RELAP5 to satisfy the Appendix K requirements. The M-RELAP5 modifications for these Appendix K requirements are as follows.

[

]

[

]

REQUEST 4-14

(Related RAI 4-7)

[

]

RESPONSE

[

]

REQUEST 4-15

(Related RAI 4-10)

PIRT Tables have some rankings that are break size dependent. Is the ranking in PIRT Table (4.3.2-1, MUAP-07013-P) the highest value for all break sizes? If not, please revise the table and provide the highest ranking for each phenomenon. Also, is there a method (for example a sensitivity analyses) of confirming the ranking in the PIRT?

RESPONSE

Section 4.3-1 of MUAP-07013 states that the (*) ranking implies that the ranking is break size dependent and that it may be insignificant for certain break sizes. Therefore, the (*) ranking indicates that the table represents the highest value for all transients. It is emphasized here that MHI’s ranking are primarily expert based, combining the technical know-how of internal MHI experts and international LOCA experts. This method is primarily applied to confirm the ranking in the PIRT.

Furthermore, a comprehensive quantitative scaling analysis for the US-APWR is being performed as discussed in the responses to RAIs 1-2 and 5-2. In the process of scaling analysis, the importance of each phenomenon addressed in the PIRT will be quantitatively examined.

REQUEST 4-16
(Related RAI 4-11)

PIRT tables provide ranking of all phenomena as they impact the figure of merit. However, it is not clear how high and medium rank phenomena are treated. Why are some high ranked phenomena (Table 4.3.2-2) not validated (Table 4.4.2-1)? Are medium ranked phenomena validated? Are high and medium ranked phenomena, not covered by Appendix K, modeled with best estimate or conservative models in the SBLOCA analyses?

RESPONSE

On how high and medium rank phenomena are treated and validated
Medium ranked phenomena are not assessed with high level of detail. Highly ranked phenomena are investigated through separate effects assessments, but medium and low ranked phenomena are assessed indirectly during integral assessments. Thus, from a practical point of view, there is not much difference between medium and low rankings.

On why some high ranked phenomena (Table 4.3.2-2) not validated (Table 4.4.2-1)
Some high ranked phenomena in Table 4.3.2-2 do not appear in Table 4.4.2.1. These are conservatively treated for the safety analysis as follows, and are not addressed in the code validation plan.

Decay heat – Conservative Appendix K model is applied with a multiplication factor of 1.2.

Local power, 3-D power distribution – Conservative input or assumption is applied (i.e. worst case peaking factors)

Critical flow – Appendix K model is applied. Verification was performed to determine that the implementation was correct. Break spectrum analysis was performed to determine worst case break size and location (Ref. 1).

Break flow enthalpy – Sensitivity calculations were performed to determine the worst break orientation, top, bottom, and side connections (Ref. 1). The break orientation influences the two-phase flow behavior to be discharged from the break that eventually affects the energy to be discharged through the break.

DVI/SI water flow rate – Flow rate and temperature of the safety injection are treated by conservative input and assumption to obtain limiting results.

Reference:

1. Mitsubishi Heavy Industries, Ltd., Small Break LOCA Sensitivity Analyses for US-APWR, Technical Report, MUAP-07025-P (R0).

REQUEST 4-17
(Related RAI 4-12)

Section 4.4.2 refers to confirmation plan for high ranking phenomena. What are the acceptance criteria for confirming the model of a given phenomenon? How is it established that the code model will accurately represent the phenomenon (e.g., percentage difference)? How is it determined that the code prediction is conservative? How is the uncertainty of measurement accounted for? Is there any sensitivity study?

RESPONSE

On the acceptance criteria for confirming the model of a given phenomenon, the response to RAI 4-12 (Ref. 1) already describes the process in general. The objectives are (1) to confirm that the models do not result in significantly non-conservative predictions, and (2) to verify that the Appendix K models provide sufficient conservatism in the safety analysis.

The RELAP5-3D, which is the based code for the M-RELAP5 that incorporates the Appendix-K Evaluation Model, has been verified of being capable to capture all phenomena during a small-break LOCA postulated to occur in a conventional PWR. All important phenomena and phases during a SBLOCA transient in the US-APWR are identical to that of conventional PWR. All the high-ranking phenomena are identified in the PIRT and are validated by both separate and integral effect tests. The results of M-RELAP5 prediction showed conservatisms in certain phenomena and realistic for other certain phenomena.

The thermal-hydraulic models in M-RELAP5 were initially developed for best-estimate method. Therefore, some discrepancies and deviation are obviously observed, that were caused by model uncertainty. The implementation of Appendix K evaluation models result in the accommodation of all these deviation. In other words, the conservative Appendix K evaluation model well bound the deviation.

On the sufficiency of conservativeness of the Appendix-K evaluation models, the decay heat model that multiplied with a factor of 1.2 demonstrates the sufficiency of the models. In this context, the M-RELAP5 has also been validated using the THTF Uncovered-Bundle Heat Transfer Test data. Figures 8.1.2-31 and 32 in the topical report MUAP-07013-P (R0) show the results of a sensitivity study in which the rod power is raised 1.2 times of the nominal power to conform to the Appendix K requirement that affect local power. The results show that by applying the Appendix K model yields significant conservativeness in the mixture level and rod surface temperature predictions. A similar investigation has also been done in addressing the code applicability to SBLOCAs by using the integral test data obtained in the ROSA/LSTF test facility (refer to Figures 8.2.1-53 to 60 of MUAP-07013-P (R0)).

Reference:

1. Mitsubishi Heavy Industry, Ltd., MHI’s Partial Responses to NRC’s Requests for Additional Information on Topical Report MUAP-07013-P (R0) “Small Break LOCA Methodology for US-APWR”, UAP-HF-09002, January 16, 2009.

REQUEST 4-18

(Related RAIs 4-1 and 4-13)

[

]

RESPONSE

[

]

REQUEST 5-1

Section 5.2
The prototype plant in the scaling analysis of the test facilities is a reference PWR and not the US-APWR. Though the reference PWR is a 4-loop plant with 17x17 fuel assemblies, there are significant differences between the reference PWR and the US-APWR, e.g. active fuel height (12 ft. for the reference and 14 ft. for the US-APWR) and number of grid spacers (9 for the reference PWR and 11 for the US-APWR). Provide an evaluation of the impact of not using US-APWR design parameters in the scaling analysis.

RESPONSE

In principle, there is no impact of not implementing US-APWR's fuel assembly design parameters such as the active fuel length of 14 ft instead of 12 ft. The top grid spacer #1 and the bottom grid spacer #11 do not contribute to the change of scalability. The intrinsic neutronics and thermal-hydraulics characteristics are maintained in the nine (9) grid spacers to be the same as that of reference plants. The additional 2 ft is to accommodate the additional grid spacers.

The US-APWR fuel design uses 11 grid spacers that span the 14-ft active fuel length.
The upper and lower grid spacers are made of nickel-chromium-iron Alloy-718 (Inconel 718), and the nine intermediate grid spacers are made of Zircaloy-4. The influencing parameter is the span between grids. The grid span for the US-APWR design is almost the same as that for the 12-ft Mitsubishi fuel with a 9 grid spacer design. The intermediate grid spacer is designed based on current version in use in Mitsubishi-fueled reactors with advanced mixing vanes. Additionally, the reduced power density in 14-ft fueled PWR compared to that of 12-ft moderates the impact by having an added thermal margin for PCT.

The response to REQUEST 8.1-1 contains the evaluation results of US-APWR design parameters in the scaling analysis. MHI has performed a comparison of the main fuel and core design parameters between the US-APWR and conventional PWR. As shown in Table RAI-8.1-1.2 and Table RAI-8.1-1.3 in the response to REQUEST 8.1-1, it is confirmed that the difference does not cause negative impact or introduce new phenomenon. It is clarified that the effect of differences are properly simulated by the code and can be concluded that the conventional (reference) model is applicable to the US-APWR.

REQUEST 5-2
(Related RAI 5-1)

The MHI response does not provide quantitative scaling analysis that supports their claim that the differences between the US-APWR and a conventional PWR in active core height and number of grid spacers is negligible.

Provide M-RELAP5 validation runs for the prediction of CHF and PCT in a 12-ft fuel assembly and the scaling analysis that demonstrates the validity of extending the M-RELAP5 capability to predict CHF and PCT in a 14-ft fuel assembly typical of the US-APWR core.

RESPONSE

[

]

REQUEST 6-1

Section 6.1.2
The M-RELAP5 documentation must be reasonably self-contained. The existing references for M-RELAP5 in the topical report refer to documentation for RELAP5-3D and RELAP5Mod3.3 extensively. There are no stand-alone M-RELAP5 code manuals. Provide stand-alone M-RELAP5 manuals and in particular a user manual on how to call for the EM models in M-RELAP5.

RESPONSE

A stand alone M-RELAP5 input manual has been developed based on the RELAP5-3D input manual, with the addition of the features of Appendix-K model. The document has been submitted to the US-NRC as follows: **"M-RELAP5 Input Manual, 6AS-1E-UAP-080014(R0), Proprietary",** which is the derivation of RELAP5-3D Volume II, Appendix A: Input Data Requirements. Table RAI-6-1.1 summarize on how to find the Appendix-K EM in the M-RELAP5 input manual.

There are no others stand-alone manuals for M-RELAP5. The rest are the same as for RELAP5-3D Code Manuals, prepared by the RELAP5-3D Code Development Team, Idaho National Laboratory, INEEL-EXT-98-00834, Revision 2.4, published in June 2005, consisting of:

Volume I: Code Structure, System Models and Solution Methods
Volume II: User's Guide and Input Requirements
Volume IV: Models and Correlations
Volume V: User's Guidelines

The RELAP5-3D is not equipped with a particular Volume III. It uses the previously prepared Volume III manual for RELAP5/Mod3, entitled: RELAP5/Mod3 Code Manual Volume III: Developmental Assessment Problems (Draft), NUREG/CR-5535, EGG-2596 (Draft), INEL, June 1990.

Table RAI-6-1.1 Correspondence of Appendix-K EM to M-RELAP5 input manual

No.	Important Parameters of Appendix-K Requirements	Corresponding Sections and Pages in M-RELAP5 Input Manual
1	Initial Stored Energy (Gap conductance model consistent with the fuel design code is installed)	Cards 1CCCGXNN, Heat Structure Input - Card 1CCCG001, Gap Conductance Model Initial Gap Pressure Data, p8-3
2	Fission Product Decay (ANS standard 1971 is installed)	Section 15 Cards 30000000 through 30099999, 15.3 Card 30000002, Fission Product Decay Information, p15-3.
3	Metal Water Reaction Rate (The Baker-Just equation is installed)	Section 8.3 Card 1CCCG003, Metal-Water Reaction Control: W1(R) Initial oxide thickness on cladding's outer surface (m, ft). Add 1.0 (m ft) to initial oxide thickness to use **Baker-Just oxidation model**, p8-4.
4	Cladding Swelling and Rupture ✓ Cladding swelling and rupture model for ZIRLO^{TM} alloy is installed. ✓ Gap conductance calculation for rupture node is installed.	Section 8.4 Card 1CCCG004, Fuel Cladding Deformation Model Control. W2(I) ZIRLO model flag. Enter 0 if ZIRLO cladding deformation model is not to be calculated. Enter 1 if ZIRLO cladding deformation model is to be calculated. Either a 0 or a 1 must be entered, p8-4.
5	Discharge Model (The Moody model is installed)	2.1 Card 1, Developmental Model Control. Option 22. This option uses Moody critical plow model rather than modified Henry-Fauske critical flow model. This option has no effect if the modified Henry-Fauske critical flow model is not selected.
6	Return to Nucleate Boiling (The logic to prevent return to nucleate boiling during blowdown is installed)	Section 8.15 Card 1CCCG800, Additional Left Boundary Option. W3(I) Flag for CHF degradation model at high void fraction. Enter 0 if CHF degradation model is not to be calculated. Enter 1 if CHF degradation model is to be calculated. Either a 0 or a 1 must be entered, p8-15
7	Return to Transition Boiling (The logic to prevent return to transition boiling during blowdown is installed)	The same as above.

REQUEST 6-2

Section 6.1.2
Table 6.1-1 summarizes independent assessments of RELAP5/MOD3 performed by the CAMP members specifically for SBLOCA. M-RELAP5 has not been assessed for all the integral effect tests and separate effects test listed in the table.
Has there been any systematic comparison of RELAP5/MOD3 and M-RELAP5 simulations of the assessment matrix in Table 6.1-1 to identify the effects of implementing the EM methodology?
Do the EM models in M-RELAP5 predict more conservative results for assessment tests when compared with RELAP5/MOD3?

RESPONSE

Not all the integral- and separate-effect tests (IETs/SETs) listed in the Table 6.1-1 are required for the assessment of M-RELAP5. Only those IETS/SETs that correspond to the high-ranked phenomena are used for the code assessment. The rest of the models are based on the well verified and validated RELAP5/MOD3.2, which was the subject of an extensive NRC program to demonstrate its adequacy for SBLOCA analysis. Experience has shown that RELAP5-3D predicts results that are close to those obtained with RELAP5/MOD3.2 for problems that do not exercise its new models and features. The Topical Report contains Table 4.4.2-1, the Assessment Matrix for M-RELAP5 for Small Break LOCA that identifies the effects of implementing the EM methodology.

A summary of the assessment results is included in Table RAI-6-2.1. In addition, we also performed one sensitivity analysis case by simulating the ROSA-IV/LSTF 5% Small Break LOCA Test (SB-CL-18), with all Appendix-K options turned-off, resulting in a best-estimate (BE) calculation. Note that neither calculation included the 20% increase in the decay heat required by Appendix K. The results were then compared with the Appendix-K results as shown in the Figures RAI-6-2.1 through 10. The most noticeable differences were that the calculated heater temperatures differed slightly because of the changes to the heat transfer logic concerning return to nucleate boiling and return to transition boiling. The other Appendix-K models were not applicable for this test. Consequently, the other parameters were nearly identical.

These results demonstrate that M-RELAP5 predicts nearly identical results with and without the Appendix-K models for cases in which the Appendix-K models are not applicable. M-RELAP5 will also predict results that are identical to RELAP5-3D when the Appendix-K models are not used. Therefore, repeating all the simulations of the assessment matrix in Table 6.1-1 using M-RELAP5 is not necessary.

The analysis described by MHI in Section 8.2.1 confirms that the Appendix-K model, including the required 20% increase in decay heat, predicts much more conservative results than obtained in the base calculation. For example, compare Figures 8.2.1-41 and 8.2.1-57 in the Topical Report. By the logic described previously, the results with the M-RELAP5 evaluation model would be much more conservative than those obtained with a best estimate RELAP5/MOD3 calculation.

The Road-Map of M-RELAP5 Code Development and Assessment is provided as an Appendix for the Response to REQUEST 6-2. The Appendix provides a brief summary of M-RELAP5 development and assessment for its application to the small break LOCA analysis of the US-APWR.

Table RAI-6-2.1 Summary of M-RELAP5 Validation and Assessment for US-APWR Small Break LOCA Analysis

Models to be Assessed	**Names of Test Activities / Facilities**	**Summary of Assessment Result**	**Corresponding Chapter in Reference**
Void model (Interfacial heat transfer and drag)	ROSA/LSTF Void Profile Test	Three tests conducted at 7.3MPa were selected for the code assessment. M-RELAP5 is capable of predicting the axial void distribution and the average void fraction in each test accurately.	8.1.1
✓ Void model ✓ Two-phase mixture level model ✓ Core uncovery heat transfer model	ORNL/THTF Void Profile & Uncovered Heat Transfer Test	10 tests of the steady-state 3.09.10 series were selected for the code assessment. The axial void distributions below the mixture level calculated by M-RELAP5 well agree with the measurements. Furthermore, M-RELAP5 accurately predicts the mixture level, and the simulated fuel rod surface temperature rise above the mixture level as well as the superheated vapor temperature.	8.1.2
✓ Two-phase mixture level model ✓ Core uncovery heat transfer model ✓ Reflood and rewet model	ORNL/THTF Reflood Test	2 tests of the transient flooding 3.09.10 series were selected for the code assessment. The upward quench velocity estimated by M-RELAP5 is slower than the measurements. M-RELAP5 also calculates fuel rod surface temperatures higher than measurements due to the conservative heat transfer models relevant to the reflood behavior.	8.1.3
CCFL model in hot leg *(water hold-up in SG inlet plenum)*	UPTF SG Plenum CCFL Test	Two pressure conditions of the hot leg injection test were selected. The CCFL model parameters for M-RELAP5 were derived in each case by applying the linear regression analysis to the measured data. The verification demonstrates that the M-RELAP5 is capable of reproducing the observed CCFL phenomena.	8.1.4
CCFL model in SG tube *(water hold-up in SG U-tube uphill side)*	Dukler Air-Water Flooding Test	In order to verify the M-RELAP5 CCFL model (Hewitt & Wallis model) applicability to the small diameter pipe like the SG tube, the Dukler air-water low-pressure flooding test was selected as a validation problem. Analysis shows that the M-RELAP5 model is adequately applicable to the CCFL behavior in the SG U-tube.	8.1.5
Code applicability to SBLOCA	ROSA-IV/LSTF Small Break (5%) LOCA Test	The SB-CL-18 test was selected as a representative SBLOCA problem. M-RELAP5 correctly simulates the key thermal-hydraulic phenomena occurring during SBLOCA. In particular, the PCT in the loop seal period is accurately predicted by M-RELAP5, and is conservatively evaluated in the boil-off period.	8.2.1

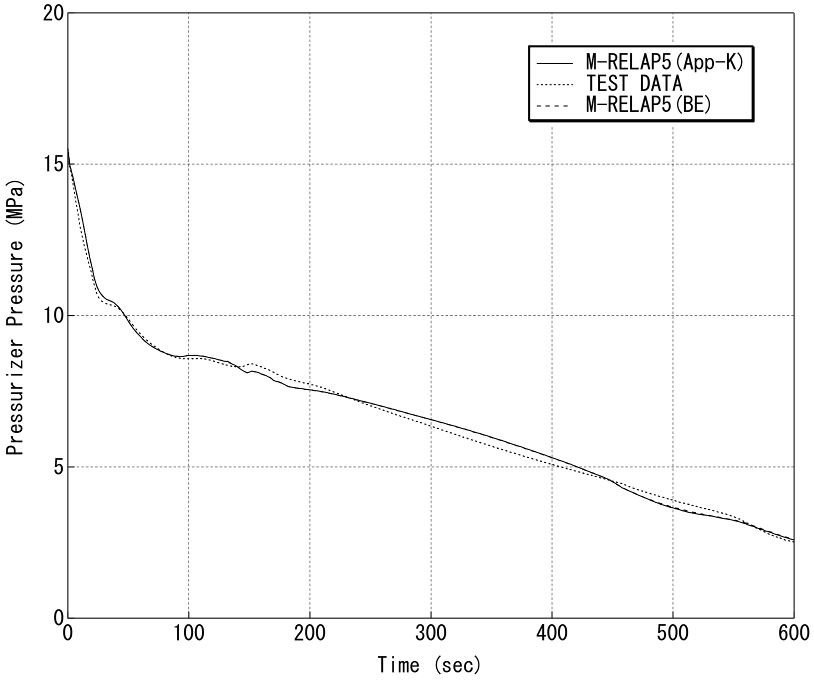

Figure RAI-6-2.1 Pressurizer Pressure
(Sensitivity Analysis of Appendix-K versus Best-Estimate)

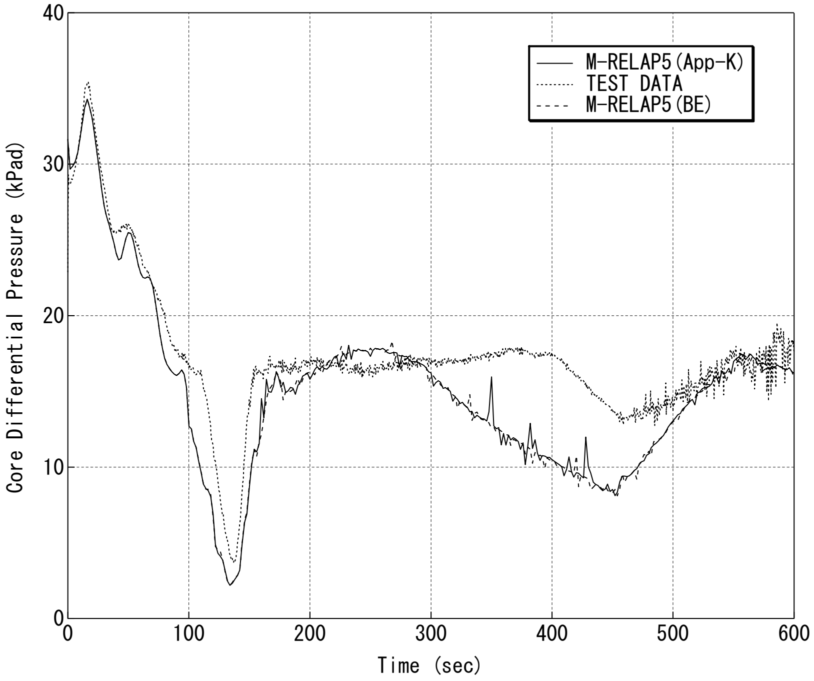

Figure RAI-6-2.2 Core Differential Pressure
(Sensitivity Analysis of Appendix-K versus Best-Estimate)

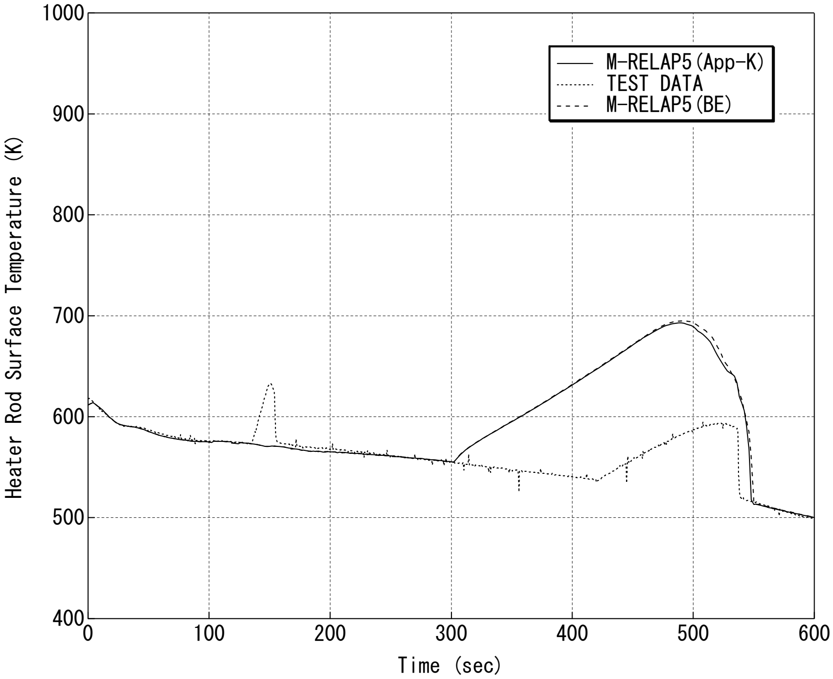

Figure RAI-6-2.3 Heater Rod Surface Temperature (Node17)
(Sensitivity Analysis of Appendix-K versus Best-Estimate)

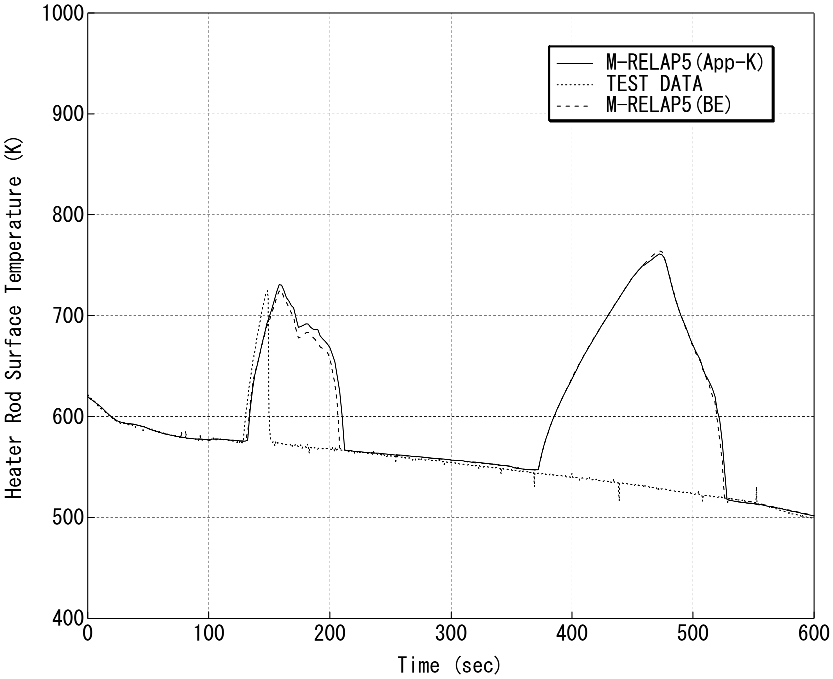

Figure RAI-6-2.4 Heater Rod Surface Temperature (Node11)
(Sensitivity Analysis of Appendix-K versus Best-Estimate)

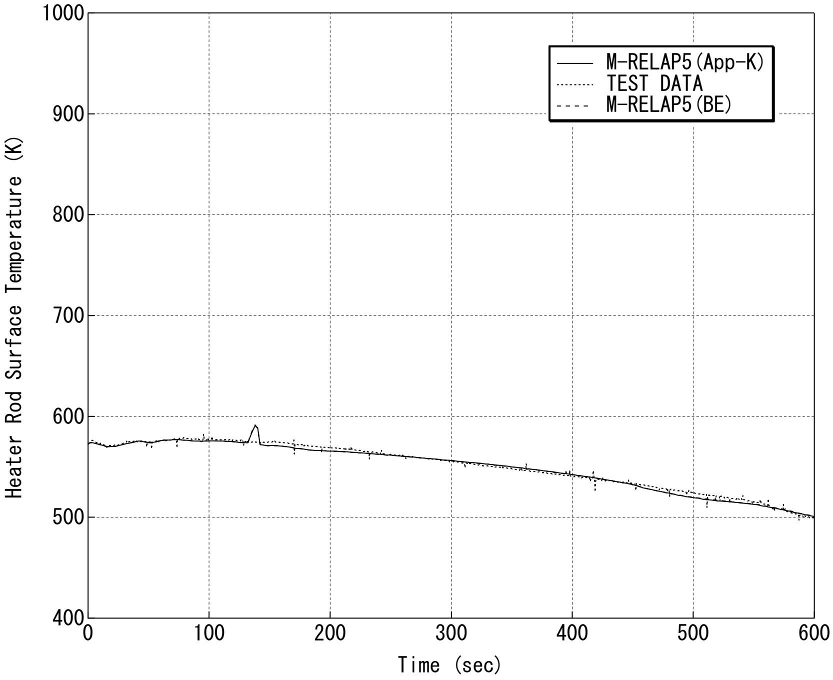

Figure RAI-6-2.5 Heater Rod Surface Temperature (Node1)
(Sensitivity Analysis of Appendix-K versus Best-Estimate)

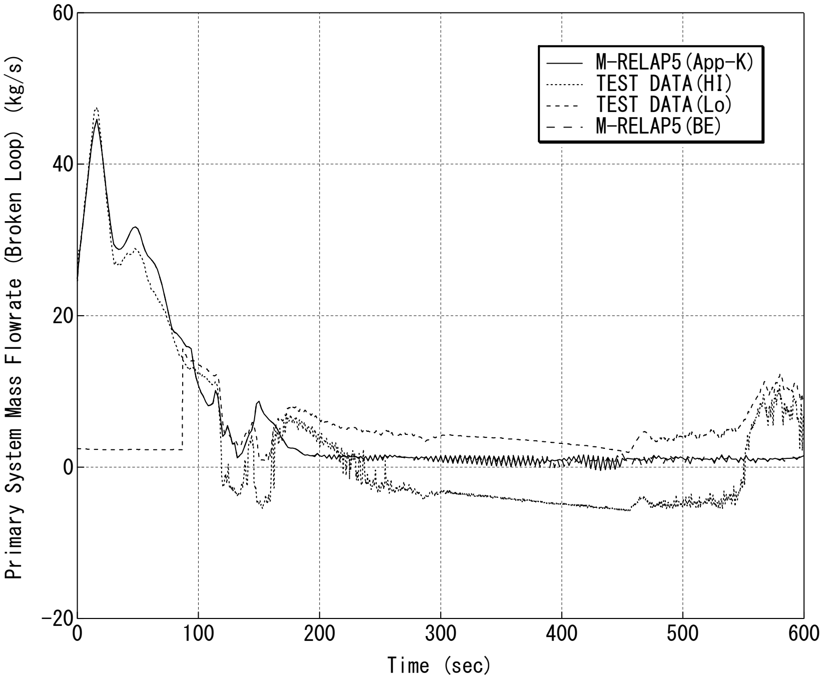

Figure RAI-6-2.6 Primary System Mass Flowrate (Broken Loop)
(Sensitivity Analysis of Appendix-K versus Best-Estimate)

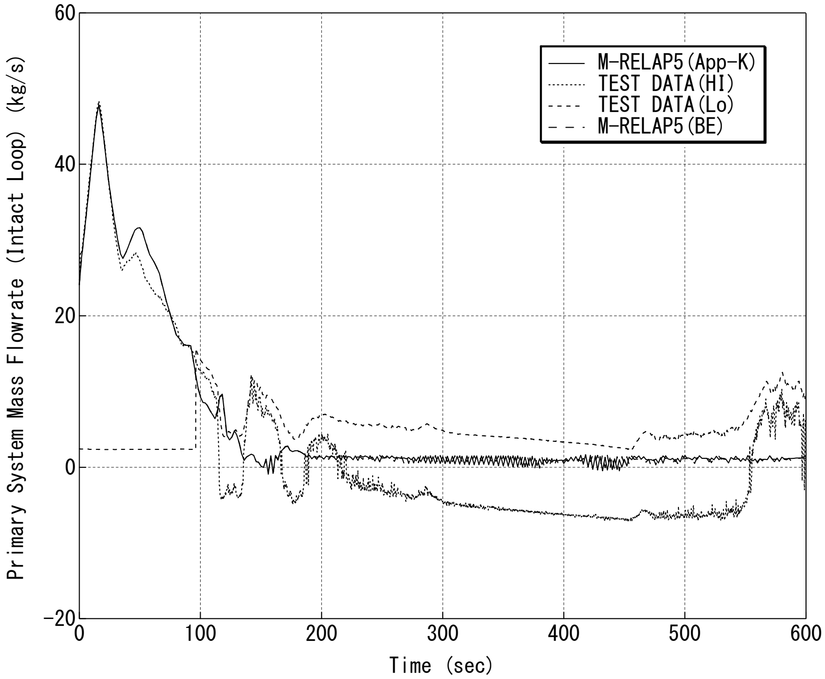

Figure RAI-6-2.7 Primary System Mass Flowrate (Intact Loop)
(Sensitivity Analysis of Appendix-K versus Best-Estimate)

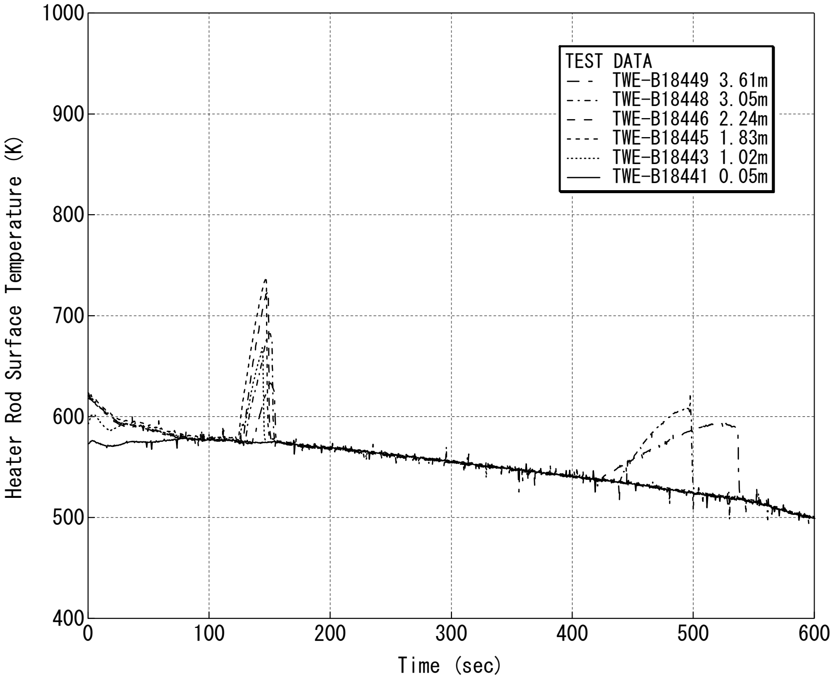

Figure RAI-6-2.8 Heater Rod Surface Temperature (Test Data)
(Sensitivity Analysis of Appendix-K versus Best-Estimate)

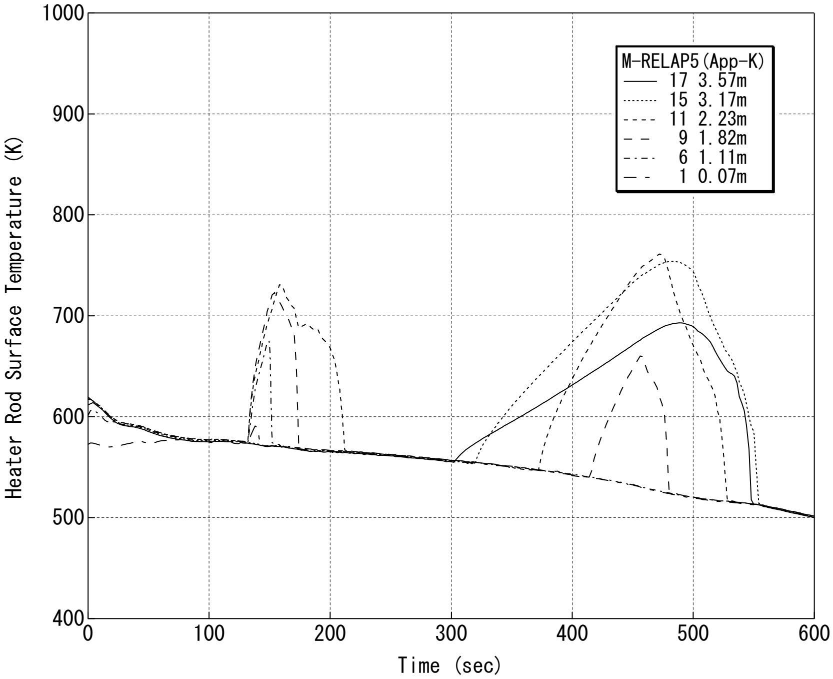

Figure RAI-6-2.9 Heater Rod Surface Temperature (App-K)
(Sensitivity Analysis of Appendix-K versus Best-Estimate)

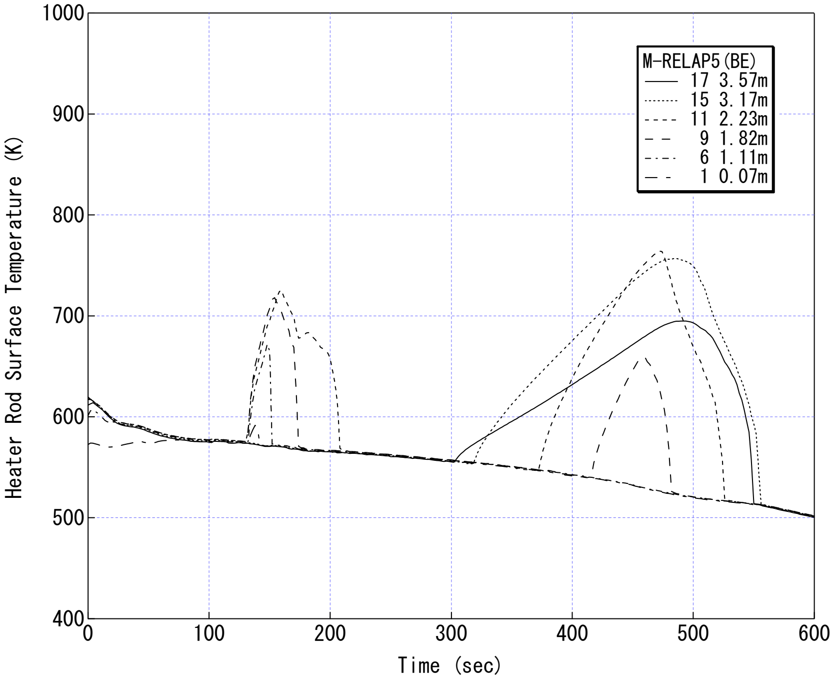

Figure RAI-6-2.10 Heater Rod Surface Temperature (BE)
(Sensitivity Analysis of Appendix-K versus Best-Estimate)

Appendix for Response to REQUEST 6-2
Road-Map of M-RELAP5 Code Development and Assessment

1. Introduction

This document provides a brief summary of M-RELAP5 development and assessment for its application to the small break LOCA analysis of the US-APWR, which is embodied in the pre-licensing Topical Report issued by Mitsubishi Heavy Industries, Ltd (MHI)(Ref.1). The purpose of the Topical Report is to demonstrate the applicability of M-RELAP5 for the Appendix-K based small-break LOCA analysis for the US-APWR. The objective is to pursue NRC's review and approval on the SB-LOCA Methodology for the US-APWR Standard Design. This summary also discusses the unique technical features in M-RELAP5 and its verification & validation status. In the end of this document, the adopted road-map for the regulatory evaluation of the M-RELAP5 SBLOCA methodology is presented.

2. Road-Map in Regulatory Technical Evaluation for M-RELAP5

M-RELAP5 has been developed and assessed in conformance to the RG 1.203 (EMDAP). In the EMDAP, adequacy in (1) PIRT, (2) assessment matrix, (3) applied evaluation model, and (4) the evaluation model assessment are the key issues, and the evaluation model applicability to the defined transient and accident analyses shall be reasonably qualified. The adopted 'road-map' in the regulatory technical evaluation for M-RELAP5 is depicted in **Figure 1**.

3. Basic Principle in Code Development and Assessment

M-RELAP5 has been developed and assessed for its application to the SBLOCA analysis of the US-APWR. The assessment is in conformance with the Regulatory Guide 1.203 (Evaluation Model Development and Assessment Process, EMDAP) (Ref.2). （Chapter 1 of Reference 1）

The primary feature of the M-RELAP5 evaluation model is that the code is applicable for the SBLOCA analysis by satisfying the conservative requirements prescribed in the 10 CFR 50 Appendix K (Ref.3). Hence, several conservative models and correlations have been implemented in its base-code, RELAP5-3D (Ref.4). The M-RELAP5 also incorporates the advanced accumulator model, which is a new engineered-safety feature specific to the US-APWR.

MHI has verified and validated the M-RELAP5 capabilities using available experimental data based on the PIRT (Phenomena Identification and Ranking Table), developed by the internal experts of MHI then independently reviewed by international experts. The code models and correlations, including those specific to M-RELAP5, are capable of predicting the important phenomena and SBLOCA system responses.

4. Evaluation Model Structure

Basic Thermal-Hydraulics Model

The basic thermal-hydraulic field equations and relevant models and correlations in M-RELAP 5 are equivalent to those in the RELAP5-3D. Hence, it is assured that the basic thermal-hydraulic model complies with the 10 CFR 50 Appendix K requirements. （Chapter 6 of Reference 1）

Appendix K Model Implementation

In order to fully satisfy the conservative requirements prescribed in the Appendix K, conservative models and correlations listed in **Table 1** have been incorporated in RELAP5-3D, completing the evaluation model structure of M-RELAP5. (Chapter 7.1 of Reference 1)

New Component Model Specific to US-APWR

The advanced accumulator component model is newly equipped to M-RELAP5. (Chapter 7.2 of Reference 1)

5. Evaluation Model Assessment

High-Ranked Process/Phenomena for US-APWR/SBLOCA

The important process and phenomena occurring under the US-APWR/SBLOCA scenario are extracted from the aforementioned PIRT and listed in **Table 2**. (Chapter 4.1-3 of Reference 1)

Assessment Matrix

In corresponding to the high-ranked processes and phenomena in **Table 2**, MHI has developed the M-RELAP assessment matrix shown in **Table**. (Chapter 4.4 of Reference 1)

Code/Model Assessment

Capabilities in terms of the basic thermal-hydraulic models equivalent between RELAP5-3D and M-RELAP5 have been adequately verified and validated by INL (Ref.4). （Chapter 6 and Table 6.1-1 of Reference 1） M-RELAP5 code applicability to perform SBLOCA analysis for the US-APWR is evaluated using the experimental data, and its brief summary is given in **Table 4**. （Chapter 8 of Reference 1） The implementation of the conservative models specific to M-RELAP5 are also validated, as summarized in **Table 5**. （Chapter 7 of Reference 1）

6. References

1. MHI, Small Break LOCA Methodology for US-APWR, MUAP-07013-P (R0), July 2007.
2. USNRC, Regulatory Guide 1.203 - Transient and Accident Analysis Methods, December 2005.
3. 10 CFR Part 50 Appendix-K, ECCS Evaluation Models.
4. Idaho National Laboratory, RELAP5-3D Code Manual, INEEL-98-00834, Revision 2.4, June 2005.

Table 1. New models in M-RELAP5 to meet the Appendix-K Requirements as compared to RELAP5-3D
(Extracted from Table 7.1.1-1 of Reference 1)

ID	Important Parameters of Appendix-K Requirements	Acceptance Criteria	M-RELAP5 models to meet the Appendix K Requirements *(Modification from RELAP5-3D)*	Corresponding Chapter in Reference 1
I.A.1	Initial Stored Energy	Steady state temperature distribution and stored energy in the fuel shall be calculated for the burn-up that yield highest PCT.	Gap conductance model consistent with the fuel design code is installed.	7.1.2
I.A.4	Fission Product Decay	Fission product decay heat shall be 1.2 times the values for infinite operating time in the ANS standard 1971.	ANS standard 1971 is installed.	7.1.3
I.A.5	Metal Water Reaction Rate	Influence of the metal-water reaction shall be calculated using the Baker-Just equation. The reaction shall be assumed not to be steam limited.	The Baker-Just equation is installed.	7.1.4
I.B	Cladding Swelling and Rupture	Cladding swelling and rupture calculations shall be based on applicable data in such a way that the degree of swelling and incidence of rupture are not underestimated. The gap conductance shall be varied in accordance with changes in gap dimensions and any other applicable variables.	✓ Cladding swelling and rupture model for ZIRLO^{TM} alloy is installed. ✓ Gap conductance calculation for rupture node is installed.	7.1.5 Appendix-B
I.C.1b	Discharge Model	Two-phase discharge rate shall be calculated using the Moody model, with at least three values of discharge coefficient. The discharge coefficient will span from 0.6 to 1.0 or a lower value if a maximum PCT may be calculated at such values.	The Moody model is installed.	7.1.6 Appendix-C
I.C.4e	Return to Nucleate Boiling	After CHF is predicted during blowdown, the calculation shall not use nucleate boiling heat transfer correlations subsequently during the blowdown.	The logic to prevent return to nucleate boiling during blowdown is installed.	7.1.7
I.C.5b	Return to Transition Boiling	Transition boiling heat transfer shall not be used during the blowdown after the temperature difference between the clad and the saturated fluid first exceeds 300 ^{o}F.	The logic to prevent return to transition boiling during blowdown is installed.	7.1.7

Table 2 PIRT for Small Break LOCA (High Rank)

(Extracted from Table 4.3.2-2 of Reference 1)

Table 3 Assessment Matrix for M-RELAP5 for Small Break LOCA Analysis of the US-APWR

(Extracted from Table 4.4.2-1 of Reference 1)

	CHF/Core Dryout	Uncovered Core Heat Transfer	Rewet	Core Mixture Level	Water Hold-Up in SG Inlet Plenum	Water Hold-Up in U-Tube Uphill Side	SG Primary and Secondary Heat Transfer	Water Level in SG Outlet Piping	Loop Seal Formation and Clearance	Downcomer Mixture Level/Void Distribution
Separate Effect Tests (SETs)										
ROSA/LSTF Void Profile Test				X						
ORNL/THTF Void Profile Test				X						
ORNL/THTF Uncovered Heat Transfer Test	X	X								
ORNL/THTF Reflood Test		X	X							
UPTF SG Plenum CCFL Test					X					
Dukler Air-Water Flooding Test						X				
Integral Effect Tests (IETs)										
ROSA-IV/LSTF Small Break (5%) LOCA Test	X	X	X	X	X	X	X	X	X	X

Table 4 Summary of M-RELAP5 Validation and Assessment for US-APWR Small Break LOCA Analysis

Models to be Assessed	Names of Test Activities / Facilities	Summary of Assessment Result	Corresponding Chapter in Reference 1
Void model (Interfacial heat transfer and drag)	ROSA/LSTF Void Profile Test	Three tests conducted at 7.3MPa were selected for the code assessment. M-RELAP5 is capable of predicting the axial void distribution and the average void fraction in each test accurately.	8.1.1
✓ Void model ✓ Two-phase mixture level model ✓ Core uncovery heat transfer model	ORNL/THTF Void Profile & Uncovered Heat Transfer Test	10 tests of the steady-state 3.09.10 series were selected for the code assessment. The axial void distributions below the mixture level calculated by M-RELAP5 well agree with the measurements. Furthermore, M-RELAP5 accurately predicts the mixture level, and the simulated fuel rod surface temperature rise above the mixture level as well as the superheated vapor temperature.	8.1.2
✓ Two-phase mixture level model ✓ Core uncovery heat transfer model ✓ Reflood and rewet model	ORNL/THTF Reflood Test	2 tests of the transient flooding 3.09.10 series were selected for the code assessment. The upward quench velocity estimated by M-RELAP5 is slower than the measurements. M-RELAP5 also evaluate the simulated fuel rod surface temperature higher than the measurements due to the conservative heat transfer models relevant to the reflood behavior.	8.1.3
CCFL model in hot leg *(water hold-up in SG inlet plenum)*	UPTF SG Plenum CCFL Test	Two pressure conditions of the hot leg injection test were selected. The CCFL model parameters for M-RELAP5 were derived in each case by applying the linear regression analysis to the measured data. The verification demonstrates that the M-RELAP5 is capable of reproducing the observed CCFL phenomena.	8.1.4
CCFL model in SG tube *(water hold-up in SG U-tube uphill side)*	Dukler Air-Water Flooding Test	In order to verify the M-RELAP5 CCFL model (Hewitt & Wallis model) applicability to the small diameter pipe like the SG tube, the Dukler air-water low-pressure flooding test was selected as a validation problem. Analysis shows that the M-RELAP5 model is adequately applicable to the CCFL behavior in the SG U-tube.	8.1.5
Code applicability to SBLOCA	ROSA-IV/LSTF Small Break (5%) LOCA Test	The SB-CL-18 test was selected as a representative SBLOCA problem. M-RELAP5 correctly simulates the key thermal-hydraulic phenomena occurring during SBLOCA. In particular, the PCT in the loop seal period is accurately predicted by M-RELAP5, and is conservatively evaluated in the boil-off period.	8.2.1

Table 5 Summary of Validation Status for M-RELAP5-Specific Models

Required Appendix-K Model Implemented in M-RELAP5	Summary of Validation Status	Corresponding Chapter in Reference 1
Initial Stored Energy (FINE Code Gap Conductance Model)	The gap heat transfer model, which is consistent with that implemented on the MHI fuel design code FINE, is incorporated in M-RELAP5. The model has been adequately validated. In M-RELAP5 application to the safety analysis, the initial fuel-cladding gap conductance shall be adjusted to reproduce the fuel temperature computed by FINE to satisfy the Appendix-K requirement.	7.1.2
Fission Product Decay (ANS Standard 1971 Decay Heat Model)	A set of the decay heat model parameters in M-RELAP5 is replaced by that reproducing the ANS 1971 decay heat accurately. The temporally integral decay power as well as the heat decay after reactor shutdown is validated in the chapter 7.1.3 of Reference 1.	7.1.3
Metal Water Reaction Rate (Baker-Just Model)	The Baker-Just metal-water reaction model is newly implemented on M-RELAP5. This model adequately bounds the possible oxidation of ZIRLO^{TM} used in the US-APWR. The reaction area enhancement due to the cladding deformation is appropriately taken into account in M-RELAP5. In addition, the metal-water reaction on the inside surface of cladding is modeled, which is necessary when the cladding results in rupture.	7.1.4
Cladding Swelling and Rupture (ZIRLO^{TM} Cladding Swelling/Rapture Model)	The cladding burst temperature, burst strain, and assembly flow blockage models specific to ZIRLO^{TM} are implemented on M-RELAP5 in accordance to NUREG-0630. In M-RELAP5, the flow blockage effect is considered only in the flow diversion from the cladding rupture region, not in the enhanced steam cooling on heat-up cladding. The cladding swelling and rupture affect the fuel-cladding gap conductance in M-RELAP5.	7.1.5 Appendix-B
Discharge Model (Moody Critical Flow Model)	The Moody critical flow model, which is prescribed in Appendix K for its licensed application to safety analyses, is newly implemented on M-RELAP5. This model is used for the discharge flow calculation under the two-phase condition. The model implementation has been carefully validated by comparing the calculated discharge flow with the original Moody critical flow.	7.1.6 Appendix-C
CHF and Post-CHF Heat Transfer Models (Modification to Post-CHF Heat Transfer Logic)	M-RELAP5 intends to use the well-validated CHF and heat transfer models originally implemented on RELAP5-3D. However, several modifications are added for its application to safety analyses, for example the CHF multiplier and its control logic. The conservative heat transfer logic is also implemented, in which rewetting during the blowdown period is inhibited, and return to the transition boiling heat transfer is not allowed during blowdown period once the cladding surface superheat temperature exceeds 300 ^{o}R. These conservative modifications are validated through the benchmarking using the experimental data obtained in the THTF uncovered heat transfer and reflood tests, and in the ROSA-IV/LSTF small break LOCA test.	7.1.7
Advanced Accumulator Model	The advanced accumulator flow model is newly implemented on M-RELAP5. This model is validated using the experimental test data conducted by MHI, showing its good predictability for the transient behavior of the advanced accumulator.	7.2 Appendix-D

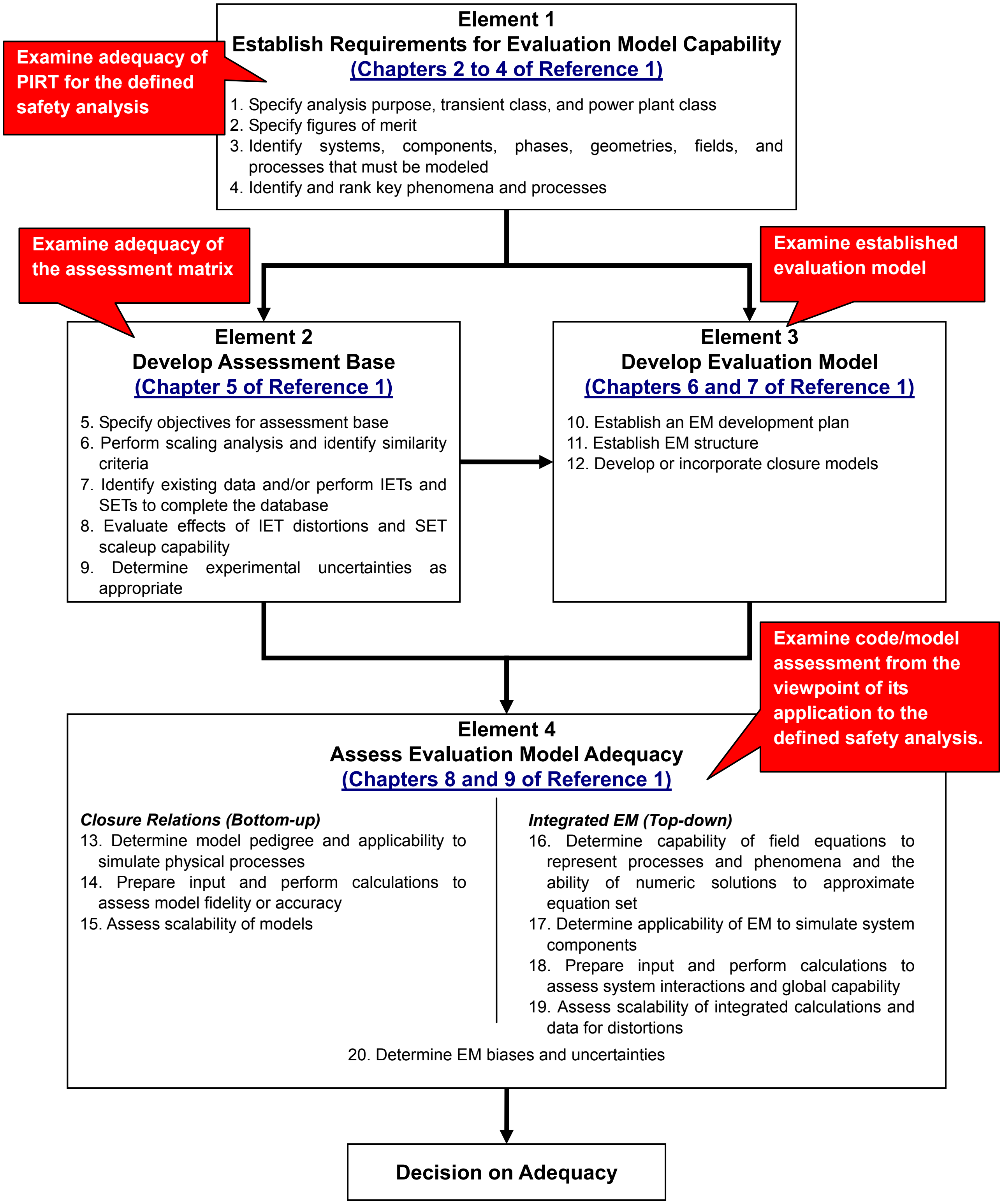

Examine adequacy of PIRT for the defined safety analysis

Element 1
Establish Requirements for Evaluation Model Capability
(Chapters 2 to 4 of Reference 1)

1. Specify analysis purpose, transient class, and power plant class
2. Specify figures of merit
3. Identify systems, components, phases, geometries, fields, and processes that must be modeled
4. Identify and rank key phenomena and processes

Examine adequacy of the assessment matrix

Examine established evaluation model

Element 2
Develop Assessment Base
(Chapter 5 of Reference 1)

5. Specify objectives for assessment base
6. Perform scaling analysis and identify similarity criteria
7. Identify existing data and/or perform IETs and SETs to complete the database
8. Evaluate effects of IET distortions and SET scaleup capability
9. Determine experimental uncertainties as appropriate

Element 3
Develop Evaluation Model
(Chapters 6 and 7 of Reference 1)

10. Establish an EM development plan
11. Establish EM structure
12. Develop or incorporate closure models

Examine code/model assessment from the viewpoint of its application to the defined safety analysis.

Element 4
Assess Evaluation Model Adequacy
(Chapters 8 and 9 of Reference 1)

Closure Relations (Bottom-up)

13. Determine model pedigree and applicability to simulate physical processes
14. Prepare input and perform calculations to assess model fidelity or accuracy
15. Assess scalability of models

Integrated EM (Top-down)

16. Determine capability of field equations to represent processes and phenomena and the ability of numeric solutions to approximate equation set
17. Determine applicability of EM to simulate system components
18. Prepare input and perform calculations to assess system interactions and global capability
19. Assess scalability of integrated calculations and data for distortions

20. Determine EM biases and uncertainties

Decision on Adequacy

Figure 1 Adopted Road-Map in for M-RELAP5 Developmental Assessment
(From Table 1.1-1 of Reference 1)

REQUEST 6-3

Section 6.2.1.3
In Table 6.2.1-4a why does the separator component not apply for the secondary side of SG?

RESPONSE

Reviewer is correct. It is a typo. The separator component does apply for the secondary side of SG. The Table has been revised accordingly.

REQUEST 6-4
(Related RAI 6-1)

Provide documentation of the changes made to RELAP5-3D that created M-RELAP5. The level of documentation detail should be the same as the RELAP5-3D manual. Either the changes can be added to the RELAP5-3D documentation and a complete code manual provided, or an Addendum can be issued. The documentation needs to identify any RELAP5-3D features that are not relevant for M-RELAP5.

RESPONSE
[

]

REQUEST 6-5
(Related RAI 6-2)

To satisfy TMI action plan requirements in NUREG-0737 requires assessing against Semiscale and LOFT data. MHI is requested to include Semiscale test S-UT-8 and LOFT test L3-1 in their assessment matrix.

RESPONSE
[

]

REQUEST 6-6
Related RAI 6-2

Based on the information provided in UAP-HF-09041-P, “MHI's 2nd Part Responses to the NRC's Requests for Additional Information on Topical Report MUAP-07013-P (RO) "Small Break LOCA Methodology for US-APWR", February 2009, in response to Request 6.2, in Table 5, “Summary of Validation Status for M-RELAP5-Specific Models,” it is not clear how the assessments were performed. Provide a table that lists all Appendix K features that were used for each of the assessment cases

.

RESPONSE

The M-RELAP5, which is based on the RELAP5-3D, in its current state, has already contained a number of models that enable it to meet many of the Appendix K requirements with no modification. Therefore, many of the Appendix K requirements can be met by simply providing the appropriate input in the plant model. This includes the appropriate plant nodalization together with appropriate initial conditions, boundary conditions, and the proper code options and also performing sensitivity calculations, if necessary. However, some Appendix K requirements can only be achieved through the implementation of new models or the modification of existing RELAP5-3D models. A few models must be also validated by additional comparison with appropriate test data to confirm the applicability of the models to Small Break LOCA Evaluation Model calculations for the US-APWR.

Actions to conform to Appendix K requirements are divided into three categories:

Category 1: required no action (addressed by conservative input data)
Category 2: required models are missing and need to be added into M-RELAP5 with appropriate verification
Category 3: additional validation using test data needs to be performed before utilized in M-RELAP5

Table RAI-6-6.1 lists the new functions in M-RELAP5 that based on the Appendix K models utilized in the assessment cases in the US-APWR SBLOCA analyses.

Table RAI-6-6.1 Appendix K Models used for the Assessment Cases of US-APWR SBLOCA Analyses *(Only those New Functions in M-RELAP5 described here)*

No.	Appendix-K Models Implemented in M-RELAP5	Category	Assessment Approach	Test Facilities
1	Initial Stored Energy (FINE Code Gap Conductance Model)	1	Provide appropriate input. Steady state temperature distribution and stored energy in the fuel are calculated for the burn-up that yield highest PCT.	None
2	Fission Product Decay (ANS Standard 1971 Decay Heat Model)	2	ANS Standard 1971 is installed. Fission product decay heat shall be 1.2 times the values of infinite operating time in the ANS Standard 1971.	None
3	No Return to Transition Boiling/Nucleate Boiling during Blowdown Phase	2	Coding modification. Return to transition boiling or nucleate boiling is not allowed during the blowdown phase.	None
4	Metal Water Reaction Rate (Baker-Just Model)	2	Coding modification. Baker-Just equation is installed. Influence of the metal/water reaction was calculated. The reaction was assumed non-steam limited and the inside of the cladding reacts after the rupture.	None
5	Cladding Swelling and Rupture (ZIRLO^{TM} Cladding Swelling/Rapture Model)	2	Coding modification. The gap conductance was varied in accordance with changes in gap dimensions and other applicable variables.	None
6	Discharge Model (Moody Critical Flow Model)	2	Sensitivity study was performed. Two-phase discharge rate was calculated using the Moody model with at least three (3) values of discharge coefficient.	None
7	CHF and Post-CHF Heat Transfer Models (Modification to Post-CHF Heat Transfer Logic)	3	Coding modification and assessment were performed. The conservative modifications were validated through benchmarking using the test data obtained from the THTF uncovered heat transfer and reflood tests, and from the ROSA-IV/ LSTF SBLOCA test.	ORNL-THTF ROSA-IV/LSTF

REQUEST 6-7

(Related RAI 6-4)

[

]

RESPONSE

[

]

REQUEST 7-1

Table 7.1.1-1(4/4)
Appendix K requirement #15 ECC water bypass is taken as not applicable to SBLOCA. The bypass flow between upper head and downcomer could potentially provide a path for steam to enter the downcomer during the loop seal clearance period. Confirm that none of the SBLOCA analyses, including sensitivity cases, experience the effect of steam impeding ECC flow.

RESPONSE

As a complete core uncovery does not occur in SBLOCA transients, the vapor generated in the core does not directly escape into the break through the downcomer. Then, the ECC water bypass phenomenon which is typical for LBLOCA transients will not occur in SBLOCA transients.

As the loops are sealed at the cross-over legs during the loop seal clearance period, upper head/downcomer bypass flow path has the potential for relieving vapor generated in the core. The break size spectrum analyses for the cold leg break are performed for US-APWR (Ref.1). The loop seal clearance periods for various break sizes are shown in Figure RAI-7-1.1. The assumed break orientation for these cases is the bottom of the cold leg. ECC water injection start time of the high head safety injection systems and the accumulators are also shown in Figure RAI-7-1.1. Only the high head safety injection system injects ECC water during the loop seal clearance period.
ECC water from the high head safety injection systems is injected into the downcomer in the downward direction between the vessel wall and the barrel wall through the direct vessel injection line shown in Figure RAI-7-1.2. So, even if the steam flow through the bypass line exists, it does not impede ECC flow into the core.
The collapsed liquid level transients in the vessel upper head and the end of the loop seal clearing period for several break sizes are shown together with top of bypass line elevation in Figure RAI-7-1.3. The bypass line is covered by the water during the loop seal clearance period. So, the vapor generated in the core hardly escape to the downcomer through the bypass line.
For these reasons, ECC flow will not be impeded by the steam flow through the upper head/downcomer bypass line for the cold leg break with the break orientation of bottom.

Following sensitivity analyses are also performed for US-APWR (Ref.1).

- Break Orientation (bottom, top and side of cold leg)
- Break Location (cold leg, hot leg, crossover leg, DVI injection line, pressurizer steam phase)
- Noding near break point
- Noding of SG U-tube and crossover leg
- Time Step Size
- No single Failure Assumption
- Offsite Power Available

As the effect of break orientation on the RCS behavior is negligible small, break orientation hardly affects the loop seal clearance period, the ECC water injection start time, and the collapsed liquid level in the vessel upper head. Then, impeding of ECC water by steam flow does not occur in the calculation with any break orientation.
As the loop seal formation will not occur in the cases of hot leg, crossover leg and pressurizer steam phase break, impeding of ECC water by steam flow will not occur. As only ECC water

from the high head safety injection systems is injected during the loop seal clearance period in the DVI injection line break, impeding of ECC water by steam flow does not occur as in the cold leg break.

None of the sensitivity analyses of the noding and time step size experience impeding of ECC water by steam flow, as the sensitivities to these parameters are small.

The sensitivity analyses for no single failure assumption and offsite power available are performed for 7.5 inch and 1.0ft^2 cold leg breaks. The loop seal formation occurs only in 7.5 inch break. ECC water injection will not occur during loop seal clearance period for the case of no single failure assumption, and only ECC water from the high head safety injection systems is injected during the loop seal clearance period for the case of offsite power available. Then, impeding of ECC water by steam flow will not occur in both cases.

References

1. MHI, Small Break LOCA Sensitivity Analyses for US-APWR, MUAP-07025-P (R0), December 2007.

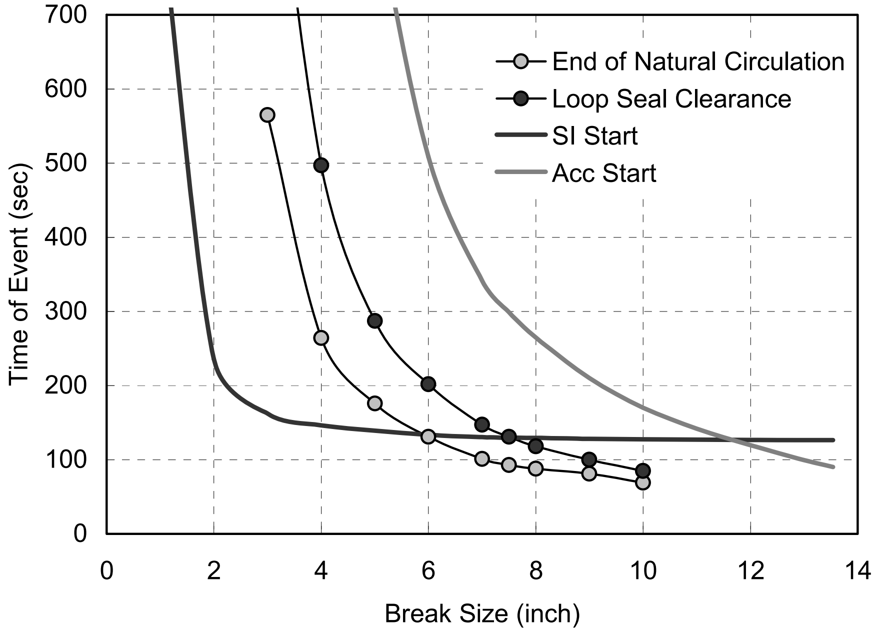

Figure RAI-7-1.1 Loop seal clearance period and SI/Acc injection start time

Figure RAI-7-1.2 ECC water flow from the high head safety injection systems

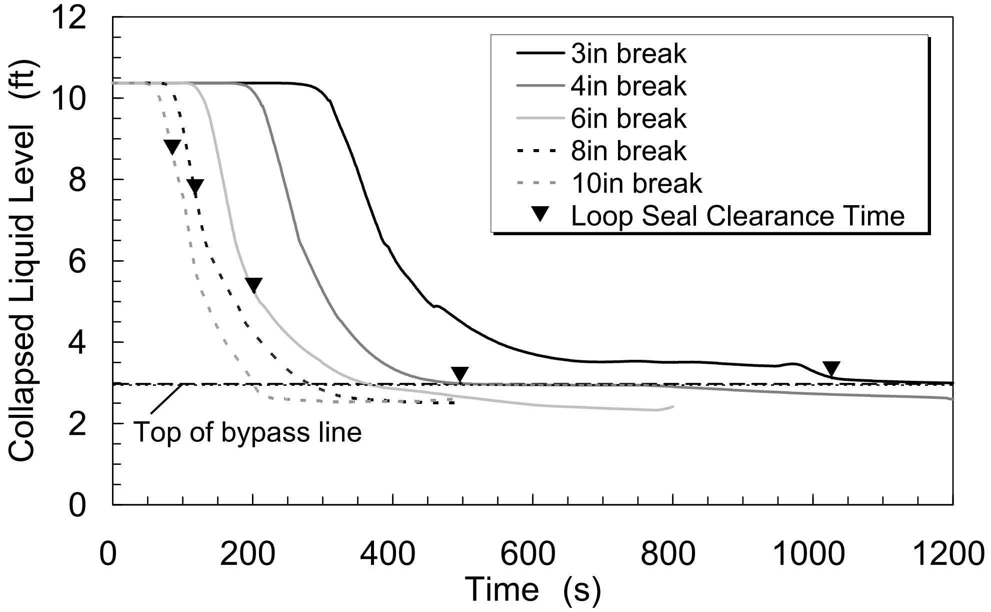

Figure RAI-7-1.3 Collapsed liquid level in the vessel upper head

REQUEST 7-2

Table 7.1.1-1(4/4)
Appendix K requirement #29 refill/reflood heat transfer is taken as not applicable to SBLOCA. However, there could be core uncovery during the loop seal clearance period resulting in cladding superheat. Confirm that all SBLOCA cases do not require refill/reflood heat transfer. If they do require refill/reflood heat transfer then explain why Appendix K requirement #29 is not for SBLOCA.

RESPONSE

Appendix K requirement #29 requires that an applicable FLECHT heat transfer correlation shall be used for reflood rates of one inch per second or higher. And it also requires that when reflood rates are less than one inch per second, heat transfer calculations shall be based on the assumption that cooling is only by steam rather than a FLECHT heat transfer correlation, and shall take into account any flow blockage due to cladding swelling or rupture. The requirement #29 limits the use of a FLECHT heat transfer correlation. As a FLECHT heat transfer correlation is not used in M-RELAP5, this requirement is taken as not applicable to SBLOCA. But, additional form loss coefficients due to flow blockage are applied in M-RELAP5 when a fuel rod ruptures in accordance with the requirement #29.

The reflood heat transfer after the core uncovers is calculated by the heat transfer package incorporated in M-RELAP5, and it is validated by ORNL/THTF high-pressure reflood tests.

REQUEST 7-2

Section 7.1.2
The discussion of gap conductance model is in the form of one equation and one reference to the fuel design code FINE. Provide validation analysis of the gap conductance model as expressed in Equation (7.1.2-1). Provide verification of the implementation of the gap conductance model in M-RELAP5 and demonstrate the integration of the gap conductance model with the rest of the gap heat transfer model in RELAP5-3D, such as thermal radiation across the gap.

RESPONSE

The following gap conductance model considering pellet offset in the fuel-cladding gap is incorporated in RELAP5-3D (Ref.1).

$$h_g = \frac{k_g}{N}\sum_{n=1}^{N}\frac{1}{t_n + 3.2(R_F + R_C) + (g_1 + g_2)} \qquad (1)$$

Where

h_g = conductance through the gas in the fuel-cladding gap
n = number of circumferential segment
N = total number of circumferential segments = 8
k_g = thermal conductivity of gas
t_n = width of fuel-cladding gap at the n-th circumferential segment
$R_{F,}, R_{C,}$ = surface roughness of the fuel and cladding
$g_{1,}, g_{2,}$ = temperature jump distance terms for fuel and cladding

Fuel temperature calculated by FINE is used in SBLOCA analysis as an initial fuel temperature. The gap conductance model incorporated in FINE is given by

(2)

(3)

(4)

Where

h_{gap} = conductance through the gas in the fuel-cladding gap (Btu/hr-ft^2-deg F)
k_{mix} = gas mixture thermal conductivity (Btu/hr-ft-deg F)
gap = diameteral gap (in)
EXO = surface roughness factor

The gap conductance model incorporated in FINE is validated in combination with other models through assessment calculations that compare the code prediction results to fuel temperature measurement data. The results of validation study are reported in the topical report of Mitsubishi Fuel Design Criteria and methodology (Ref.2).

Equation (3) for smaller gap is applied to calculate the fuel temperature for SBLOCA. As the consistent gap conductance model with equation (3) in FINE is required in SBLOCA analysis, the original gap conductance model in RELAP5-3D is transformed into the following concentric gap conductance model.

$$h_g = \frac{k_g}{g + 3.2(R_F + R_C) + (g_1 + g_2)} \qquad (5)$$

Where

g = concentric fuel-cladding gap width

As the temperature jump distance terms in equation (5) are considered in the gas mixture thermal conductivity in equation (3), both equations are equivalent.

The gap conductance is calculated by M-RELAP5 and FINE at equivalent conditions and is compared to verify that the gap conductance model is adequately implemented in M-RELAP5.

Analytical conditions are followings.

Cladding outer diameter: 0.374 in
Cladding thickness: 0.0224 in
Pellet diameter: 0.322 in
Pellet density: 97 %TD
Burn up: 0.0 MWD/T
Radial power distribution in pellet: flat distribution is assumed.
[ ]
Core pressure: 2250 psia

M-RELAP5 noding scheme is shown in Figure RAI-7-3.1. Heat structure HS010 represents a fuel rod, and single volume SV010 represents fluid volume containing the fuel rod. Vapor temperature of time dependent volume TV100 is selected so that the calculated cladding surface temperature agrees with that predicted by FINE. Pressure of time dependent volume TV400 is adjusted to make the SV010 pressure to be 2250psia. Internal pressure calculated by FINE is used in M-RELAP5. The input values for surface roughness of the fuel and cladding for M-RELAP5 are selected so that the effect of surface roughness on gap conductance is same between M-RELAP5 and FINE.

The comparisons of the calculated gap conductance by M-RELAP5 and FINE are shown in Figure RAI-7-3.2. The gap conductance is also calculated by M-RELAP5 using the pellet offset gap conductance model presented in equation (1). The pellet offset gap conductance model gives larger values than FINE. On the other hand, gap conductance with the concentric gap conductance model agrees with the prediction by FINE. However, a small difference remains between the two predictions. Two causes are pointed out. First, the gap conductance by M-RELAP5 includes the additional thermal radiation term across the gap. But, its contribution to the gap conductance is too small at normal conditions to explain the difference as discussed later. Next, as M-RELAP5 uses the same thermal expansion models for cladding and fuel as RELAP5-3D, the applied thermal expansion models for cladding and fuel are different between M-RELAP5 and FINE. These differences affect the predicted gap size by each code. The gap conductance calculated by M-RELAP5 is divided by the ratio of gap size calculated by FINE to gap size calculated by M-RELAP5. The obtained gap conductance agrees well with that by FINE shown in Figure RAI-7-3.3. It is concluded that the concentric gap conductance model consistent with FINE is adequately implemented in M-RELAP5.

In addition to the conductance through the gas in the fuel-cladding gap, the following thermal radiation across the fuel-cladding gap is considered in RELAP5-3D.

$$h_r = \sigma F\left(T_F^2 + T_C^2\right)\left(T_F + T_C\right)$$

$$F = \frac{1}{\left\{\dfrac{1}{\varepsilon_F} + \left(\dfrac{R_F}{R_C}\right)\left[\dfrac{1}{\varepsilon_C} - 1\right]\right\}} \qquad (6)$$

Where

h_r = conductance by thermal radiation across the gap
σ = Stefan-Boltzmann constant
F = view factor
$\varepsilon_F, \varepsilon_C$ = emissivity of fuel and cladding
R_F, R_C = outer radius of fuel and inner radius of cladding
T_F, T_C = temperature of fuel outer surface and temperature of cladding inner surface

M-RELAP5 uses the same thermal radiation term as RELPA5-3D. Radiation gap conductance mainly depends on the gap average temperature, and slightly depends on the ratio of outer fuel radius to inner cladding radius. Radiation gap conductance dependency on the average gap temperature is shown in Figure RAI-7-3.4.

As the gap average temperature is less than 1000 deg F under the normal operating conditions, the radiation gap conductance is less than 10 Btu/ft^2-h-F. It is less than 1% compared with the gap conductance through the gas in the gap, and it can be neglected under the normal operating conditions. However, radiation gap conductance increases as the gap average temperature rises, and the gap conductance through the gas in the gap decreases when the cladding swelling or rapture occurs under LOCA transient. The contribution of radiation gap conductance can not be neglected under LOCA. So, the radiation gap conduction term is implemented in M-RELAP5. Radiation gap conductance is calculated at a SBLOCA simulated condition by M-RELAP5. Calculations are performed using noding scheme shown in Figure RAI-7-3.1 and the same conditions as the previous study except the followings.

Linear power density: 0.0617kW/ft (power at decay heat level)
Core pressure: 1000 psia

Fuel rod temperatures are increased by setting the vapor temperature of time dependent volume TV100. The obtained radiation conductance is shown in Figure RAI-7-3.4. It agrees with the prediction with equation (6). It is concluded that the radiation conductance model across the gap is adequately implemented in M-RELAP5.

References

1. RELAP5-3D CODE MANUAL VOLUME I: CODE STRUCTURE, SYSTEM MODELS, AND SOLUTION METHODS, INEEL-EXT-98-00834, Revision 2.4, June 2005.
2. MHI, Mitsubishi Fuel Design Criteria and Methodology, MUAP-07008-P, May 2007.

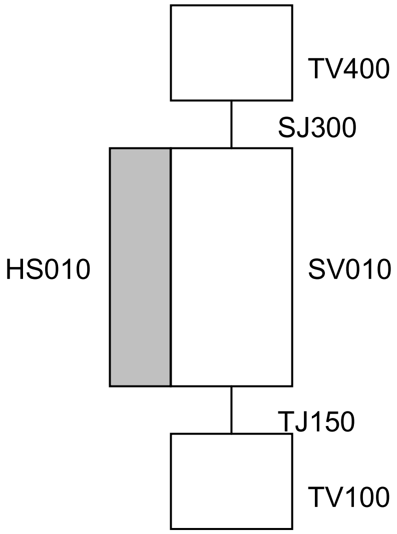
TV400
SJ300
HS010
SV010
TJ150
TV100

Figure RAI-7-3.1 M-RELAP5 noding scheme

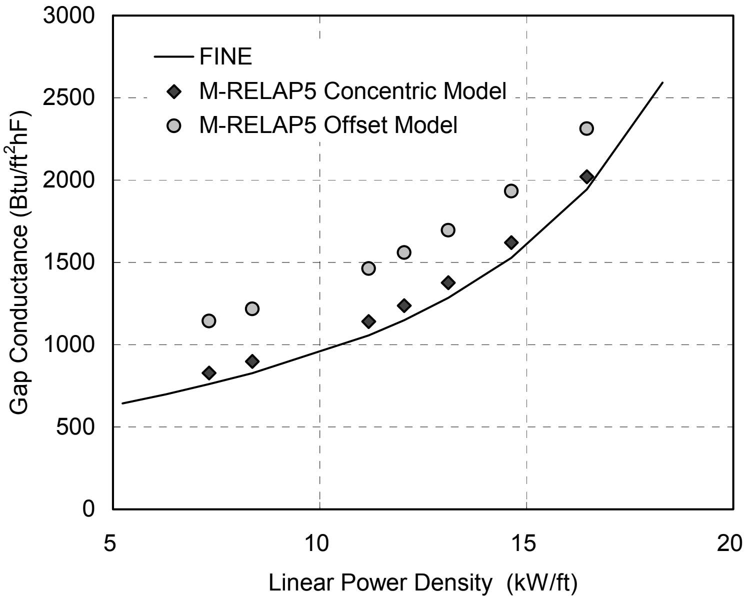

Figure RAI-7-3.2 Comparisons of the gap conductance

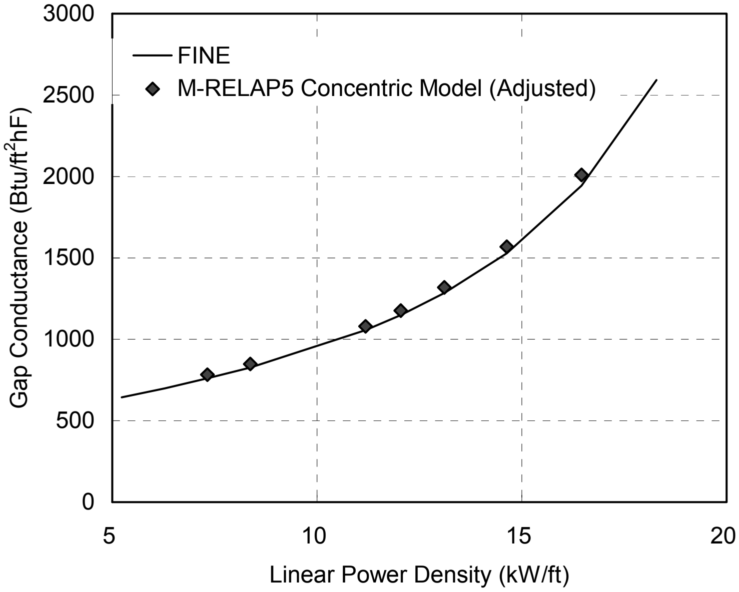

Figure RAI-7-3.3 Comparisons of the gap conductance (gap size is adjusted)

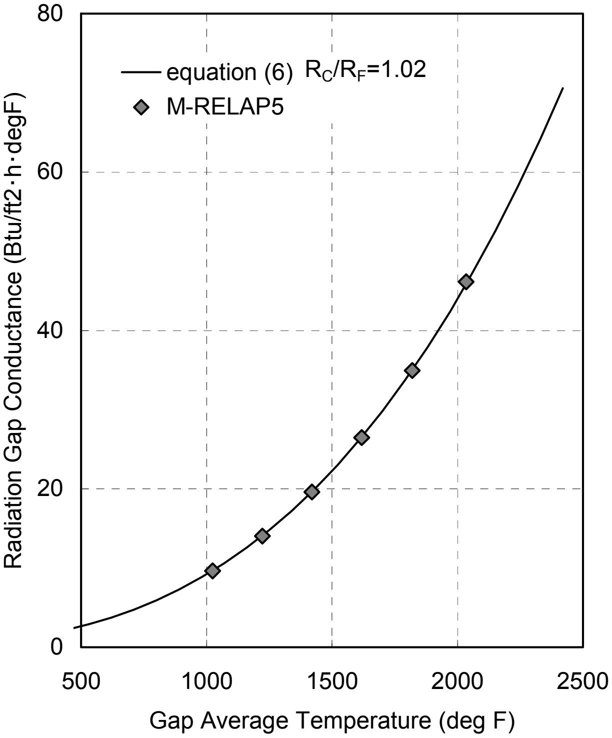

Figure RAI-7-3.4 Radiation gap conductance dependency on gap average temperature

REQUEST 7-4

Section 7.1.3
Provide a reference or fuel cycle calculation to justify the claim that the default values of the ANSI/ANS 5.1-1979 standard are appropriate for the US-APWR and yield the highest decay heat from the actinide series.

RESPONSE

The default values described in the topical report include the yield of ^{239}U produced per a nuclear fission, the released energy from the decay of an actinide nucleus and the decay constant. The released energy from the decay of an actinide nucleus and the decay constant are particular values for each actinide nucleus. These values, therefore, are independent from fuel cycle calculation of the US-APWR and are appropriate for the US-APWR.

On the other hand, the yield of ^{239}U produced per a nuclear fission is dependent on the fuel specifications, especially, the fuel enrichment and the fuel burnup. Figure RAI-7-4.1 shows that the calculation results of the US-APWR based on its expected fuel enrichment were covered by the default value 1.0 in M-RELAP5 over the broad fuel burnup. Therefore, it is conservative to use the default value 1.0.

Figure RAI-7-4.1 Yield of ^{239}U produced per a nuclear fission

REQUEST 7-5

Section 7.1.4.1
Provide verification of the implementation of the Metal Water Reaction Rate Model in M-RELAP5. Confirm that the hydrogen generation rate and the heat generation rate are consistent with the metal/water reaction rate.

RESPONSE

The thickness of the cladding converted to oxide, the metal-water reaction heat release rate, and hydrogen mass generated by the metal-water reaction at an isothermal condition are calculated by M-RELAP5 and are compared with analytical calculation results to verify that the Baker-Just correlation is adequately implemented in M-RELAP5.
The assumed analytical conditions follow.

Fuel rod specification: 17x17 fuel rod (cladding outer diameter is 9.5mm)
Initial oxide thickness: 0.0mm
Oxidation temperature: 1200 deg C constant
Oxidation time: 100sec

M-RELAP5 noding scheme is shown in Figure RAI-7-5.1. Heat structure HS010 represents a fuel rod with 100mm axial length, and single volume SV010 represents fluid volume containing the fuel rod. Vapor temperature of time dependent volume TV100 is set be 1200 deg C and junction vapor flow of time dependent junction TJ150 is set to be 1.0x10^{6}kg/s to maintain the cladding surface temperature at 1200 deg C. Fluid pressure is maintained to be 10MPa by time dependent volume TV400. Fission and decay heat power are neglected and a large rod surface heat transfer coefficient is applied so that the metal-water reaction heat rate can be estimated from the heat transfer rate from cladding to vapor. Cladding swelling and rupture calculations are skipped so that the M-RELAP5 and analytical results can be easily compared.

The Baker-Just correlation is given by

$$W^2 = 33.3\times10^6\, t \exp\left[-\frac{45{,}500}{RT}\right] \qquad (1)$$

Where

W = the amount of zirconium reacted (mg/cm^2)
t = the time（s）
$\boldsymbol{R}$ = the gas constant, 1.987 (cal/mole-K)
T = the temperature (K)

The amount of zirconium reacted can be expressed in terms of the thickness of the cladding reacted for convenience as follows.

$$W = 100\times\rho_{Zr}\delta = 6.5\times10^5\,\delta \qquad (2)$$

Where

ρ_{Zr} = zirconium density, 6500 (kg/m^3)
δ = the thickness of cladding reacted (m)

Substituting equation (2) into equation (1) gives:

$$\delta = \sqrt{33.3\times10^6\, t \exp\left[-\frac{45{,}500}{RT}\right]}\Big/100\rho_{Zr} = \sqrt{33.3\times10^6\, t \exp\left[-\frac{45{,}500}{RT}\right]}\Big/6.5\times10^5 \qquad (3)$$

Equation (3) gives the thickness of cladding reacted at constant temperature.

The amount of reacted zirconium weight per unit length is given by

$$M = \rho_{Zr}\pi\left\{r_0^2 - (r_0 - \delta)^2\right\} = \rho_{Zr}\pi\left\{2r_0\delta - \delta^2\right\} \tag{4}$$

Where

M = the amount of reacted zirconium weight per unit length (kg/m)

r_0 = the cladding outer radius (m)

Differencing equation (4) for the time gives the reacted zirconium weight per unit length and per unit time as follows.

$$\begin{aligned}\frac{dM}{dt} &= 2\rho_{Zr}\pi(r_0 - \delta)\frac{d\delta}{dt} = \rho_{Zr}\pi(r_0 - \delta)\sqrt{33.3\times10^6 \exp\left[\frac{-45{,}500}{RT}\right]\frac{t^{-0.5}}{100\rho_{Zr}}} \\ &= \pi(r_0 - \delta)\sqrt{33.3\times10^6 \exp\left[\frac{-45{,}500}{RT}\right]\frac{t^{-0.5}}{100}}\end{aligned} \tag{5}$$

As reaction heat release incorporated in M-RELAP5 is 5.94 × 10^8 J/(kg･mol), and molecular weight of zirconium is 91.22 kg/(kg･mol), the reaction heat release rate per unit length is given by

$$Q'_{MWR} = \pi(r_0 - \delta)\sqrt{33.3\times10^6 \exp\left[\frac{-45{,}500}{RT}\right]\frac{t^{-0.5}}{100}}\times\frac{5.94\times10^8}{91.22} \tag{6}$$

Where

Q'_{MWR} = the reaction heat release rate per unit length（W/m）

The total hydrogen mass generated by the metal-water reaction is calculated by multiplying the mass of zirconium reacted by the ratio of the four hydrogen atoms to one zirconium atom. Then, the total hydrogen mass generated by the metal-water reaction per unit length is given by

$$M_{H2} = M \times \frac{4.0}{91.22} = \rho_{Zr}\pi\left\{2r_0\delta - \delta^2\right\}\times\frac{4.0}{91.22} \tag{7}$$

Where

M_{H2} = the total hydrogen mass generated by metal-water reaction (kg/m）

The comparisons of the calculated results of the zirconium reacted thickness, the reaction heat release rate and the hydrogen mass generated by M-RELAP5 with the results by equation (3), equation(6) and equation (7) are shown in Table RAI-7-5.1 and Figure RAI-7-5.2, Figure RAI-7-5.3 and Figure RAI-7-5.4. The calculated results by M-RELAP5 agree with the results by the analytical method well. It is concluded that the Baker-Just correlation is adequately implemented in M-RELAP5 and the hydrogen generation rate and the heat generation rate are also adequately calculated.

Table RAI-7-5.1 Comparison between analytical method and M-RELAP5

time	Reacted Zirconium Thickness(m)		Reaction Heat (W/m)		H2 Generation (kg/m)	
(sec)	Equation(3)	M-RELAP5	Equation(6)	M-RELAP5	Equation(7)	M-RELAP5
5	8.36426E-06	8.36433E-06	1054.7	1054.7	7.10889E-05	7.10894E-05
10	1.18289E-05	1.18288E-05	745.27	745.26	1.00498E-04	1.00498E-04
20	1.67285E-05	1.67283E-05	526.44	526.44	1.42052E-04	1.42051E-04
30	2.04882E-05	2.04879E-05	429.49	429.49	1.73909E-04	1.73906E-04
40	2.36577E-05	2.36573E-05	371.70	371.70	2.00746E-04	2.00742E-04
50	2.64501E-05	2.64496E-05	332.27	332.26	2.24374E-04	2.24370E-04
60	2.89747E-05	2.89741E-05	303.15	303.15	2.45724E-04	2.45720E-04
70	3.12962E-05	3.12956E-05	280.53	280.52	2.65348E-04	2.65342E-04
80	3.34571E-05	3.34564E-05	262.29	262.28	2.83604E-04	2.83598E-04
90	3.54866E-05	3.54858E-05	247.18	247.18	3.00743E-04	3.00736E-04
100	3.74061E-05	3.74053E-05	234.40	234.40	3.16946E-04	3.16940E-04

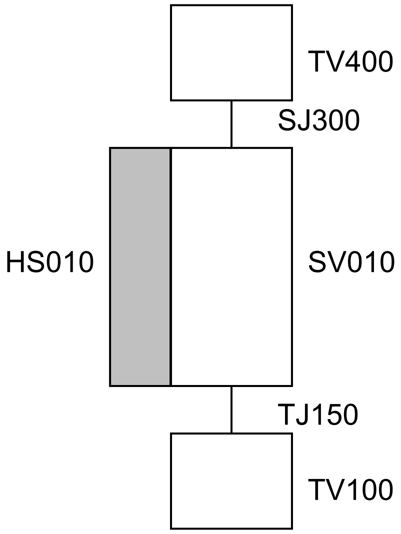
TV400
SJ300
HS010
SV010
TJ150
TV100

Figure RAI-7-5.1 M-RELAP5 noding scheme

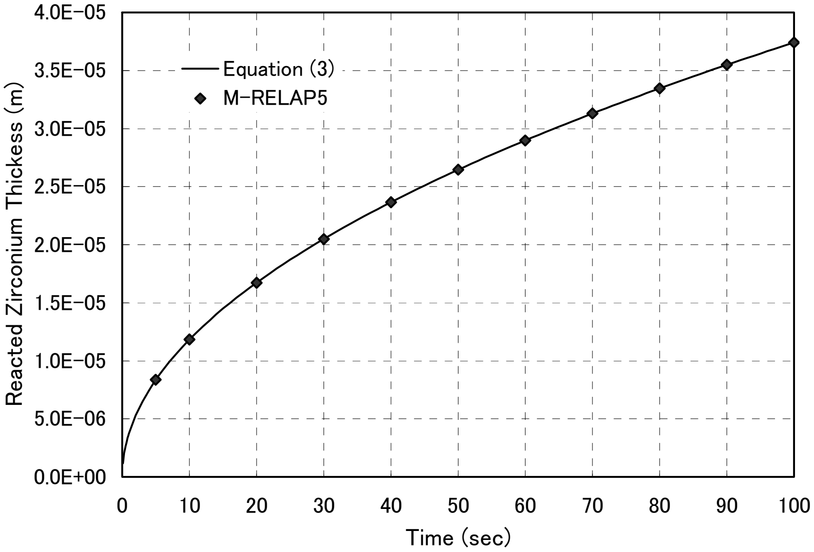

Figure RAI-7-5.2 Comparison of the thickness of zircaloy reacted

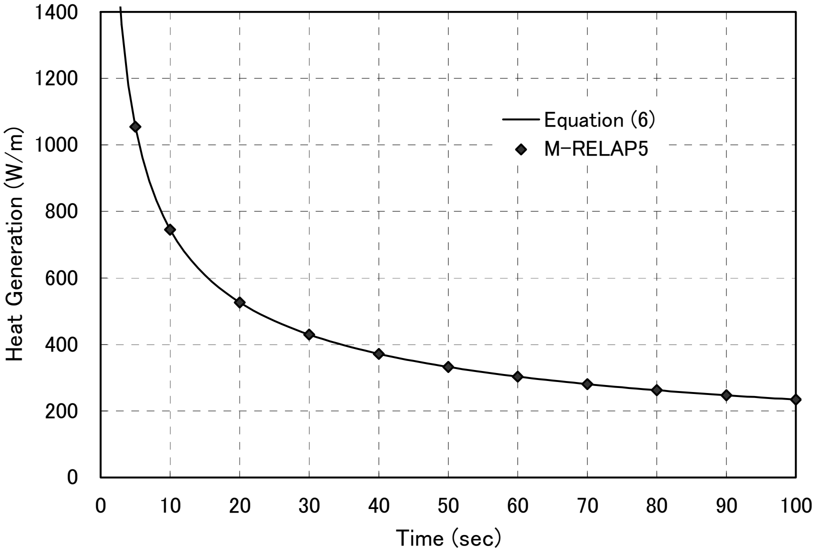

Figure RAI-7-5.3 Comparison of the reaction heat release rate

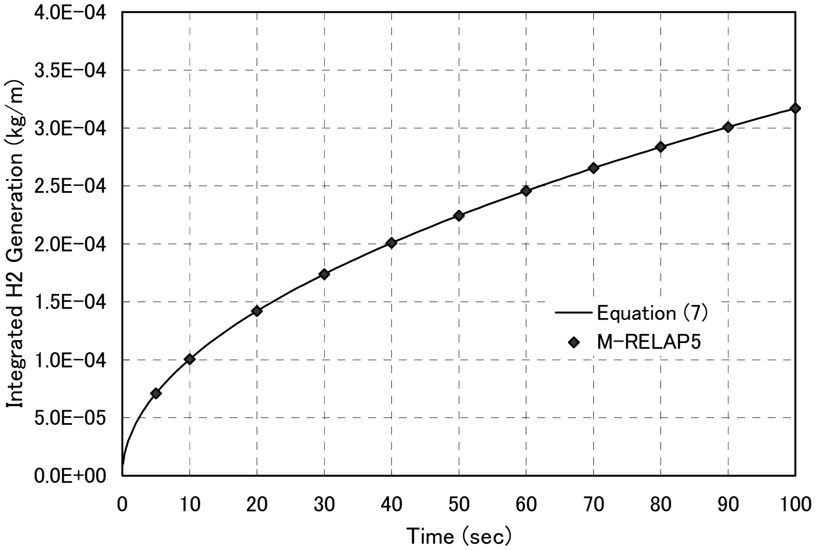

Figure RAI-7-5.4 Comparison of the hydrogen mass generated

REQUEST 7-6

Section 7.1.4.2
Verify the correctness of the exponential term in Equation (7.1.4-8). It appears a negative sign is missing.

RESPONSE

The Equation (7.1.4-8) in the topical report is shown here again. There is certainly a negative sign in the exponent term.

$$dr_n = \left[\left(d\tilde{r}_{n-1} \right)^2 + K \Delta t e^{-\frac{A}{RT}} \right]^{1/2} \qquad (7.1.4\text{-}8)$$

REQUEST 7-8

[

]

RESPONSE

[

]

[

]

REQUEST 7-9

Section 7.1.6
It appears with non-condensable quality □□□□ the two-phase critical flow will be calculated by using the extended Henry-Fauske model instead of the Moody model. Explain this switch in two-phase critical flow model. The operation of the advanced accumulator may introduce non-condensable to the system. Did the SBLOCA analysis ever reach a state that required the use of the extended Henry-Fauske model?

RESPONSE

The pressure of the advanced accumulator when nitrogen gas begins to flow out is around **[ ]** psia. In the analysis of core-cooling performance during the course of small-break LOCA's periods, the primary system pressure is considerably higher than the nitrogen flow-out pressure, even for the maximum break size case, as shown in Figure RAI-7-9.1. Therefore, small-break-LOCA analysis for the US-APWR does not result in any state that requires the use of the extended Henry-Fauske model.

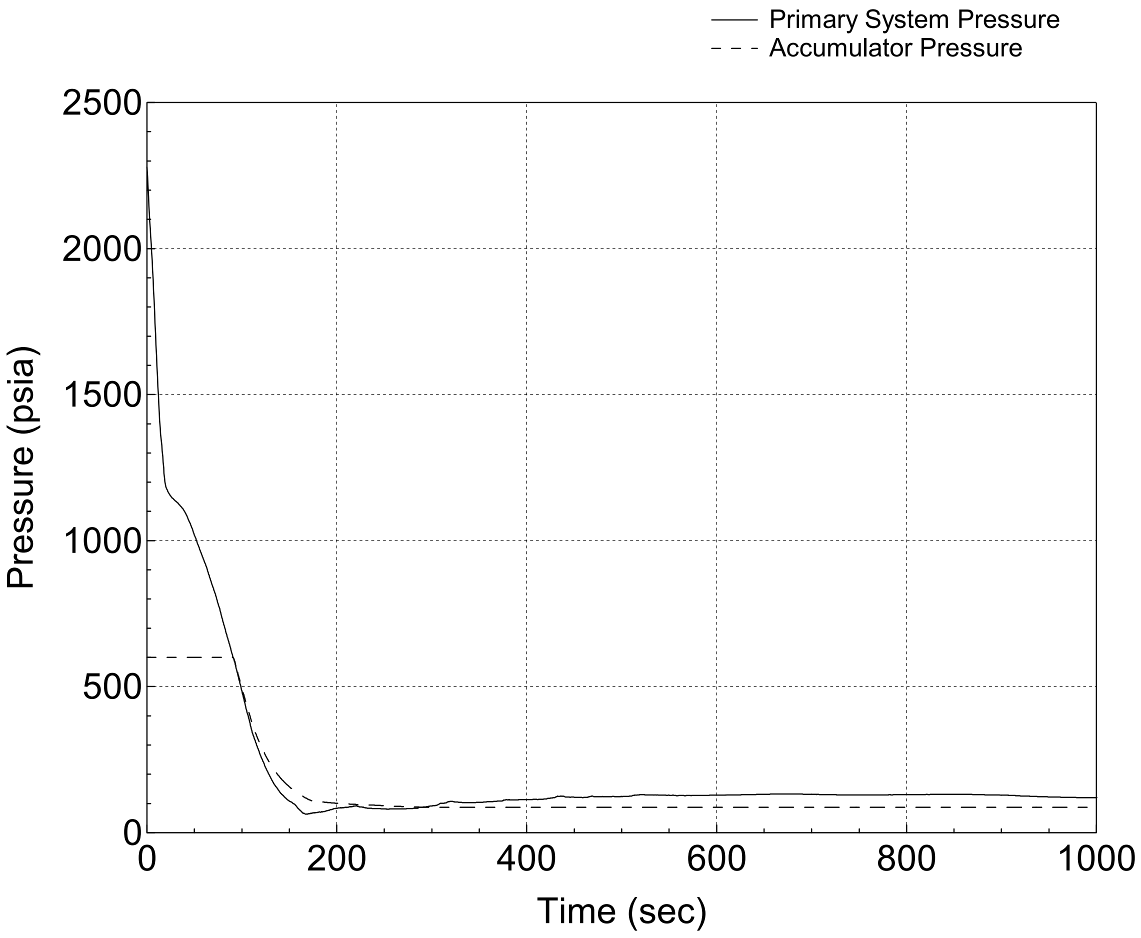

Figure RAI-7-9.1 Primary System and Accumulator Pressure for 1ft^2 Cold-Leg Break

REQUEST 7-10

Section 7.1.7.2
When the AECL-UO look-up table is used to calculate the CHF, M-RELAP5 has a special logic that will bypass the use of the bundle factor multiplier (numerically less than unity) when certain condition is met. The discussion in this section does not clearly define the technical basis for this logic. Provide the technical analysis and benchmark that form the basis for this logic of bypassing the bundle factor.

RESPONSE

Predicted CHF with and without the bundle factor are shown in Figure RAI-7-10.1 and Figure RAI-7-10.2. DNB occurs early in the transient when the bundle factor is applied for both cases of 7.5 inch break and 1.0ft^2 break, because the bundle factor extremely reduces CHF. However, the bundle factor is based on a limited amount of data that is not specified in the original paper (Ref.1). The approach described below is used to avoid extremely conservative calculations and confirm that DNB does not occur early in the transient.

The bundle factor accounts for the effect of the geometry difference between a tube and a rod bundle, the effect of an unheated wall and the effect of the enthalpy distribution in the bundle due to the rod power distribution (Ref.2). Each effect related to the bundle factor is evaluated below. Finally, the possibilities of DNB occurrence early in the transient are estimated for the US-APWR SBLOCA transients.

Applicability of the look-up table to the bundle geometry (typical cell)
Core pressure is from 12 to 14MPa, and mass velocity is from 1500 to 2500 kg/m^{2}s during the approach to DNB in the early stage of the US-APWR SBLOCA transients. Comparison of CHF calculated by the WRB-2 correlation (Ref.3), which is developed for the PWR fuel assembly, and the 1986 CHF look-up table without the rod bundle factor for these conditions is shown in Figure RAI-7-10.3. The geometry parameters of the typical cell which is surrounded by four fuel rods for the US-APWR fuel assembly are applied to the CHF calculation by the WRB-2 correlation. And, the hydraulic diameter of the fuel assembly is applied to obtain CHF using the look-up table in the same way as the plant analysis with M-RELAP5. The CHF calculated by WRB-2 for the typical cell is larger than that obtained from the look-up table above the specific quality which depends on the core pressure and the mass velocity. The look-up table can be conservatively applied above this specific quality to predict CHF of the typical cell without the bundle factor.

Applicability of the look-up table to the flow channel with unheated wall (thimble cell)
CHF is also calculated by the WRB-2 correlation for the subchannel with unheated wall of control rod guide thimble using the geometry parameters of the thimble cell for the US-APWR fuel assembly. Ten percent less mass velocity than that of the assembly average is used to account for the difference of the hydraulic diameter between the thimble cell and fuel assembly. Comparison of the calculated CHF with the CHF obtained from the look-up table is shown in Figure RAI-7-10.4. The CHF calculated by WRB-2 is larger than that obtained from the look-up table above the specific quality which depends on the core pressure and the mass velocity. The look-up table can be also conservatively applied above this specific quality to predict CHF of the thimble cell without the bundle factor.

Evaluation of the effect of the enthalpy distribution in the fuel assembly on CHF

The rod power distribution in the fuel assembly causes the enthalpy distribution in the fuel assembly. The subchannel with the highest enthalpy usually reaches DNB before a subchannel at cross-section average conditions. MHI judges that the main purpose of the bundle factor is to account for the effect of the enthalpy distribution in the fuel assembly on CHF. Extremely conservative calculations were performed to justify not using the bundle factor. The hot rod power was applied to the entire hot assembly in the M-RELAP5 calculations to conservatively account for the effect of the enthalpy distribution in the fuel assembly. Results of the bounding analyses for 7.5 inch break and 1.0 ft^2 break are shown in Figure RAI-7-10.5 and Figure RAI-7-10.6, respectively. CHF obtained from the look-up table without the bundle factor is greater than the actual heat flux.

The coolant conditions from the boundary calculations at the time when the DNB margin is least are shown in Table RAI-7-10.1. The CHF obtained from the look-up table and CHF calculated with WRB-2 at these conditions which are consistent with Figure RAI-7-10.3 and Figure RAI-7-10.4 are also shown in Table RAI-7-10.1. CHF obtained from the look-up table is less than that calculated by the WRB-2 for the typical cell and the thimble cell for both break cases. Therefore, the look-up table without the bundle factor can be conservatively applied to judge whether DNB occurs or not. As the CHF obtained from the look-up table is greater than the actual heat flux early in the transient for both cases as shown in Figure RAI-7-10.5 and Figure RAI-7-10.6, it is concluded that DNB does not occur early in the transient and the analyses bypassing the bundle factor early in the transient are adequately conservative.

References

1. D. C. Groenveld, et al., 1986 AECL-UO Critical Heat Flux Lookup Table, Heat Transfer Engineering, Vol.7, 1-2, 1986.
2. D. C. Groeneveld and C. W. Shoek, A Comprehensive Examination of Heat Transfer Correlations Suitable for Reactor Safety Analysis, in: Multiphase Science and Technology, vol. 2, Hemiphere Publ. Co., 1986
3. MHI, Thermal Design Methodology, MUAP-07009-P, May 2007.

Table RAI-7-10.1 Comparison of CHF for bounding analysis

		7.5inch	1.0ft2
Coolant Conditions at minimum DNB margin	Pressure (MPa)	13.6	13.2
	Mass Velocity (kg/m^{2}s)	2170	1730
	Quality	0.14	0.17
CHF (MW/m^2)	look-up table without bundle factor	1.44	1.39
	WRB-2 (Typical cell)		
	WRB-2 (Thimble cell)		

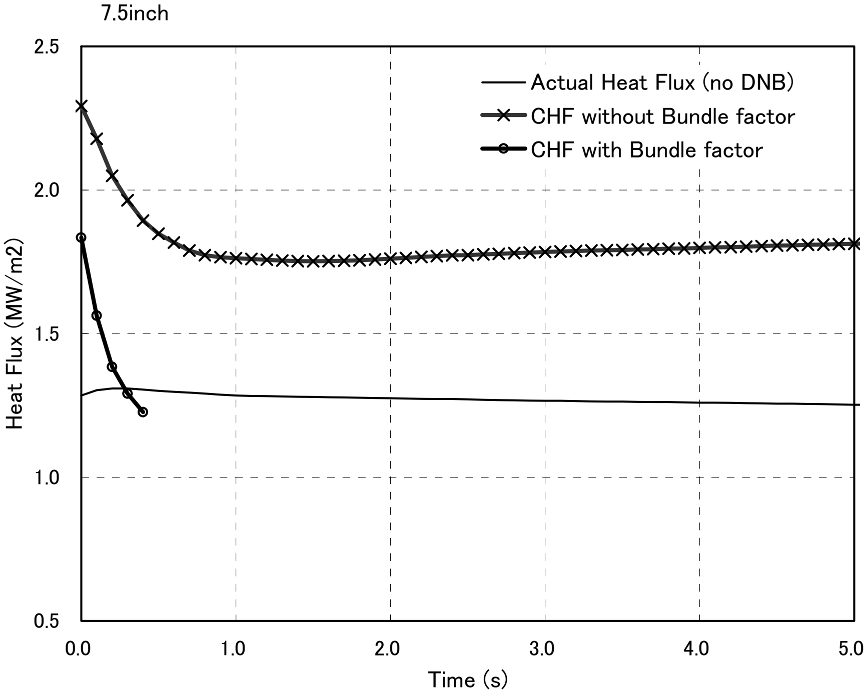

Figure RAI-7-10.1 CHF transient with and without Bundle Factor - 7.5inch break -

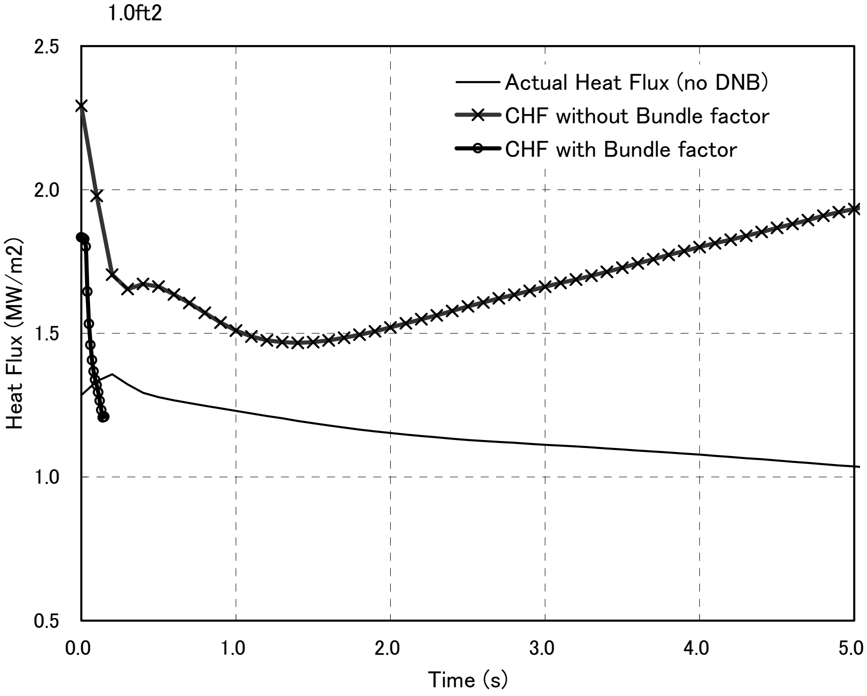

Figure RAI-7-10.2 CHF transient with and without Bundle Factor - 1.0ft^2 break -

Figure RAI-7-10.3 Comparison of look-up Table CHF with WRB-2 - Typical Cell -

Figure RAI-7-10.4 Comparison of look-up Table CHF with WRB-2 - Thimble Cell -

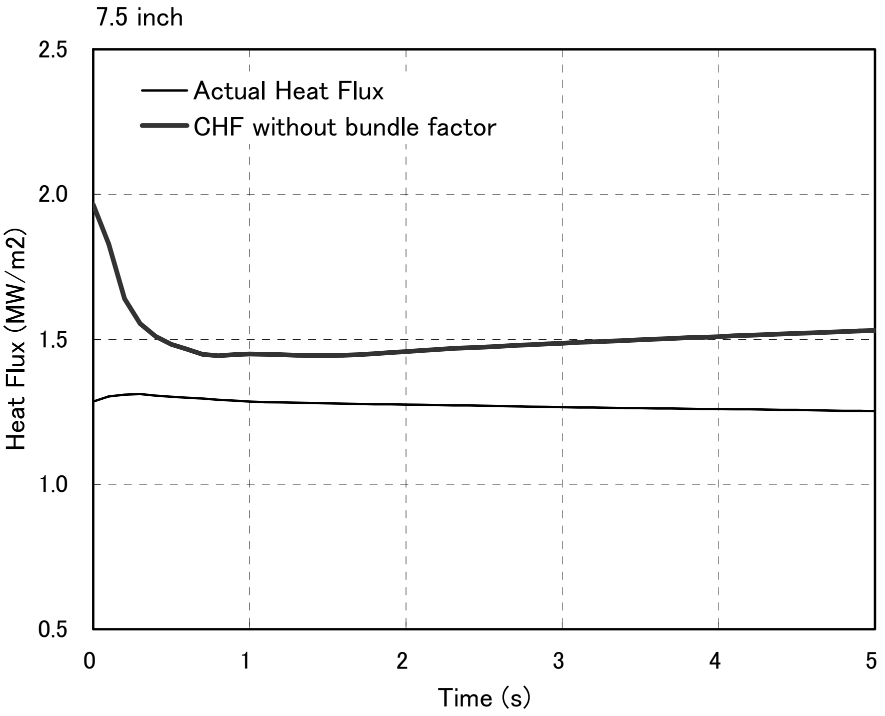

Figure RAI-7-10.5 CHF of bounding analysis - 7.5inch break –

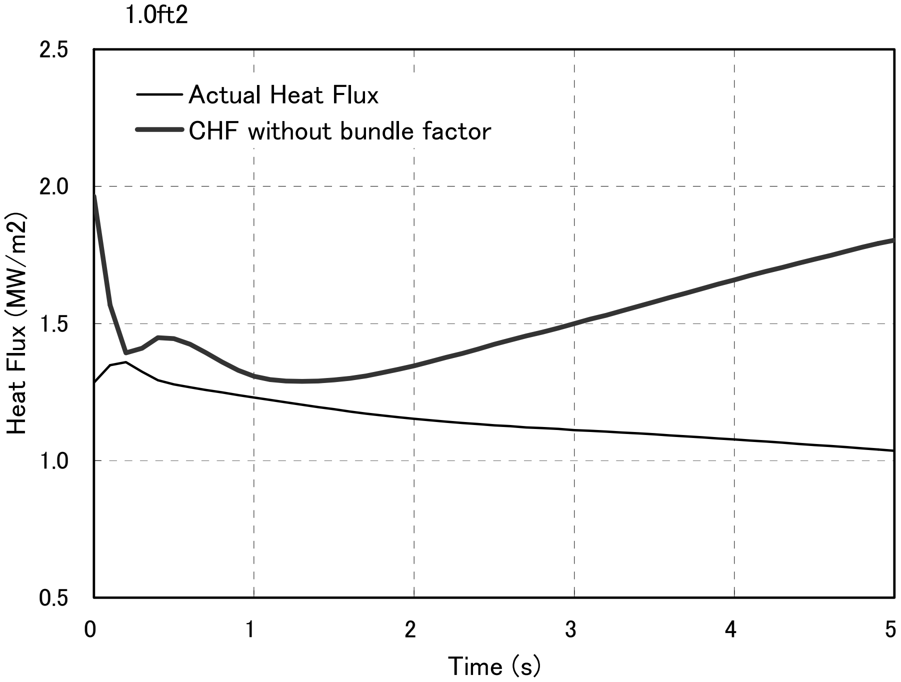

Figure RAI-7-10.6 CHF of bounding analysis - 1.0ft^2 break -

REQUEST 7-11

Section 7.1.7.2
The AECL look-up table for CHF has been under continuing improvement. The 1986 version implemented in M-RELAP5 is an older version, the latest being the 2006 version. Explain why in lieu of more recent development the 1986 version of the AECL look-up table still remains relevant or at least conservative.

RESPONSE

The validation of the AECL-UO CHF look-up table is described in the code manual (Ref.1). The look-up table is also validated using the ORNL/THTF uncovered-bundle heat transfer tests as shown in the topical report.

CHF occurrence might be expected in the early stage of the transient before the reactor trip and in the loop seal clearance or boil-off periods when the core uncovers in the SBLOCA transients. The differences of the CHF predicted by the 1986 version (Ref.2) and the 2006 version (Ref.3) and its effects on the SBLOCA calculation results are discussed for the early stage of the transient and the core uncovery period, respectively.

Values in the CHF table and the exponent n of the diameter correction factor $(D/8)^n$ differ between the 1986 version and the 2006 version. D is the tube diameter in millimeters. The exponent n is -1/3 for the 1986 version, and is -1/2 for the 2006 version. The 2006 version gives about 5 percent smaller CHF than the 1986 version due to the difference of the exponent n for the US-APWR assembly geometry.

Representative core pressure is from 12 to 14MPa and representative mass velosity is from 1500 to 2500 kg/m^{2}s in the early stage of the transients before the reactor trip when CHF occurrence might be expected. CHF values for the diameter of 8mm obtained from the 1986 version and the 2006 version are shown in Figure RAI-7-11.1 and Figure RAI-7-11.2. CHF values are almost the same below the quality of 0.2. The quality where CHF is expected is less than 0.2 in the early stage of the transients. Therefore, the 2006 version gives 5 percent less CHF than the 1986 version considering the difference of the diameter correction factor. As it is considered that the margin to DNB is greater than 5 percent in the early stage of the transient, DNB would not occur before the reactor trip even if the 2006 version is applied, and the calculation results would not be affected.

In the US-APWR SBLOCA analysis, CHF occurs during the loop seal clearance period for the 7.5 inch break and during the boil off period for the1.0 ft^2 break. Fluid conditions around CHF occurrence at the PCT location are shown in Figure RAI-7-11.3 and Figure RAI-7-11.4, respectively. CHF occurs at low flow rate conditions in the upward direction. CHF occurs at a pressure of about 9MPa and a mass velocity of below 20kg/m^{2}s for the 7.5 inch break. CHF occurs at a pressure of about 3MPa and a mass velocity of about 20kg/m^{2}s for the 1.0ft^2 break. CHF values of the 1986 version and the 2006 version are compared for these conditions.
In the 1986 version, CHF for low flow conditions is calculated using CHF value at the pool boiling condition (mass velocity is 0.0 and the quality is 0.0) and the vertical flow factor K_7 which is shown as follows.

$$q''_{CHF} = q''_{table}\left\{P^*, G = 0.0, Xe = 0.0\right\} \times k_7 \qquad G^* < 10$$

$$q''_{CHF} = q''_{table}\left\{P^*, G = 0.0, Xe = 0.0\right\} \times k_7 \times \frac{100 - G^*}{90} + q''_{table}\left\{P^*, G = 100, Xe^*\right\} \times \frac{G^* - 10}{90} \qquad 10 < G^* < 100$$

$$q''_{CHF} = q''_{table}\left\{P^*, G^*, Xe^*\right\} \qquad 100 < G^*$$

$$k_7 = 1 - \alpha \qquad \alpha < 0.8$$

$$k_7 = (1-\alpha)\frac{0.8 + 0.2\rho_f/\rho_g}{\alpha + (1-\alpha)\rho_f/\rho_g} \qquad \alpha > 0.8$$

Where

q''_{CHF} = CHF at $P = P^*, G = G^*$ and $Xe = Xe^*$ without any correction factor except K_7
q''_{table} = CHF in the look-up table for diameter of 8mm
P = Pressure (kPa)
G = Mass velocity (kg/m^{2}s)
Xe = equilibrium quality
α = void fraction

CHF values at the mass velocity of 0.0 and the quality of 0.0 of the 1986 version are shown in Figure RAI-7-11.5 together with CHF values calculated with the Zuber correlation for the pool boiling. These values are in agreement with each other. CHF values at the mass velocity of 0.0 and the quality of 0.0 of the 2006 version are also shown in Figure RAI-7-11.5. The values of the 2006 version are considerably smaller than the values of the 1986 version or values calculated with the Zuber correlation even though the 2006 paper says that the Zuber correlation is used. The reason for this difference is not described and also the vertical factor is not included in the original paper of the 2006 version (Ref.3). Therefore, CHF values at low flow conditions for the 2006 version are decided to be obtained directly from the look-up table by interpolation rather than using the CHF value at the pool boiling condition and the vertical flow factor K_7. As the flow pattern is considered to be pool boiling rather than flow boiling at low flow conditions, the static quality is used to obtain CHF values from the look-up table instead of the equilibrium or flow quality.

CHF values for the low flow conditions obtained from the 1986 version and the 2006 version are shown in Figure RAI-7-11.6 and Figure RAI-7-11.7. These CHF values already include the diameter correction factor for the US-APWR fuel assembly. The 1986 version gives equal to or less CHF than the 2006 version at the quality conditions where CHF is expected to occur. Therefore, the 1986 version of the AECL look-up table is more conservative during the loop seal clearance and the boil off periods in the US-APWR SBLOCA analyses.

References

1. RELAP5-3D CODE MANUAL VOLUME IV: MODELS AND CORRELATIONS, INEEL-EXT-98-00834, Revision 2.4, June 2005.
2. D. C. Groenveld, et al., 1986 AECL-UO Critical Heat Flux Lookup Table, Heat Transfer Engineering, Vol.7, 1-2, 1986.
3. D. C. Groenveld, et al., The 2006 CHF look-up table, Nuclear Engineering and Design, Vol.237, 2007.

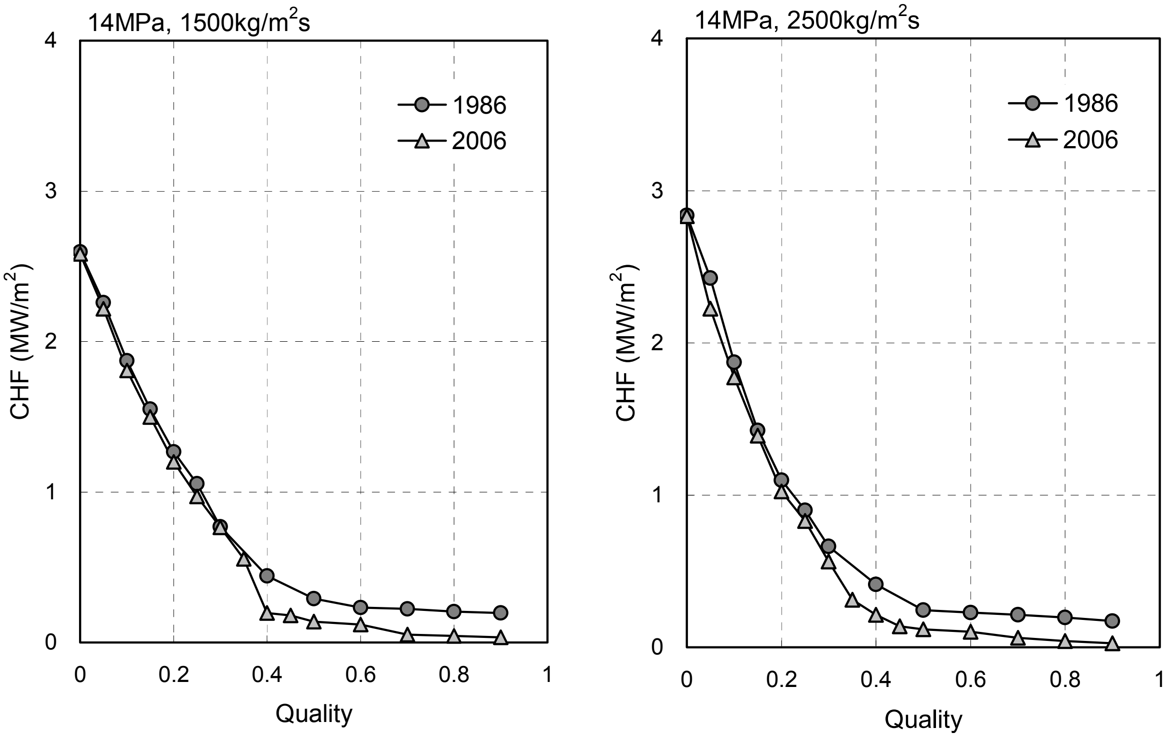

Figure RAI-7-11.1 Comparison of CHF lookup table between 1986 and 2006 (14MPa)

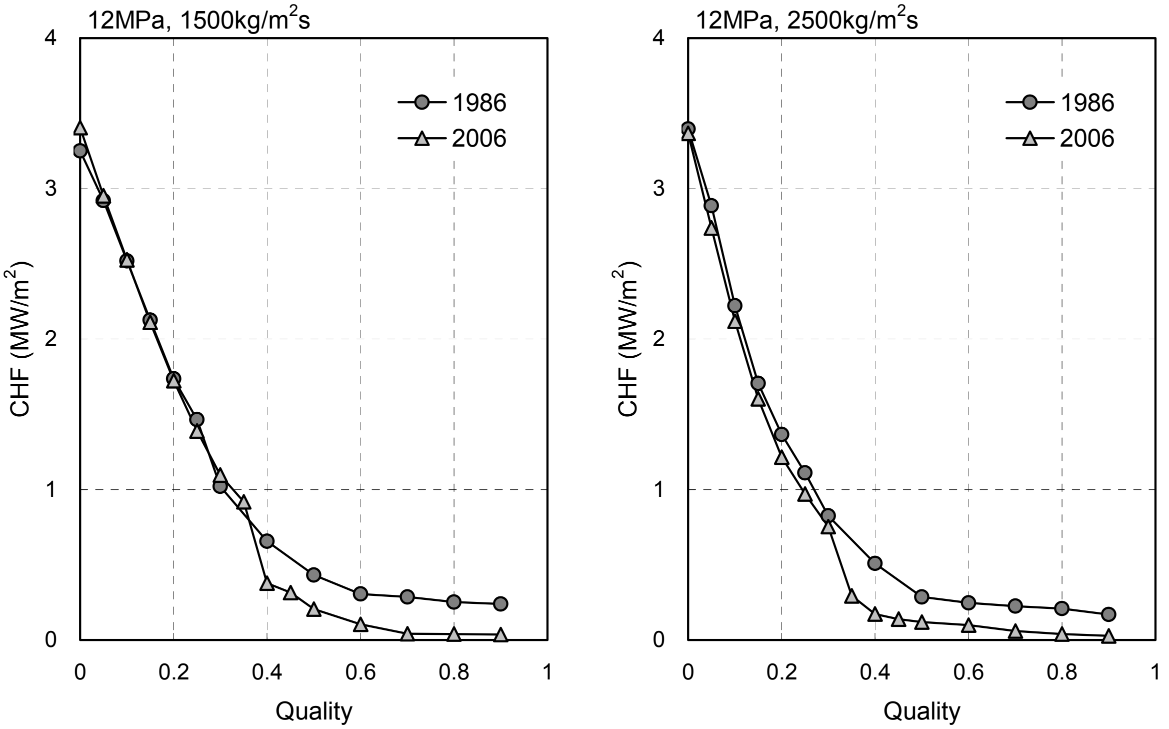

Figure RAI-7-11.2 Comparison of CHF lookup table between 1986 and 2006 (12MPa)

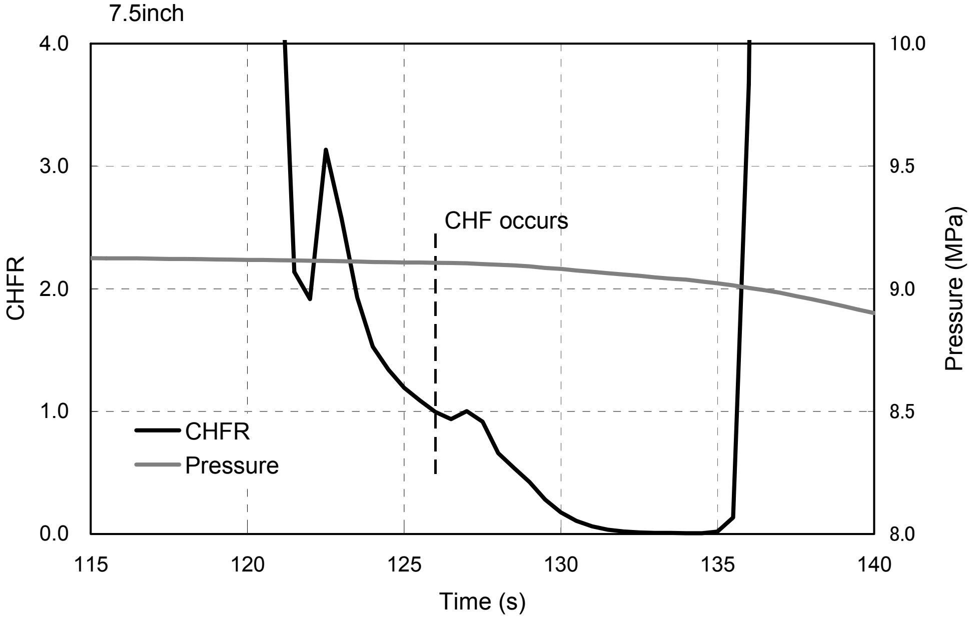

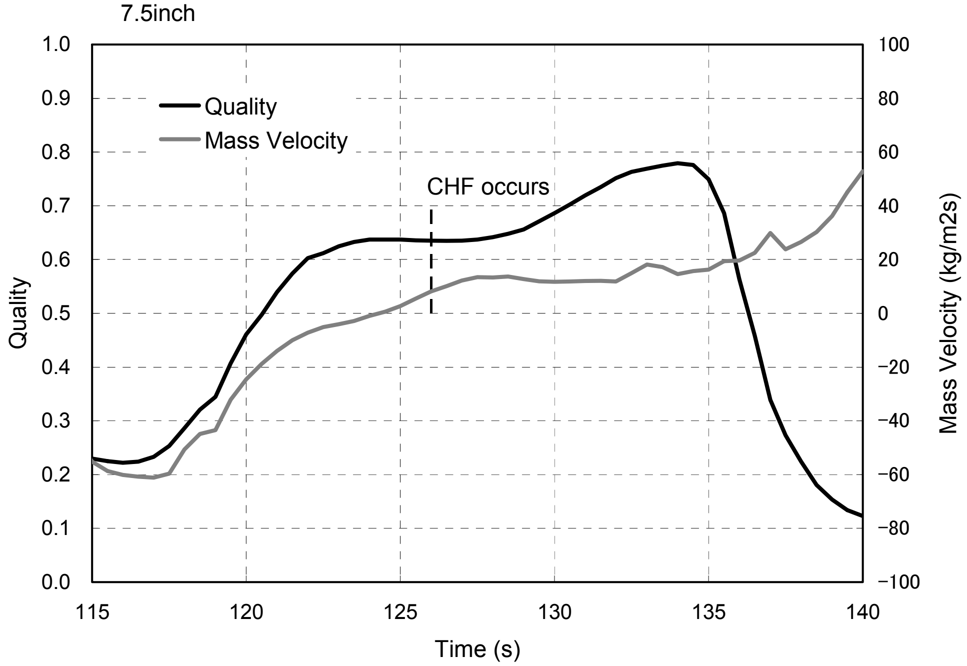

Figure RAI-7-11.3 Fluid Conditions at CHF occurrence -7.5 inch break-

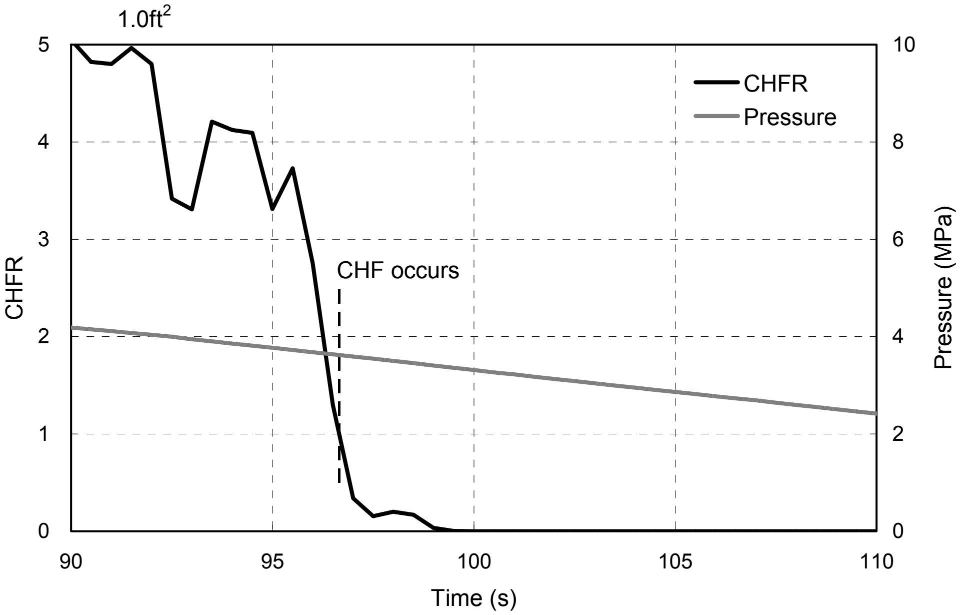

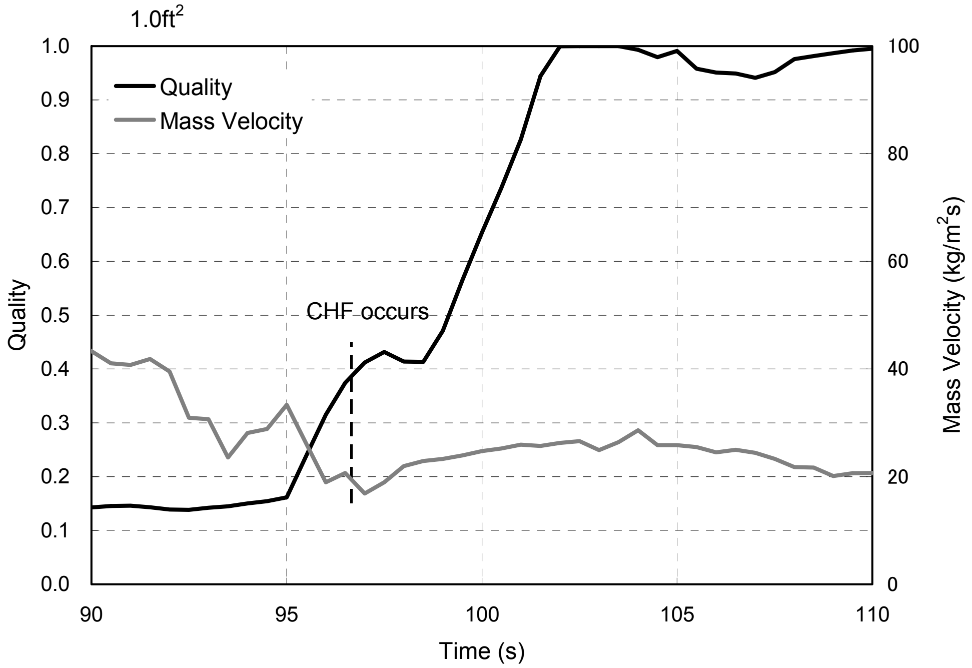

Figure RAI-7-11.4 Fluid Conditions at CHF occurrence -1.0ft^2 break-

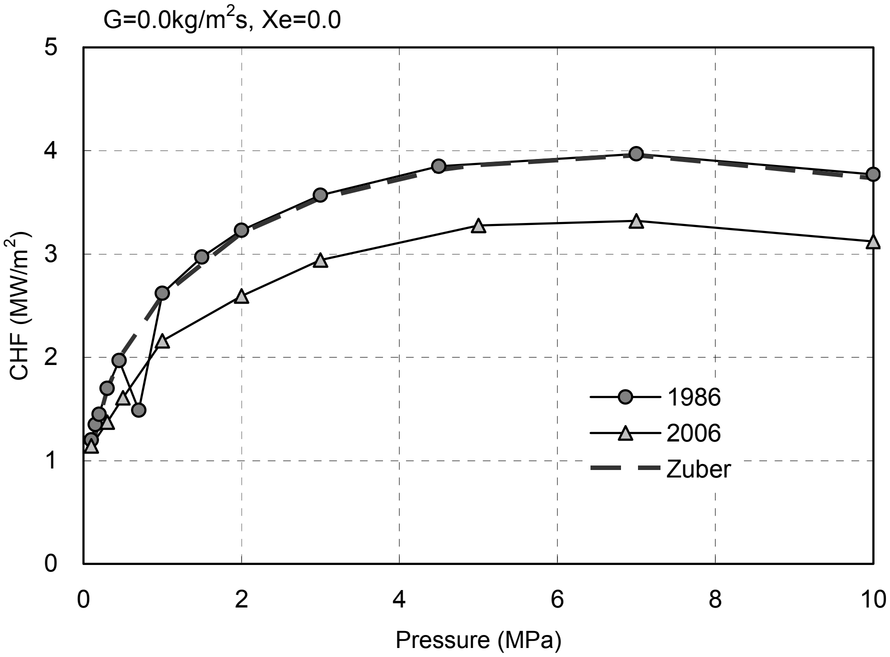

Figure RAI-7-11.5 Lookup Table CHF at zero flow and equilibrium quality of 0.0

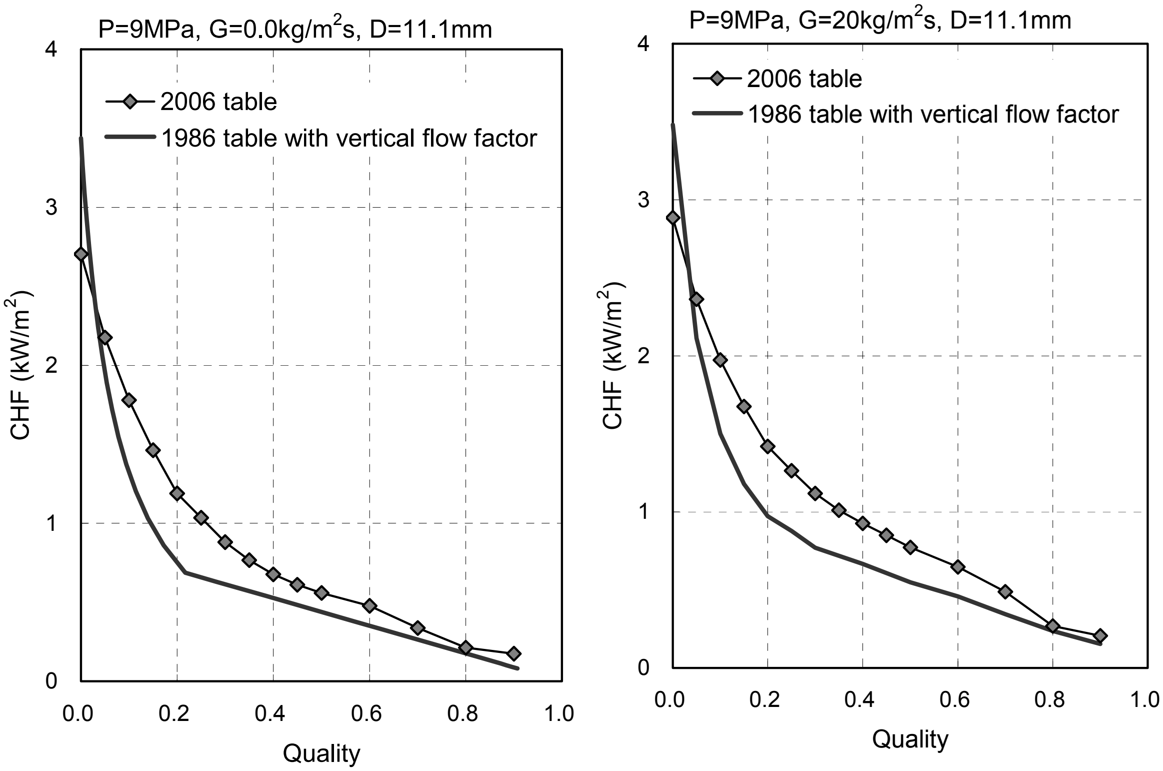

Figure RAI-7-11.6 Comparison of CHF under low flow conditions (9MPa)

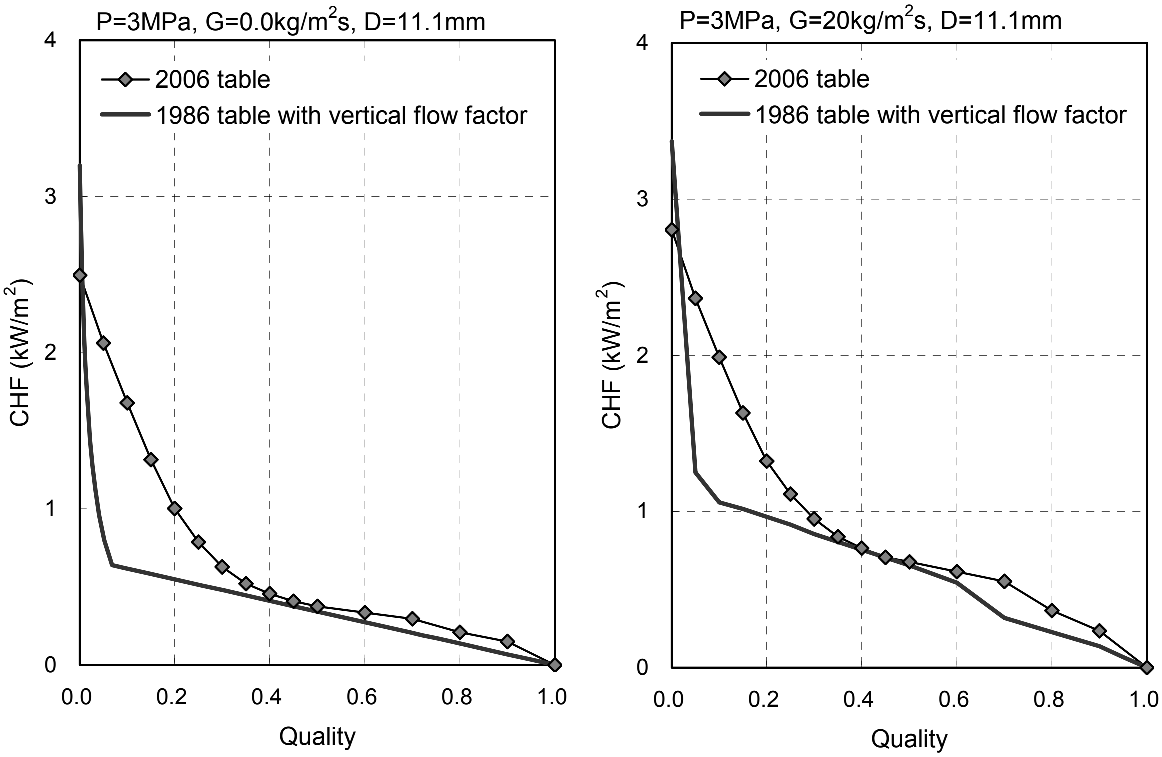

Figure RAI-7-11.7 Comparison of CHF under low flow conditions (3MPa)

REQUEST 7-12

Section 7.1.7.6
The logic to prevent return to nuclear boiling and transition boiling is only necessary (per Appendix K) during the blowdown phase of a LOCA. Provide the criteria used to define the blowdown phase when the prevention logic is applicable.

RESPONSE

SBLOCA transients are generally divided into five periods: blowdown, natural circulation, loop seal clearance, boil-off and core recovery. The boundaries of these periods are described in the response to REQUEST 4-1. The blowdown period starts from the initiation of the break. It ends when the primary system pressure has decreased to nearly equal the secondary system pressure. The blowdown period is generally followed by the natural circulation and loop seal clearance periods during SBLOCA transients.

Even if CHF or excess cladding over-heating occurs in the early stage of the blowdown period, the return to nucleate boiling or the return to transition boiling can be expected soon after the reactor trip because the rod surface heat flux greatly reduces and the sufficient coolant exist in the core. However, these rewetting phenomena are not validated by any experimental data. Therefore, the prevention logic of the Appendix K requirement is conservatively applied during over the blowdown period in the SBLOCA analysis.

Return to nucleate boiling after CHF or return to transition boiling after excess cladding over-heating during loop seal clearance or core recovery periods due to the core mixture level recovery is validated by ORNL/THTF high pressure reflood tests and the ROSA-IV/LSTF test. Therefore, the prevention logic is not necessary for these periods.

[

]

REQUEST 7-13
(Related RAI 7-1)

Does the M-RELAP5 model of the US-APWR include a bypass flow path between the upper head and the downcomer that could potentially allow steam to leak from the core region? If this bypass flow path is present in the model evaluate its effect on the progression of the SBLOCA and the potential for the bypassed steam to sweep some of the ECC water out the break.

RESPONSE

The bypass flow path between the upper head and the downcomer is considered in the US-APWR SBLOCA analyses. This flow path is modeled by **[ ]** as shown in **Figure RAI-7-13.1**.

As the loops are sealed at the cross-over legs during the loop seal clearance period, the bypass flow path between the upper head and the downcomer has the potential for relieving vapor generated in the core. If the vapor is relieved through this bypass flow path, the pressure above the core is reduced and then the core liquid level depression is reduced. The reduction of the liquid level depression lowers the cladding temperature when the core is uncovered. In this way, there is a possibility that the bypass flow path affects the PCT during the loop seal clearance period.

However, a large amount of liquid still remains in the upper head, and the bypass flow path is covered by the liquid during the loop seal clearance period for the break sizes in which the core is uncovered. Then, there is essentially no vapor relief through the bypass flow path during the loop seal clearance period, and the PCT is hardly affected by the bypass flow path. The collapsed liquid level transients in the upper head are shown in Figure RAI-7-1.3 of the response to RAI 7-1 (Ref. 1).

When the liquid level in the upper head is lower than the top of the spray nozzles, the vapor generated in the core flows directly into the upper downcomer and from there towards the broken cold leg. As ECC water from the high head safety injection systems is injected into the downcomer in the downward direction below the cold legs by the flow guide, the vapor flow from the spray nozzles does not impede this ECC water flow into the core. For the larger break sizes, the accumulator injects ECC water when the primary pressure decreases. The vapor from the intact steam generator sweeps part of this ECC water out the break. There remains a possibility that the vapor from the spray nozzles also sweeps part of the ECC water out the break. The vapor mass flow at the outlet of the intact reactor coolant pumps and at the spray nozzles for the 1.0ft^2 cold break is shown in **Figure RAI-7-13.2.** As the vapor flow from the spray nozzles is negligible compared with the vapor flow from the intact loop, its effect on the ECC water is considered to be small.

The bypass flow path between the upper head and the downcomer is considered in the US-APWR SBLOCA analyses, but its effect on the PCT or on the sweep of ECC water out the break is considered to be small.

References:

1. Mitsubishi Heavy Industry, Ltd., MHI’s Partial Responses to NRC’s Requests for Additional Information on Topical Report MUAP-07013-P (R0) “Small Break LOCA Methodology for US-APWR”, UAP-HF-09002, January 16, 2009.

Figure RAI-7-13.1 Nodalization Scheme of Reactor Vessel

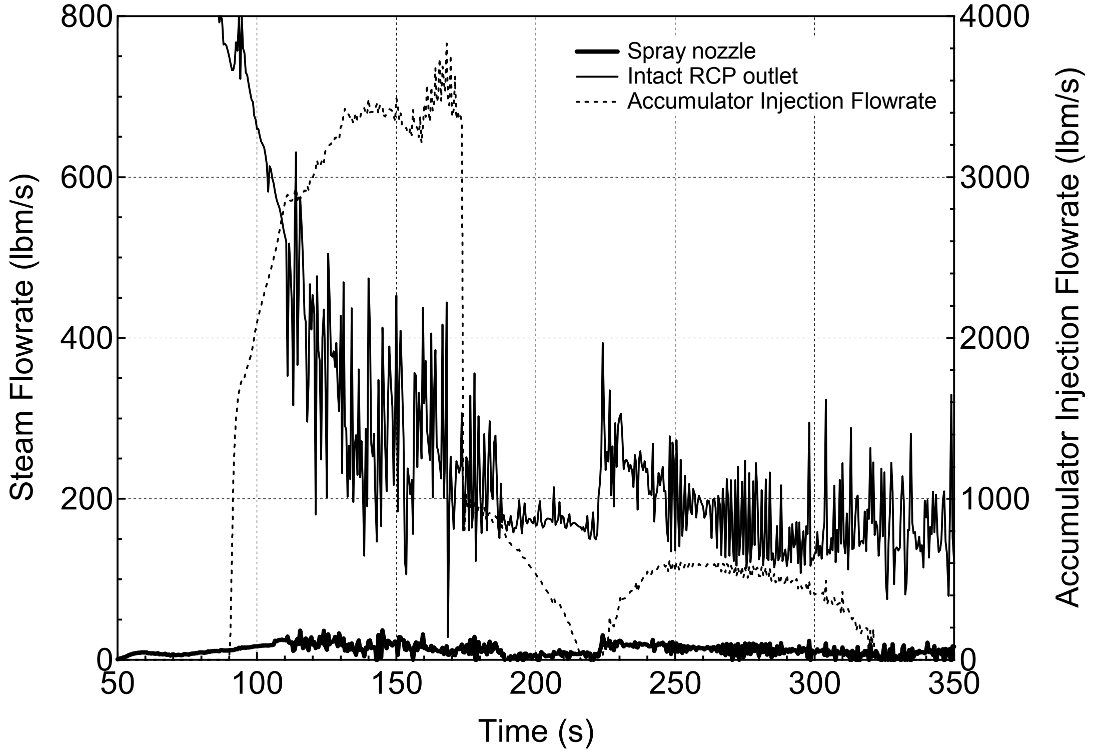

Figure RAI-7-13.2 Steam Flowrate at Intact RCP Outlets and at Spray Nozzles

REQUEST 7-14

(Related RAI 7-2)

The break size spectrum for the APWR is different than previously considered by the NRC for SBLOCA, since the limiting case is at the high end of the range (1.0 ft^2). For PWRs limiting breaks have historically been in the range of 2 to 4 inches. It is not certain that the APWR break size range can be characterized fully by SBLOCA phenomena. To assist the NRC in determining whether the governing phenomena are more like a SBLOCA or LBOCA (e.g. to resolve end of bypass, FLECHT heat transfer applicability, amount of dissolved Nitrogen in RCS from accumulator based on accumulator water level) the following information is requested:

For the limiting 1.0 ft^2 break and the 7.5 in break, provide plots of the following parameters:

a. the cold leg to downcomer mass rate for each loop,
b. the downcomer to lower plenum mass flow rate,
c. the mass flow rate into and exiting the average and hot channel (vapor and liquid components as appropriate),
d. the core bypass inlet mass flow rate,
e. the neutron reflector inlet mass flow rate,
f. the accumulator water levels as functions of time,
g. the equivalent two-phase levels in the average and hot channel as functions of time,
h. the peak cladding temperature as a function of time and identify the SBLOCA phase (i.e., blowdown, loop-seal clearing, natural circulation, etc.) time spans on the plots.
i. the heat transfer coefficient at the peak clad temperature location and the heat transfer correlation identifier and annotate the plot to indicate the time when an Appendix K heat transfer lockout occurs.

RESPONSE

The requested data are provided in **Figures RAI-7-14.1 to RAI-7-14.26**.

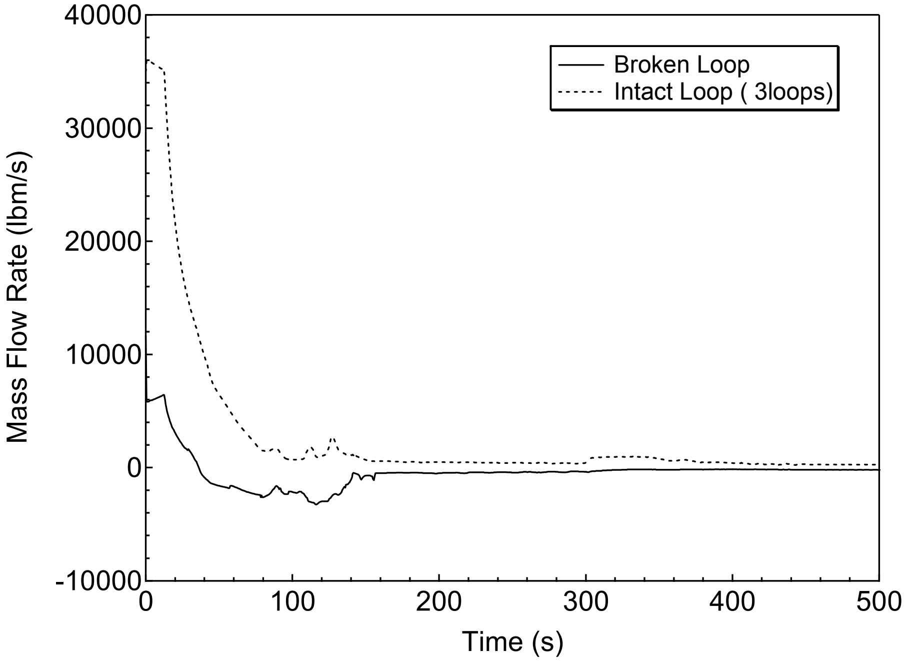

Figure RAI-7-14.1 Cold-leg to Downcomer Mass Flowrates for 7.5-inch Break

0)

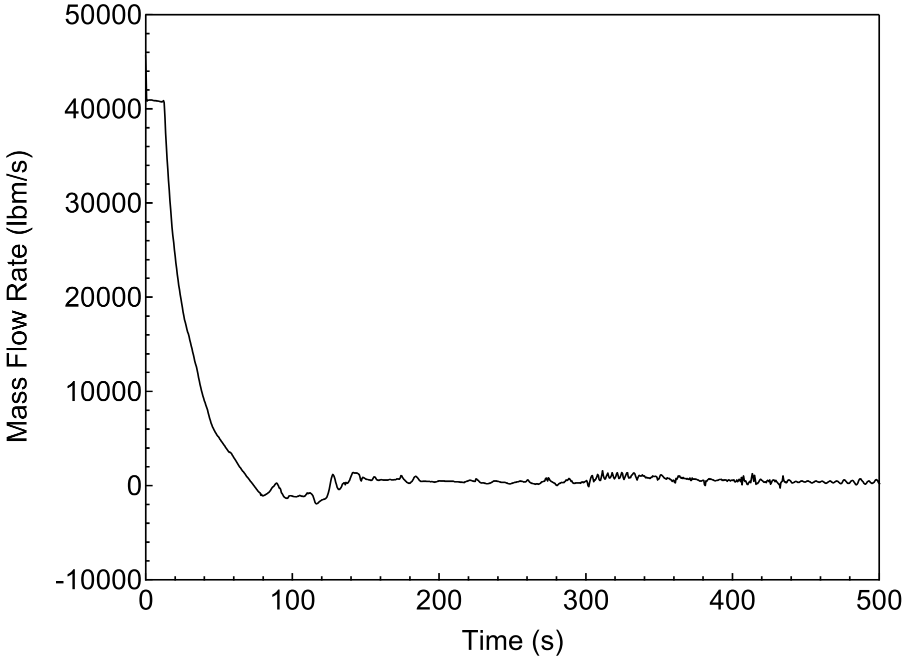

Figure RAI-7-14.2 Downcomer to Lower Plenum Mass Flowrate for 7.5-inch Break

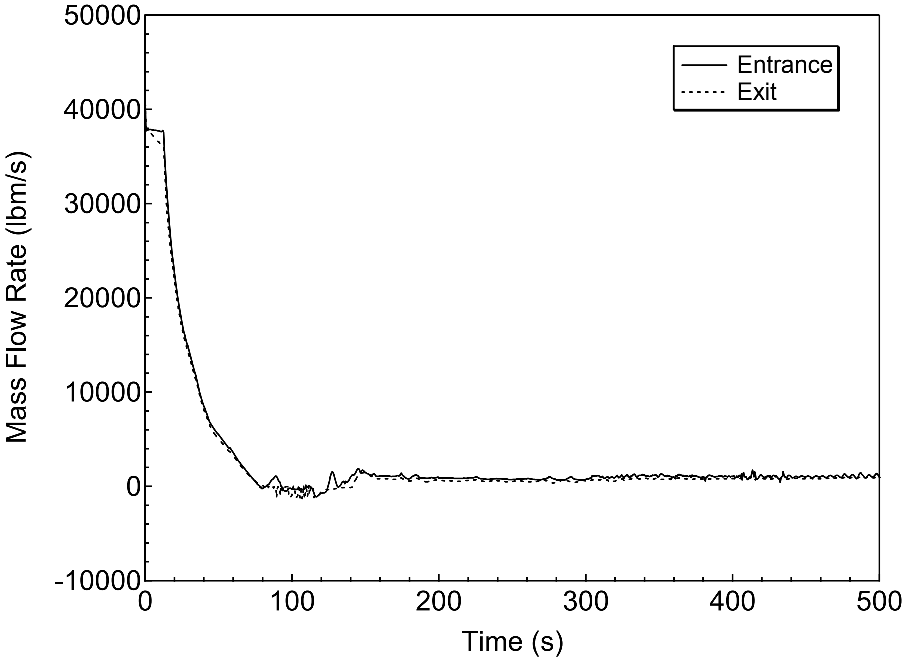

Figure RAI-7-14.3 Average Core Entrance and Exit Liquid Mass Flowrates for 7.5-inch Break

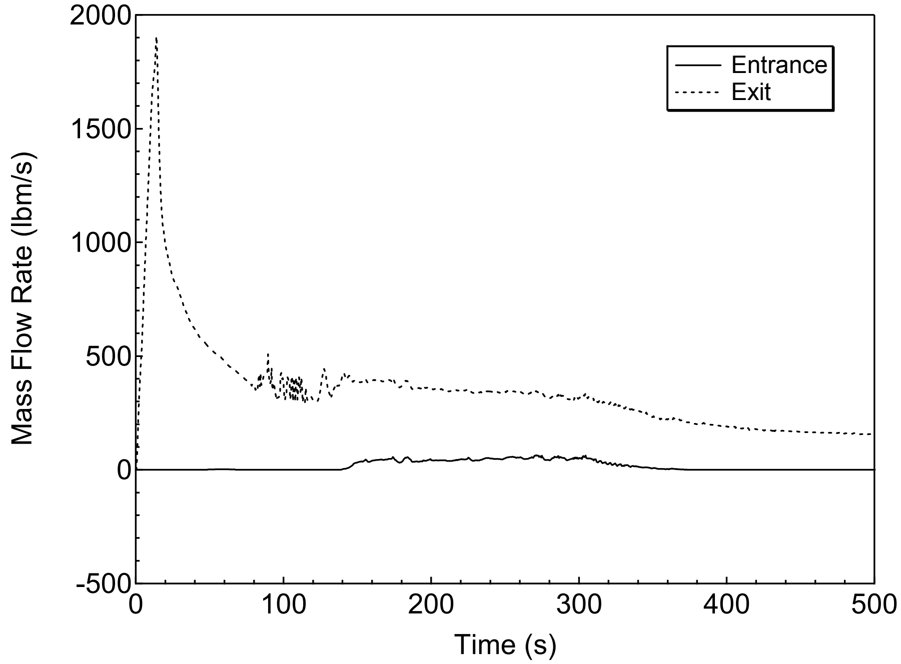

Figure RAI-7-14.4 Average Core Entrance and Exit Vapor Mass Flowrates for 7.5-inch Break

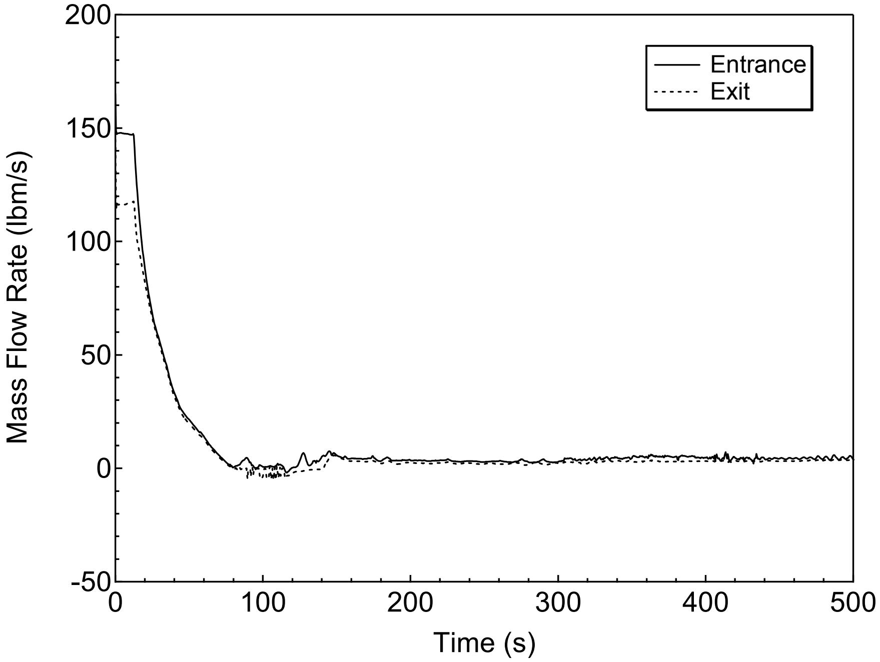

Figure RAI-7-14.5 Hot Assembly Entrance and Exit Liquid Mass Flowrates for 7.5-inch Break

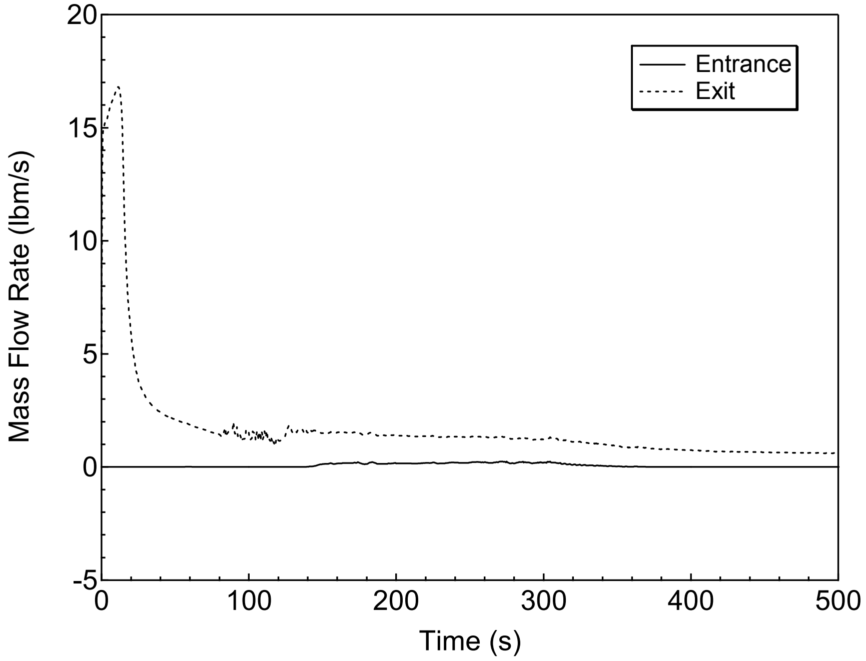

Figure RAI-7-14.6 Hot Assembly Entrance and Exit Vapor Mass Flowrates for 7.5-inch Break

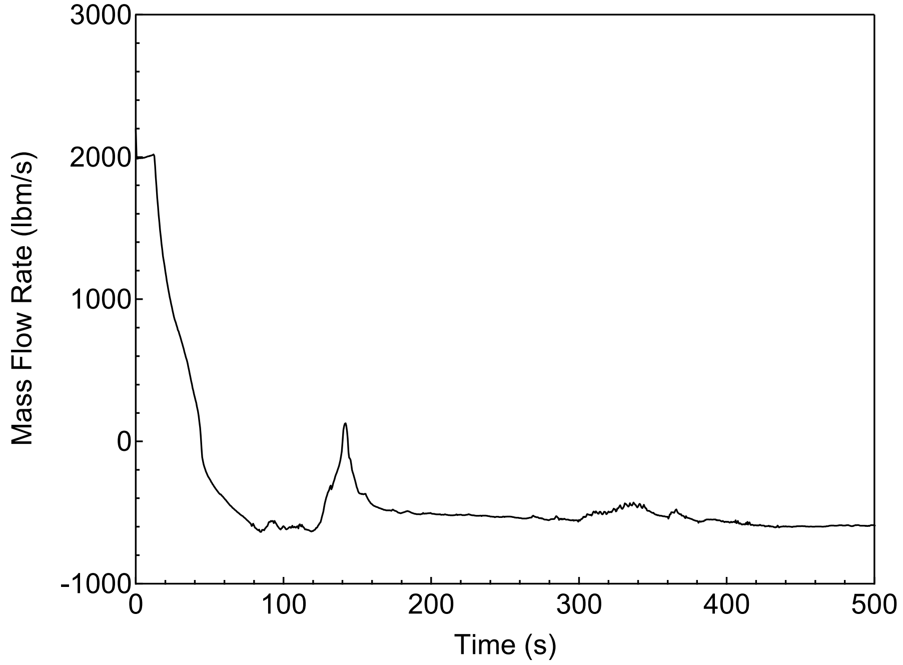

Figure RAI-7-14.7 Core Bypass Entrance Mass Flowrate for 7.5-inch Break

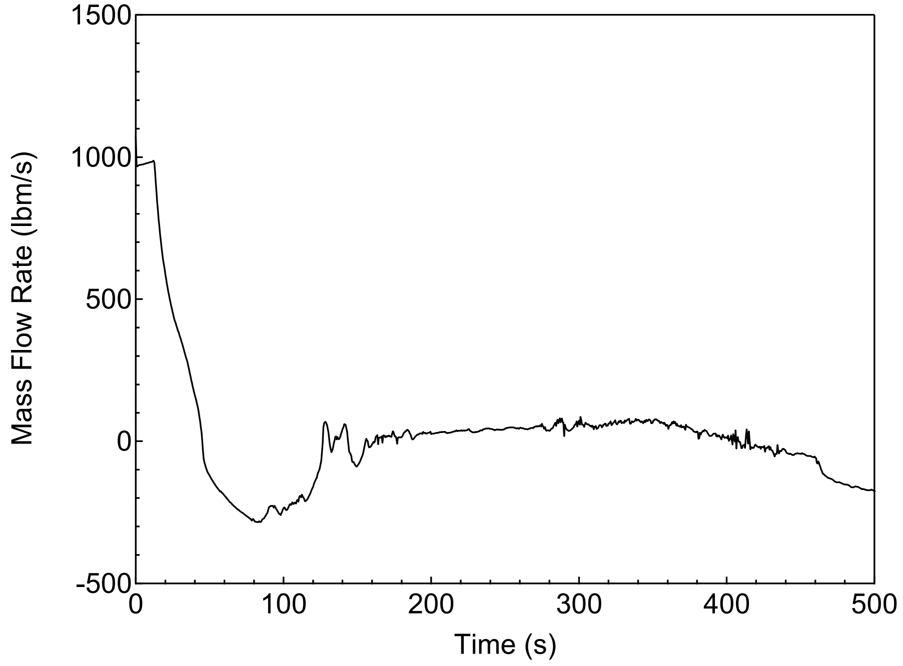

Figure RAI-7-14.8 Neutron Reflector Entrance Mass Flowrate for 7.5-inch Break

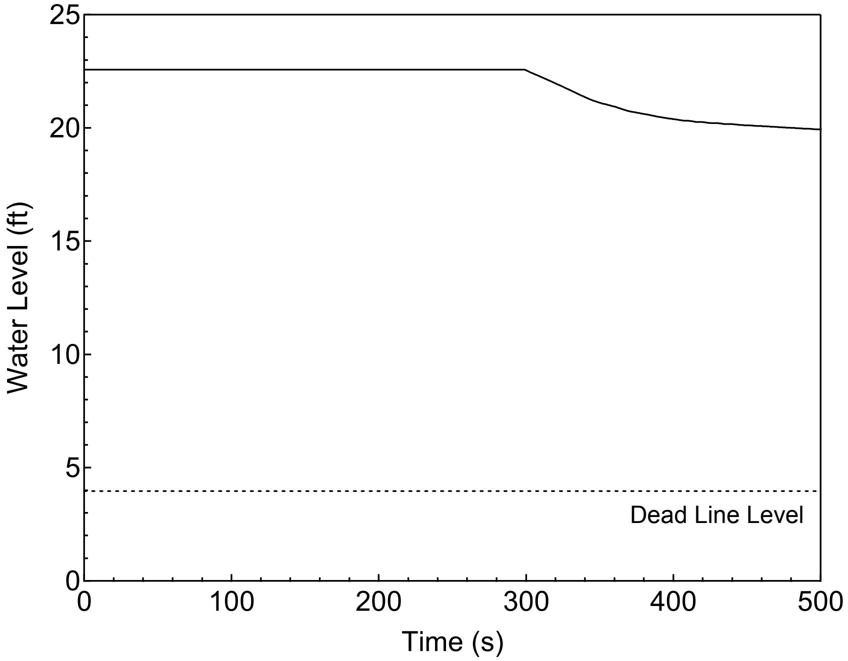

Figure RAI-7-14.9 Accumulator Water Level for 7.5-inch Break

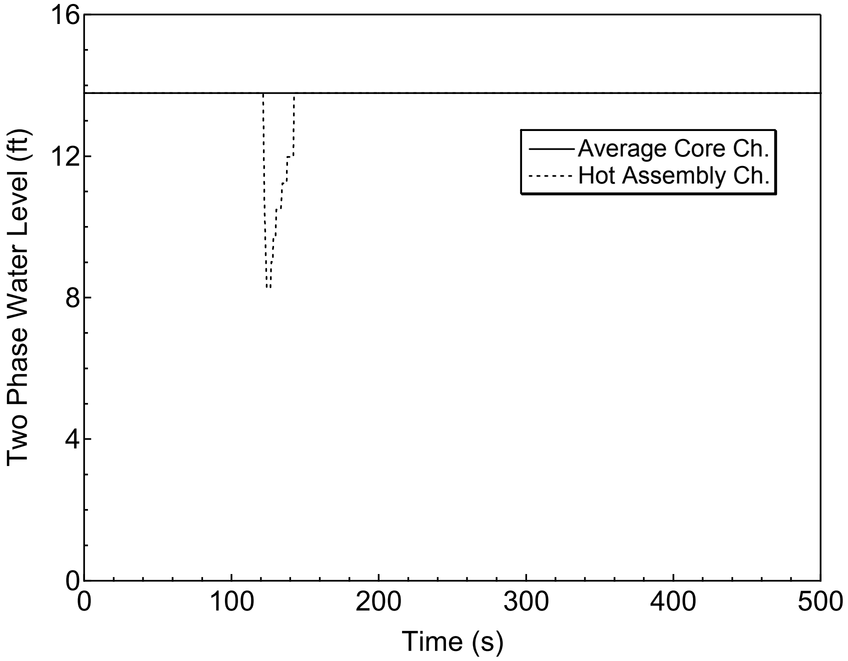

Figure RAI-7-14.10 Core Two-Phase Level for 7.5-inch Break

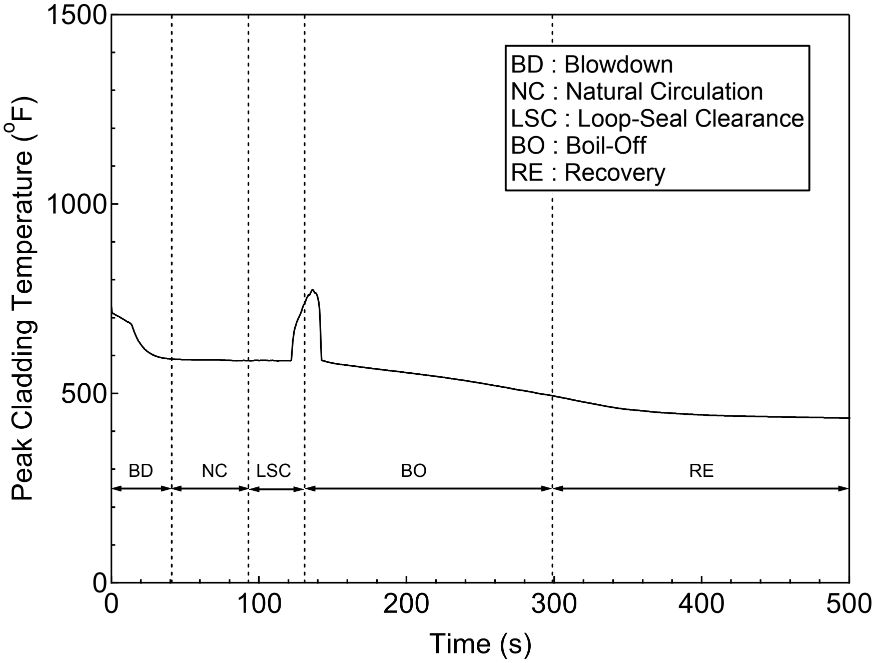

Figure RAI-7-14.11 PCT at ALL Elevations for Hot Rod in Hot Assembly for 7.5-inch Break

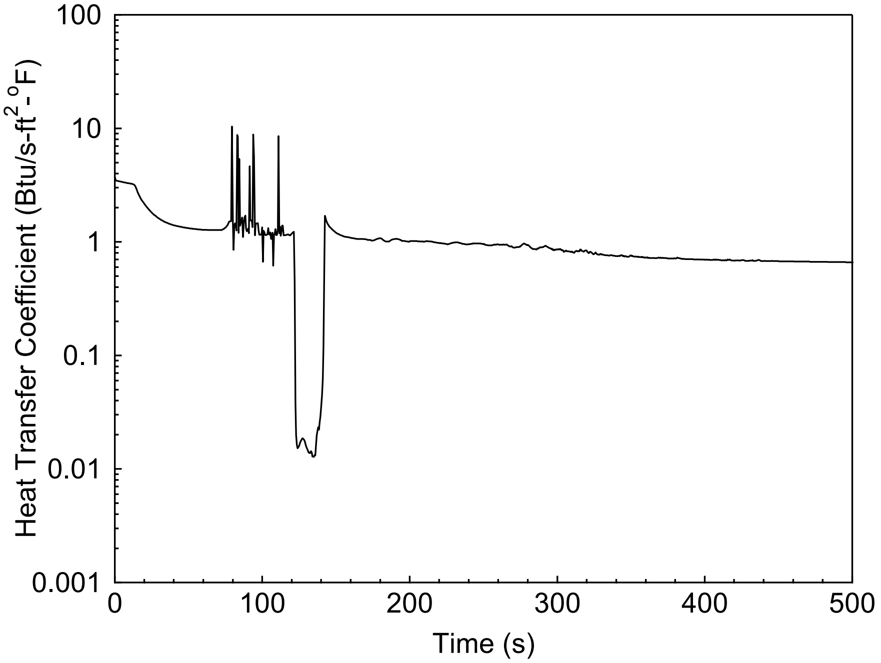

Figure RAI-7-14.12 Heat Transfer Coefficient at PCT Location for 7.5-inch Break

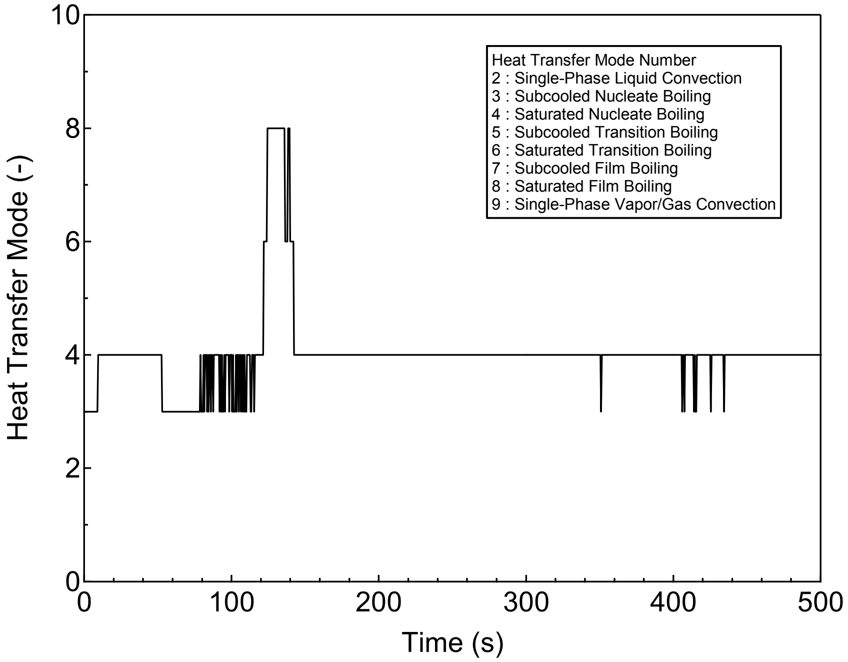

Figure RAI-7-14.13 Heat Transfer Mode at PCT Location for 7.5-inch Break

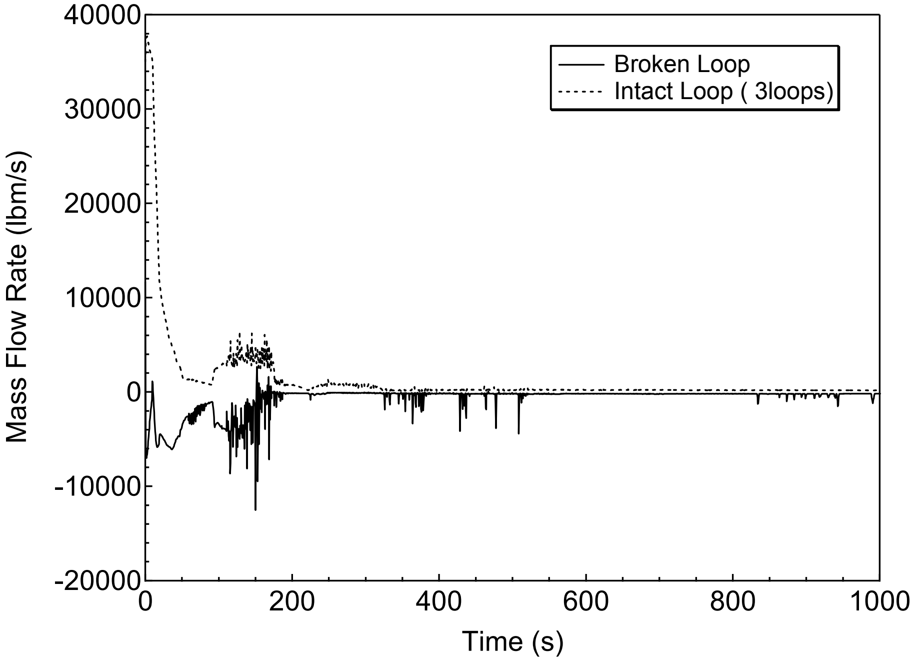

Figure RAI-7-14.14 Cold-leg to Downcomer Mass Flowrates for 1-ft^2 Break

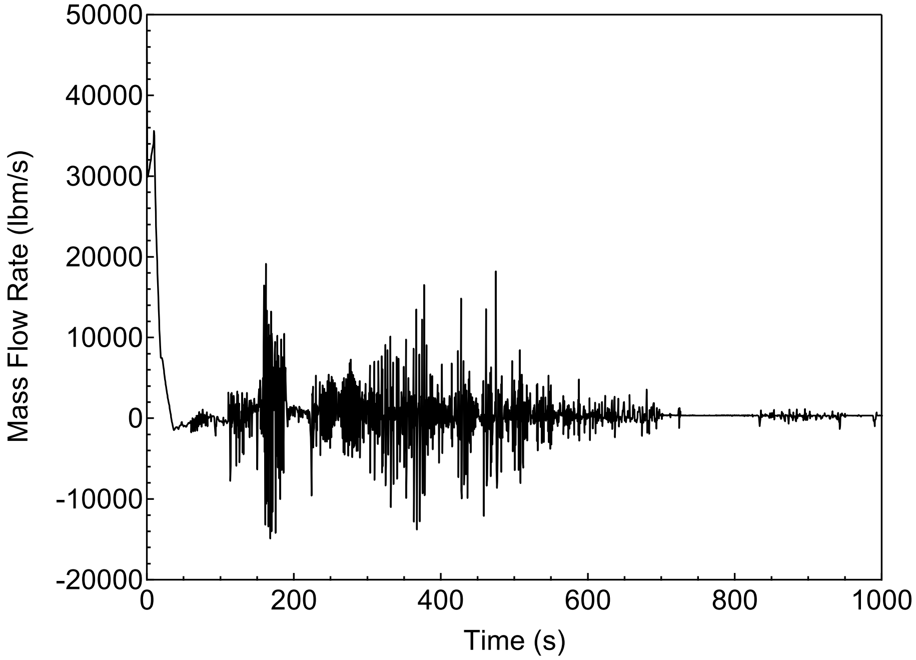

Figure RAI-7-14.15 Downcomer to Lower Plenum Mass Flowrate for 1-ft^2 Break

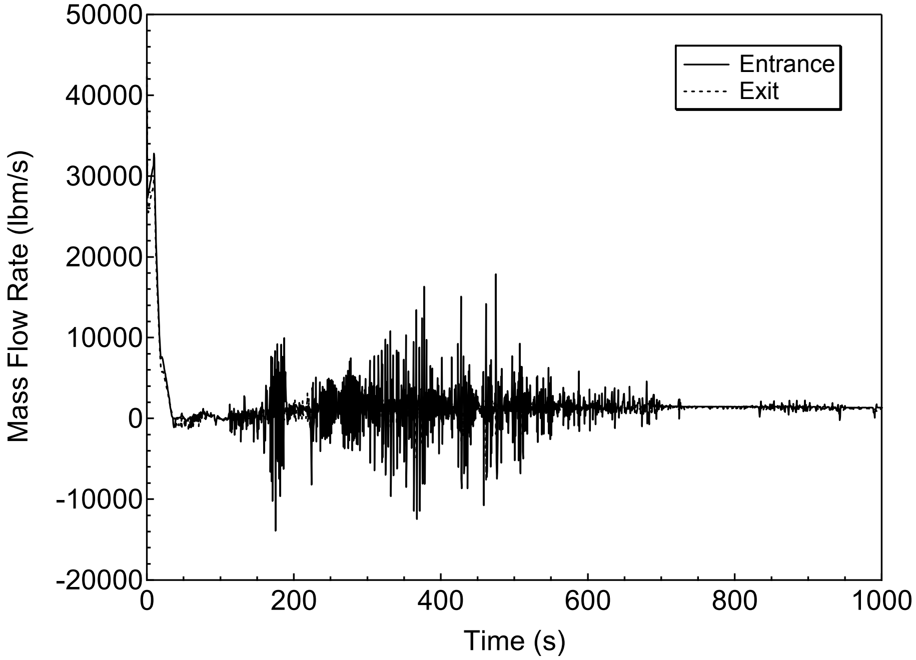

Figure RAI-7-14.16 Average Core Entrance and Exit Liquid Mass Flowrates for 1-ft^2 Break

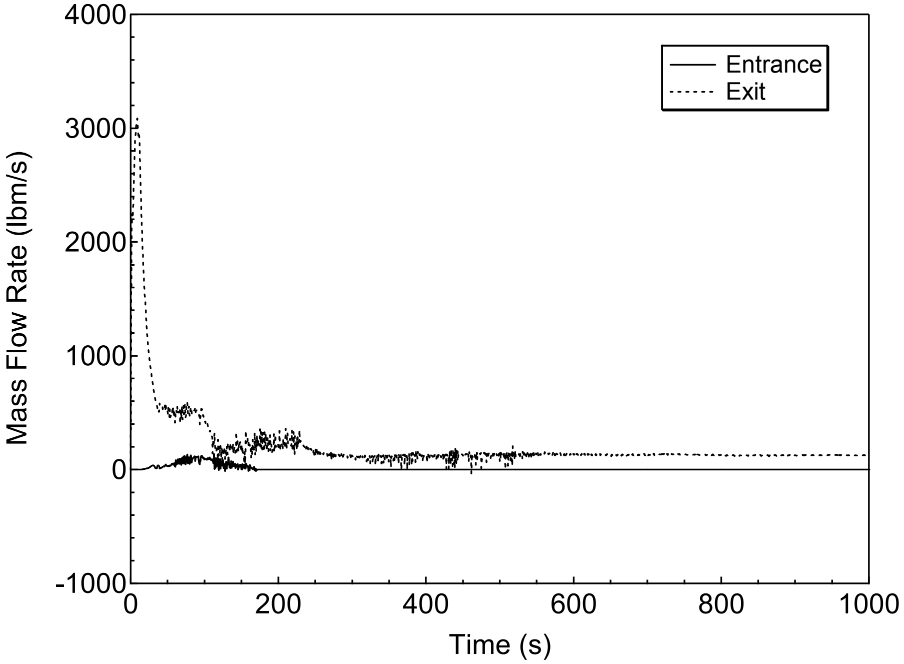

Figure RAI-7-14.17 Average Core Entrance and Exit Vapor Mass Flowrates for 1-ft^2 Break

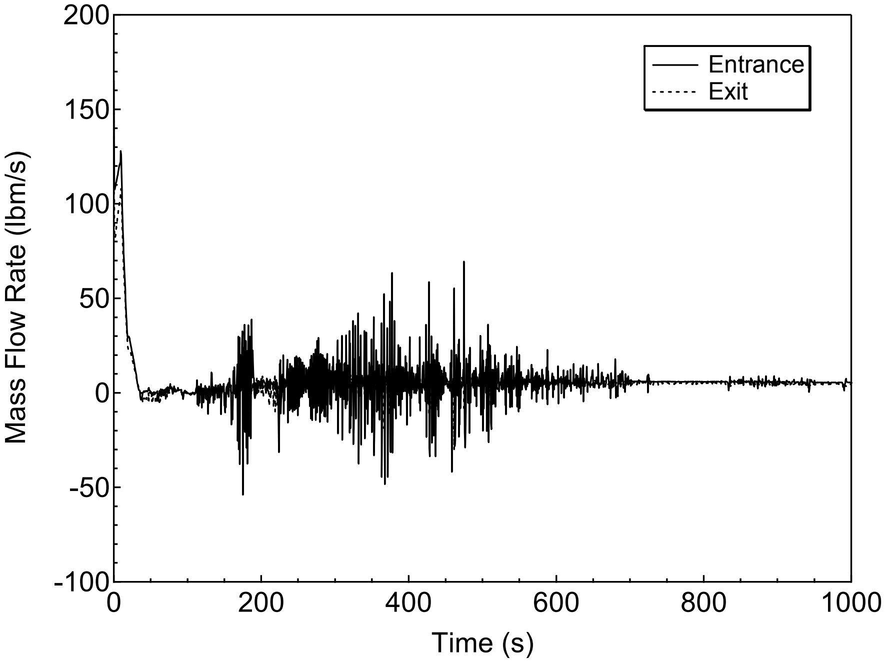

Figure RAI-7-14.18 Hot Assembly Entrance and Exit Liquid Mass Flowrates for 1-ft^2 Break

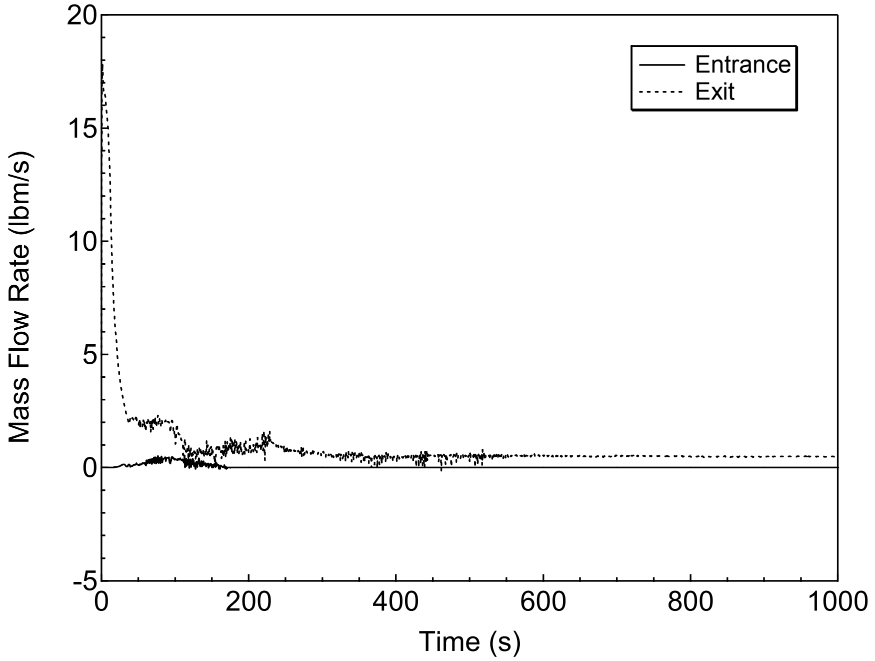

Figure RAI-7-14.19 Hot Assembly Entrance and Exit Vapor Mass Flowrates for 1-ft^2 Break

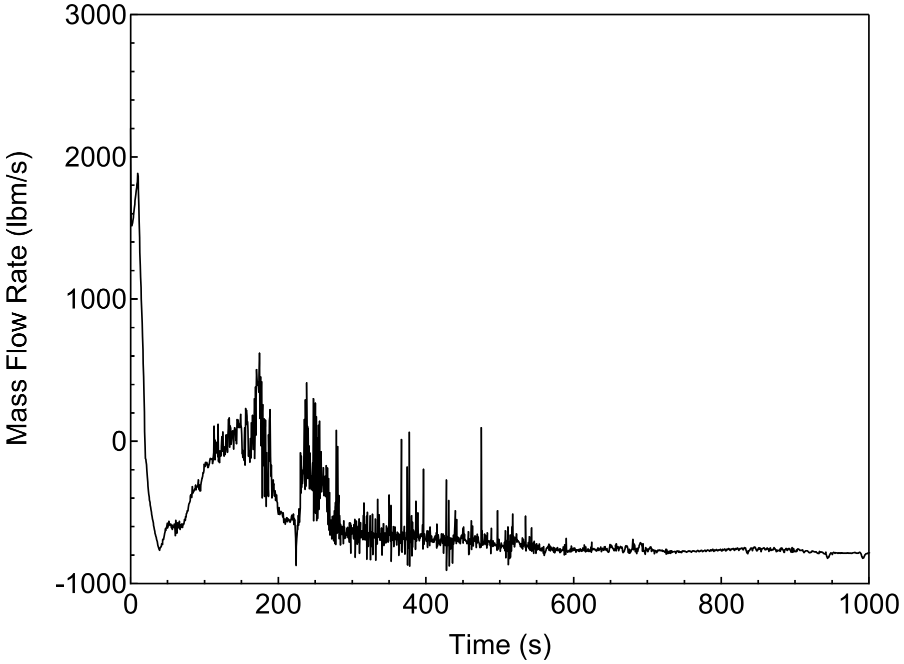

Figure RAI-7-14.20 Core Bypass Entrance Mass Flowrate for 1-ft^2 Break

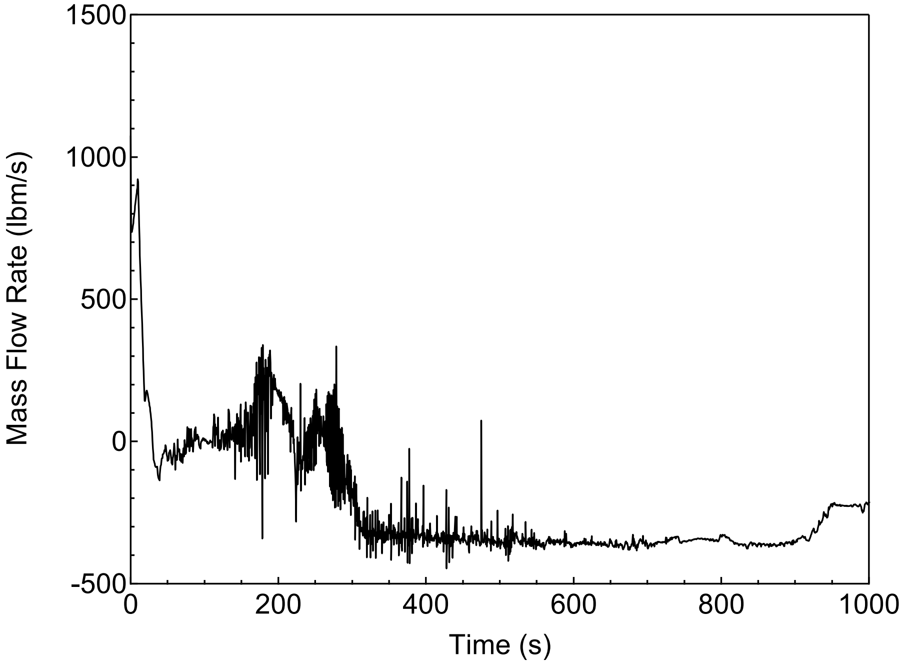

Figure RAI-7-14.21 Neutron Reflector Entrance Mass Flowrate for 1-ft^2 Break

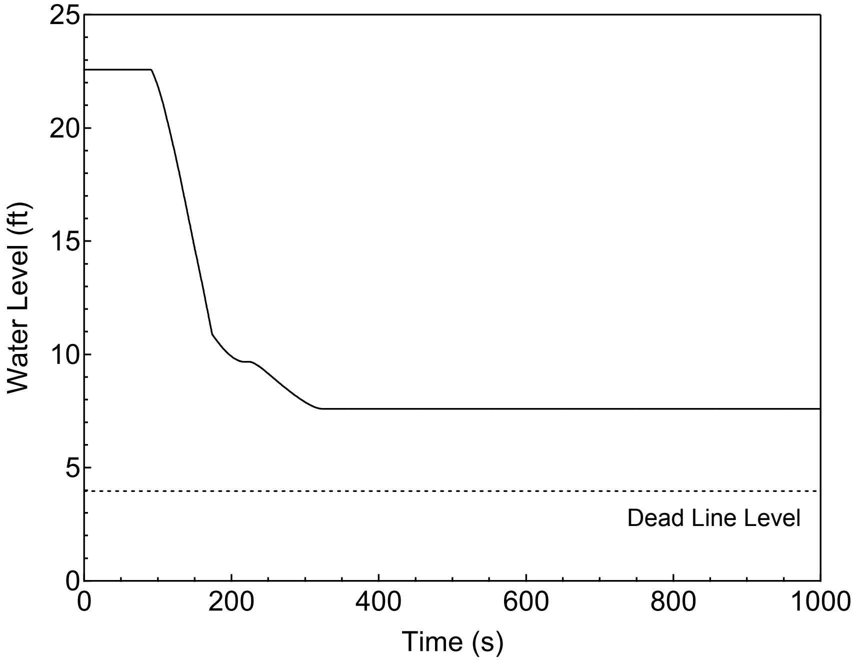

Figure RAI-7-14.22 Accumulator Water Level for 1-ft^2 Break

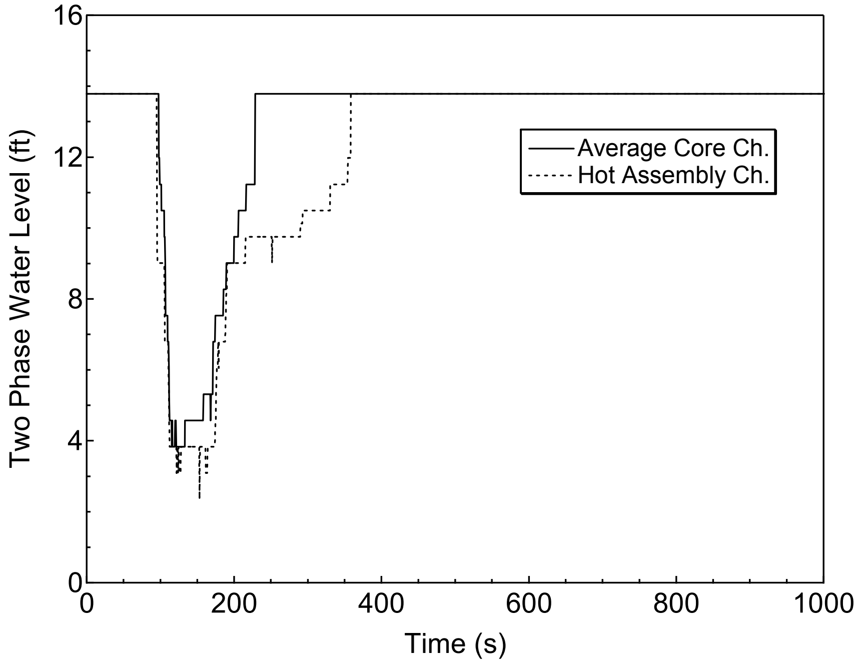

Figure RAI-7-14.23 Core Two-Phase Level for 1-ft^2 Break

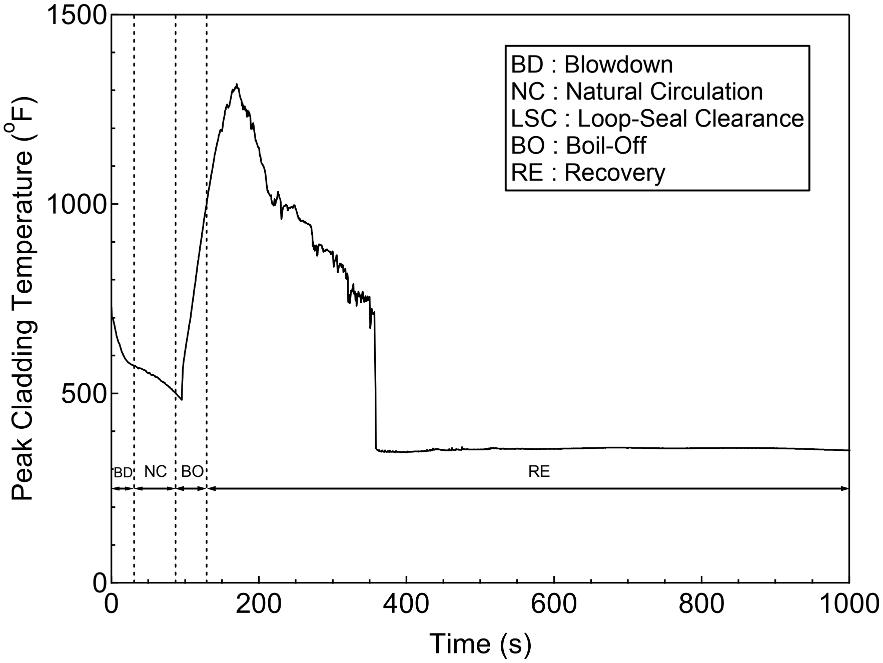

Figure RAI-7-14.24 PCT at ALL Elevations for Hot Rod in Hot Assembly for 1-ft^2 Break

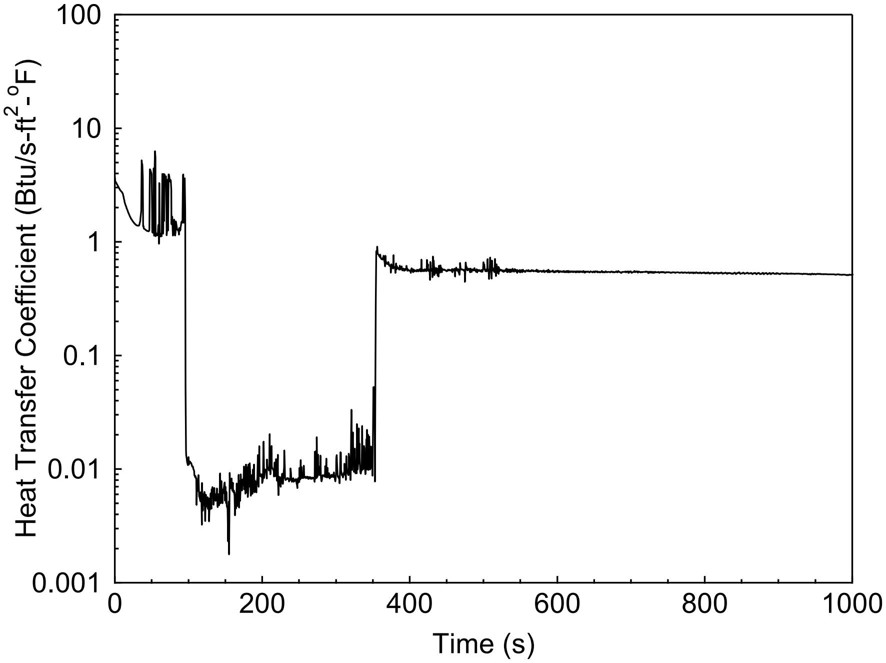

Figure RAI-7-14.25 Heat Transfer Coefficient at PCT Location for 1-ft^2 Break

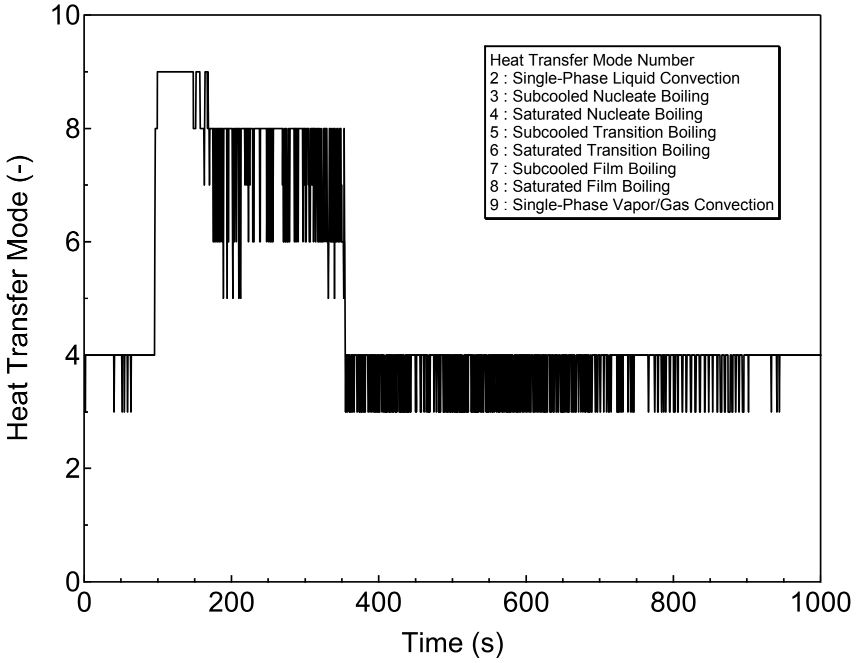

Figure RAI-7-14.26 Heat Transfer Mode at PCT Location for 1-ft^2 Break

REQUEST 7-15

(Related RAI 7-2)

Based on Section 4.4, “Reflood Model,” in Volume IV of the RELAP-3D code description, “Paul Scherrer Institute (PSI) in Switzerland developed updates to improve the quench front behavior during the reactor core reflood process. A modified version of these updates was incorporated into RELAP5-3D along with a new quench front plotting capability.” A literature search suggests a multiplier of 0.6 should be applied to the heat transfer coefficient for flooding rate greater than 1 inch/sec to meet Appendix K requirements, based on an assessment against FLECHT-SEASET tests.

Is the 0.6 multiplier used for SBLOCA reflood rates greater than 1 inch/second? If not, why? Are any other modifications used in M-RELAP5, such as a multiplier, to meet the Appendix K requirements?

RESPONSE

Liang et al. intend to apply the RELAP5-3D to the LOCA analysis in accordance with the Appendix K of 10 CFR 50. They performed the assessment calculations against the five FLECHT-SEASET tests to use the PSI reflood model for the reflood heat transfer calculation for a flooding rate greater than 1 inch/sec. They concluded based on this assessment that the heat transfer coefficient calculated by the original PSI model should be reduced by a factor of 0.6 to ensure reasonable conservatism (Ref. 1).

The applicability of the PSI reflood model to the high pressure condition of the SBLOCA transients has not been validated. On the other hand, it was confirmed that the default heat transfer model in the M-RELAP5 can be conservatively applied to SBLOCA conditions by the comparison with the ORNL/THTF high-pressure reflood tests. Thus, the default heat transfer model is used in the US-APWR SBLOCA analyses with M-RELAP5. As the PSI reflood model is not used in the US-APWR SBLOCA analyses, the multiplier of 0.6 is not applicable. Multipliers to the heat transfer coefficient are not introduced to meet the Appendix K requirements.

The Dougall-Rohsenow correlation is applied to the two-phase vapor convection heat transfer calculation in M-RELAP5. As described in the topical report of SBLOCA methodology for the US-APWR, the vapor physical properties of thermal conductivity, viscosity and specific heat capacity are evaluated at the film temperature and the vapor temperature is used as the sink temperature. The original correlation used the saturation temperature to evaluate the vapor properties and as the sink temperature. MHI believes that M-RELAP5 meets the Appendix K requirement about the Dougall-Rohsenow correlation, because of the lower heat transfer coefficient and the higher sink temperature.

References:

1. Thomas K. S. Liang, et al., Development of LOCA licensing calculation capability with

RELAP5-3D in accordance with Appendix K of 10 CFR50.46, Nucl. Eng. Des. Vol. 211, 2002

REQUEST 7-16
(Related RAI 7-2)

Comparisons to FLECHT heat transfer correlation for reflood rates greater than 1” per second. MHI previously stated that this did not apply to SBLOCA based on NOTRUMP SER, but the APWR limiting break size is much larger than typical PWRs (3-4 inches).

Please provide a discussion addressing the larger limiting break size for the APWR which justifies the MHI position of not comparing to FLECHT data.

RESPONSE

[

]

[

]

REQUEST 7-17
(Related RAI 7-2)

During refill and during reflood when reflood rates are less than one inch per second, heat transfer calculations shall be based on the assumption that cooling is only by steam. The M-RELAP reflood model uses the Forsland-Rohsenow correlation which includes heat transfer to droplets and does not comply with the Appendix K requirement for steam cooling only.

Please explain how using the heat transfer coefficient model, which includes the Forsland-Rohsenow correlation, satisfies the Appendix K steam cooling only requirement.

In M-RELAP5, radiation to droplets is then added to the final film boiling coefficient. Please explain how this term satisfies the Appendix K steam only criterion.

RESPONSE

The FLECHT tests which simulate the flow blockage were performed before Appendix K to 10 CFR 50 was issued. With reflood rate of one inch per second or higher, improvement of heat transfer was found around the blockage. The improved heat transfer was shown to be caused by break-up of the entrained droplets and increased turbulence by the blockage. On the contrary, heat transfer was degraded for the blockage test at a reflood rate of 0.6 inch per second. The degradation was presumed to be the result of a lack of the entrained droplet effect and the steam flow reduction around the blockage. Based on the test results, heat transfer coefficient based on unblocked FLECHT tests is approved when the reflood rate is one inch per second or higher even if the flow blockage occurs. And the assumption that cooling is only by steam, and the flow blockage might affect both local steam flow and heat transfer is required when the reflood rate is less than one inch per second. The actual purpose of Appendix K requirement for the steam cooling is considered to neglect the entrained droplet effect by the blockage and to account the heat transfer degradation due to the flow reduction around the blockage for low flood rate condition.

The Forsland-Rohsenow correlation is used in PSI reflood model. As the PSI reflood model is not used in US-APWR SBLOCA analyses, the Forsland-Rohsenow correlation is not applied.

The general heat transfer model incorporated in M-RELAP5 considers not only convective cooling to steam but also film boiling cooling to liquid through vapor film and radiation to water droplets is applied to the reflood heat transfer calculations in the US-APWR SBLOCA analyses. The conservatism of this heat transfer model is confirmed by the comparison with ORNL/THTF high-pressure reflood test data. MHI intends to evaluate the FLECHT-SEASET data to confirm the conservatism of the heat transfer model under the lower pressure condition which is typical to larger break size in the response to RAI 7-16. It is expected that the heat transfer model of M-RELAP5 is conservative and is adequately applied to the reflood heat transfer calculation for no blockage cases.

When fuel cladding deformation due to cladding swelling or rupture occurs, the resulting flow blockage affects hydrodynamic behavior. Flow area change and additional pressure loss due to the flow blockage are considered in M-RELAP5 regardless of the reflood rate. The flow blockage will reduce the coolant flow around the blockage and will degrade the heat transfer. In addition, the entrained droplet effect caused by the blockage is conservatively neglected in M-RELAP5. Thus, the flow blockage effect on the heat transfer is conservatively considered in M-RELAP5 regardless the reflood rate. The flow blockage does not occur in the US-APWR SBLOCA analyses.

A reflood rate for 1.0ft^2 of cold leg break is shown in **Figure RAI-7-17.1**. As the initial fuel rod stored energy is already released before the reflood starts, and decay heat in the reflood period is small in the SBLOCA, steam generation in the core is small compared with the LBLOCA. So, the steam binding effect is negligible in SBLOCAs. This causes a higher reflood rate in SBLOCA than in LBLOCA. The estimated reflood rate is greater than 1.0 inch per second as shown in Figure RAI-7-17.1. Therefore, the Appendix K requirement for steam cooling does not apply to the SBLOCA analyses of the larger break sizes.

It can be concluded that the reflood heat transfer model in M-RELAP5 satisfies the Appendix K requirement.

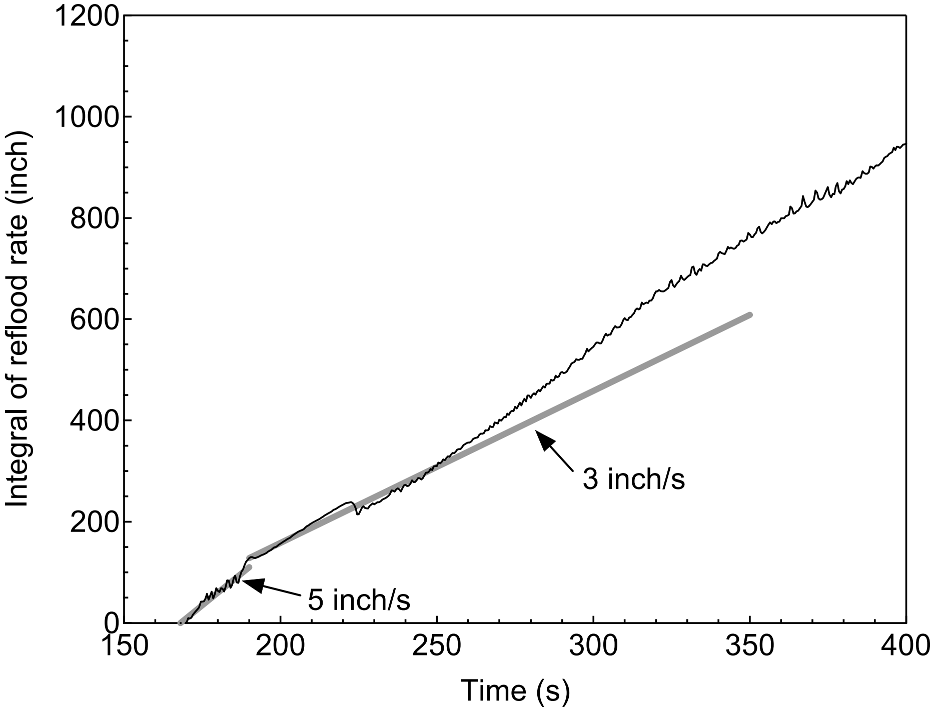

Figure RAI-7-17.1 Estimated Reflood Rate for 1.0ft^2 of Cold-leg Break

REQUEST 7-18

(Related RAI 7-2, 7-10)

[

]

RESPONSE

[

]

[

]

[

]

REQUEST 7-19
(Related RAI 7-8)
[

]

RESPONSE
[

]

REQUEST 7-20
(Related RAI 7-8)

M-RELAP5 has implemented its own model for the transition from subcooled single-phase critical flow to two-phase critical flow. From the original response to RAI 7-8 it appears that MHI is taking credit for a lower critical flow rate when vapor phase exists with subcooled liquid in the volume upstream of the break. Also a special numerical scheme was implemented to smooth out the prediction of critical flow when the transition occurs.

Provide validation analyses against critical flow tests that span conditions of subcooled liquid with vapor and also transition from single-phase liquid to two-phase critical flow.

Is the under-relaxation method part of the Appendix K modification or part of the M-RELAP5 base code (i.e. the under-relaxation method is in operation even if none of the Appendix K model is activated)?

RESPONSE
[

]

[

]

REQUEST 7-21

(Related RAI 7-8)

[

]

RESPONSE

[

]

REQUEST 7-22

(Related RAI 7-10)

[

]

RESPONSE

[

]

[

]

REQUEST 7-23

(Related RAI 7-14)

Fig RAI-7-14.15, 16 and especially 18 of the July response (UAP-HF-09362) show very large and rapid oscillations in the vessel, including the core, flows. This raises the question about whether these flow oscillations promote core cooling. Appendix K, Section C.7.a on Core Flow Distribution During Blowdown" requires that "The calculated flow shall be smoothed to eliminate any calculated rapid oscillations (period less than 0.1 seconds). Discuss the manner in which this Appendix K requirement is satisfied.

RESPONSE

In SBLOCA analyses using M-RELAP5, the core heat transfer calculation and the system fluid calculation are concurrently performed to evaluate the PCT, without using the smoothed core flowrate. Therefore, PCTs obtained by M-RELAP5 calculations inherently contain the effect of the flow oscillation at the core inlet, particularly for the 1-ft^2 break case.

Appendix K to 10 CFR 50 requires that the calculated flow shall be smoothed to eliminate any calculated rapid oscillations with periods less than 0.1 seconds. In the US-APWR SBLOCA with the 1-ft^2 cold leg break, significant oscillations at the core inlet appear after the end of the blowdown phase. The period of the flow oscillations is about 0.2 seconds during the boil-off phase in the 1-ft^2 break, and is greater than 1 second during the core recovery phase, as shown in Figures RAI-7-23.1 and 2. Therefore, there are no rapid oscillations required to be smoothed according to Appendix-K.

[

]

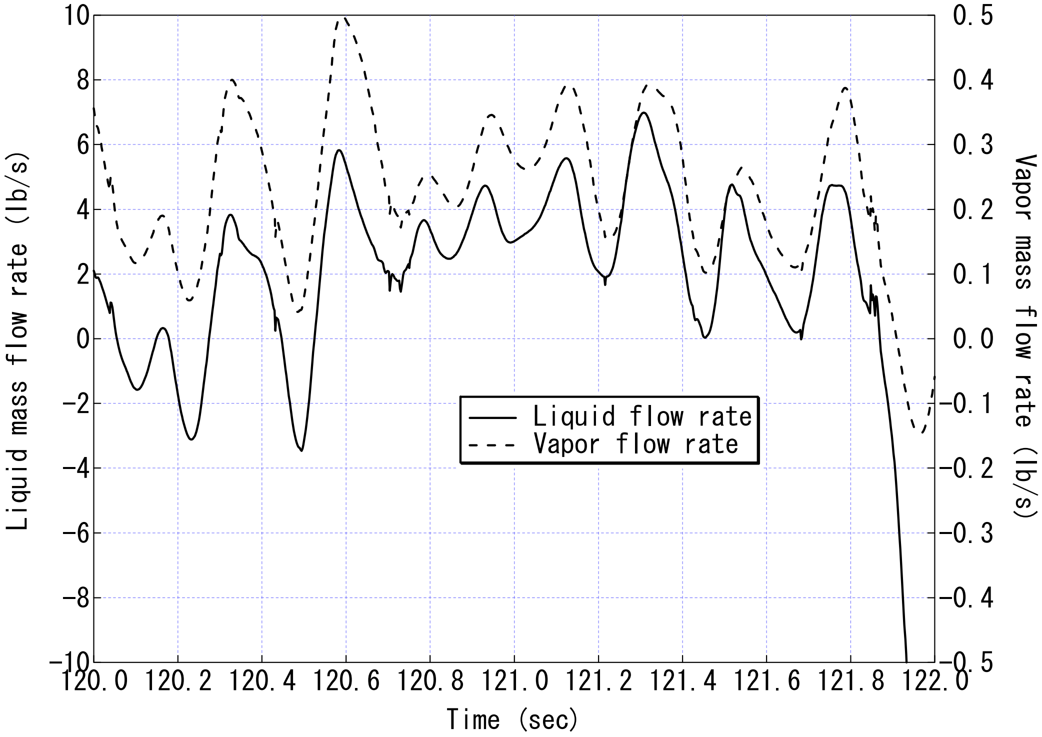

Figure RAI-7-23.1 Hot Assembly Flowrate Oscillation during Boil-off Phase

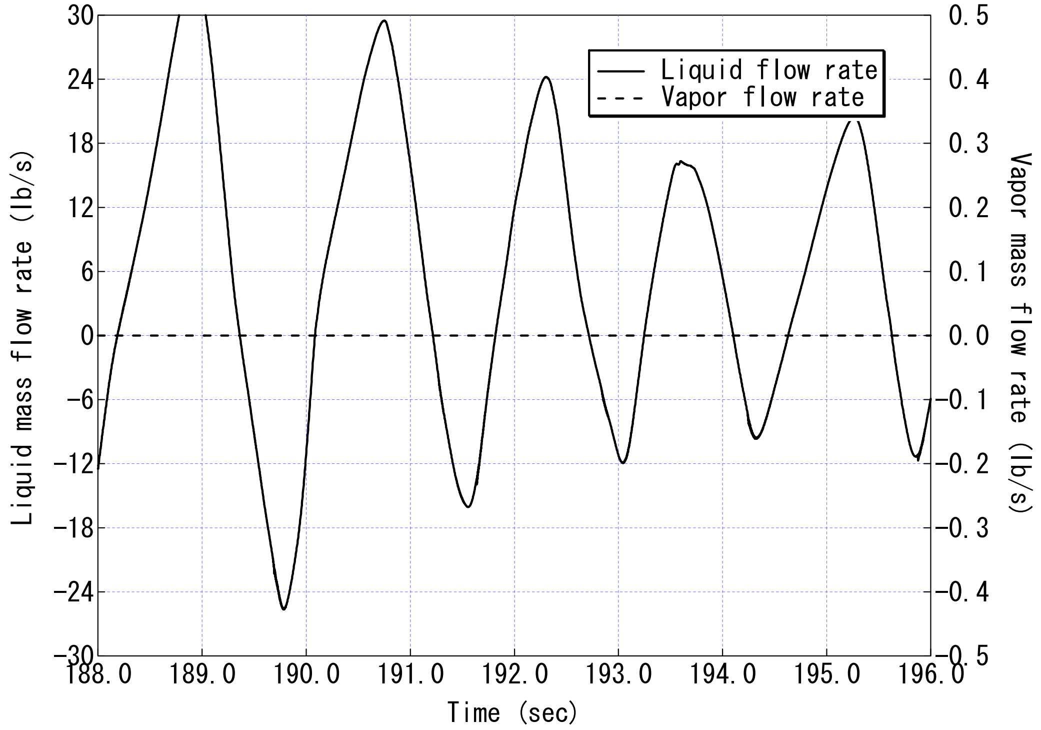

Figure RAI-7-23.2 Hot Assembly Flowrate Oscillation in Core Recovery Phase

REQUEST 8-1

Section 8.0
M-RELAP5 was created by modifying RELAP5-3D. Does any of the change have a direct impact on the result of the M-RELAP5 assessment? Are the differences in the results produced by using M-RELAP5 and RELAP5-3D consistent with the differences in the two codes?

RESPONSE

M-RELAP5 has been developed and assessed for its application to the SBLOCA analysis for US-APWR without altering the original features of its base code, RELAP5-3D.

The primary feature of the M-RELAP5 evaluation model is that the code is applicable to the SBLOCA analysis and satisfies the conservative requirements prescribed in 10 CFR 50, Appendix K, "ECCS Evaluation Models." In developing M-RELAP5, several conservative models and correlations have been implemented in its base code, RELAP5-3D. M-RELAP5 has also incorporated the model of the advanced accumulator, which is the only new engineered safety feature specific to US-APWR when compared to other 4-loop PWR plants.

Unless the models specific to M-RELAP5 are switched on, M-RELAP5 is identical to RELAP5-3D in terms of its calculation results.

REQUEST 8-2

Section 8.0
Was a single frozen version of M-RELAP5 used in all the assessments presented in this section? If yes, was the same version of M-RELAP5 used in the SBLOCA analysis?

RESPONSE

A single frozen version of M-RELAP5 was used in all the assessments presented in Section 8.0 of the topical report. A slightly different yet ultimately the same version of M-RELAP5 was used in the SBLOCA analysis for the preparation of the Design Control Document (DCD) for the US-APWR (Ref.1).

The difference between the two M-RELAP5 versions used in the calculations for the topical report and the DCD consists only in the difference in the way to read in the input data, i.e., the READ format. There is no difference between the two versions to make the calculation results of the two versions different.

Therefore it can be concluded that the two versions of M-RELAP5 used in the SBLOCA analyses for the topical report and the DCD are ultimately the same.

References

1. MHI, Design Control Document for US-APWR, Chapter 15 Transient and Accident Analyses, MUAP-DC015 Revision 0, December 2007.

REQUEST 8-3

The 1/2 scale test will be simulated with RELAP5/MOD3.3 as part of the confirmatory calculations. The purpose is to benchmark the advanced accumulator modeling approach used in RELAP5/MOD3.3 (uses control systems) against experimental data.

Please provide the M-RELAP5 input file that was used for the 1/2 scale advanced accumulator tests.

RESPONSE

The M-RELAP5 input files are supplied in ENCLOSURE 4 of this document, and the M-RELAP5 input data for the 1/2-scaled advanced accumulator test analysis are recorded on the attached CD-R. The detail of these inputs is described in Reference 1.

References:

1. Mitsubishi Heavy Industry, Ltd., Transmittal of the Calculation Book and Input Deck of Full Height 1/2 Scale Test Analysis on Advanced Accumulator for WCOBRA/TRAC and M-RELAP5., UAP-HF-08030, January 17, 2008.

REQUEST 8-4

[

]

RESPONSE

[

]

[

]

[

]

[

]

REQUEST 8-4

[

]

RESPONSE (Revision 1)

[

]

[

]

[

]

[

]

REQUEST 8-5

[

]

RESPONSE

[

]

[

]

REQUEST 8-3
(Related RAI 8-2)

Have there been error fixes in M-RELAP5 since MUAP-07013-P (R0) was issued? What impact do these error fixes have on the SBLOCA methodology as presented in MUAP-07013-P (R0) and the technical report MUAP-07025-P (R0)?

RESPONSE

Followings are differences in M-RELAP5 between the versions used in MUAP-07013-P (R0) and MUAP-07025-P (R0).

[

]

These error fixes have no impact to MUAP-07013-P (R0) experimental validation calculation.

Differences between the current M-RELAP5 and the version used in MUAP-07015-P (R0) are as follows.

[

]

The impacts of these error fixes to PCT are -1°F and +20°F for 7.5in break and 1ft^2 break cases, respectively, as reported in Reference 1.

References:

1. Mitsubishi Heavy Industry, Ltd., Reporting of Modifications and Corrections in ECCS Evaluation Models for the US-APWR LOCA Analyses, UAP-HF-08120, July 4, 2008.

REQUEST 8.1-1

Discuss the scaling of each test in Sections 8.1.1 (ROSA-IV LSTF) and 8.1.2 (ORNL/THTF) vs. US-APWR (in terms of vessel and rod heights, volume, flow areas, rod diameter, power/heat flux ratio, grid spacers, ratio of heated and unheated rods, and SG elevation, tube diameter and tube length, etc.), and justify the scaling (i.e., why the differences in these scales, if any, are not an issue) in using these tests for the US-APWR assessment.

RESPONSE

To validate M-RELAP5, the Phenomena Identification and Ranking Table (PIRT) for small break LOCA in the US-APWR has been developed. The phenomena ranked as “High” in the PIRT have been either conservatively modeled based on the Appendix-K requirements or confirmed by validation of the corresponding models in M-RELAP5 through simulations of selected tests. Table RAI-8.1-1.1, which is Table 4.4.2-1 in the Topical Report MUAP-07013-P(R0), lists the simulated tests for the validation of M-RELAP5 along with the high-ranking phenomena for which models have been validated for small break LOCA analysis for US-APWR.

Referring to Table RAI-8.1-1.1, the ROSA-IV/LSTF separate effect test was conducted for the assessment of the core mixture level, which is strongly dependent on the void fraction profile. The core mixture level was also assessed through the ORNL/THTF separate effect test programs. The ORNL/THTF separate effect test facility was also used in the uncovered core heat transfer and reflood tests to investigate the phenomena of CHF / core dryout, uncovered core heat transfer, and rewetting.

Since the ROSA-IV/LSTF and ORNL/THTF tests mentioned in this REQUEST were separate effect tests considering only the core thermal-hydraulic phenomena as described above, the scaling of the core parameters for ROSA-IV/LSTF and ORNL/THTF are described and discussed against a typical 4-loop PWR and the US-APWR in Tables RAI-8.1-1.2 and RAI-8.1-1.3, respectively. Overall, both ROSA-IV/LSTF and ORNL/THTF are quite well scaled with respect to US-APWR.

The key parameters in CHF/rewetting phenomena are the hydraulic diameter and heated diameter. These parameters in the THTF test facility were adequately scaled as shown in Table RAI-8.1-1.3. In addition, the grid span is another important parameter, because the droplet impingement on the grid spacers causes significant effect on the CHF/rewetting behaviors. However, the CHF/rewetting phenomena assessed by the THTF test data are limited only to the reflood condition, where the flooding velocity is relatively low and few droplets are generated. Therefore, the grid span can be excluded from the key parameters. It is noted that significant generation of droplet might occur in a LOCA transient having larger break size, because both the HHIS and ACC flow are injected to the sufficiently depressurized primary system. Consequently, this results in the higher flooding flow rate. Under such a condition, the grid effect tends to facilitate the rewetting behavior. However, the current M-RELAP5 has no model that specifically accounts for this phenomenon, which is conservative from the viewpoint of code application to SBLOCA analyses.

As for the uncovered core heat transfer, the vapor Reynolds number can be the most important parameter, because it dominates the convective heat transfer from the wall to vapor. No design parameter would affect the vapor Reynolds number, while the test conditions such as thermal power and flow rate can be carefully discussed for the code assessment.

The key parameter in the core mixture level is the void profile. The void profile is primarily sensitive to the flow geometry and hydraulic diameter except the test conditions (pressure, flow rate, thermal power and so on). The flow geometry employed in both the LSTF and THTF tests was the rod bundle which adequately simulated the 17X17 PWR fuel assembly. Thus, their hydraulic diameters were adequately scaled against US-APWR as shown in Tables RAI-8.1-1.2 and RAI-8.1-1.3.

The heated length is also important parameter for the CHF/rewetting and void profile (mixture level). The LSTF and THTF test facilities were targeting on the existing PWR core with 12-ft active fuel length, while the US-APWR employs the design of 14-ft active fuel length. However, the power density of the US-APWR core is sufficiently comparable with the existing PWR (without power uprate). Therefore, there is basically no significant difference in the thermal-hydraulic behavior between the US-APWR and the reference or existing PWR.

To this end, MHI concludes that the scalabilities of ROSA-IV/LSTF and ORNL/THTF separate effect test facilities are applicable to the US-APWR assessment.

Table RAI-8.1-1.1 Validation Tests for High Ranking Phenomena for Small Break LOCA

	CHF/Core Dryout	Uncovered Core Heat Transfer	Rewet	Core Mixture Level	Water Hold-Up in SG Inlet Plenum	Water Hold-Up in U-Tube Uphill Side	SG Primary and Secondary Heat Transfer	Water Level in SG Outlet Piping	Loop Seal Formation and Clearance	Downcomer Mixture Level/Void Distribution
Separate Effect Tests (SETs)										
ROSA/LSTF Void Profile Test				X						
ORNL/THTF Void Profile Test				X						
ORNL/THTF Uncovered Heat Transfer Test	X	X								
ORNL/THTF Reflood Test		X	X							
UPTF SG Plenum CCFL Test					X					
Dukler Air-Water Flooding Test						X				
Integral Effect Tests (IETs)										
ROSA-IV/LSTF Small Break (5%) LOCA Test	X	X	X	X	X	X	X	X	X	X

Table RAI-8.1-1.2 Scaling of Core Parameters for ROSA-IV/LSTF against PWR and US-APWR

Table RAI-8.1-1.3 Scaling of Core Parameters for ORNL/THTF against PWR and US-APWR

REQUEST 8.1-2

For each of the tests discussed in Sections 8.1.1, 8.1.2 and 8.1.3 scale the testing power in comparison with the timing of the US-APWR decay power (120% of ANS curve).

RESPONSE

The times of the Peak Cladding Temperature (PCT) occurrences after the reactor shutdown (SD) for the US-APWR SBLOCA scenarios were obtained from the US-APWR DCD as shown in Table RAI-8.1-2.1.

The Linear Heat Generation Rates (LHGRs) for the ROSA-IV/LSTF tests selected for the M-RELAP5 assessment are specified in Table RAI-8.1-2.2. The LHGR ranged from 0.92 to 1.28 kW/m.

Figure RAI-8.1-2.1 represents the LHGRs corresponding to the ANS-1971 standard decay heat model and 1.2 times the ANS-1971 standard, which was used in the M-RELAP5 analyses of the US-APWR SBLOCA scenarios, along with the LHGRs for the ROSA-IV/LSTF tests selected for the M-RELAP5 assessment. As shown in Figure RAI-8.1-2.1, the range of the LHGRs for the simulated ROSA-IV/LSTF tests fully covers the range of the LHGRs for the 120% of the ANS-1971 standard decay heat curve at the times of the PCT occurrences after the reactor shutdown for the US-APWR SBLOCA scenarios.

The LHGRs for the ORNL/THTF tests selected for the M-RELAP5 assessment are specified in Table RAI-8.1-2.3. The LHGR ranged from 0.32 to 1.29 kW/m.

Figure RAI-8.1-2.2 represents the LHGRs corresponding to the ANS-1971 standard decay heat model and 1.2 times the ANS-1971 standard, which was used in the M-RELAP5 analyses of the US-APWR SBLOCA scenarios, along with the LHGRs for the ORNL/THTF tests selected for the M-RELAP5 assessment. As shown in Figure RAI-8.1-2.2, the range of the LHGRs for the simulated ORNL/THTF tests fully covers the range of the LHGRs for the 120% of the ANS-1971 standard decay heat curve at the times of the PCT occurrences after the reactor shutdown for the US-APWR SBLOCA scenarios.

Table RAI-8.1-2.1 PCT Time after Reactor Shutdown from US-APWR DCD/SBLOCA

Scenario	CR-In Time(2) (sec)	SD Time(3) (sec)	PCT Time(4) (sec)	PCT-SD Time(5) (sec)
CLB 7.5 in	11.1	[ ]	136	[ ]
CLB 1.0 ft^2	8.7	[ ]	166	[ ]
CR-In Time Duration(1) (sec)	[ ]			

(1) Time duration for the control rod insertion
(2) Initiating time for the control rod insertion
(3) Time of the reactor shutdown completed: (3) = (1)+(2)
(4) Time of the PCT occurrence
(5) Time of the PCT occurrence after the reactor shutdown: (5) = (4)-(3)
(2) through (4): Time after the blowdown initiation

Table RAI-8.1-2.2 LHGRs for ROSA-IV/LSTF Tests Simulated by M-RELAP5

Test ID	LHGR (kW/m)
ST-NC-01	0.92
ST-NC-06E	1.01
SB-CL-16L	1.28
Min.	0.92
Max.	1.28

Table RAI-8.1-2.3 LHGRs for ORNL/THTF Tests Simulated by M-RELAP5

Test ID	LHGR (kW/m)	Note
3.09.10J	1.07	Level Swell
3.09.10K	0.32	Level Swell
3.09.10M	1.02	Level Swell
3.09.10N	0.47	Level Swell
3.09.10AA	1.27	Void
3.09.10BB	0.64	Void
3.09.10CC	0.33	Void
3.09.10DD	1.29	Void
3.09.10EE	0.64	Void
3.09.10FF	0.32	Void
3.09.10P	0.997	Reflood
3.09.10Q	1.02	Reflood
Min.	0.32	
Max.	1.29	

Figure RAI-8.1-2.1 Comparison of LHGRs for ROSA-IV/LSTF Tests Simulated by M-RELAP5 and Those for US-APWR SBLOCA Decay Power

Figure RAI-8.1-2.2 Comparison of LHGRs for ORNL/THTF Tests Simulated by M-RELAP5 and Those for US-APWR SBLOCA Decay Power

REQUEST 8.1-3

Sections 8.1.1, 8.1.2 and 8.1.3
The submittal concluded that M-RELAP5 was conservative based on the results of test simulations which used only one nodalization for each test. However, sometimes results can vary depending on nodalization. Discuss if any nodalization sensitivity studies were performed to make sure the results were conservative regardless of the nodalization for each test simulation.

RESPONSE

The M-RELAP5 nodalization schemes for the ROSA-IV/LSTF and ORNL/THTF test simulations were developed to be consistent with the scheme used to model the US-APWR. These schemes have been shown to accurately model important thermal-hydraulic parameters such as liquid levels.

The M-RELAP5 input model for the US-APWR SBLOCA analysis was developed following the INL's RELAP5-3D user's guidelines (Ref.1) for the analyses of Westinghouse-designed PWRs.
[

]

The axial nodalization schemes used in the M-RELAP5 simulations of both the ROSA-IV/LSTF and ORNL/THTF test bundles were similar to that used in the US-APWR SBLOCA analyses. The average axial node lengths for both test simulations were about **[ ]** which is almost the same as that used in the US-APWR SBLOCA analyses.

Since the M-RELAP5 nodalization schemes for the ROSA-IV/LSTF and ORNL/THTF test simulations were developed on the basis of the same noding philosophy as the nodalization scheme used in the US-APWR SBLOCA analyses, no nodalization sensitivity study was performed for each test simulation.

References
1. RELAP5-3D© Code Manual Volume V: User's Guidelines, INEEL-EXT-98-00834, Revision 2.4, June 2005.

REQUEST 8.1-4

(Related RAI 8.1-2)

The timings of PCT in the RAI response of 8.1-2 cover 7.5-inch and 1 ft^2 break.

Discuss whether the LHGR of the tests cover the range of PCT timing of other break sizes.

Also discuss if the mass flux of these simulations cover the range of mass flux of entire SBLOCA spectrum of break sizes.

RESPONSE

In discussing whether the linear heat generation rate (LHGR) of the tests covers the range of PCT timing during US-APWR SBLOCAs, the break spectrum being addressed is reasonably extended from 2-in to 1.0-ft^2 break at the cold-leg. The PCT occurrence timing after the reactor SCRAM is listed in **Table RAI 8.1-4.1**. Significant fuel cladding heat-up are shown during the loop seal clearance phase from 6 to 8-in break cases, while the heat-up occurs during the boil-off and recovery phase from 12-in to 1.0-ft^2 break cases. No significant heat-up appears for the other break sizes in US-APWR.

The PCT timing and the corresponding LHGR data ranges in US-APWR SBLOCAs are compared with the experimental test conditions, ROSA/LSTF and ORNL/THTF void profile, uncovered-bundle heat transfer, and high-pressure reflood tests which are used in M-RELAP5 code assessment (see MHI response to RAI 8.1-2 (Ref. 1)), in **Figure RAI-8.1-4.1**. The PCT occurs from 100 to 180 seconds after the reactor SCRAM for US-APWR, and the test data cover the range from 15 seconds after the SCRAM when the ANS-1971 decay heat power is assumed. Even if the 20% conservatism is taken into account for the decay heat, the test data satisfy the PCT timing range expected in US-APWR SBLOCAs as shown in Figure RAI-8.1.4-1.

The core inlet mass flux condition expected in US-APWR SBLOCAs is compared with the experimental test range. From the viewpoint of the impact on PCT, the core inlet mass flux plays an important role from the loop seal clearance to core recovery periods in US-APWR SBLOCAs. Therefore, the corresponding data in the ORNL/THTF tests are compared with the US-APWR SBLOCA flow range.

The mass flux data in the experiments are listed in **Table RAI-8.1.4-2**. The plant core flow range are shown in **Table RAI-8.1.4-3**, each of which is obtained by averaging the core inlet flow from the beginning of the loop seal clearance period to the end of core recovery period. These data are compared in **Figure RAI-8.1.4-2**, indicating that the test data sufficiently cover the range expected in US-APWR SBLOCAs.

Reference:

1. Mitsubishi Heavy Industry, Ltd., MHI's Partial Responses to NRC's Requests for Additional Information on Topical Report MUAP-07013-P (R0) "Small Break LOCA Methodology for US-APWR", UAP-HF-09002, January 16, 2009.

Table RAI-8.1-4.1 PCT Time after Reactor SCRAM

Scenario	PCT Duration	PCT Time after SCRAM (sec)
CLB 2.0 in	-	-
CLB 4.0 in	-	-
CLB 6.0 in	LSC	**[ ]**
CLB 7.5 in	LSC	**[ ]**
CLB 8.0 in	LSC	**[ ]**
CLB 10 in	-	-
CLB 12 in	BO	**[ ]**
CLB 1.0 ft^2	BO	**[ ]**

LSC: Loop Seal Clearance BO : Boil-off/Core Recovery

Table RAI-8.1-4.2 Mass Flux Data in ORNL/THTF and FLECHT-SEASET Tests

Test	Case	Flooding Mass Flux (lbm/ft^2-s)	Remarks
ORNL/THTF	3.09.10J	12.93	Uncovery Test
	3.09.10K	2.22	Uncovery Test
	3.09.10M	13.38	Uncovery Test
	3.09.10N	4.33	Uncovery Test
	3.09.10AA	21.15	Void Profile Test
	3.09.10BB	9.44	Void Profile Test
	3.09.10CC	7.22	Void Profile Test
	3.09.10DD	19.82	Void Profile Test
	3.09.10EE	11.00	Void Profile Test
	3.09.10FF	4.83	Void Profile Test
	3.09.10P	16.55	High-Pressure Reflood Test
	3.09.10Q	10.74	High-Pressure Reflood Test

Table RAI-8.1-4.3 Core Inlet Mass Flux Condition in US-APWR SBLOCAs

Scenario	PCT Duration	Core Inlet Mass Flux (lbm/ft^2-s)
CLB 2.0 in	-	-
CLB 4.0 in	-	**[ ]**
CLB 6.0 in	LSC	**[ ]**
CLB 7.5 in	LSC	**[ ]**
CLB 8.0 in	LSC	**[ ]**
CLB 10 in	-	**[ ]**
CLB 12 in	BO	**[ ]**
CLB 1.0 ft^2	BO	**[ ]**

LSC: Loop Seal Clearance BO: Boil-off/Recovery

Figure RAI-8.1-4.1 Comparison of LHGR Range between Experimental Tests and US-APWR SBLOCAs

Figure RAI-8.1-4.2 Comparison of Mass Flux Range between Experimental Tests and US-APWR SBLOCAs

REQUEST 8.1-5
(Related RAI 8.1-3)

Sensitivity study in the nodalization of the plant model is not a substitute for sensitivity study for the test simulation.

Demonstrate that conclusions derived from the simulation do not depend on the nodalization of the test facilities (especially for the nodalization of the ROSA/LSTF cross-over legs, which are substantially different from the plant model).

RESPONSE

[

]

[

]

[

]

Appendix A

Additional Information in Response to REQUEST 8.1-5

MITSUBISHI HEAVY INDUSTRY, LTD.

[

]

REQUEST 8.1.1-1

ROSA is an integral test facility including pressurizer and steam generators (SGs). But the simulations were performed only for the vessel. Are the selected tests vessel only tests, or is the vessel isolated for the simulations?

RESPONSE

The vessel was not isolated in the present experiment. However, only the vessel was simulated because this test was conducted under the steady-state condition and MHI judged that the vessel thermal-hydraulics including the core void profile has no significant affect from the rest of the system.

The boundary conditions for the vessel model were obtained from experimental measurements. Specifically, the measured crossover leg flow rate and cold leg temperature were used as boundary conditions at the vessel inlet, and the hot leg pressure was uses as a boundary condition at the vessel outlet.

REQUEST 8.1.1-2

[

]

RESPONSE

[

]

REQUEST 8.1.1-3

[

]

RESPONSE

[

]

REQUEST 8.1.1-4

[

]

RESPONSE

[

]

REQUEST 8.1.1-5

Compare how the grid spacers are modeled in the test and in plant simulations (e.g., flow areas, friction factors), and discuss the impact of these modeling differences, if any, on the void fraction distributions.

RESPONSE

[

]

References

1. The RELAP5-3D© Code Development Team, 2005, "RELAP5-3D© Code Manual Volume II: User's Guide and Input Requirements," INEEL-EXT-98-00834 Revision 2.4

REQUEST 8.1.1-6

[

]

RESPONSE

[

]

REQUEST 8.1.1-7

Figure 8.1.1-6 shows a comparison of the predicted and measured void fraction profiles. The void fraction decreases at the highest node in the M-RELAP5 prediction. One would expect the void fraction to continuously increase. Please explain this prediction.

RESPONSE

The reason why the void fraction is lower at the highest node of the core is numerically due to the junction-based interface friction factor applied there. The highest node is connected to the upper plenum node, which has a larger flow area than that of the core-heated section. The change of the flow area causes the reduced mass flux, resulting in the smaller friction factor at the top of the core-heated section due to the applied model (Refs. 1 and 2), and in the smaller void fraction there.

A sensitivity calculation in which the flow area of the upper plenum node is changed to be identical to that of the core-heated section has additionally been performed. As shown in the Figure 8.1.1-7.1, the void fraction continuously increases in the sensitivity case, different from the base case.

It is not experimentally confirmed whether the void fraction continuously increases or begins to decrease near the top of the heated core as shown in the base case. However, this void fraction degradation appears only at the core highest node and there is no impact on the PCT. The noding scheme for the upper plenum is consistent between the experimental test calculation and the US-APWR SBLOCA calculation.

References:

1. RELAP5-3D Code Manual Volume IV: Models and Correlations, INEEL-EXT-98-00834, Revision 2.4, June 2005.
2. B. Chexal and G. Lellouche, A Full-Range Drift-Flux Correlation for Vertical Flows (Revision 1), EPRI NP-3989-SR, September 1986.

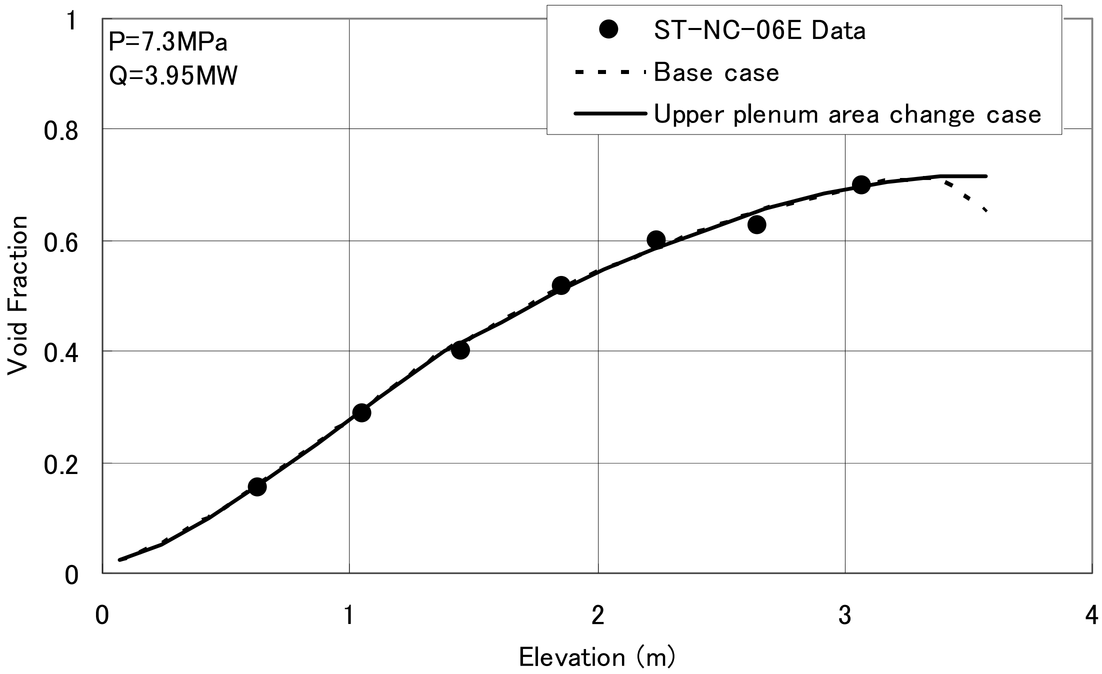

Figure 8.1.1-7.1 Sensitivity Calculation for Upper Plenum Flow Area

REQUEST 8.1.2-1

Figure 8.1.2-2 shows a “shroud plenum annulus”. Is this space filled with water? Is there any water flowing through this space? How is this space handled in the test and the simulation?

RESPONSE

As described in Section 5.2.1.2 (a) of MUAP-07013-P (R0), the bottom of the “shroud plenum annulus” was connected to the pressurizer surge line and the top of the annulus to the test section (heater section) outlet. Flow through the annulus was controlled by opening or closing valves equipped in these inlet and outlet lines.

Referring to descriptions in terms of the test procedure (Ref.1), both inlet and outlet line valves were left open to facilitate rapid equalization of the test section and annulus mixture-levels during the boiloff process prior to the measurement. Once steady-state was reached, the lines were closed, thus isolating the annulus from the rest of the system, starting the data scan (about 20 seconds). This operation prohibited unfavorable flow leakage from the test section to the annulus during the data measurement. Hence, mixture level was formulated in the annulus region without any flow communication to the rest of the system during the measurement period.

[

]

References

1. T. M. Anklam et al., Experimental Investigations of Uncovered-Bundle Heat Transfer and Two-Phase Mixture-Level Swell under High-Pressure Low-Heat Conditions, NUREG/CR-2456, ORNL-5848, 1982.

REQUEST 8.1.2-2

[

]

RESPONSE

[

]

REQUEST 8.1.2-3

[

]

RESPONSE

[

]

REQUEST 8.1.2-4

How is the “measured mixture level” (in Figures 8.1.2-7 and 8.1.2-30) determined in the tests? How is the predicted mixture level (in Figure 8.1.2-30) defined and calculated?

RESPONSE

In the experiment, the two-phase mixture level was identified by observing the average temperature at the FRS (fuel rod simulator) thermocouple levels. The measured two-phase mixture levels in Figures 8.1.2-7 and 8.1.2-30 of MUAP-07013-P (R0) were assumed to be midway between the highest level where the average temperature of thermocouples indicated nucleate boiling and the lowest where the average temperature indicated dryout. This is described in Section 5.2.1.2 (4) b of MUAP-07012-P (R0).

Similarly, the two-phase mixture-level predicted by M-RELAP5 was defined to be midway between the highest calculation node where the convective heat transfer mode of the FRS indicated nucleate boiling and the lowest calculation node where the heat transfer mode showed dryout. **[**

]

REQUEST 8.1.2-5

Section 8.1.2.3 states that “Eventually, the THTF settled into a quasi-steady state with the bundle partially uncovered and inlet flow just sufficient to make up for the liquid being vaporized.” Then, please explain why the mass fluxes of Tests K and CC in Table 8.1.2-1 are widely different (2.22 vs. 7.22) for the similar pressure, inlet subcooling and linear heat power. (Comparison of J and AA also.) (Also test FF, which has a higher pressure and higher subcooling, has a higher mass flux, i.e. higher vapor production, than test K for the same power, which is an anomaly). Did all tests result in vaporizing 100% of the incoming liquid? Please provide a table showing the SS energy balance for each test (i.e., Outlet enthalpy- Inlet enthalpy= Heat Input - loss).

RESPONSE

THTF 3.09.10I to N test series was primarily conducted to obtain the heat transfer data in the uncovered-bundle region, where the remarkable two-phase mixture level was formulated in the test section by reducing inlet flow sufficient to make up for the liquid being vaporized. Therefore, much of input thermal power was consumed for steam heat-up to maintain the long uncovered-bundle region.

On the other hand, THTF 3.09.10AA to FF test series was conducted to measure the longer void distribution, where the mixture-level approached the top of the test section as shown in Figures 8.1.2-23 to 8.1.2-28 of MUAP-07013-P (R0). In this latter test series, much of the input power was consumed for coolant boiling, less than the thermal power necessary to maintain longer uncovered-bundle region.

The difference in the generated uncovered-bundle length between two test series induced the different input thermal power (different steady-state heat balance) even under the similar inlet flow, temperature, and pressure conditions, as recognized in comparison between Tests K and CC.

The above explanation is valid also in comparison among Tests K, CC and FF. Test FF had a higher pressure and higher subcooling than Tests K and CC. Hence, Test FF needed higher thermal power to vaporize all the inlet coolant than that of test CC, if inlet flows in Tests CC and FF had been same. Namely, smaller inlet flow was necessary to be fully vaporized in Test FF than Test CC under the same thermal power condition. Finally, Test K resulted in the smaller inlet flow than Tests CC and FF to maintain longer uncovered-bundle region as described above.

Table RAI-8.1.2-5.1 shows the steady-state heat balance based on the measured data for each test (Ref.1). This table validates that input energy meets the exit energy with good accuracy, although slightly large deviations are found in a few cases.

References

1. T. M. Anklam et al., Experimental Investigations of Uncovered-Bundle Heat Transfer and Two-Phase Mixture-Level Swell under High-Pressure Low-Heat-Flux Conditions, NUREG/CR-2456, ORNL-5848, 1982.

Table RAI-8.1.2-5.1 Measured Heat Balance Data for THTF 3.09.10 Test Series

Test	(a)FRS Thermal Power (kW)	(b) Heat Loss (kW)	[fraction]	Pressure (MPa)	Mass Flux (kg/m^2s)	Inlet Temperature (K)	Outlet Temperature (K)	(c) Inlet Flow Energy (kW)	(d) Outlet Flow Energy (kW)	{(a)-(b) +(c)-(d)}/(d) (-)
3.09.10I	487.19	8.61	[0.018]	4.50	29.76	473.0	774.1	156.24	629.70	0.81%
3.09.10J	234.82	12.13	[0.052]	4.20	12.93	480.3	728.4	70.49	266.53	10.00%
3.09.10K	70.23	12.33	[0.176]	4.01	3.13	466.5	935.0	15.87	73.41	0.48%
3.09.10L	476.22	8.13	[0.017]	7.52	29.11	461.3	715.6	143.76	582.54	5.03%
3.09.10M	223.85	9.46	[0.042]	6.96	13.38	474.4	746.5	70.85	274.69	3.84%
3.09.10N	103.14	16.73	[0.162]	7.08	4.60	473.1	947.9	24.21	108.10	2.33%
3.09.10AA	278.71	5.58	[0.020]	4.04	21.15	450.9	547.0	98.27	373.50	-0.56%
3.09.10BB	140.45	4.83	[0.034]	3.86	9.44	458.2	540.8	45.73	166.98	8.61%
3.09.10CC	72.42	2.53	[0.035]	3.59	7.22	467.6	531.6	36.81	126.91	-15.92%
3.09.10DD	283.10	8.46	[0.030]	8.09	19.82	453.4	595.4	93.67	350.88	4.97%
3.09.10EE	140.45	5.52	[0.039]	7.71	11.00	455.9	581.0	52.71	192.47	-2.51%
3.09.10FF	70.23	6.46	[0.092]	7.53	4.83	451.4	565.8	22.56	83.45	3.46%

REQUEST 8.1.2-6

How was the fractional heat loss in Table 8.1.2-1 determined (measured, or calculated to match the energy balance)? Why are they widely different from less than 2% to 17%?

RESPONSE

As described in the end of Section 5.2.1.2 (1) b of MUAP-07013-P (R0), heat loss was calculated by ORNL based on the measured thermocouple data. A typical instrumentation site consisted of a pair of thermocouples embedded in the shroud box wall as illustrated in Figure 5.2.1.2-6 of MUAP-07013-P (R0). Because the thermocouples were equipped separately in the radial direction, heat loss could be determined by the temperature gradient. Pairs of thermocouples were settled at the various axial levels as shown in Figure 5.2.1.2-7 of MUAP-07013-P (R0), and each local heat loss was spatially integrated to obtain the total heat loss from the test section.

The test report (Ref.1) describes that the fractional heat loss was dependent on the spatial position, if there existed a longer uncovered-bundle region. Heat loss in the upper portion of the test section was greater than in the lower portion, because the larger temperature gradient across the shroud box occurred in the upper portion due to superheated steam. This indicates that the fractional heat loss was significantly sensitive to the uncovered-bundle length, as demonstrated by the relation between the measured mixture-level and fractional heat loss in Figure RAI-8.1.2-6.1. A relevant description is given in Section 8.1.2.5 of MUAP-07013-P (R0).

References

1. T. M. Anklam et al., Experimental Investigations of Uncovered-Bundle Heat Transfer and Two-Phase Mixture-Level Swell under High-Pressure Low-Heat Conditions, NUREG/CR-2456, ORNL-5848, 1982.

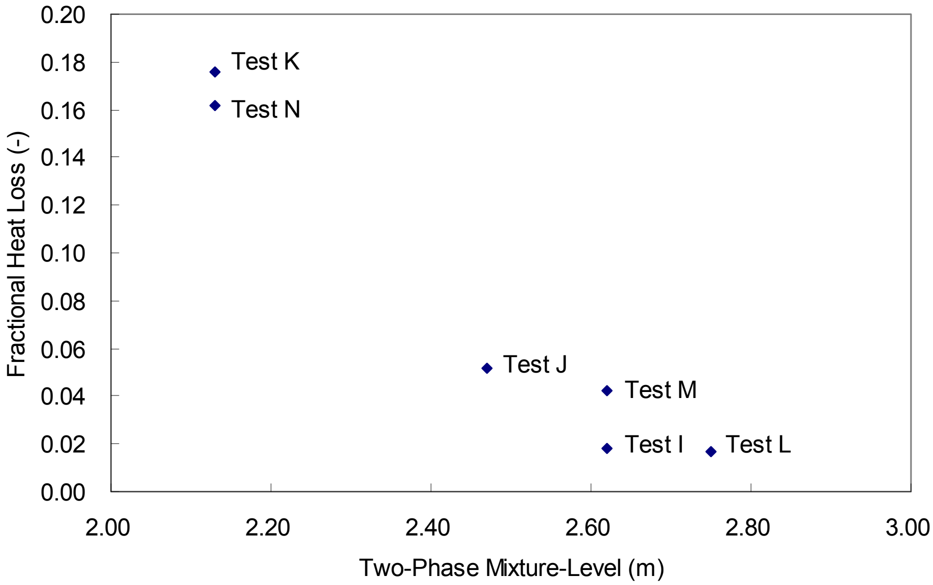

Figure RAI-8.1.2-6.1 Relation between Measured Mixture-Level and Fractional Heat Loss

REQUEST 8.1.2-7

It is observed in Section 8.1.2.5 that “in most cases the calculated void fractions are slightly larger than the experimental values.” Please discuss the implication of this observation, particularly in relation to the mixture level. Is this systematic deviation, an indication of the code deficiency?

RESPONSE

M-RELAP5, as well as RELAP5-3D, determines the void profile based on the liquid-vapor interfacial shear derived by the Chexal-Lellouche drift-flux model for the rod bundle geometry. By investigating the calculated results in terms of THTF 3.09.10AA to FF, it is found that M-RELAP5 slightly overestimates the void fraction under the lower pressure condition (Tests AA to CC) and accurately reproduces the measurement under the higher pressure condition (Tests DD to FF). The similar tendency can be recognized in the original report of the Chexal-Lellouche drift-flux model (Ref.1). A tendency observed in the uncovered-bundle heat transfer tests (Tests I to N) is to be discussed in the response to REQUEST 8.1.2-9.

Overestimation in predicted void fraction generally tends to induce the higher two-phase mixture swell. However, its impact is quite limited, because the mixture-level is significantly sensitive to the transition void fraction that defines the boundary from the churn flow regime (two-phase flow) to the mist flow regime (mixture-level generation). The transition void fraction is known to be dependent on pressure, coolant flow and void fraction itself, and affects the velocity slip between liquid and vapor (the liquid-vapor interfacial shear in the two-fluid model as employed in M-RELAP5 code), determining where the mixture-level can be formed. Again, the interfacial shear is determined by the Chexal-Lellouche drift-flux model in M-RELAP5.

In conclusion, M-RELAP5 is able to accurately predict the measured mixture-level as shown in Figure 8.1.2-30 of MUAP-07013-P (R0), which is an evidence that the interfacial shear model in M-RELAP5 is sufficiently valid not only for the void profile prediction but also for the transition void fraction to determine the mixture-level.

References

1. B. Chexal and G. Lellouche, A Full-Range Drift-Flux Correlation for Vertical Flows, EPRI-NP-3989-SR Revision 1, 1986.

REQUEST 8.1.2-8

The calculated vapor temperature is higher than measured (by about 20K) in Figure 8.1.2-9. Based on the energy balance shouldn't they be the same? Please explain (Note that boundary conditions, i.e., inlet temp, flow rate, vapor pressure and heat generation, are the same.) Is this due to entrainment?

RESPONSE

MHI would like to refer to the comments by ORNL in terms of the vapor temperature measurement (Ref.1). The vapor temperature was derived by two methods. In one method, the vapor temperature was based on local vapor temperature measurements made by the thermocouple array rods described in Section 5.2.1.3 of MUAP-07013-P (R0). In the other method, an energy balance was employed to back calculate the vapor temperature in the heated bundle from the vapor temperatures measured at the end of the heated length by the subchannel thermocouple rake. When heat transfer coefficients were calculated using the two methods, excellent consistency was observed for the high mass-flux tests. At very low flow rates, however, the two methods diverged widely, and the energy balance method appeared to yield the most reasonable results. Although the reason for this discrepancy was not fully understood, installation and fabrication problem were suspected regarding thermocouple array rods measurements. ORNL used the energy balance method in all their heat transfer calculations. Therefore, all the temperature distributions shown in MUAP-07013-P (R0) are based on the energy balance method. Uncertainty of the vapor temperature by the energy balance was computed by propagating uncertainties in the physical parameters used for the method. Details of the methods are given in Appendix A of Reference 1.

The test report indicates that the measurement errors for the vapor temperature were about 21K (Test J), 37K (Test K), 14K (Test M), and 18K (Test N), respectively (Ref.1). Thus, the reported uncertainty is about the same as the discrepancy between the calculated and measured values. The measurement error was not so large as to invalidate the code assessment.

The discrepancy between the calculated and measured vapor temperatures is also affected by the uncertainties in the measured parameters used as boundary conditions for the calculations. The uncertainties in the measured mass flux (4.1%), pressure (2.0 - 9.9%), inlet temperature (3.7 - 10.3K), bundle power (1.1%), and bundle heat loss all affect the calculated vapor temperature. Thus, the discrepancy between the calculated and measured vapor temperatures can be accounted for by uncertainties in the measurements. The uncertainties specified above are discussed in Appendix D of Reference 2.

References

1. T. M. Anklam et al., Experimental Investigations of Uncovered-Bundle Heat Transfer and Two-Phase Mixture-Level Swell under High-Pressure Low-Heat Conditions, NUREG/CR-2456, ORNL-5848, 1982.
2. D. K. Felde et al., Facility Description - THTF MOD 3 ORNL PWR BDHT Separate-Effects Program, NUREG/CR-2640, ORNL/TM-7842, 1982.

REQUEST 8.1.2-9

The large difference and a sudden jump of void fractions in Figure 8.1.2-11 for Test K was explained by heat loss at boundary (Section 8.1.2.5). But this was observed only in this test and not in Test N where the heat rate and mass flux were similarly low, and heat loss was similarly high. Explain this anomaly.

RESPONSE

As discussed in MHI response to REQUEST 8.1.2-6, the uniform axial variation of heat loss assumed in MUAP-07013-P (R0) caused the heat loss below the mixture level to be larger than in the actual test. This increased heat loss below the mixture level reduces the void fraction, and thus causes the flow regime transition from bubbly/churn flow to mist flow to occur at a higher spatial position in the calculations. This was particularly apparent in Tests K and N because these two tests each had a relatively large heat loss.

A change in heat loss below the mixture level affects both the steam quality and the void fraction. However, the impact on the void fraction becomes larger in a low pressure test (Test K, 4.01MPa) than in a high pressure test (Test N, 7.08MPa) as shown in Figure RAI-8.1.2-9.1 (Ref.1), even if the change in steam qualities (which depends on the change in the heat loss) is the same in the two cases. This phenomenological investigation indicates that the possible uncertainty in heat loss below the mixture level affects the void distribution more significantly in Test K than in Test N.

Next, MHI has conducted additional sensitivity studies to make clear how the spatial variation in heat loss affects the void distributions for Tests K and N. In the sensitivity calculations, the spatial variation of heat loss is tentatively simulated by imposing a temperature distribution on the outer surface boundary of the shroud box wall. The temperature below the mixture level of the test section is assumed to be subcooled (the saturation temperature minus 12K is assumed for both Tests K and N), and the temperature above the mixture level to be saturated. The heat transfer coefficient of the wall surface is assumed to be axially uniform, and is adjusted to reproduce the total heat loss measured in the experiment (Ref.2). Although these boundary conditions are assumed rather than measured (Ref.2), these can simulate a reasonable spatial variation of the heat loss with elevation that can be compared with the base case.

Figures RAI-8.1.2-9.2 and 3 compare the results from the sensitivity calculations with the base cases, which assumed a uniform heat loss distribution, for Tests K and N, respectively. In Test K, the sensitivity calculation provides a better agreement with the measurement, in particular, in the spatial location where the flow regime transits from bubbly/churn to mist. A much smaller change is observed in Test N. Therefore, these sensitivity studies validate the MHI comment that the uniform heat loss distribution employed in MUAP-07013-P (R0) affected the calculated void distribution, especially in Test K.

In conclusion, MHI judged that M-RELAP5 is able to reproduce the void distribution measured in the THTF tests reasonably well when a uniform spatial variation of heat loss is assumed. This assumption slightly increases the uncertainty in the analysis results, particularly for the large heat loss test under the low pressure condition. However, the uncertainty never disturbs the conclusion of MUAP-07013-P (R0) in terms of the M-RELAP5 validation using THTF void profile test data as discussed above.

References

1. A. Inoue et al., Void Measurement of BWR Fuel Assembly, J. Atomic Energy Society of Japan, 37, 8, pp710-720, 1995 (*in Japanese*).
2. T. M. Anklam et al., Experimental Investigations of Uncovered-Bundle Heat Transfer and Two-Phase Mixture-Level Swell under High-Pressure Low-Heat Conditions, NUREG/CR-2456, ORNL-5848, 1982.

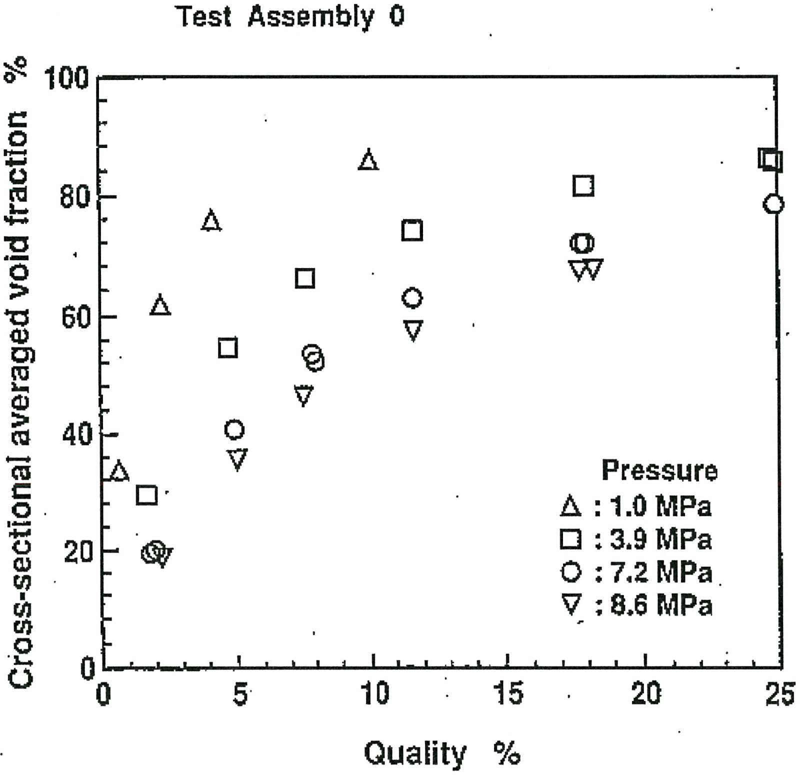

Fig. 7 Effect of pressure and quality on void fraction

Figure RAI-8.1.2-9.1 Pressure and Quality Sensitivities to Void Fraction (Ref.1)

Figure RAI-8.1.2-9.2 Void Distribution with Space-Dependent Heat Loss Condition (Test K)

Figure RAI-8.1.2-9.3 Void Distribution with Space-Dependent Heat Loss Condition (Test N)

REQUEST 8.1.2-10

1) The measured heat transfer coefficients in the vapor region generally increases rapidly with temp increase while the calculated coefficients generally unchanged, indicating the MRELAP5 model may be deficient. Explain this discrepancy between data and model prediction.

2) In three (J, M, N) of the four tests, the measured heat transfer coefficients show sudden drops after peaking in the vapor region. Are these considered real? Is there any concern that these are not shown in the simulations, and thus the M-RELAP5 model may be deficient. Explain.

RESPONSE

1) THTF test report (Ref.1) describes as follows: '*The shape of the heat transfer profiles is the combined result of changes in convective heat transfer, radiative transfer, and grid effect. The axial variation in convective heat transfer tends to be dominated by variations in viscosity and vapor thermal conductivity. Viscosity increases with vapor temperature and thus elevation; this caused the vapor Reynolds number to decrease with elevation. Conductivity increases with vapor temperature and thus elevation as well. Therefore, increases in conductivity tend to offset decreases in Reynolds number. The result is that the convective heat transfer coefficient, excluding grid effects, can either increase or decrease with elevation, depending on particular test conditions. In all tests with the exception of 10M the convective heat transfer coefficient is calculated to increase overall with respect to elevation. The radiative heat component of heat transfer increases with elevation in all tests.*'

In the experimental investigation, the total heat transfer was determined from the measured FRS and steam vapor temperatures, while the radiative heat transfer (radiation to vapor) was calculated by using the Hottel empirical method (Ref.2) with the measured temperatures. The convective heat transfer component was derived by subtracting the radiative component from the total heat transfer data.

In M-RELAP5, the wall heat transfer to the single-phase vapor is computed as follows:

$$Nu = Max\left(Nu_{ForcuedTurbulent}, Nu_{ForcedLa\min ar}, Nu_{Free}\right).$$

The turbulent forced convection $Nu_{ForcedTurbulent}$, the laminar forced convection $Nu_{ForcedLa\min ar}$, and the natural convection Nu_{Free} are based on the Dittus-Boelter correlation, Sellars ($Nu = 4.6$), and the Churchill-Chu or McAdams correlations, respectively. It can be concluded that the turbulent forced convection (modeled by the Dittus-Boelter correlation in M-RELAP5) dominated the overall convective heat transfer for the THTF uncovered-bundle tests, because the vapor Reynolds numbers estimated in the test report (Ref.1) were generally greater than 2,000, which places the tests in the turbulent regime (Ref.3). The spatial variation in the M-RELAP5 heat transfer coefficient must be discussed carefully as follows.

First, the convective enhancement due to abrupt flow area change at the grid position is not accounted in the current M-RELAP5 modeling for the THTF analysis. This resulted in no rapid increase in the calculated heat transfer coefficient near the grid position, which was observed in the measured data. Details are to be discussed in the response to item 2) of this REQUEST.

Second, M-RELAP5 has no explicit radiative heat transfer model for the single-phase vapor convection mode. This significantly affects the spatial variation, because the radiative heat transfer increased with elevation in all the tests. The measured heat transfer coefficient is decomposed to the convective and radiative components (digital data of these two components are reported in Appendix B of the test report (Ref.1) with their uncertainties), which are compared with the M-RELAP5 heat transfer coefficient in Figures RAI-8.1.2-10.1 to 4.

The figures show that the measured convective heat transfer coefficient either increases or decreases with elevation, depending on the test, while the measured radiative component always increases with elevation. Furthermore, the spatial variation of the M-RELAP5 heat transfer coefficient tends to agree with that of the measured convective heat transfer coefficient except for Test K. MHI suspects that uncertainty of the measured radiative heat transfer might distorted the accuracy of the convective heat transfer, particularly in the upper portion of the test bundle, for Test K, because the error in the radiative component was significantly larger than in the other tests. (Note that the convective heat transfer was obtained by subtracting the radiative component from the total heat transfer in the experiment, again.)

Figures RAI-8.1.2-10.1 to 4 also show that the heat transfer coefficient computed by M-RELAP5 based on the Dittus-Boelter correlation is generally larger than the measured convective component. A similar result was reported by Reference 1. However, by neglecting the radiative component, the M-RELAP5 heat transfer coefficient in the steam cooling region is generally less than the measured total heat transfer coefficient. This can be the conservative basis for the code application to safety analyses.

In conclusion, M-RELAP5 tends to reproduce spatial variations observed in the measured convective heat transfer which can either increase of decrease with elevation, depending on particular test conditions. This implies that M-RELAP5 physically simulates the phenomena relevant to the convective vapor heat transfer. In addition, M-RELAP5 has no explicit model specific to the radiative heat transfer in the steam cooling mode. Thus, the code tends to generate smaller values than the measurements in terms of the total heat transfer coefficient, which results in the prediction of conservative wall temperatures.

2) THTF test report (Ref.1) describes that the sudden change in the heat transfer was due to the grid effect on local heat transfer. The effect can be generally classified under the following mechanism: (1) convective enhancement, (2) grid rewet by droplet impingement, and (3) droplet breakup. In the THTF uncovered-bundle heat transfer test, there occurred few droplets because of its extremely low inlet coolant flow, and then the first mechanism, convective heat transfer enhancement by abrupt flow area change at the grid position, could be the dominant factor. This grid effect tends to be greater under the higher Reynolds condition as shown in Figure RAI-8.1.2-10.5 (Ref.4). Therefore, a remarkable convective enhancement was not found in the lower inlet flow test, Test K. (See Figure RAI-8.1.2-10.6.)

In M-RELAP5 modeling for the THTF test analysis, the abrupt flow area change at the grid position is ignored so that the code appropriately computes vapor and liquid momentum sources at the numerical junctions (including the grid positions) which determine the void distribution, as well as in modeling for the US-APWR SBLOCA analysis. Hence, the convective enhancement due to the grid is not addressed in the current M-RELAP5 analysis, as described in Section 8.1.2.6 of MUAP-07013-P (R0).

From the viewpoint of the conservative basis in safety analyses, the above modeling in M-RELAP5 tends to compute smaller heat transfer coefficient than a case where any grid effect model is taken into account, leading to a higher peak cladding temperature value.

References

1. T. M. Anklam et al., Experimental Investigations of Uncovered-Bundle Heat Transfer and Two-Phase Mixture-Level Swell under High-Pressure Low-Heat Conditions, NUREG/CR-2456, ORNL-5848, 1982.
2. H. C. Hottel and A. F. Sarofilm, Radiative Transfer, McGraw-Hill, New York, 1967.
3. B. Metais and E. R. G. Eckert, Forced, Mixed, and Free Convection Regimes, J. Heat Transfer, **86**, 295, 1964.
4. USNRC, Compendium of ECCS Research for Realistic LOCA Analysis, NUREG-1230 Revision 4, 1988.

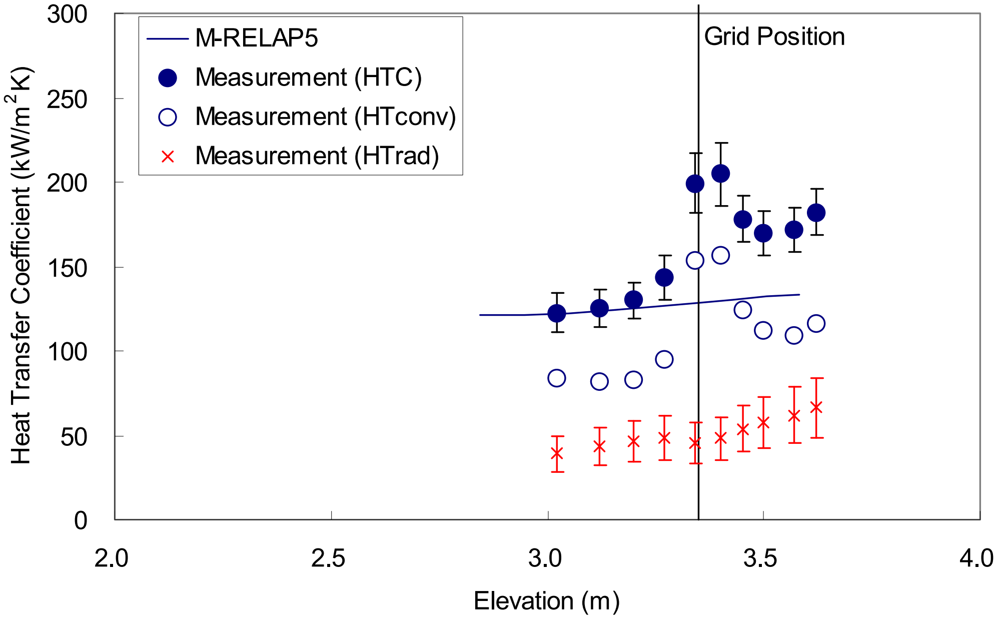

Figure RAI-8.1.2-10.1 Comparison between Calculated and Measured HTC (Test J)

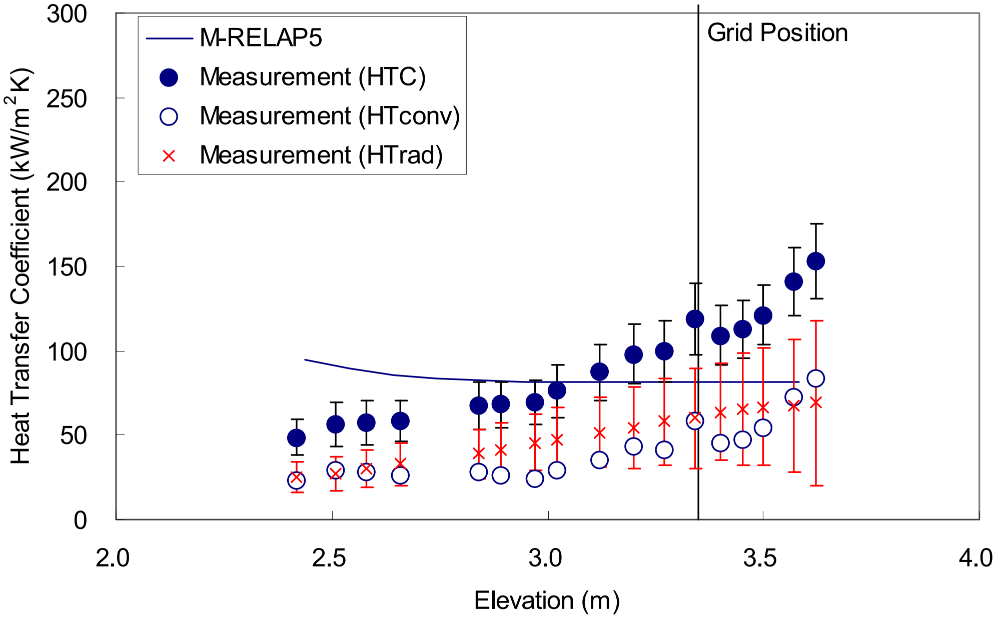

Figure RAI-8.1.2-10.2 Comparison between Calculated and Measured HTC (Test K)

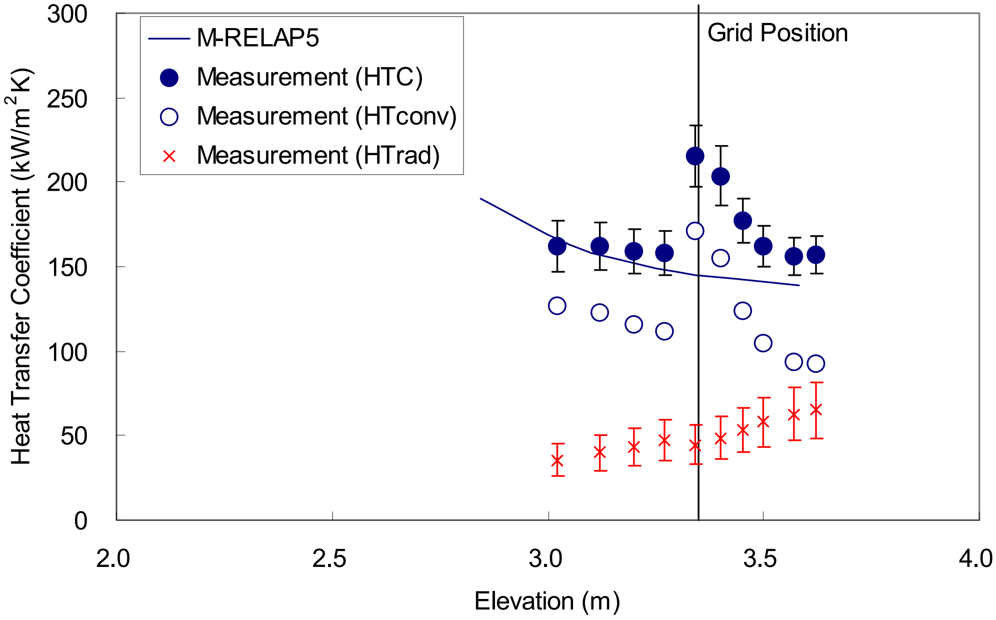

Figure RAI-8.1.2-10.3 Comparison between Calculated and Measured HTC (Test M)

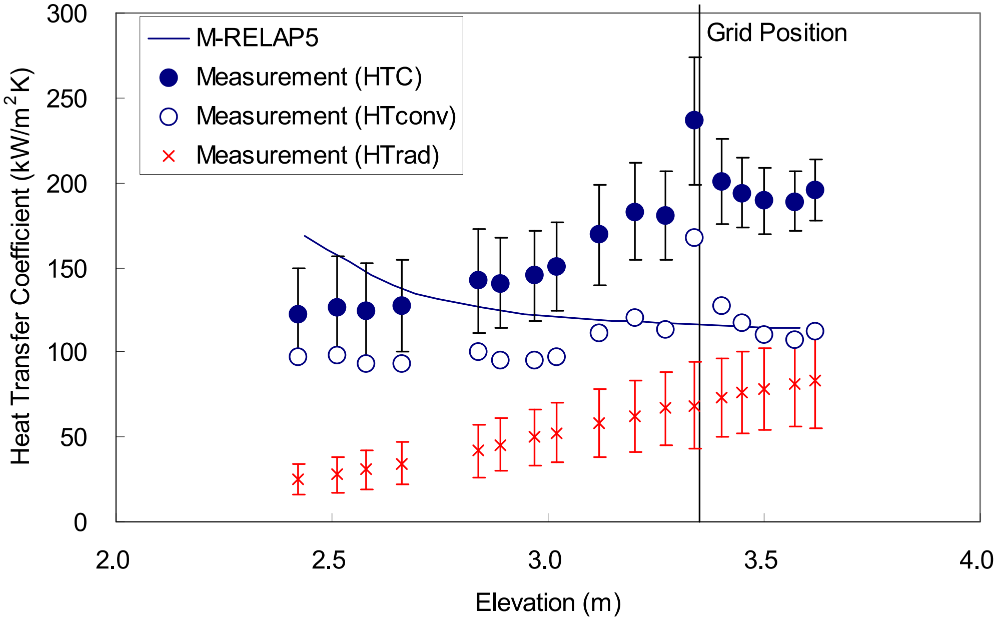

Figure RAI-8.1.2-10.4 Comparison between Calculated and Measured HTC (Test N)

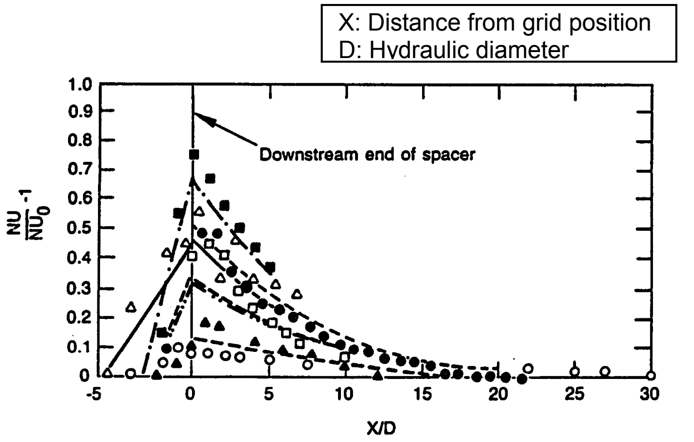

Symbol	Author	Type of grid reported in reference —	Re x 10^{-4}	ϵ	Calculated $\frac{NU}{NU_0}-1$ $= 5.55\,\epsilon^2$
■	REHME	B.3	12.7	0.348	0.672
△	VELCEK	6 cm	15.5	0.289	0.463
●	KIDD	4.3	5	0.245	0.333
□	KRETT	C	9.5	0.303	0.509
▲	VELCEK	5 mm	12.5	0.237	0.311
○	HUDINA	Lb. smooth	1.5-5	0.156	0.135

6 9324

Figure 6.4-50. Heat transfer near straight spacers in single-phase flow.

6.4-70

Figure RAI-8.1.2-10.5 Grid Effect Dependency on Reynolds Number (Ref.4)

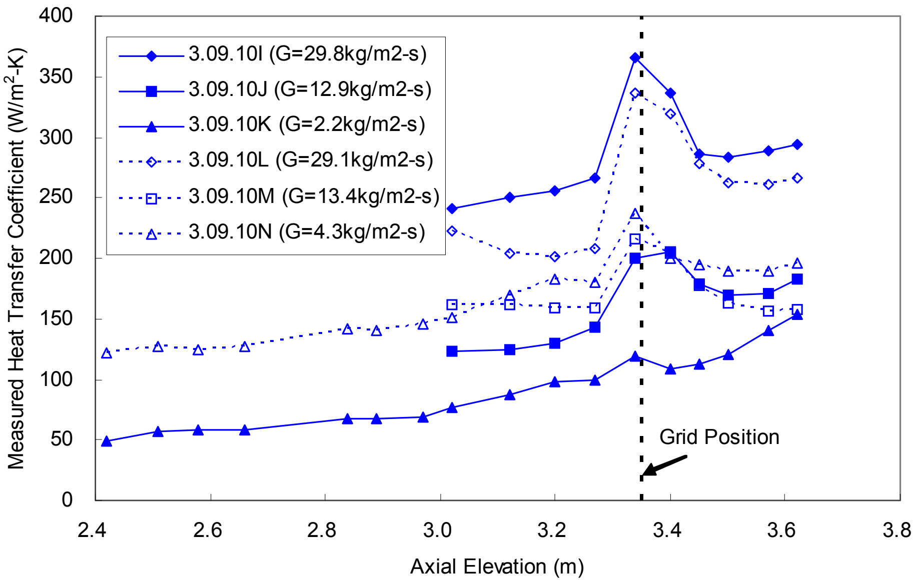

Figure RAI-8.1.2-10.6 Measured Heat Transfer Profile in THTF Experiments

REQUEST 8.1.2-11

Provide more detailed explanations of sensitivity study 1. Are these simulations only or also tests? (It appears the measured levels of tests are unchanged. What is the significance of comparing cases of different power level?)

RESPONSE

As described in Section 6 and 7 of MUAP-07013-P (R0), M-RELAP5 has been developed based on the best-estimate code RELAP5-3D with inclusion of Appendix K conservative models listed in Table 7.1.1-1. However, no conservative treatment and modification is directly taken into account for the models relevant to the two-phase mixture-level evaluation, thus the M-RELAP5 shows its best-estimate predictability for the mixture-level as shown in Figure 8.1.2-30.

A conservative basis for safety analysis exists in treatment of the thermal power; core decay power is simulated by the ANS 1971 model with multiplication factor of 1.2. This hypothetically causes larger vaporization, inducing longer uncovered-bundle region and slower quench rate. In order to identify this conservatism, MHI had conducted a sensitivity analysis using the THTF mixture-level test data, where the FRS power level was tentatively increased to the 1.2 times of the experimental value for the sensitivity study only. The results are shown in Figures 8.1.2-31 and 32 of MUAP-07013-P (R0) as ‘sensitivity 1’. It is found that the predicted mixture-level was conservatively depressed by about 20% in ‘sensitivity 1’ than the nominal result.

REQUEST 8.1.2-12

[

]

RESPONSE

[

]

REQUEST 8.1.2-13
(Related RAI 8.1.2-5)

The mass fluxes for Test K and N in Table RAI-8.1.2-5.1 are not the same as those in Table 8.1.2-1. This should be clarified. Also, note there is substantial energy imbalance, especially for tests J, BB and CC (Some of them are more than 15%. They will be even larger when divided by (d)-(c) rather than (d).)

Discuss the impact of these imbalance on the conclusion that the code prediction is reasonable and validates the code.

RESPONSE

First, the boundary condition in terms of the mass flux used for M-RELAP5 THTF test analysis is described as follows. In the experiment, the volumetric flow rate was measured both at the channel inlet and outlet sections, and one low-flow orifice meter and one turbine meter were equipped at each of the inlet and outlet sections. The fluid density was also measured by using the densitometer equipped in the outlet spool piece to determine the mass flux from the volumetric flow rate. However, the experimental test report states that the vapor density computed from the measured pressure and steam temperature was used in determining the mass flux at the channel outlet. As discussed later, there observed significant uncertainties in the measured steam temperature; therefore, the mass flux at the inlet channel section is used throughout the M-RELAP5 calculation with the exception of the ultimately high flow tests (Tests I and L) where the inlet mass fluxes were not correctly measured. It is noted that the Tests I and L are excluded from our code assessment database because of the higher power density in comparison with that expected in the actual plant accident.

Next is our consideration in confirming the heat balance from the test data. In the experiment, the vapor temperature distribution was determined from the energy conservation based upon the steam temperature measured by the subchannel thermocouple rake at the end of heated length. Although the vapor temperature distribution was directly measured by using the thermocouple array rods, the direct measurement indicated several unphysical behaviors, especially, for the ultimately low mass flux tests (Tests K and N). The details are described in Section 5.3.2.1 and Appendix A.5 of Reference 1.

In determining the experimental vapor temperature distribution for the upper portion of the test channel (steam cooling region), the measured outlet mass flux was used along with the energy conservation. Because a large deviation is found between the inlet and outlet mass fluxes only for the lower flow tests (Tests K and N), we decided to apply the mass fluxes measured at the outlet in derivation of the heat balance only for these two tests, while the measured inlet mass flux is used for the other tests as M-RELAP5 THTF test analysis. Test FF was also performed under the low flow rate condition. However, the measured two-phase mixture level was higher than Tests K and N and approached beneath the end of the heated length in Test FF. Under this condition, assumption of the steam only flow at the channel outlet was uncertain and the temperature distribution shall not be evaluated based on the energy conservation with the measured outlet mass flux. Therefore, the measured inlet mass flux was used in the heat balance calculation for Test FF.

The above is the reason why the mass fluxes for Tests K and N in Table RAI-8.1.2-5.1 (Ref.2) are not the same as those in Table 8.1.2-1 of MUAP-07013-P (R0). The mass fluxes used for each of the M-RELAP5 test analysis and heat balance calculation prepared for the NRC's request are compared with the measured inlet and outlet mass fluxes in **Table RAI-8.1.2-13.1**.

Hereafter, the imbalance observed in derivation of the heat balance calculation is discussed. As reviewer pointed out there remains a significant imbalance in the derived heat balance table as shown in **Table RAI-8.1.2-13.2**. To clarify possible sources of this imbalance, first, errors contained in the measured parameters used for the heat balance calculation are summarized in **Table RAI-8.1.2-13.3**, which are referred to appendices of the experimental test report (Ref.1). The table shows that significant measurement uncertainties (above 30%) were included in the measured fluid temperatures, while errors of the measured bundle power are below about 6 % and those of the mass flux are below 10% except for Test FF. Therefore, the uncertainties included in the measured parameters can be one of the possible sources.

MHI would like to give a comment regarding the significantly large uncertainty in the measured temperature. First, Section 5.3.2 of the experimental test report (Ref.1) shows that uncertainties of the bundle cross-section average vapor temperature were about ±50 °F (±28 K) near the end of the heated length for Test K, while Appendix A of the same report indicates uncertainties of the outlet temperature reached ±260 K. The latter uncertainties are shown in Table RAI-8.1.2-13.3, although the experimental test report mentions nothing about the difference between the two series of the uncertainties. One possibility is that the temperature shown in Section 5.3.2 may be the data obtained by the thermocouple array rods and the uncertainty is primarily corresponding to the equipment uncertainty and to the deviation caused by averaging several temperatures measured at the same axial elevation. On the other hand, the temperature shown in Appendix A may be obtained by the energy balance along with the vapor temperature measured by the subchannel thermocouple rake. For the latter, Section A.6 of the test report states "*Use of an energy balance to calculate vapor temperature requires computation of bundle heat losses*", and the heat loss was determined from axial integral of the measured temperature gradient across the test channel shroud box. This indicates a possibility that the temperature uncertainty shown in Appendix A involves the uncertainty due to the heat loss measurement and calculation in addition to the uncertainty of the thermocouple rake. In other words, the imbalance in the heat balance calculations may be due to the uncertainty of the heat loss in addition to the measurement uncertainties.

Second, in the mixture level swell tests, Tests AA to FF, where the mixture level was high approached beneath the end of the heated length, there possibly remains the liquid film and entrainment even at the channel outlet. In calculating the heat balance (Ref.2), on the other hand, we approximately assumed the steam only flow even for the mixture level swell tests. This may induce the additional uncertainty for Tests AA to FF.

The above are the possible sources of the imbalance appearing in the heat balance calculations, and MHI supposes that the primary sources come from the measurement uncertainties. The uncertainties are taken into account also in the measured uncovery heat transfer coefficient for Tests I to N, and in the mixture level swell for all the subject tests, independently from the heat balance calculations MHI performed.

Figures RAI-8.1.2-13.1 to RAI-8.1.2-13.6 compare the M-RELAP5 calculation results with the measurements in terms of the uncovery heat transfer and the collapsed and mixture level with the errors. Taking account the measurement uncertainties, M-RELAP5 is capable of predicting these key parameters with best-estimate or conservative accuracy. (Note that the axial variation of the predicted and measured uncovery heat transfer coefficient is addressed in MHI response to REQUEST 8.1.2-10 in Reference 2.) In addition, 2% increase in the core thermal power assumed for the US-APWR DCD Small Break LOCA analyses assures the sufficient conservatism required in the safety analyses.

References:

1. T. M. Anklam et al., Experimental Investigations of Uncovered-Bundle Heat Transfer and Two-Phase Mixture-Level Swell under High-Pressure Low-Heat Conditions, NUREG/CR-2456, ORNL-5848, 1982.
2. Mitsubishi Heavy Industry, Ltd., MHI's Partial Responses to NRC's Requests for Additional Information on Topical Report MUAP-07013-P (R0) "Small Break LOCA Methodology for US-APWR", UAP-HF-09002, January 16, 2009.

Table RAI-8.1.2-13.1 Mass Fluxes used for M-RELAP5 Test Analysis and Heat Balance Calculation

Test	Inlet Mass Flux ($kg/s/m^2$)	Outlet Mass Flux ($kg/s/m^2$)	Mass Flux$^{1)}$ ($kg/s/m^2$)	Mass Flux$^{2)}$ ($kg/s/m^2$)
3.09.10I	-	29.76	29.76	29.76
3.09.10J	12.93	12.66	12.93	12.93
3.09.10K	2.22	3.13	2.22	3.13
3.09.10L	-	29.11	29.11	29.11
3.09.10M	13.38	12.63	13.38	13.38
3.09.10N	4.33	4.60	4.33	4.60
3.09.10AA	21.15	20.26	21.15	21.15
3.09.10BB	9.44	9.62	9.44	9.44
3.09.10CC	7.22	5.03	7.22	7.22
3.09.10DD	19.82	19.48	19.82	19.82
3.09.10EE	11.00	9.62	11.00	11.00
3.09.10FF	4.83	3.85	4.83	4.83

1) Mass flux used for M-RELAP5 calculations.
Based on the inlet mass flux except for the high flow tests (Tests I and L).
2) Mass flux used for the heat balance calculations.
Based on the inlet mass flux except for the low and high flow tests (Tests, I, K, L, N)

Table RAI-8.1.2-13.2 Heat Balance Calculation Results

Test	(a)FRS Thermal Power (kW)	(b) Heat Loss (kW)	[fraction]	(c) Inlet Flow Energy (kW)	(d) Outlet Flow Energy (kW)	{(a)-(b) +(c)-(d)}/ (d)	{(a)-(b) +(c)-(d)}/ {(d)-(c)}
3.09.10I	487.19	8.61	[0.018]	156.24	629.70	0.81%	1.08%
3.09.10J	234.82	12.13	[0.052]	70.49	266.53	10.00%	13.59%
3.09.10K	70.23	12.33	[0.176]	15.87	73.41	0.48%	0.61%
3.09.10L	476.22	8.13	[0.017]	143.76	582.54	5.03%	6.68%
3.09.10M	223.85	9.46	[0.042]	70.85	274.69	3.84%	5.17%
3.09.10N	103.14	16.73	[0.162]	24.21	108.10	2.33%	3.00%
3.09.10AA	278.71	5.58	[0.020]	98.27	373.50	-0.56%	-0.76%
3.09.10BB	140.45	4.83	[0.034]	45.73	166.98	8.61%	11.85%
3.09.10CC	72.42	2.53	[0.035]	36.81	126.91	-15.92%	-22.43%
3.09.10DD	283.10	8.46	[0.030]	93.67	350.88	4.97%	6.77%
3.09.10EE	140.45	5.52	[0.039]	52.71	192.47	-2.51%	-3.46%
3.09.10FF	70.23	6.46	[0.092]	22.56	83.45	3.46%	4.74%

Table RAI-8.1.2-13.3 Measurement Errors relevant to Heat Balance Calculation

Test	Bundle Power		Inlet Temperature		Outlet Temperature		Mass Flux		Heat Loss	Mixture Level
	(kW)	Error	(K)	Error	(K)	Error	(kg/m^2/s)	Error	(-)	(m)
3.09.10I	487.19	5.3%	473.0	54.8%	774.1	33.5%	29.76	6.7%	0.02	2.62
3.09.10J	234.82	5.3%	480.3	53.9%	728.4	35.6%	12.93	4.8%	0.05	2.47
3.09.10K	70.23	6.3%	466.5	55.5%	935.0	31.3%	3.13	8.3%	0.18	2.13
3.09.10L	476.22	5.3%	461.3	56.2%	715.6	36.2%	29.11	5.6%	0.02	2.75
3.09.10M	223.85	5.4%	474.4	54.6%	746.5	34.7%	13.38	4.6%	0.04	2.62
3.09.10N	103.14	5.4%	473.1	54.8%	947.9	28.8%	4.60	5.9%	0.16	2.13
3.09.10AA	278.71	5.3%	450.9	57.5%	547.0	47.4%	21.15	3.0%	0.02	3.42
3.09.10BB	140.45	5.4%	458.2	56.5%	540.8	47.9%	9.44	6.7%	0.03	3.31
3.09.10CC	72.42	5.4%	467.6	55.4%	531.5	48.8%	7.22	8.7%	0.04	3.60
3.09.10DD	283.10	5.3%	453.4	57.2%	595.4	43.5%	19.82	3.2%	0.03	3.23
3.09.10EE	140.45	5.4%	455.9	56.8%	581.0	44.6%	11.00	5.8%	0.04	3.47
3.09.10FF	70.23	5.5%	451.4	57.4%	565.8	45.8%	4.83	13.2%	0.09	3.23

All the errors refer to the appendices of the experimental test report (NUREG/CR-2456).
Measurement uncertainty of heat loss from the channel is not available.

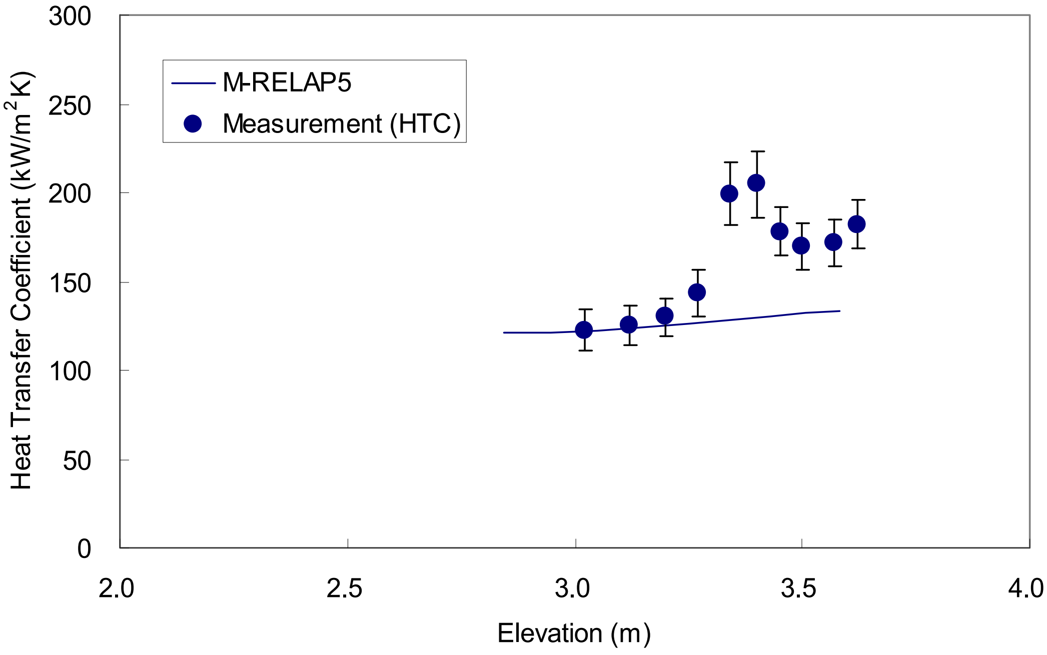

Figure RAI-8.1.2-13.1 Comparison Measured and Predicted Uncovery Heat Transfer Coefficients (Test J)

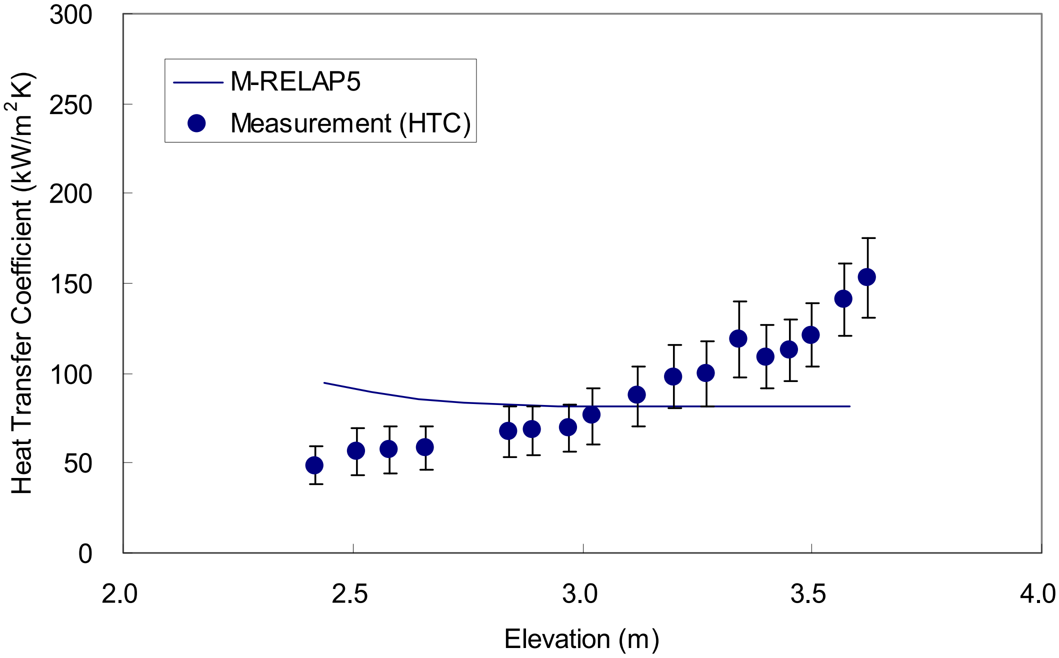

Figure RAI-8.1.2-13.2 Comparison Measured and Predicted Uncovery Heat Transfer Coefficients (Test K)

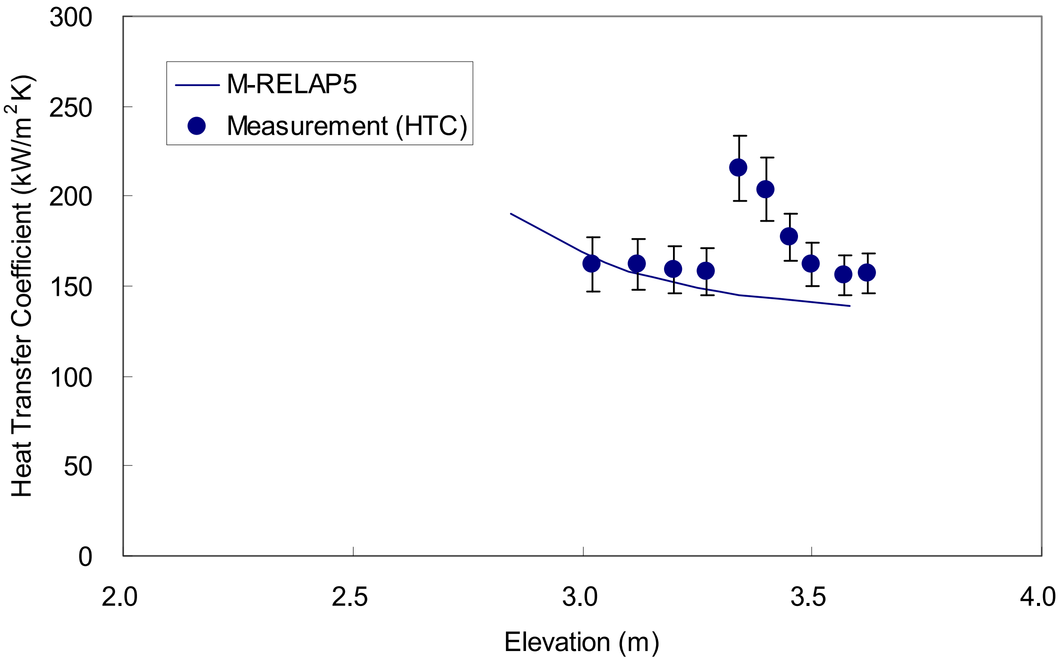

Figure RAI-8.1.2-13.3 Comparison Measured and Predicted Uncovery Heat Transfer Coefficients (Test M)

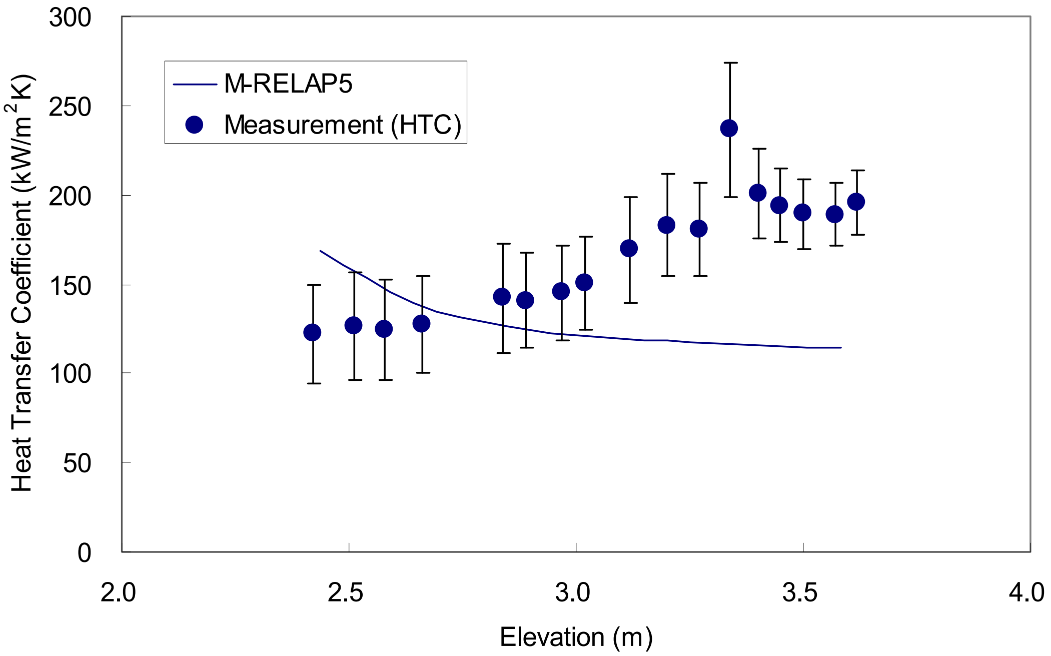

Figure RAI-8.1.2-13.4 Comparison Measured and Predicted Uncovery Heat Transfer Coefficients (Test N)

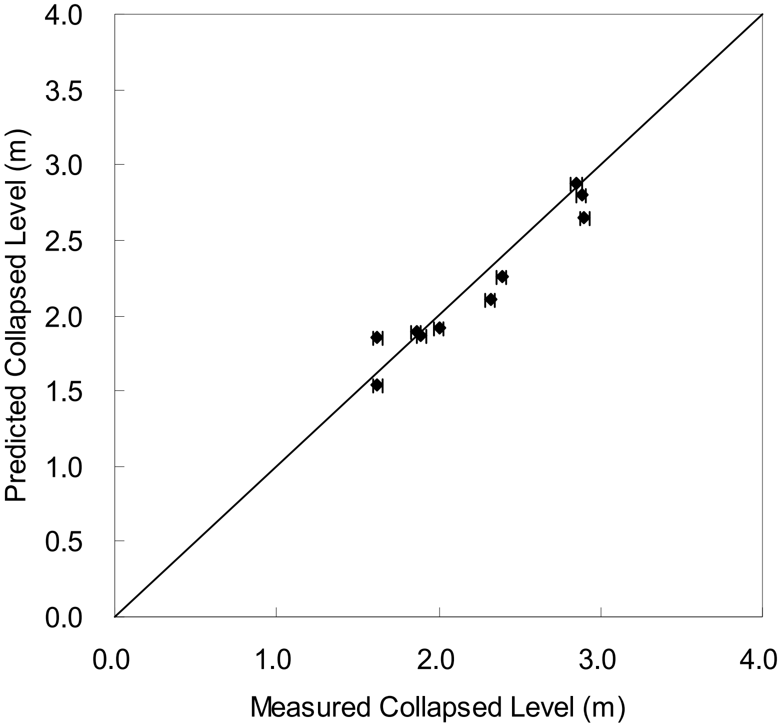

Figure RAI-8.1.2-13.5 Comparison Measured and Predicted Collapsed Levels

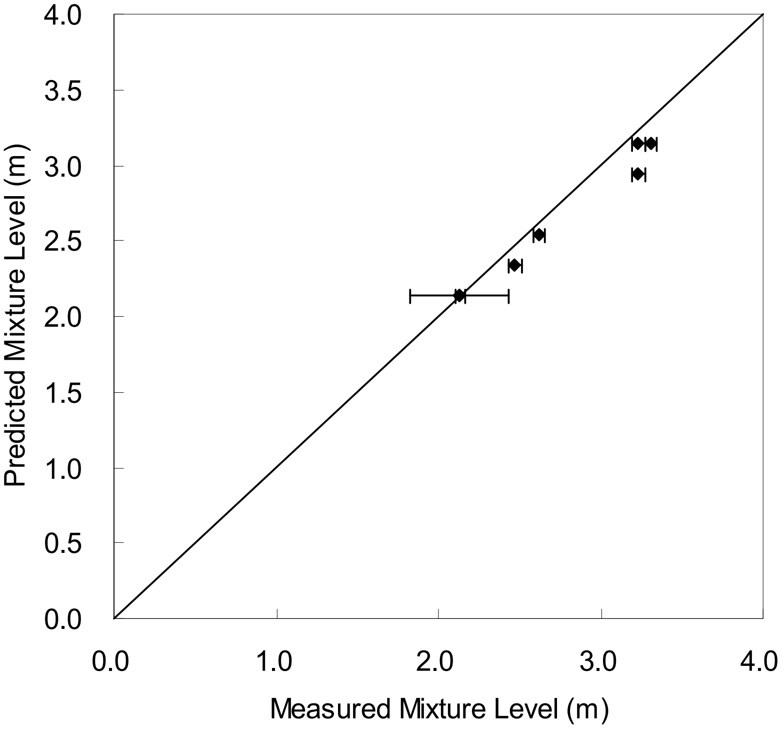

Figure RAI-8.1.2-13.6 Comparison Measured and Predicted Mixture Levels

REQUEST 8.1.2-14

[

]

RESPONSE

[

]

REQUEST 8.1.2-14-1

(Related RAI 8.1.2-14)

[

]

RESPONSE

[

]

[

]

REQUEST 8.1.2-14
(Related RAI 8.1.2-13)

The explanation provided in the July response (UAP-HF-09362) is difficult to follow and needs to be made more concise to directly respond to the question. The presence of significant uncertainties in the experimental data is known, although the ±260 K outlet temperature uncertainty quoted on page 44 does not appear to be correct. Address concisely the effect of the uncertainty on the code validation.

RESPONSE

(1) Mass Flux for Tests K and N
The mass fluxes in Table 8.1.2-1 of Reference 1 are based on the data measured at the test section inlet. On the other hand, the mass fluxes for Tests K and N in Table RAI-8.1.2-5.1 of Reference 2, which are used for the heat balance calculations, are based on the data measured at the test bundle outlet. The reason why the outlet mass flux data are used for the heat balance calculations is as follows:

In Reference 3, ORNL computed vapor temperatures for heat transfer calculations based on two methods. The first method was based on averaging local temperature measurements by the thermocouple array rods. The second method was based on vapor temperatures measured by a subchannel thermocouple rake at the outlet of the test bundle and an energy balance to extrapolate results back into the bundle (refer to Appendix A of Reference 3). The two methods were in excellent agreement for the high mass flux tests, but in poor agreement for very low mass flux tests, such as Tests K and N. As an example, Test K at the 2.42-m elevation was calculated to have a local-measurement-based Nusselt number of about 40 for a vapor Reynolds number of roughly 1900. If an energy balance is used for the same case, the Nusselt number is roughly 4.0, which is more consistent with a vapor Reynolds number typical of laminar flow. Consequently, ORNL used the second method to experimentally evaluate all the vapor temperatures and heat transfer coefficients of the steam region.

Therefore, the mass flux and exit temperature given in Table RAI 8.1.2-5.1 for Tests K and N were based on the measured outlet mass flux and the temperatures from the thermocouple rake consistent with the values used by ORNL in their heat transfer analysis based on the energy balance.

(2) Energy Balance
As described above, vapor temperatures and heat transfer coefficients of the steam region were experimentally derived from the energy balance with the mass flux measured at the bundle outlet. In other words, the energy balance must be evaluated using the mass flux measured at the bundle outlet when the vapor temperatures extrapolated from the temperature by the thermocouple rake are compared with the calculations in the M-RELAP5 code assessment.

In order to qualify the measured data, the energy balance calculation is revised in the present RESPONSE, in which the bundle outlet mass flow is used for all tests and the vapor temperature extrapolated from the thermocouple rake temperature is used when available. It is noted that the previously reported energy balance calculation in Table RAI-8.1.2-5.1 (Ref.2) employs the inlet mass fluxes and steam temperatures measured at the bundle outlet spool piece, except for Tests K and N. Table RAI-8.1.2-14.1 lists parameters used for the energy balance calculation reported here. The revised energy balances are shown in Table RAI-8.1.2-14.2, in which the error of energy balance is normalized to the outlet flow energy. Although small deviations in the energy balance remain, the result is generally improved compared to the previous one.

The uncertainties in the energy balance calculations are estimated by propagating the uncertainties due to power (heat flux), pressure, mass flow, and inlet and outlet temperatures, which are extracted from References 3 and 4 listed in Table RAI-8.1.2-14.3. The uncertainties in the table represent the 2σ error bands, which correspond to 95% confidence intervals. Deviations in the energy balances in Table RAI-8.1.2-14.2 are reasonably consistent with those expected based on the uncertainties due to the measurements.

The 260 K uncertainty for the inlet and outlet temperatures comes from Appendix B.1 of Reference 3, but is obviously in error. The temperature uncertainties shown in Table RAI-8.1.2-14.3 come from Appendix B.2 of Reference 3.

(3) M-RELAP5 Sensitivity Calculations
Sensitivities of the M-RELAP5 calculated results to the instrumentation uncertainties are investigated for the ORNL/THTF uncovered-bundle heat transfer tests. Power, pressure, inlet flow and temperature are used as boundary conditions, and the instrumentation uncertainties in power, pressure, flowrate and temperature are ±1.1%, ±0.2MPa, 4.1% and ±3.9K, respectively, as listed in Table RAI-8.1.2-14.3. The uncertainty in the inlet liquid temperature instrumentation (±3.9K) is significantly smaller than that in the outlet vapor temperature (±23.5K), which contains uncertainties due to the energy balance calculation to extrapolate the thermocouple rake temperature back to the bundle outlet temperature.

Sensitivity calculation results are shown in Figures RAI-8.1.2-14.1 to 5 for the power instrumentation uncertainty, Figures RAI-8.1.2-14.6 to 10 for the pressure instrumentation uncertainty, Figures RAI-8.1.2-14.11 to 15 for the flowrate instrumentation uncertainty, and Figures RAI-8.1.2-14.16 to 20 for the inlet temperature instrumentation uncertainty, respectively. The results contain the most important parameters from the safety analysis point of view, including the heater rod surface temperature distribution and two-phase mixture level for the Tests J, K, M, and N.

Sensitivities of the calculated results to the power, pressure and temperature instrumentation uncertainties are negligibly small. The sensitivity due to the flowrate instrumentation uncertainty is relatively larger than the others. However, the flowrate sensitivity is never significant enough to invalidate the M-RELAP5 results in Reference 1. Even when the flowrate is assumed to be higher than the measurement within 95% confidence (2σ), M-RELAP5 generally provides conservative predictions in terms of the heater rod temperature (Figures RAI-8.1.2-14.11 to 14). As for the mixture level, M-RELAP5 tends to predict slightly higher values than the measured (Figure RAI-8.1.2-14.15) with the higher flowrate, but the sensitivity is much smaller than when the Appendix K requirement for heater power (power multiplied by 1.2) is used, which is shown in Figure 8.1.2-32 of Reference 1. Because the mixture level is assumed to be at the center of the lowest node in the post-CHF heat transfer regime, even small changes in the dryout location (ex. Figure 8.1.2-14.14) can cause relatively big changes in the estimated mixture level (see Figure 8.1.2-14.15).

To summarize, sensitivities due to uncertainties in the input parameters are not significant, and the uncertainties do not change the conclusions discussed in the M-RELAP5 topical report (Ref.1).

References:

1. Mitsubishi Heavy Industries, Ltd., Small Break LOCA Methodology for US-APWR, MUAP-07013-P (R0), July 2007.
2. Mitsubishi Heavy Industries, Ltd., MHI's Partial Responses to the NRC's Requests for Additional Information on Topical Report MUAP-07013-P (R0) "Small Break LOCA Methodology for US-APWR", UAP-HF-09002, January 2009.
3. T. M. Anklam et al., Experimental Investigations of Uncovered-Bundle Heat Transfer and Two-Phase Mixture-Level Swell under High-Pressure Low-Heat-Flux Conditions, NUREG/CR-2456, ORNL-5848, March 1982.
4. R. L. Durall et al, Facility Description – THTF MOD3 ORNL PWR BDHT Separate-Effects Program, NREG/CR-2640, ORNL/TM-7842, September 1982.

Table RAI-8.1.2-14.1 Revised Parameter used in Energy Balance Calculation for ORNL/THTF Test 3.09.10

Test	LHGR	Power	Heat Loss		Press	Mass Flux*	Mass Flow*	Inlet Temp	Outlet Temp	Inlet Liquid Enthalpy	Outlet Vapor Enthalpy
	(kW/m)	(kW)	(kW)	[fraction]	(MPa)	(kg/m^2s)	(kg/s)	(K)	(K)	(kJ/kg)	(kJ/kg)
3.09.10I	2.22	487.19	8.61	[0.018]	4.50	29.76	0.1840	473.03	792.38	855.17	3484.53
3.09.10J	1.07	234.82	12.13	[0.052]	4.20	12.66	0.0783	480.34	826.24	887.69	3565.42
3.09.10K	0.32	70.23	12.33	[0.176]	4.01	3.13	0.0193	466.47	934.97	825.08	3817.49
3.09.10L	2.17	476.22	8.13	[0.017]	7.52	29.11	0.1799	461.32	720.61	805.72	3274.03
3.09.10M	1.02	223.85	9.46	[0.042]	6.96	12.63	0.0781	474.43	792.77	864.30	3459.14
3.09.10N	0.47	103.14	16.73	[0.162]	7.08	4.60	0.0285	473.07	947.93	858.35	3827.82
3.09.10AA	1.27	278.71	5.58	[0.020]	4.04	20.26	0.1252	450.92	547.02	754.54	2882.05
3.09.10BB	0.64	140.45	4.83	[0.034]	3.86	9.62	0.0595	458.24	540.83	787.59	2870.42
3.09.10CC	0.33	72.42	2.53	[0.035]	3.59	5.03	0.0311	467.58	531.57	829.63	2853.41
3.09.10DD	1.29	283.10	8.46	[0.030]	8.09	19.48	0.1204	453.39	595.38	770.24	2883.84
3.09.10EE	0.64	140.45	5.52	[0.039]	7.71	11.00	0.0680	455.87	581.04	781.12	2839.56
3.09.10FF	0.32	70.23	6.46	[0.092]	7.53	4.83	0.0299	451.43	565.77	760.74	2775.40

*Mass flow measured at the channel outlet is used.

Table RAI-8.1.2-14.2 Revised Energy Balance Calculation for ORNL/THTF Test 3.09.10

Test	(a)FRS Thermal Power (kW)	(b) Heat Loss (kW)	(c) Inlet Flow Energy (kW)	(d) Outlet Flow Energy (kW)	Energy Balance Error[1] ([(a)-(b)+(c)-(d)]/(d))	Energy Balance Error[2]
3.09.10I	487.19	8.61	157.31	640.98	-0.79% ±6.29%	0.81%
3.09.10J	234.82	12.13	69.46	279.01	4.71% ±7.71%	10.00%
3.09.10K	70.23	12.33	15.96	73.86	0.01% ±7.55%	0.48%
3.09.10L	476.22	8.13	144.98	589.11	4.07% ±7.75%	5.03%
3.09.10M	223.85	9.46	67.47	270.05	4.37% ±7.70%	3.84%
3.09.10N	103.14	16.73	24.43	108.95	1.74% ±7.65%	2.33%
3.09.10AA	278.71	5.58	94.49	360.92	1.86% ±7.58%	-0.56%
3.09.10BB	140.45	4.83	46.83	170.68	6.89% ±7.96%	8.61%
3.09.10CC	72.42	2.53	25.79	88.72	7.86% ±7.92%	-15.92%
3.09.10DD	283.10	8.46	92.74	347.24	5.80% ±8.11%	4.97%
3.09.10EE	140.45	5.52	53.11	193.07	-2.60% ±7.32%	-2.51%
3.09.10FF	70.23	6.46	22.71	82.86	4.37% ±8.26%	3.46%

1) Energy balance error normalized to the outlet flow energy.
The uncertainty is estimated by propagating the measurement uncertainties in power, pressure, mass flow, and inlet and outlet temperatures.

2) Energy balance error from Table RAI-8.1.2-5.1.

Table RAI-8.1.2-14.3 Measurement Uncertainties related to Energy Balance Calculation for ORNL/THTF Test 3.09.10

Type	Uncertainty		Reference
Power	1.1	(%)	NUREG/CR-2640
Heat flux(1)	5.5	(%)	NUREG/CR-2456
Pressure	0.2	(MPa)	NUREG/CR-2456
Flowrate(2)	4.1	(%)	NUREG/CR-2640
Flowrate(3)	5.7	(%)	NUREG/CR-2456
T-inlet	3.9	(K)	NUREG/CR-2456
T-outlet	23.5	(K)	NUREG/CR-2456

1) Uncertainty computed by propagating uncertainties in power, thermocouple, and material properties.

2) Uncertainty in flowmeter instrumentation.

3) Uncertainty in mass flowrate computed by propagating uncertainties in flowmeter, temperature, and pressure.

Figure RAI-8.1.2-14.1 Comparison of Predicted and Measured FRS Surface Temperature Profiles for ORNL/THTF Test 3.09.10J (Heater Rod Power Uncertainty)

Figure RAI-8.1.2-14.2 Comparison of Predicted and Measured FRS Surface Temperature Profiles for ORNL/THTF Test 3.09.10K (Heater Rod Power Uncertainty)

Figure RAI-8.1.2-14.3 Comparison of Predicted and Measured FRS Surface Temperature Profiles for ORNL/THTF Test 3.09.10M (Heater Rod Power Uncertainty)

Figure RAI-8.1.2-14.4 Comparison of Predicted and Measured FRS Surface Temperature Profiles for ORNL/THTF Test 3.09.10N (Heater Rod Power Uncertainty)

Figure RAI-8.1.2-14.5 Comparison of Predicted and Measured Mixture Levels for ORNL/THTF Tests (Heater Rod Power Uncertainty)

Figure RAI-8.1.2-14.6 Comparison of Predicted and Measured FRS Surface Temperature Profiles for ORNL/THTF Test 3.09.10J (Pressure Uncertainty)

Figure RAI-8.1.2-14.7 Comparison of Predicted and Measured FRS Surface Temperature Profiles for ORNL/THTF Test 3.09.10K (Pressure Uncertainty)

Figure RAI-8.1.2-14.8 Comparison of Predicted and Measured FRS Surface Temperature Profiles for ORNL/THTF Test 3.09.10M (Pressure Uncertainty)

Figure RAI-8.1.2-14.9 Comparison of Predicted and Measured FRS Surface Temperature Profiles for ORNL/THTF Test 3.09.10N (Pressure Uncertainty)

Figure RAI-8.1.2-14.10 Comparison of Predicted and Measured Mixture Levels for ORNL/THTF Tests (Pressure Uncertainty)

Figure RAI-8.1.2-14.11 Comparison of Predicted and Measured FRS Surface Temperature Profiles for ORNL/THTF Test 3.09.10J (Inlet Flow Uncertainty)

Figure RAI-8.1.2-14.12 Comparison of Predicted and Measured FRS Surface Temperature Profiles for ORNL/THTF Test 3.09.10K (Inlet Flow Uncertainty)

Figure RAI-8.1.2-14.13 Comparison of Predicted and Measured FRS Surface Temperature Profiles for ORNL/THTF Test 3.09.10M (Inlet Flow Uncertainty)

Figure RAI-8.1.2-14.14 Comparison of Predicted and Measured FRS Surface Temperature Profiles for ORNL/THTF Test 3.09.10N (Inlet Flow Uncertainty)

Figure RAI-8.1.2-14.15 Comparison of Predicted and Measured Mixture Levels for ORNL/THTF Tests (Inlet Flow Uncertainty)

Figure RAI-8.1.2-14.16 Comparison of Predicted and Measured FRS Surface Temperature Profiles for ORNL/THTF Test 3.09.10J (Inlet Temperature Uncertainty)

Figure RAI-8.1.2-14.17 Comparison of Predicted and Measured FRS Surface Temperature Profiles for ORNL/THTF Test 3.09.10K (Inlet Temperature Uncertainty)

Figure RAI-8.1.2-14.18 Comparison of Predicted and Measured FRS Surface Temperature Profiles for ORNL/THTF Test 3.09.10M (Inlet Temperature Uncertainty)

Figure RAI-8.1.2-14.19 Comparison of Predicted and Measured FRS Surface Temperature Profiles for ORNL/THTF Test 3.09.10N (Inlet Temperature Uncertainty)

Figure RAI-8.1.2-14.20 Comparison of Predicted and Measured Mixture Levels for ORNL/THTF Tests (Inlet Temperature Uncertainty)

REQUEST 8.1.3-1

Scale the inlet mass flux in Table 8.1.3-1 in terms of the US-APWR scaling and compare them with the appropriate/typical core inlet flow rate during the reflood period of US-APWR SBLOCA.

RESPONSE

Table RAI-8.1.3-1.1 shows a comparison of the experimental flooding mass flux with that expected under the typical SBLOCAs in US-APWR. The US-APWR flooding mass flux data are extracted from the calculations for the core recovery period of the 7.5-in and 1-ft^2 cold leg break accidents described in the design control document (Ref.1). The 7.5-in break generates the highest peak cladding temperature (PCT) during the 'loop seal' period. The 1-ft^2 cold leg break is the limiting case and generates the severest PCT during the 'boiloff' period.

The experimental flooding mass flux conditions are representative of those expected during the typical SBLOCAs in the US-APWR, as shown in Table RAI-8.1.3-1.1.

It is noted that the THTF mass flux data in Table RAI-8.1.3-1.1 are different from the values specified in Table 8.1.3-1 of MUAP-07-13-P (R0), which correspond to the mass flux at the initial steady-state just before the start of the transient. Refer to the response to REQUEST 8.1.3-3.

References

1. MHI, Design Control Document for US-APWR, Chapter 15 Transient and Accident Analyses, MUAP-DC015 Revision 0, December 2007.

Table RAI-8.1.3-1.1 Comparison of Experimental Flooding Velocity with Typical US-APWR SBLOCAs

		Mass Flux	
		(lbm/ft^2)	(kg/m^2)
US-APWR	7.5in cold leg break		
	1ft^2 cold leg break		
THTF	3.09.10P	16.55	80.80
	3.09.10Q	10.74	52.45

REQUEST 8.1.3-2

The flow in Table 8.1.3-1 is given in inlet mass flux (kg/s.m^2), while the flow in Figure 8.1.3-2 is given in m^3/s. Revise either so that the units are consistent.

RESPONSE

Table 8.1.3-1 of MUAP-07013-P (R0) is to be replaced by the following table so that it keeps consistency with Figures 8.1.3-2 and 5. Additional information is discussed in the MHI response to REQUEST 8.1.3-3.

Table RAI-8.1.3-2.1 Revised ORNL/THTF High-Pressure Reflood Test Conditions

Test	Pressure	Initial mass flux	Initial inlet temperature	Initial inlet subcooling	Linear heat power	Flooding velocity during transient test	
	(MPa)	(kg/m^{2}s)	(K)	(K)	(kW/m)	(cm/s)	(m^3/s) × 10^{-4}
3.09.10O	3.88	25.36	447.7	74	2.03	12.2	7.50
3.09.10P	4.28	12.19	462.6	65	0.997	9.2	5.66
3.09.10Q	3.95	12.68	456.8	66	1.02	5.9	3.63
3.09.10R	7.34	27.64	449.2	113	2.16	11.7	7.20
3.09.10S	7.53	13.82	459.0	105	1.38	10.2	6.27

REQUEST 8.1.3-3

The inlet mass flux in Table 8.1.3-1 is not consistent with the flooding velocity of Table 5.2.1.4-4, or Figures 8.1.3-2 and -5. (e.g., Table 8.1.3-1 show similar inlet mass flux for Tests P and Q, but Figure 8.1.3-2 for Test P and Figure 8.1.3-5 for Test Q show substantially different flow rates). Clarify the discrepancy (the same applies to tests R and S).

RESPONSE

The inlet mass flux given in Table 8.1.3-1 is actually the mass flux in the steady condition prior to the stat of the test. Therefore, the mass flux should not be consistent with the flooding velocity, which is related to the flow during the test. Tests P and Q have similar initial conditions, but the flooding velocities vary significantly. Table 8.1.3-1 will be revised to eliminate any confusion as mentioned in the MHI response to REQUEST 8.1.3-2.

References

1. C. R. Hyman et al., Experimental Investigations of Bundle Boiloff and Reflood under High-Pressure Low Heat Flux Conditions, NUREG/CR-2455, ORNL-5846, 1982.

REQUEST 8.1.3-4

Explain how the inlet temperatures of Figure 8.1.3-3 and 8.1.3-6 were selected and compare them with the inlet temperature to the core during the reflood period in a typical SBLOCA transient.

RESPONSE

The inlet temperatures of Figures 8.1.3-3 and 6 of MUAP-07013-P (R0) are parameters used in M-RELAP5 analyses as boundary conditions. The data were measured in the test facility (TE-256 in Figure 8.1.2-1 of MUAP-07013-P (R0)), and are compared with the boundary conditions used in Figures 8.1.3-3 and 6 of MUAP-07013-P (R0).

Figure RAI-8.1.3-4.1 shows a comparison between the experimental temperature data and US-APWR SBLOCA temperature range which is derived from the design control document (Ref.1) and the topical report in terms of the SBLOCA sensitivity study (Ref.2). The US-APWR SBLOCA temperature range is specifically determined from 1-in cold leg break to 1-ft^2 cold leg break, which covers the temperature range possible under all the US-APWR SBLOCAs.

Flooding phenomena to quench the dryout fuel cladding mainly occur under the ‘recovery’ phase, where the temperature varies from 405K to 560K (270-550^{o}F) in the US-APWR SBLOCA. US-APWR, in particular, tends to generate the severest peak cladding temperature (PCT) for the larger break sizes, because the high-head injection system (HHIS) is able to provide the primary reactor coolant system with water sufficient for the smaller break sizes. Therefore, the limiting PCT occurs in the 1-ft^2 break accident when the reactor pressure is about 1MPa (145psia) and the core inlet coolant temperature is about 405K (270^{o}F).

In the THTF reflood tests used for the M-RELAP5 assessment, however, the pressure and inlet coolant temperature are limited to about 4MPa (580psia) and 460K (370^{o}F), respectively. In order to demonstrate that M-RELAP5 is sufficiently applicable to the wider pressure and temperature conditions, MHI is planning to provide an additional verification **[**

].

It is noted that each phase referred to in Figure RAI-8.1.3-4.1 is defined in the response to REQUEST 4-1.

References
1. MHI, Design Control Document for US-APWR, Chapter 15 Transient and Accident Analyses, MUAP-DC015 Revision 0, December 2007.
2. MHI. Small Break LOCA Sensitivity Analyses for US-APWR, MUAP-07025-P (R0), December 2007.

[

]

Figure RAI-8.1.3-4.1 Comparison of Core Inlet Temperature Data with US-APWR/SBLOCA

REQUEST 8.1.3-5

The inlet temperature profiles for Test P (Figure 8.1.3-3) and Test Q (Figure 8.1.3-6) are substantially different. Explain.

RESPONSE

The difference in the temperature evolutions between Tests P and Q was due to the experimental procedure employed for each test. As shown in Figure 8.1.2-1 of MUAP-07013-P (R0), there were two water-feeding lines connected to the test section inlet, the 1/2-in. steady-state inlet flow line and the 3/4-in. reflood line, in the THTF apparatus. The temperatures in Figures 8.1.3-3 and 6 are the mixture mean temperatures of the fluid from these two lines. The initial steady-state condition was attained by adjusting the flow rate through the 1/2-in. line, while the 3/4-in. reflood line was isolated. The transient was activated by feeding additional water from the 3/4-in. reflood line. Because the initially isolated water in the reflood line was cooler than that circulating through the steady-state line, the coolant temperature at the test section inlet temporarily decreased in the beginning of the transient tests as shown in Test P (Figure 8.1.3-3).

For Test Q, on the other hand, the transient flow was sufficiently manipulated by controlling the flow rate through the 1/2-in. steady-state line only. Therefore, no cooler water was supplied to the test section, nor significant transient occurred in the temperature evolution at the test section inlet as shown in Figure 8.1.3-6.

The above is described in the test report (Ref.1).

References

1. C. R. Hyman et al., Experimental Investigations of Bundle Boiloff and Reflood under High-Pressure Low Heat Flux Conditions, NUREG/CR-2455, ORNL-5846, 1982.

REQUEST 8.1.3-6

Explain how the pressures (boundary condition) in Figures 8.1.3-4 and -7 were selected.

RESPONSE

The pressures were measured at the test section outlet (PE-201 in Figure 8.1.2-1), and were used as boundary conditions for the M-RELAP5 calculations, which are compared with the measurements in Figures 8.1.3-4 and 7 of MUAP-07013-P (R0).

Figure RAI-8.1.3-6.1 shows a comparison between the experimental pressure data and the US-APWR SBLOCA pressure range which is derived from the design control document (Ref.1) and the topical report in terms of the SBLOCA sensitivity study (Ref.2).

As discussed in the response to REQUEST 8.1.3-4, the limiting peak cladding temperature (PCT) occurs in the 1-ft^2 break accident when the reactor pressure is just about 1MPa (145psia). THTF tests used for the M-RELAP5 assessment, however, are limited to about 4MPa (580psia) which corresponds to the pressure occurring in the 'recovery' phase of the 5 to 11-in break accidents. Therefore, MHI is planning to provide an additional verification using **[** **]**.

It is noted that each phase referred to in Figure RAI-8.1.3-6.1 is defined in the response to REQUEST 4-1.

References

1. MHI, Design Control Document for US-APWR, Chapter 15 Transient and Accident Analyses, MUAP-DC015 Revision 0, December 2007.
2. MHI. Small Break LOCA Sensitivity Analyses for US-APWR, MUAP-07025-P (R0), December 2007.

[

]

Figure RAI-8.1.3-6.1 Comparison of Pressure Data with US-APWR/SBLOCA

REQUEST 8.1.3-7

Explain the saw-tooth behavior of the collapsed liquid level for the M-RELAP5 results in Figures 8.1.3-10 and 14. Explain why the calculated collapsed liquid level at time=0 for test Q (Figure 8.1.3-14) does not match the measured level.

RESPONSE

The saw-tooth behavior found in the M-RELAP5 results (Figures 8.1.3-10 and 14) is caused by repetition between rewetting and dryout locally near the liquid level front. A similar behavior can be observed in the calculated FRS temperatures which are shown in Figures 8.1.3-8, 9, 12 and 13 of MUAP-07013-P (R0). Once the rewetting occurs near the liquid level front, heat transfer to the fluid suddenly increases. This induces the rapid increase in vaporization, resulting in decrease in the collapsed liquid level and in enhancement of dryout region again. This behavior is repeated until the local coolant is adequately subcooled. It is noted that this intermittent quench behavior was identified in the test report (Ref.1), and that discontinuous behaviors were found in the measured fluid temperature as shown in Figure RAI-8.1.3-7.1.

Although this phenomenon can be possible in the limited local area just near the liquid-level front microscopically, the coarser mesh scheme is employed for the present M-RELAP5 numerical simulations from the practical point of view. Therefore, just after the front of liquid level passes the discretized mesh boundary, the vaporization mentioned above occurs over the coarse mesh. This leads to the phasic mass exchange larger than that actually observed in the experiment, and to the saw-tooth behavior apparent in the simulated collapsed liquid level histories. Based on the comparison between the measured and calculated liquid level histories, however, MHI has concluded that M-RELAP5 is able to sufficiently reproduce the high-pressure reflood phenomenon notwithstanding the above numerical difficulty, as stated in Section 8.1.3.5 of MUAP-07013-P (R0).

For the latter question here, MHI is providing with several comments regarding the discrepancy between the measured and calculated initial collapsed liquid levels, in Section 8.1.3.4 of MUAP-07013-P (R0). In M-RELAP5 analyses, boundary conditions were defined at the FRS thermal power, inlet coolant flow rate, subcooling, and exit pressure. Hence, the initial FRS surface temperature and liquid level were the results from the steady-state calculation. Here, the initial FRS surface temperature was judged to be more important than the initial liquid level to simulate the reflood quench behavior because the temperature directly affects the threshold to allow rewetting. Initial calculations with the measured flow and subcooling resulted in higher FRS surface temperature than measured. These higher initial temperatures would delay the rewetting and might make the basic models appear more conservative than they actually are. Therefore, the initial values of inlet flow and subcooling were adjusted in the steady-state calculation so that the calculated FRS surface temperature sufficiently met the measured one, resulting in the slight mismatch between the measured and calculated initial liquid levels.

References

1. C. R. Hyman et al., Experimental Investigations of Bundle Boiloff and Reflood under High-Pressure Low Heat Flux Conditions, NUREG/CR-2455, ORNL-5846, 1982.

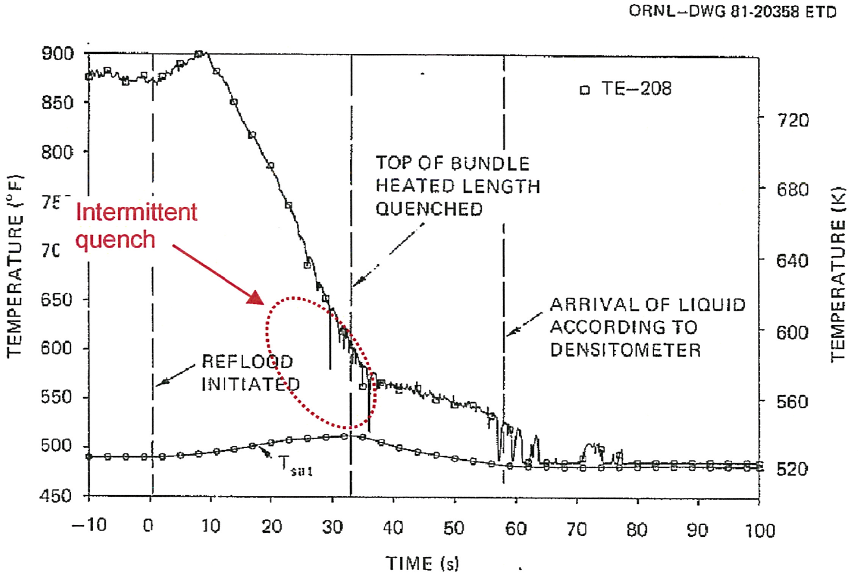

Fig. 31. Test section outlet temperature vs saturation temperature, test 3.09.10P.

Figure RAI-8.1.3-7.1 Intermittent Quench Behavior in THTF Reflood Test (Ref.1)

REQUEST 8.1.3-8

The quench velocities for test P (Figure 8.1.3-11) and test Q (Figure 8.1.3.15) are similar for the tests (about 3 cm/sec for P and 2.8 cm/sec for Q), but they are substantially different for the simulations (about 2.4 for P and 1.3 for Q). This may imply that the quench velocities for the simulation could be higher than the test for some parameter ranges, and thus the simulation may not be conservative. Please explain.

RESPONSE

The test report (Ref.1) describes that the average quench rate for Tests P and Q were 3.28cm/s and 2.78cm/s in the experiment, respectively. This difference was due to the difference in the flooding rate, 9.2cm/s for Test P and 5.9cm/s for Test Q. In addition, the test report pointed out that the dominant heat transfer mode around the quench front affected the quench rate, from investigations to dynamic behavior of the measured histories in terms of quench and collapsed levels as follow.

When the quench level is significantly above the collapsed liquid level, dispersed flow film boiling is suggested, while the inverted annular film boiling may be suggested when the quench level is near or below the collapsed level. These heat transfer and hydraulic flow regimes are schematically compared in Figure RAI-8.1.3-8.1 (Ref.2). Next, Figures RAI-8.1.3-8.2 and 3 show comparisons between the measured quench level and collapsed level histories for Tests P and Q, respectively, indicating that the dispersed flow film boiling possibly appeared in Test Q rather than Test P. Under the dispersed flow film boiling like Test Q, numerous droplets occur from the liquid level front, which effectively contribute to the precursor cooling above the liquid level before quench. This effectively decreases the vapor superheat and the fuel rod surface temperature in the uncovered-bundle region, and thus hastens the quench rate even though the flooding rate is low. This is why the difference in the measured quench rates between Tests P and Q was relatively small, in spite of the fact that the flooding rates were significantly different from each other.

On the other hand, the average quench rates by M-RELAP5 are **[** **]** for Tests P and Q, respectively. The ratio of quench-to-flooding rate is smaller in the lower flooding case (Test Q) for M-RELAP5 in contrast to the measurements, as arranged in Table RAI-8.1.3-8.1. This tendency in the M-RELAP5 prediction can be explained by modeling for the precursor cooling effect, namely by the wall heat transfer model applicable to the uncovered-bundle region in M-RELAP5. M-RELAP5 does not model an explicit droplet field and therefore does not represent the cooling effect of droplets on the heated wall and vapor just above the mixture-level. Hence, the wall heat transfer under the dispersed flow film boiling (Test Q) is conservatively represented by the vapor convection (single-phase vapor), while the inverted flow film boiling (Test P) is reasonably modeled by the Bromley heat transfer correlation.

Figures RAI-8.1.3-8.4 and 5 show comparisons between the collapsed and quench levels calculated by M-RELAP5 for Tests P and Q, respectively. The precursor cooling effect predicted by M-RELAP5 is significantly less than the measurement for Test Q. Figures RAI-8.1.3-8.6 and 7 show the axial distributions in terms of the applied heat transfer mode and computed heat transfer coefficient by M-RELAP5 for Tests P and Q, respectively. It is found that the dryout heat transfer coefficient just above the quench front in Test Q is reduced to **[** **]**, due to the heat transfer mode different from Test P. This possibly induces that the predicted precursor cooling effect is conservatively underestimated in Test Q rather than in Test P, resulting in underestimation of quench rate in Test Q.

Regarding the inverted flow film boiling regime, M-RELAP5 evaluates its heat transfer coefficient by the Bromley correlation. Because the Bromley correlation describes the heat transfer from the heated wall to the stagnant and non-contact liquid fluid without the turbulent convection effect, the correlation tends to underestimate the heat transfer coefficient with increase in the fluid Reynolds number. This indicates that M-RELAP5 tends to underestimate the heat transfer in the inverted flow film boiling regime under the relatively high flow condition.

In conclusion, M-RELAP5 theoretically tends to underestimate the heat transfer coefficient both for the low flow/dispersed flow film boiling and for the high flow/inverted flow film boiling, and to predict slower quench rates in comparison to the measurements as confirmed by Table RAI-8.1.3-8.1. Finally, it is noted that the code applicability to the wide pressure range, i.e. various break sizes, is to be verified using the additional **[** **]** IET data.

References

1. C. R. Hyman et al., Experimental Investigations of Bundle Boiloff and Reflood under High-Pressure Low Heat Flux Conditions, NUREG/CR-2455, ORNL-5846, 1982.
2. USNRC, Compendium of ECCS Research for Realistic LOCA Analysis, NUREG-1230 Revision 4, 1988.

Table RAI-8.1.3-8.1 Comparison between Measured and Calculated Quench Rate

Test	Initial pressure (MPa)	Linear heat rate (kW/m)	Average flooding rate (cm/s)	Meas. average quench rate (cm/s)	Cal. average quench rate (cm/s)
3.09.10P	4.28	1.00	9.2	3.28 (0.36)*	
3.09.10Q	3.95	1.02	5.9	2.78 (0.47)*	

*Ratio of quench-to-flooding rate

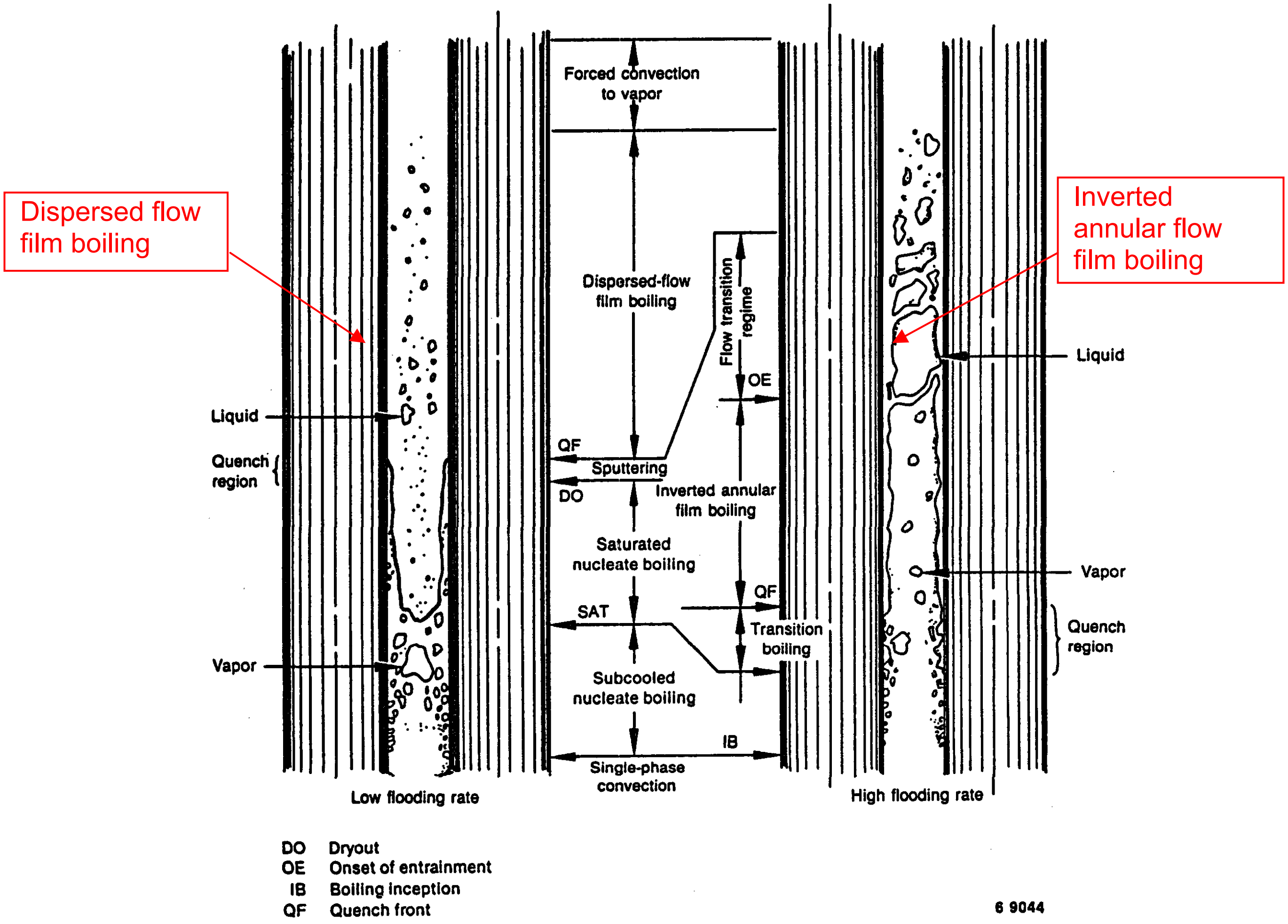
Dispersed flow film boiling
Inverted annular flow film boiling
Forced convection to vapor
Dispersed-flow film boiling
Flow transition regime
OE
QF
Sputtering
DO
Inverted annular film boiling
Saturated nucleate boiling
QF
SAT
Transition boiling
Subcooled nucleate boiling
IB
Single-phase convection
Liquid
Quench region
Vapor
Low flooding rate
Liquid
Vapor
Quench region
High flooding rate
DO Dryout
OE Onset of entrainment
IB Boiling inception
QF Quench front
6 9044

Figure 6.4-3. Heat transfer and hydraulic flow regimes for bottom reflood.

Figure RAI-8.1.3-8.1 Heat Transfer and Hydraulic Flow Regimes for Bottom Reflood (Ref.2)

ORNL–DWG 81-20399 ETD

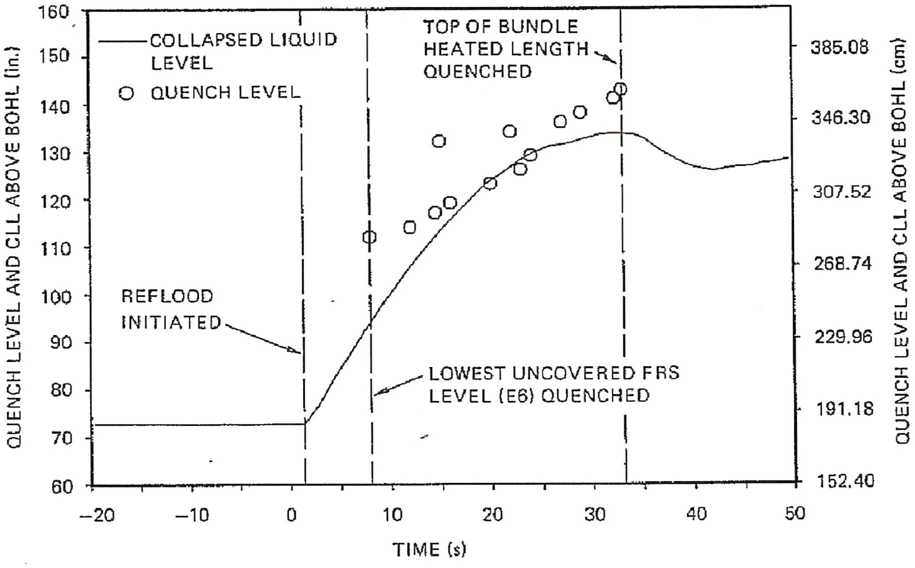

Fig. 72. Quench level and collapsed liquid level histories, test 3.09.10P.

Figure RAI-8.1.3-8.2 Measured Quench Level and Collapsed Liquid Level Histories (Test 3.09.10P)

ORNL–DWG 81-20400 ETD

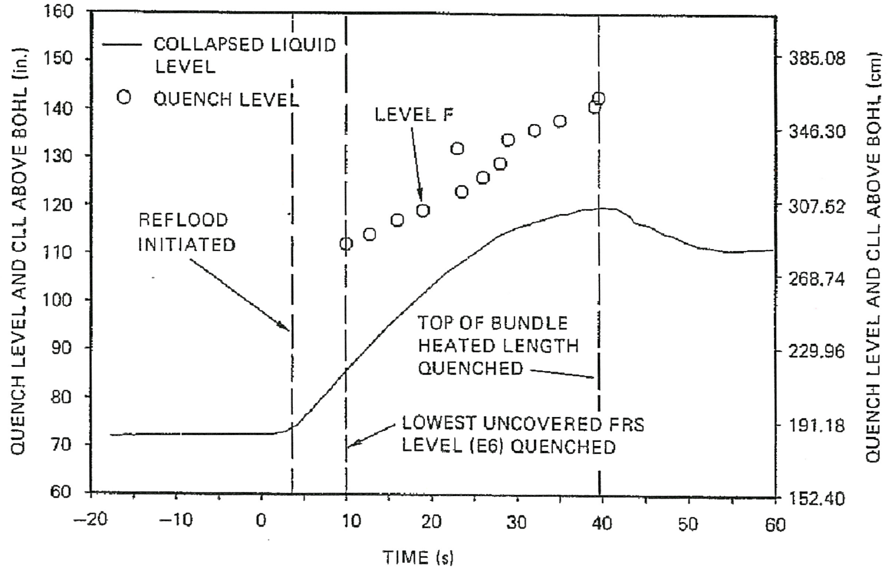

Fig. 73. Quench level and collapsed liquid level histories, test 3.09.10Q.

Figure RAI-8.1.3-8.3 Measured Quench Level and Collapsed Liquid Level Histories (Test 3.09.10Q)

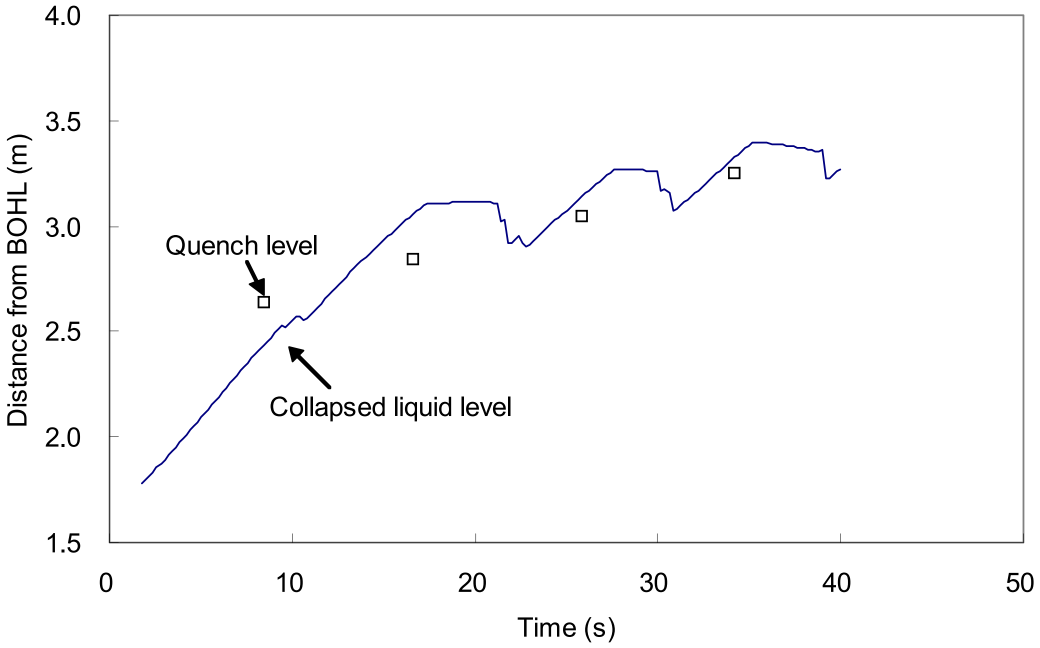

Figure RAI-8.1.3-8.4 Calculated Quench Level and Collapsed Liquid Level Histories (Test 3.09.10P)

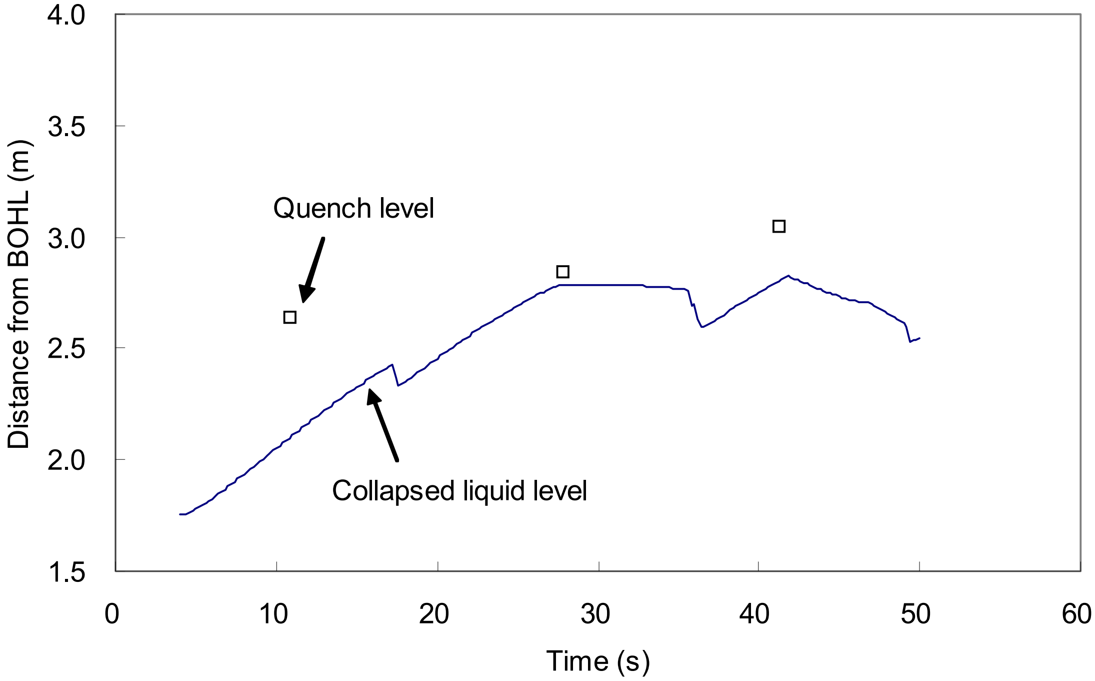

Figure RAI-8.1.3-8.5 Calculated Quench Level and Collapsed Liquid Level Histories (Test 3.09.10Q)

Figure RAI-8.1.3-8.6 Comparison of M-RELAP5 HTMODE between Tests P and Q

Figure RAI-8.1.3-8.7 Comparison of M-RELAP5 HTC between Tests P and Q

REQUEST 8.1.3-9

Figures 8.1.3-8 through 8.1.3-15 show the comparison of the predicted results to the measured data. It is noticed that the initial fluid temperature and collapsed level are lower in the prediction than in the measurement (See Figures 8.1.3-8, 8.1.3-10, 8.1.3-12, and 8.1.3-14). Please explain.

RESPONSE

As described in the third paragraph of Section 8.1.3.4 of the topical report MUAP-07013-P (R0) (Ref. 1), the initial values of inlet flow and subcooling were adjusted in the steady-state calculation such that the simulation sufficiently reproduced the measured cladding temperature under the dryout at the initial steady-state. This calibration eliminates the uncertainty in the initial cladding temperature for the reflooding test analysis. Without this calibration, the initial cladding temperature would have been higher, resulting in higher cladding temperatures during the transient and later quench times. Thus, calculated results would have appeared even more conservative than shown in Figures 8.1.3-8, -9, -12, and -13 of Ref. 1. From the onset of transient calculation, the fluid condition was put back to the measured one.

M-RELAP5 tends to slightly underpredict the steady-state mixture level compared to the measurement data. This clarifies that the code predicts longer dryout (uncovery) region than that of measurement data, as shown in Figure 8.1.2-30 of the topical report MUAP-07013-P (R0). **[**

]

Underprediction in terms of the initial collapsed level is discussed in the response to REQUEST 8.1.3-10.

Reference:

1. Mitsubishi Heavy Industries, Ltd., Small Break LOCA Methodology for US-APWR, MUAP-07013-P (R0), July 2007.

REQUEST 8.1.3-9-1

(Related RAI 8.1.3-9)

[

]

RESPONSE

[

]

[

]

REQUEST 8.1.3-10

The 1st sentence of the 3rd paragraph in Section 8.1.3.5 on page 8.1.3-3 states, “Figures 8.1.3-10 and 14 indicate good agreement between the calculated results and the experimental data.”

However, Figure 8.1.3-14 shows that the predicted initial collapsed water levels is different from the measured data. It can be seen that if the predicted initial collapsed water levels are moved up to the point of the measurement then the agreement is much better. Please explain why the initial predicted collapsed water level is different than the test data.

RESPONSE

The initial collapsed water level is not an input parameter, but instead is obtained from the initial steady-state calculation. The collapsed level is one of the calculation results dependent on the code models (particularly, interfacial shear) and experimental condition: mass flux, inlet subcooling, pressure, power, and geometry. Thus, the predicted initial collapsed level is not expected to agree exactly with the experimental data.

Analysis of Figure 8.1.2-29 of the topical report (Ref. 1) shows that the M-RELAP5 code has a mean and standard deviation of **[ ]** in predicting the steady-state collapsed level, in comparison with the measurements. This level of accuracy is judged to be good agreement. This uncertainty sufficiently accounts for the difference in the initial collapsed liquid level for Test 3.09.10Q, which was about -5 in (-0.13m) (Figure 8.1.3-14 in the topical report).

Reference:

1. Mitsubishi Heavy Industries, Ltd., Small Break LOCA Methodology for US-APWR, MUAP-07013-P (R0), July 2007.

REQUEST 8.1.3-11

MHI states in the first paragraph on page 8.1.3-4 that the delayed quenching times resulted from the fact that the M-RELAP5 predicted heat transfer for film boiling and transition boiling, which are dominant in the pre-quench cooling, is conservatively modeled. However, MHI stated in Section 8.1.2.7 that the M-RELAP5 code reasonably predicts the rod heat transfer above the two-phase mixture level.

Please provide an explanation of these two contradictory conclusions regarding the capability of M-RELAP5 to predict the heat transfer in the region above the two-phase mixture level.

RESPONSE

Section 8.1.2.7 of the topical report MUAP-07013-P (R0) (Ref. 1) summarizes the code predictability for the film boiling/dispersed flow and/or steam cooling heat transfer above the mixture two-phase level under steady-state condition. A modification was made to the Dougall-Rohsenow correlation for the vapor convective heat transfer, where the steam properties are computed based on the film temperature to provide conservative heat transfer coefficients (Refer to Section 7.1.7.5 of MUAP-07013-P (R0)) in conformance to Appendix K requirement. This approach primarily assures a reasonable conservatism in dryout heat transfer coefficients that further gives conservatism when calculating heat-up behavior.

On the other hand, the code's capability to predict the dynamic reflooding behavior is described in Section 8.1.3.6 of the topical report. **[**

] Therefore, M-RELAP5 shows explicitly conservative predictions in terms of rewetting and/or quenching behavior during reflooding.

References:
1. Mitsubishi Heavy Industries, Ltd., Small Break LOCA Methodology for US-APWR, MUAP-07013-P (R0), July 2007.
2. Mitsubishi Heavy Industries, Ltd., 'MHI's Partlal Responses to the NRC's Requests for Additional Information On Topical Report MUAP-07013-P (R0) "Small Break LOCA Methodology for US-APWR", UAP-HF-09002, January 16, 2009.

REQUEST 8.1.4-1

The UPTF test description mentions steam injection and air injection (Section 8.1.4.2). Is it correct? Was the test steam only?

RESPONSE

Injected gas phase in the UPTF test was steam only and the description of “air” injection is incorrect. The term will be revised from air to steam.

REQUEST 8.1.4-2

[

]

RESPONSE

[

]

REQUEST 8.1.4-3

RELAP5 uses CCFL correlation with three input specified parameters that indicates the effect of surface tension and gas flow rate for hold up. It correctly indicates that for large pipes surface tension is important (Kutateladze correlation) and for small pipes the length scale does not depend on surface tension.
However, there is no statement on size of the pipe where the transition occurs. Explain the criteria for selecting the use of either the “big” pipe or “small” pipe form of the CCFL correlation.

RESPONSE

The criteria could be judged between the big and small pipes based on Fig.2 in Ref.1 (shown in Figure RAI-8.1.4-3.1) and Fig.25 in Ref.2. As shown in Figure RAI-8.1.4-3.1, Kutateladze number (depending on steam flow rate) giving zero penetration of water increases with D*: ($D \cdot \left(g\left(\rho_L - \rho_G\right)/\sigma\right)^{1/2}$) and approaches to a constant value which is about 3.2 for D* greater than about 60. The value of D at D*=60 was derived as a function of pressure as shown in Table RAI-8.1.4-3.1. From this table, the Ku correlation was applied to the hot leg nozzle of the steam generator inlet plenum and was applied the correlation using hydraulic-equivalent diameter as the length-scale to the inlet of the tubes in the steam generators.

References

1. Richter, H.J., Flooding in tubes and annuli, Int. J. Multiphase Flow, Vol. 7, No. 6, pp. 647-658, 1981.
2. Bankoff, S.G. and Lee, S.C., A Critical Review of the Flooding Literature, NUREG/CR-3060, 1983.

Table RAI-8.1.4-3.1 Value of D at D*=60 under different pressure

Pressure (bar)	3	15	70	150
D (in.)	5.5	5.1	3.9	2.4

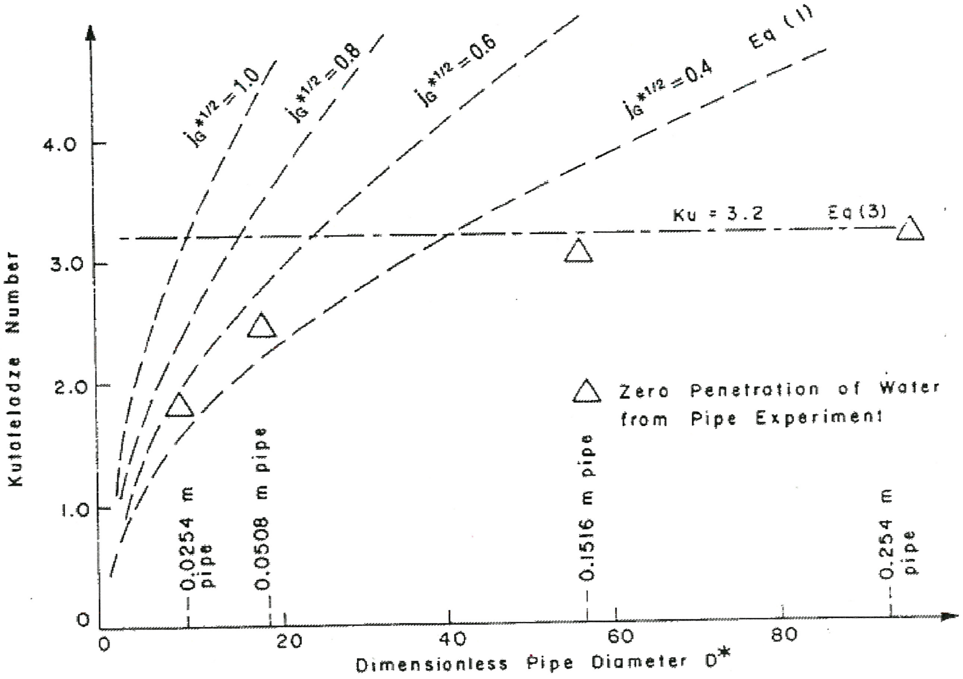

Fig. 2. Kutateladze number vs nondimensional geometric parameter and experimental results for zero penetration of liquid.

Figure RAI-8.1.4-3.1 Kutateladze number vs. nondimensional geometric parameter and experimental results for zero penetration of liquid

REQUEST 8.1.4-4

The large pipe CCFL correlation was obtained by regression analyses of the actual UPTF data. The coefficients (m, c, β), obtained from these analyses, are used to model these tests with RELAP5 as part of validation. However, this is not a validation but verification of implementation of the model. What set of coefficients will be used in plant simulation?

RESPONSE

The same set of coefficients (**[ ]**, β=1.0) was applied, which was obtained from the UPTF data in the plant simulations.

REQUEST 8.1.4-5

Figure 8.1.4-3 shows nodalization diagram for UFT test. Please explain the rationale for number of nodes in the different sections. How does this nodalization compare to nodalization of similar sections for the US-APWR?

RESPONSE

The nodalization for the hot leg part in the UPTF was the same as that used in the RELAP5 model in Ref.1. In the plant simulation, the horizontal part of the hot leg was divided into three nodes and the riser part was modeled with one node. To investigate the effect of nodalization, sensitivity analyses have been performed. The nodalization diagram is shown in Figure RAI-8.1.4-5.1 and the result is in Figure RAI-8.1.4-5.2. The number of nodes does not significantly affect the results and the application of CCFL model does not depend on the number of nodes.

Reference

1. Dillistone, M.J., Analysis of the UPTF Separate Effects Test 11 (Steam-Water Countercurrent Flow in the Broken Loop Hot Leg) Using RELAP5/MOD2, NUREG/IA-0071, 1992.

Figure RAI-8.1.4-5.1 Nodalization diagram used for the UPTF CCFL test sensitivity analysis

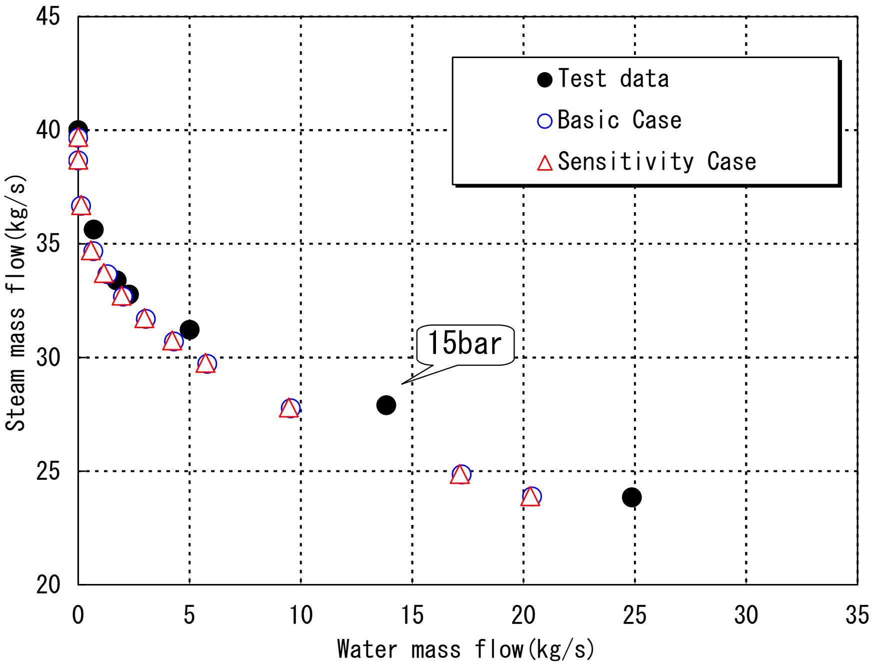

Figure RAI-8.1.4-5.2 UPTF CCFL Test sensitivity analysis, Comparison of the flooding curves of analysis results and test results

REQUEST 8.1.4-6

Figure 8.1.4-4 indicates a comparison of code prediction and the test results. Are there code results for actual test conditions? How do they compare? For 3 bar case, there are three steam flow rates with liquid upward flow but none in the data. Please explain.

RESPONSE

In the code prediction, the same steam flow rate was not set as in the UPTF test but was instead set the steam flow rate to the values given in Table 8.1.4-1. The liquid downward flow rate was evaluated under each steam flow rate in that table and therefore some different characteristics are recognized in the comparison. The liquid upward flow calculation could be attributed to the relatively large discrepancy between the test results at 3 bar and the regression relation shown in Figure 8.1.4-2.

REQUEST 8.1.4-7

(Related RAI 8.1.4-3)

The CCFL correlation has three coefficients that are provided through input. Provide locations of all the places where CCFL correlation is applied, values of CCFL coefficients, and justification.

What is the size of pipe when surface tension effect is not important? Does the set of coefficients change with a change in pressure (see Table RAI-8.1.4-3.1, January-2009 MHI response, page 93)?

RESPONSE

Table RAI-8.1.4-7.1 summarizes the location and the coefficient set of CCFL applied to US-APWR.

For the location A in the table, the hydraulic diameter is **[ ]** and is close to 0.75 m in the UPTF. Since those hydraulic diameter are classified as a large-scale pipe and the applicability of K*-scaling to such a large-scale pipe is considered to be high as described in the response to RAI 8.1.4-3 (Ref. 1). For the location B, the applicability was described in the response to RAI 8.1.5-1 (Ref.1). For the location C, the hydraulic diameter is also **[ ]** and the applicability of K*-scaling is high. K* number for ‘water zero’ penetration at the location C is about **[ ]** from the coefficient c and the value corresponds to that under a large-scale pipe in Figure RAI-8.1.4-3.1.

The effect of surface tension is relatively small where the nondimensional CCFL data are rather be correlated better with hydraulic diameter as the length-scale. The region is considered to be under D* in Figure RAI-8.1.4-3.1 (Ref.1) less than **[ ]**.

The CCFL coefficient set in Table RAI 8.1.4-7.1 is used for the whole range of pressure without modification due to pressure.

References:

1. Mitsubishi Heavy Industry, Ltd., MHI’s Partial Responses to NRC’s Requests for Additional Information on Topical Report MUAP-07013-P (R0) “Small Break LOCA Methodology for US-APWR”, UAP-HF-09002, January 16, 2009.
2. C. L. Tien and C. P. Liu, Survey on Vertical Two-Phase Countercurrent Flooding, EPRI NP-984 Research Project 1160-1, 1979.

Table RAI-8.1.4-7.1 Locations of CCFL correlations applied for US-APWR

REQUEST 8.1.4-8
(Related RAI 8.1.4-4)
[

]

RESPONSE
[

]

REQUEST 8.1.4-9

(Related RAI 8.1.4-6)

Why does the data for 3 bar in Figure 8.1.4-2 of MUAP-07013-P (R0) show less liquid down flow when compared to the 15 bar data at the same Hg? Is this an indication of pressure dependence of the coefficients (c and m) for the CCFL correlation?

Figure 8.1.4-4 of MUAP-07013-P (R0) compares analytical results and test data at two pressures, 3 bar and 15 bar. The comparison at 3 bar shows that for a given steam mass flow, the analytical result predicts higher water mass flow than the test data. Is the set of coefficients for CCFL correlation obtained from the UPTF tests conservative for SBLOCA simulation for the US-APWR? Has the validation of the CCFL correlation been done with an independent set of data, i.e. other than the UPTF data that were used to develop the coefficients for the CCFL correlation?

Also, there are CCFL models applied at the main coolant pump suction and discharge. Please describe the basis for selecting these models including the assessments that demonstrate applicability to the US-APWR application.

RESPONSE

For vertical pipes, the CCFL correlation by Hewitt & Wallis for SG U-tubes is able to apply to the high pressure ROSA/LSTF data as described in the response to RAI 8.1.5-1 (Ref. 1). However, the effect of pressure for the hot-leg CCFL is not clear because of scarce database for the special geometry. The UPTF data is reported in detail with error band in Reference 2 and the database is shown in **Figure RAI-8.1.4-9.1**. The data scattering becomes large under a low Hg of the 3 bar case and the dependency on pressure is not clear under the wide error band.

Considering the error band in Reference 2, the upper bound of water mass flow rate under 3 bar is located at around the UPTF CCFL correlation and it does not necessarily mean that the correlation gives non-conservative results. And the range of pressure is at around 80 bar that the hot-leg CCFL is important. Since the data scattering under the low pressure 3 bar case is considered to be caused by the two-phase flow instability due to density difference between gas and liquid, the hot-leg CCFL characteristics under 15 bar are supposed to be likely case under 80 bar.

The description for the CCFL model at pump suction side is included in the response to RAI 8.1.4-7 where the model applies to the location C. Please refer to the response.

References:

1. Mitsubishi Heavy Industry, Ltd., MHI's Partial Responses to NRC's Requests for Additional Information on Topical Report MUAP-07013-P (R0) "Small Break LOCA Methodology for US-APWR", UAP-HF-09002, January 16, 2009.
2. P. A. Weiss and R. J. Hertlein, UPTF Test Results: First Three Separate Effect Tests, Nuclear Engineering and Design, 108, pp.249-263, 1988.

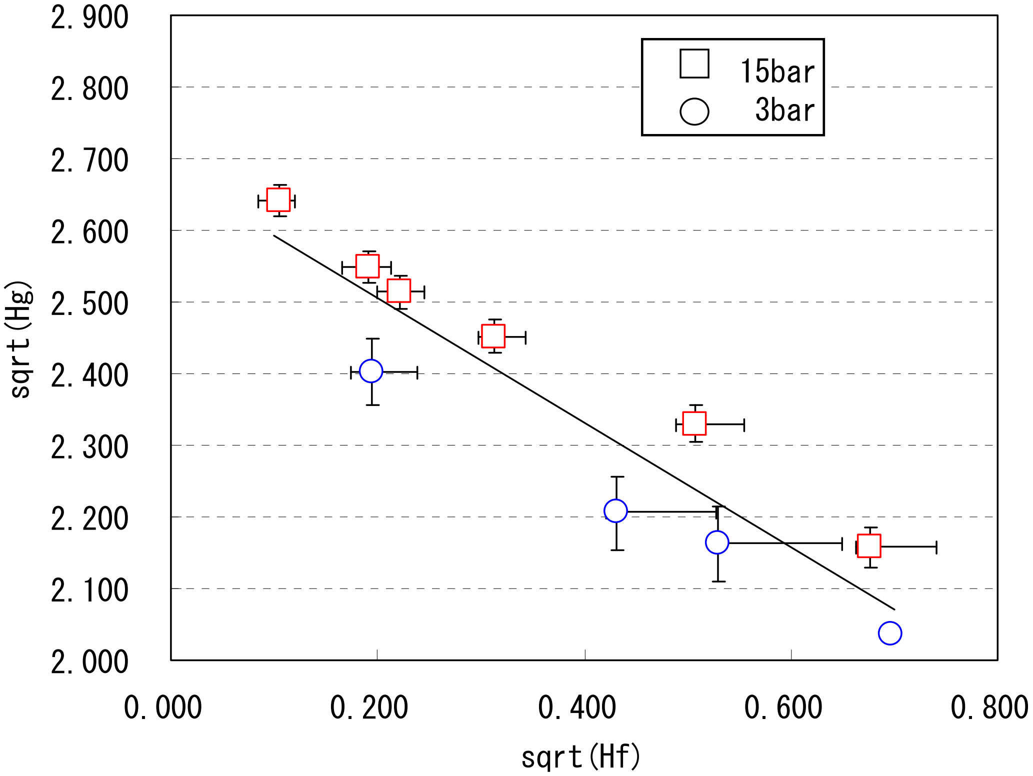

Figure RAI-8.1.4-9.1 UPTF CCFL Data with Error Band

REQUEST 8.1.4-10

[

]

RESPONSE

[

]

REQUEST 8.1.4-11
(Related RAI 8.1.4-7)
[

]

RESPONSE
[

]

REQUEST 8.1.4-11-1

(Related RAI 8.1.4-11)

[

]

RESPONSE

[

]

[

]

REQUEST 8.1.4-10

(Related RAI 8.1.4-9)

The results shown in Figure RAI-8.1.4-9.1 indicate some pressure dependency in the range from 3 to 15 bar. As stated in the response, the important pressure range for use of this CCFL correlation is around 80 bar. This indicates that there could be considerable uncertainty in using this correlation at 80 bar based on the comparison to data at 3 and 15 bar. Describe how this uncertainty is addressed in the SBLOCA methodology.

RESPONSE

The effect of pressure was recently reported in NURETH-13 by the Dresden group (Ref. 1). The hot leg geometry is simulated using a rectangular duct of 5cm in width and 25cm in height. High pressure steam-water experiments were conducted under 15bar, 30bar and 50bar. The CCFL data under different pressures were correlated reasonably well with Ku. However, it is recognized that the Ku for water down-flow rate at a steam flow rate tends to increase with pressure. **[**

] (Ref. 2) This tendency means that the UPTF correlation derived below 15bar gives conservative results under higher pressure because more water accumulates around the SG inlet plenum when using the UPTF correlation than would be expected under higher pressure. The additional water accumulation around the SG inlet plenum causes a lower liquid level in the core during the loop seal clearing period, which increases the likelihood of core dryout.

Since the CCFL correlation strongly depends on flow-path geometry, the Ku relationship by the Dresden group using the rectangular geometry can not be applied directly to the US-APWR. However, the qualitative tendency of the effect of pressure on the liquid down-flow is considered to be relevant to the US-APWR. Therefore, the use of the CCFL correlation derived from the UPTF data is considered to be conservative in the M-RELAP5 SBLOCA analyses.

References:

1. C. Vallee et al., “Counter-current Flow Limitation Experiments in a Model of the Hot Leg of a Pressurized Water Reactor – Comparison between Low Pressure Air/Water Experiments and High Pressure Steam/Water Experiments,” The 13th Int. Topical Meeting on Nuclear Reactor Thermal Hydraulics (NURETH-13), N13P1107, Sep. 2009.
2. Mitsubishi Heavy Industries, Ltd., Small Break LOCA Methodology for US-APWR, MUAP-07013-P (R0), July 2007.

REQUEST 8.1.5-1

Discuss the scaling of the Duckler Air-Water Flooding test facility in comparison with the US-APWR steam generator tubes (diameter, length, friction factor, etc.),

RESPONSE

The comparison between the Dukler test facility and the US-APWR for the configuration and the fluid combination is shown in Table RAI-8.1.5-1.1. The subject on scaling for each item is considered as follows:

1. Tube diameter: The CCFL in steam generator (SG) tubes focuses on the interaction between the liquid film condensed within the tube and the upward steam flow. This implies less impact of tube end geometry affecting the CCFL curve and then the coefficient set (m=1.0, c=0.88, β=0.0) which is recommended in Ref. 5.2.1.6-2 is adopted when end effects are minimized. The J* scaling (Eq. 5.2.1.6-4) is considered to have a high adaptability for a small-scale pipe as discussed in the response of REQUEST 8.1.4-3 and the experimental data by Dukler in this section are indeed located near the curve as shown in Figure 8.1.5-4. Figure 5.2.1.6-5 (from Ref. 5.2.1.6-2) indicates that Eq. 5.2.1.6-4 correlates well the data irrespective of the tube diameter 3/4" or 5/4". The tube diameter 3/4" is near the US-APWR and the adaptability of the correlation is considered to be high.
2. Tube length: The phenomena restricting the downward liquid flow rate in SG tubes is considered to be governed by those near the bottom of the tubes where the steam and condensed liquid flows are maximized. The effect of tube length is unlikely to be important under the situation. Figure 5.2.1.6-5 shows several experimental data but the effect of length is not reported to be an affecting parameter.
3. Tube wall material: The effect of wall friction is considered to be smaller than the interfacial friction and any experimental studies on the wall friction against CCFL have not been recognized as far as MHI concerned. The coefficient c in ROSA-IV/LSTF is shown in the next item (4. Fluid combination) and the value is the same as Eq. 5.2.1.6-4. This means the effect of tube wall material is not significant because the LSTF uses stainless-steel tubes and the Dukler experiment Plexiglas. In the penetration region, the wall friction might have some effect because the water down flow rate in Dukler experiment tends to be larger than Eq. 5.2.1.6-4.
4. Fluid combination: Ref.1 revealed that the difference of fluid combination (air/water vs. steam/water) can be scaled by J* parameter (Figure RAI-8.1.5-1.1). Furthermore ROSA-IV/LSTF tests investigated the steam flow rate giving zero water penetration at the bottom of SG tubes (Ref.2) as shown below in Figure RAI-8.1.5-1.2 and the same coefficient c=0.88 was reported. These results support the same coefficient set (m=1.0, c=0.88, β=0.0) can apply to the US-APWR analyses.

References

1. Ohnuki, A., Experimental study of counter-current two-phase flow in horizontal tube connected to inclined riser, J. Nucl. Sci. Technol., Vol. 23, No. 3, pp 219-232, 1986.
2. Kukita, Y., Anoda, Y. and Tasaka, K., Summary of ROSA-IV LSTF first-phase test program – Integral simulation of PWR small-break LOCAs and transients -, Nucl. Eng. Design, Vol. 131, pp 101-111, 1991.

Table RAI-8.1.5-1.1 Comparison of configuration and fluid combination

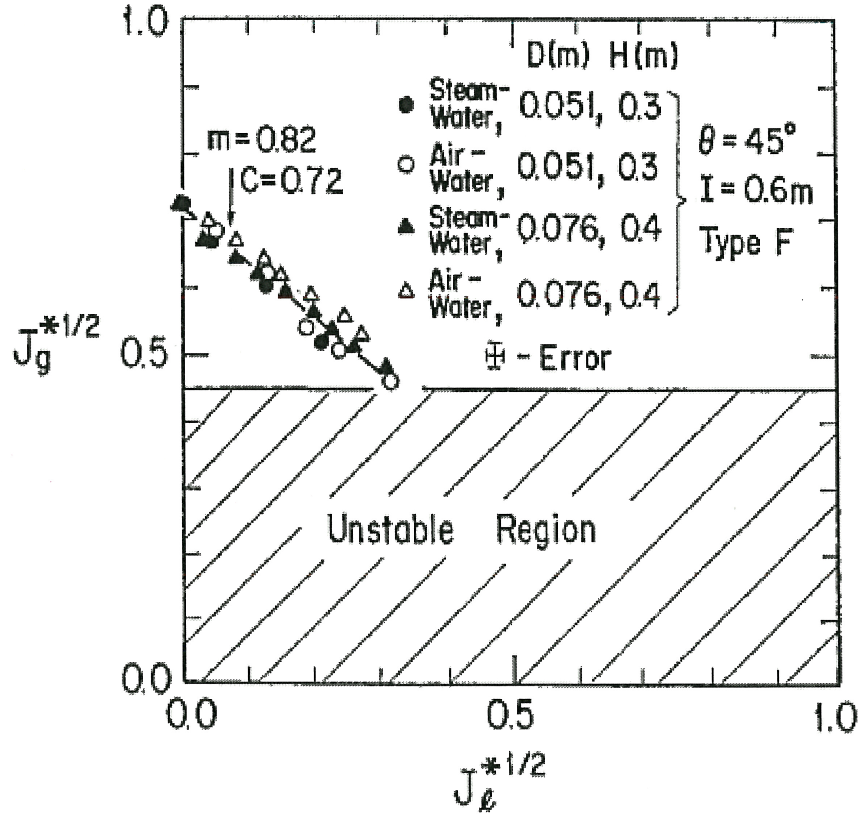

Fig. 8 Effect of fluid combinations (air/water and steam/water)

Figure RAI-8.1.5-1.1 Effect of fluid combinations

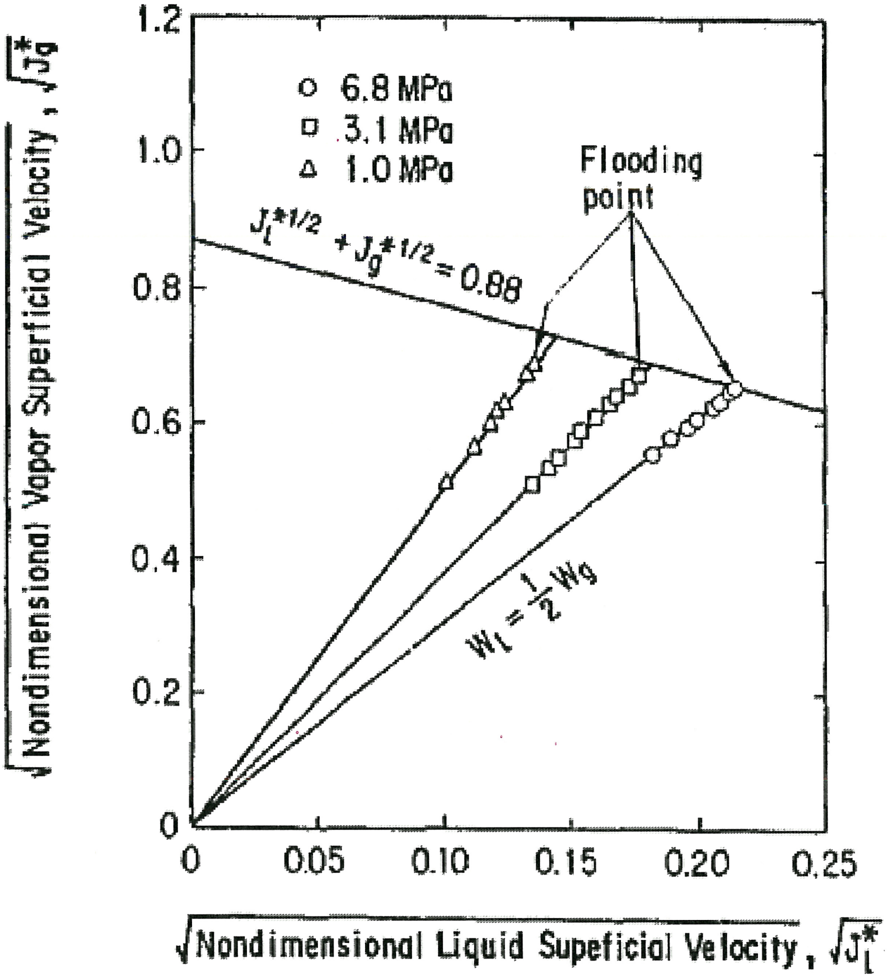

Fig. 13. Steam generator (SG) U-tube CCFL characteristics.

Figure RAI-8.1.5-1.2 SG U-tube CCFL characteristics in ROSA-IV/LSTF

REQUEST 8.1.5-2

Compare the test pressure, temperature and flow rates (both water and air) with those of the expected conditions at the SG U-tube uphill side during the loop seal clearing period, and discuss why these tests are applicable to the loop seal period of a SBLOCA.

RESPONSE

As investigated in the response of REQUEST 8.1.5-1, the CCFL correlation Eq. 5.2.1.6-4 using J* parameter has a high potential to scale the difference of the configuration and the fluid combination between the Dukler test facility and the US-APWR. Furthermore, the CCFL correlation gives an important contribution during the loop seal clearing period. Figure RAI-8.1.5-2.1 shows the transients of J* at intact loop side SG tubes in the ROSA-IV/LSTF analysis (Section 8.2). The comparison with the CCFL correlation is also included. The CCFL governs the down flow rate in the period of LS (Loop Seal) formation-clearance until the time of clearing.

Figure RAI-8.1.5-2.1 J* at intact loop side SG tube in the ROSA-IV/LSTF analysis and comparison with CCFL correlation

REQUEST 8.1.5-3

The test sections are made of Plexiglas/flexible tygon tubing while the SG tubes are made of inconel. Discuss the impact of the pipe material difference in assessing the applicability of the test results, since the surface property (friction factor and surface tension) of the pipes may influence the results. Smooth surface may be more inductive to more water going down, which the results indicate.

RESPONSE

The response on this subject is stated at the response-3 in REQUEST 8.1.5-1.

REQUEST 8.1.5-4

The test was performed with water and non-condensable gas (air), while the fluid in the SG tubes is condensable water/steam mixture during SBLOCA. Discuss the applicability of this test in spite of this difference.

RESPONSE

The response on this subject is stated at the response-4 in REQUEST 8.1.5-1.

REQUEST 8.1.5-5

Discuss if the test cover all flow regimes since reflood/reflux flow would be affected by the flow regime.

RESPONSE

In the Dukler flooding test, annular countercurrent flow was mainly investigated and a slugging flow was reported under a low air upward flow rate after flooding occurred. Basically, the same flow regime is predicted in M-RELAP5 analyses although the predictive accuracy on the flow regime boundary is not clear due to lack of experimental information especially on the axial variation of flow regime. The amount of liquid accumulation within the uphill side of SG U-tubes is one of most important values affecting the core liquid level. The CCFL characteristics and the flow regime predictions affect the value. The former subject is investigated in this section and Eq. 5.2.1.6-4 is confirmed to have a high potential to apply to the actual conditions as stated in the responses in REQUEST 8.1.5-1 and 8.1.5-2. The latter one (flow regime predictions) is indirectly evaluated in section 8.2.1 ROSA-IV/LSTF analysis through comparisons of differential pressures along the uphill side of SG U-tubes. Reasonable agreements were obtained on the differential pressure shown in Figure 8.2.1-26 and 8.2.1-27. The high adaptability of Eq. 5.2.1.6-4 and the good predictions for the differential pressures indicate no significant problems due to flow regime predictions.

REQUEST 8.1.5-6

Is the CCFL correlation described in Section 8.1.5.3.b, namely the three parameters in the Hewitt & Wallis correlation, the same one used in all SBLOCA simulations?

RESPONSE

The same parameters were used in all SBLOCA simulations.

REQUEST 8.1.5-7

[

]

RESPONSE

[

]

REQUEST 8.1.5-9

Figure number is wrong at the bottom of page 8.1.5-2. It should be changed to be Figure 8.1.5-4 from Figure 9.1.5-4.

RESPONSE

The figure number should be 8.1.5-4. MHI will correct the wrong number.

REQUEST 8.1.5-10

Figures 8.1.5-3 and 8.1.5-4 show the comparison of the calculated results to the measured data. What do the solid lines stand for in those figures?

RESPONSE

The solid lines stand for the relationship given by the Hewitt & Wallis correlation described in Section 8.1.5.3 b of the topical report MUAP-07013-P (R0) (Ref. 1). The inclusion of the solid lines is intended to show M-RELAP5 can trace the original correlation.

Reference:

1. Mitsubishi Heavy Industries, Ltd., Small Break LOCA Methodology for US-APWR, MUAP-07013-P (R0), July 2007.

REQUEST 8.2.1-1

The assessment of M-RELAP5 against the ROSA-IV/LSTF tests was for application to the US-APWR. Table 8.2.1-1 showed the scaling of the major design characteristics of the test facility against a PWR. Provide a similar table for the US-APWR.

RESPONSE

Table RAI-8.2.1-1.1 shows the scaling of the major design characteristics of the test facility against a US-APWR and a PWR. The scaling between the test facility and the US-APWR is similar to that between the test facility and a PWR.

References
1. The ROSA-IV Group, ROSA-IV Large Scale Test Facility (LSTF) System Description, JAERI-M84-237, 1985.
2. Kumamaru, H., et al., ROSA-IV/LSTF 5% Cold Leg Break LOCA Experiment RUN SB-CL-18 Data Report, JAERI-M89-113.

Table RAI-8.2.1-1.1 Major Design Characteristics of LSTF and PWR

REQUEST 8.2.1-2

In Section 8.2.1.3 (a), it was stated that “the hot and cold legs were sized to conserve the volume scaling and ratio of the length to the square root of pipe diameter, L/sqrt(D), for the reference PWR.” Does this still hold for the US-APWR? If not, discuss the implication or why this does not matter,

RESPONSE

The volume scaling and ratio of the length to the square root of pipe diameter, L/sqrt(D) are shown in Table RAI-8.2.1-1.1. MHI judged that the parameter scaling between LSTF and US-APWR does not cause any concern. The reason is as follows;
[

]

References
1. N. Zuber, Problems in Modeling of Small Break LOCA, NUREG-0724, 1980.

REQUEST 8.2.1-3

Test SB-CL-18 (5% break) was selected for analysis which is equivalent to a 6-inch break, because "both loop seal phenomena and boil off phenomena considered important for SBLOCA were observed in the experiment." However, the SBLOCA spans from 2" to 12", and it may be also important to know what phenomena occurs or does not occur at certain size breaks (and the code can simulate the non-occurrence of them at those sizes). Are there any plans to do additional assessment for other break sizes. Discuss the applicability of M-RELAP5 to break sizes other than the 6-inch break that has been assessed against data.

RESPONSE

A 5% break of ROSA/LSTF is equivalent to a 6-inch break of a 4-loop PWR, and is equivalent to a 7.5-inch break of the US-APWR. As pointed out by NRC, it may also be important to know what phenomena occur or do not occur at certain size breaks. Analyses of a 0.5% break and 10% break were performed to demonstrate the applicability of M-RELAP5 to smaller and larger breaks. The results of the analyses are shown in the following paragraphs.

For 10% break analysis, SB-CL-09 is selected. The features of this test are as follows.
- 10%(31.9mm ID) cold leg break, equivalent to 10.5-inch break of US-APWR
- No high head safety injection
- Core uncovery associated with the loop seal clearance occurred about 60 seconds after the break (Figures RAI-8.2.1-3.1 and 8.2.1-3.5)
- Loop seal clearance occurred about 75 seconds after break, but the upper core remained uncovered (Figures RAI-8.2.1-3.1, 8.2.1-3.5, and 8.2.1-3.10)
- The core power was tripped off at 111s when the maximum heater rod temperature reached 923K (Figure RAI-8.2.1-3.4, Figure RAI-8.2.1-3.8)
- The core water level rose after the core power termination and quench was observed near 150s (Figure RAI-8.2.1-3.5), before the accumulator injection began at about 200s.
- No boil-off occurred because the core power was tripped

The results of the M-RELAP5 analysis of SB-CL-09 are shown in Figures RAI-8.1.3-1 to 13. Analysis and boundary conditions are the same as described in Section 8.2.1.6 in MUAP-07013-P(R0) for Sensitivity-1. The core uncovery associated with loop seal clearance starts about 60s after the break and the loop seal clears at about 70s (Figure RAI-8.2.1-3.1). After loop seal clearance, the core water level did not fully recover (Figure RAI-8.2.1-3.1). M-RELAP5 well simulates the timing of core uncovery, loop seal clearance, and the subsequent core water level increase. At 111s, core power is tripped off, the core water level increases again, and the core is fully quenched by about 180s (Figures RAI-8.2.1-3.1 and 5 to 13). M-RELAP5 simulates the 10% break transient qualitatively well. The core water level drop is larger than in the test at 50s, and core heat up starts because of CHF rather than a top-down dryout. There are no boil-off and subsequent core recovery periods because of the core power trip.

[

]

[

]

M-RELAP5 conservatively simulates the SBLOCA tests that are equivalent to 2.5-inch and 10.5-inch breaks in the US-APWR. It is concluded that M-RELAP5 is applicable for a wide range of break sizes.

References

1. JAEA, A Study on ROSA/LSTF SB-CL-09 Test Simulating PWR 10% Cold Leg Break LOCA, JAEA-Research 2008-087, 2008.
2 JAERI, Results of 0.5% Cold-Leg Small-Break LOCA Experiments at ROSA-IV/LSTF Effect of Break Orientation, Experimental Thermal and Fluid Science, 1990.
3 Y.Kukita, et. al., Summary of ROSA-IV LSTF first-phase test program – integral simulation of PWR small-break LOCAs and transients -, Nuclear Engineering and Design 131, 1991, pp.101-111.

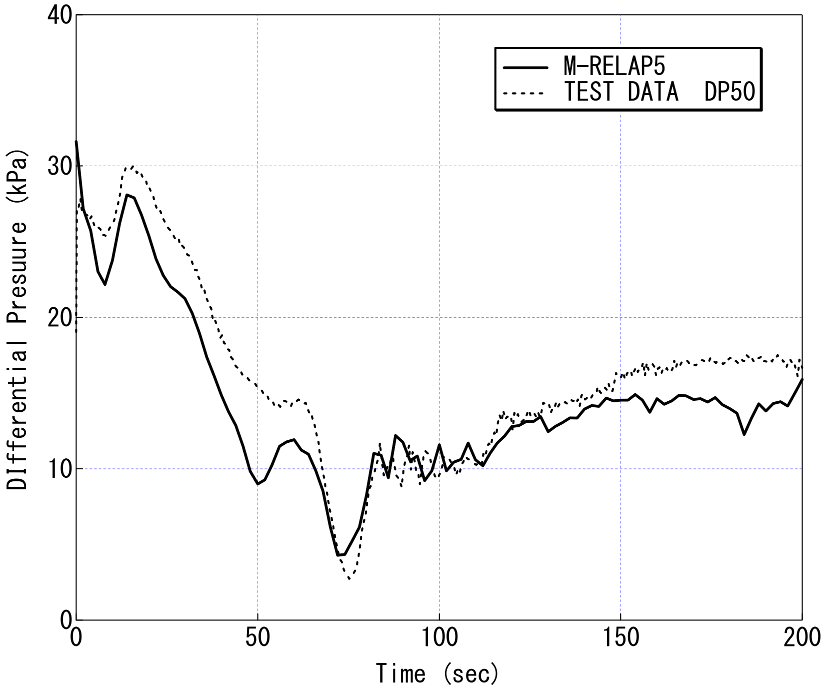

Figure RAI-8.2.1-3.1 Core Differential Pressure (10% break)

Figure RAI-8.2.1-3.2 Break Flow Rate (10% break)

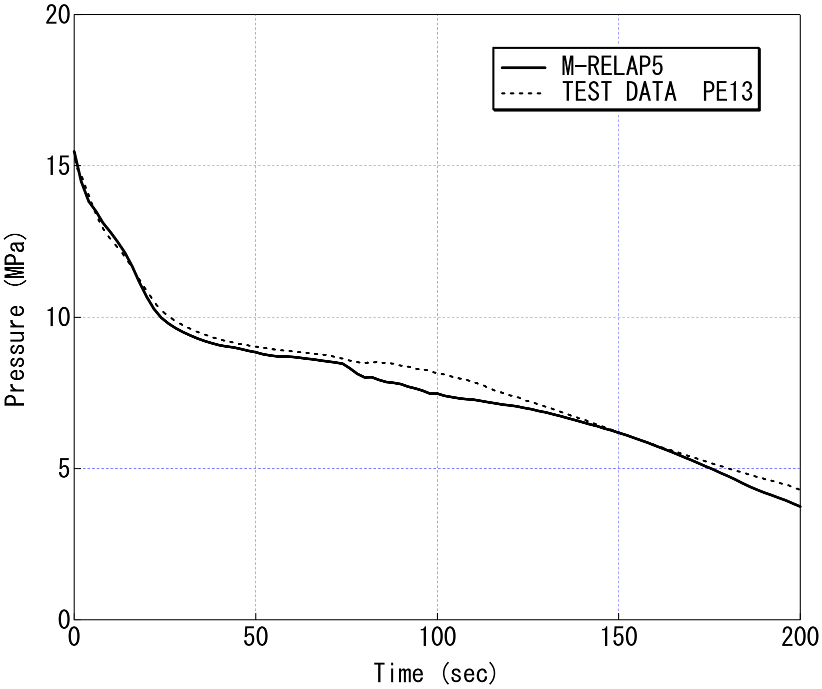

Figure RAI-8.2.1-3.3 Primary Pressure (10% break)

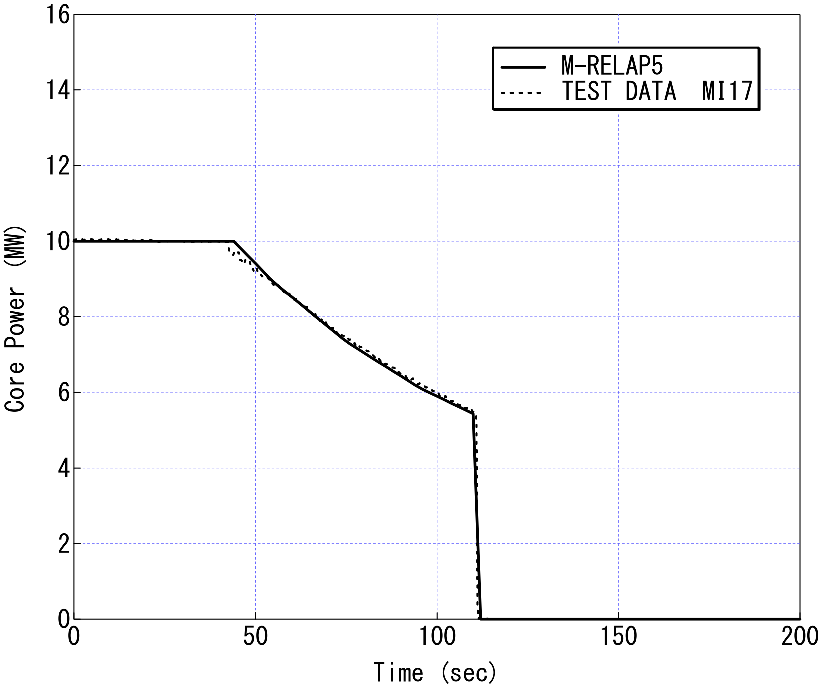

Figure RAI-8.2.1-3.4 Core Power (10% break)

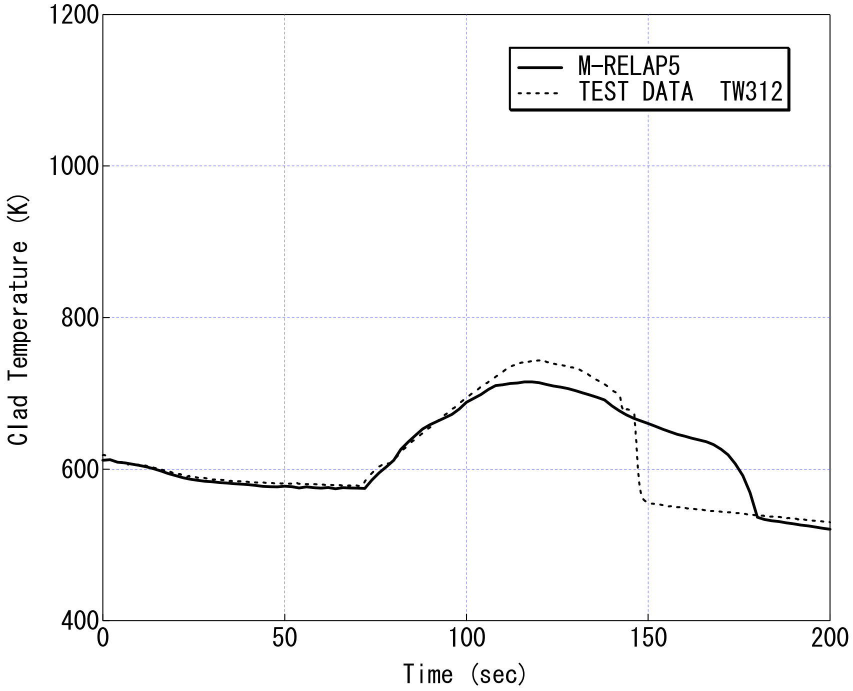

Figure RAI-8.2.1-3.5 Heater Rod Surface Temperature at 3.61m (Test Data) and at 3.57m (M-RELAP5) (10% break)

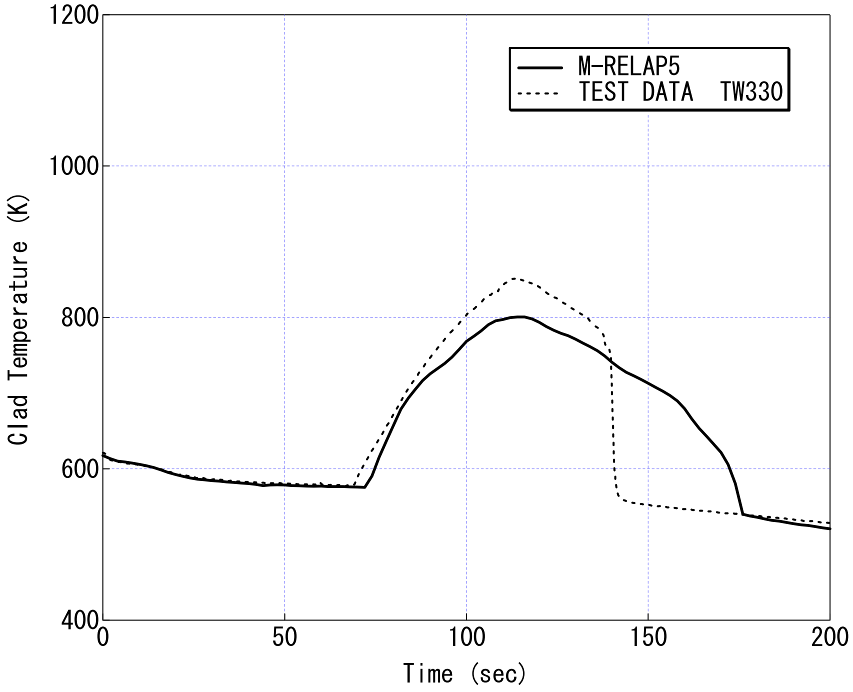

Figure RAI-8.2.1-3.6 Heater Rod Surface Temperature at 3.05m (Test Data) and at 3.17m (M-RELAP5) (10% break)

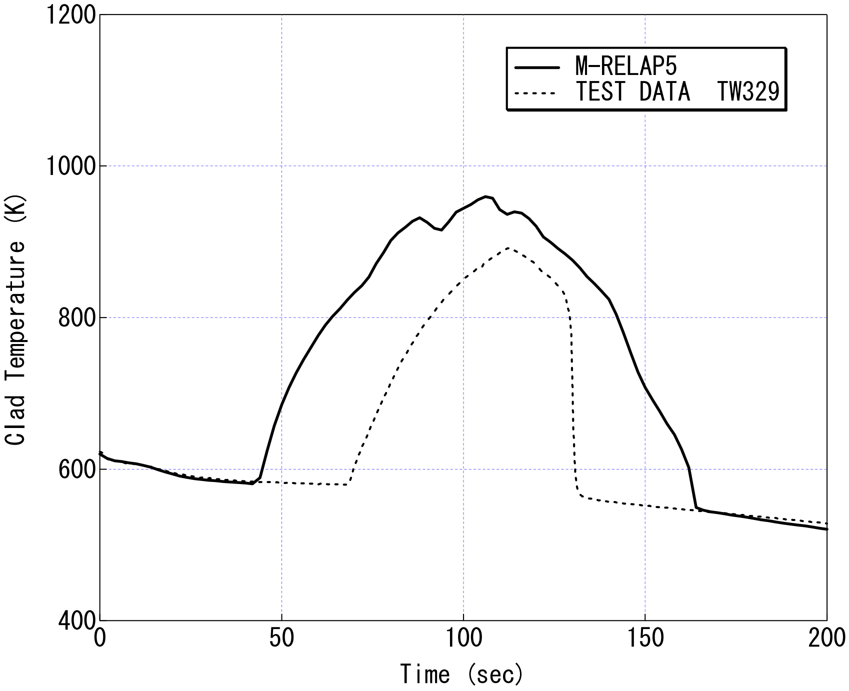

Figure RAI-8.2.1-3.7 Heater Rod Surface Temperature at 2.64m (Test Data) and at 2.68m (M-RELAP5) (10% break)

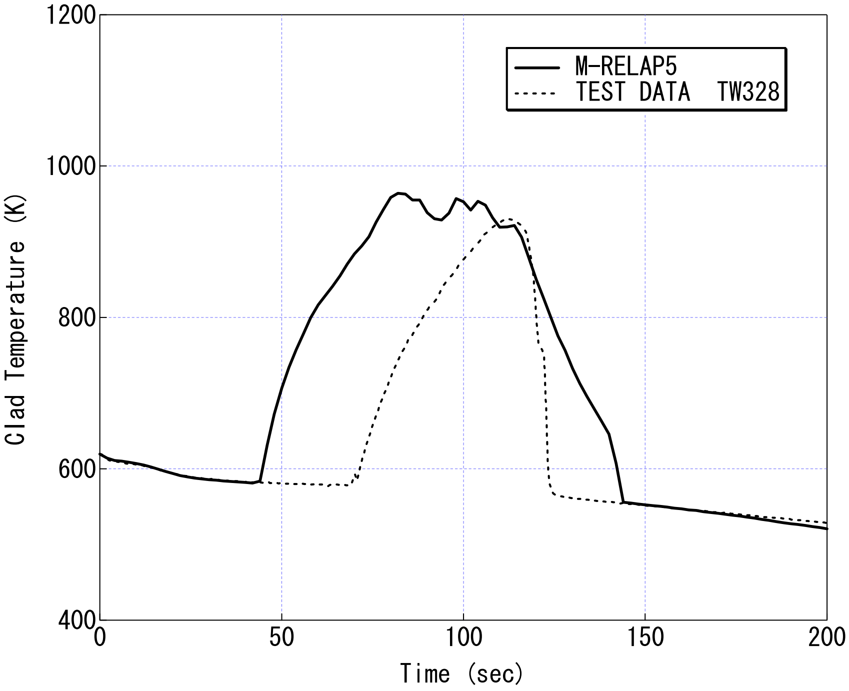

Figure RAI-8.2.1-3.8 Heater Rod Surface Temperature at 2.24m (Test Data) and at 2.23m (M-RELAP5) (10% break)

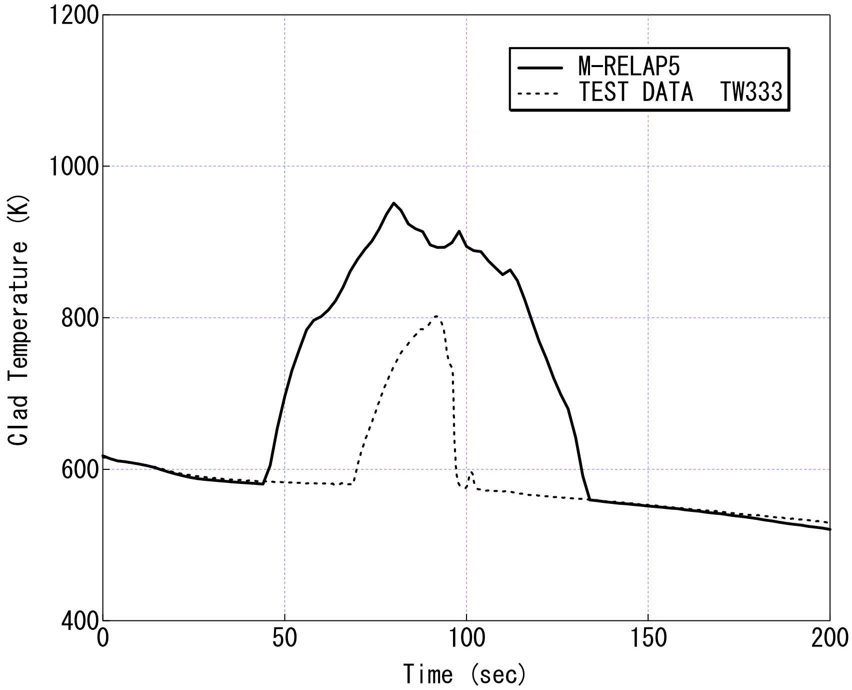

Figure RAI-8.2.1-3.9 Heater Rod Surface Temperature at 1.83m (Test Data) and at 1.82m (M-RELAP5) (10% break)

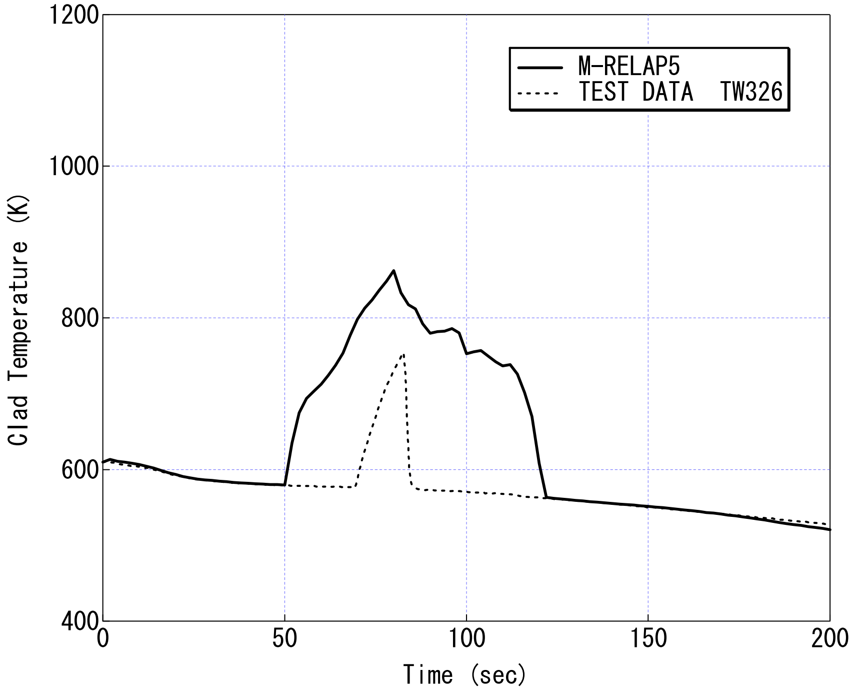

Figure RAI-8.2.1-3.10 Heater Rod Surface Temperature at 1.42m (Test Data) and at 1.38m (M-RELAP5) (10% break)

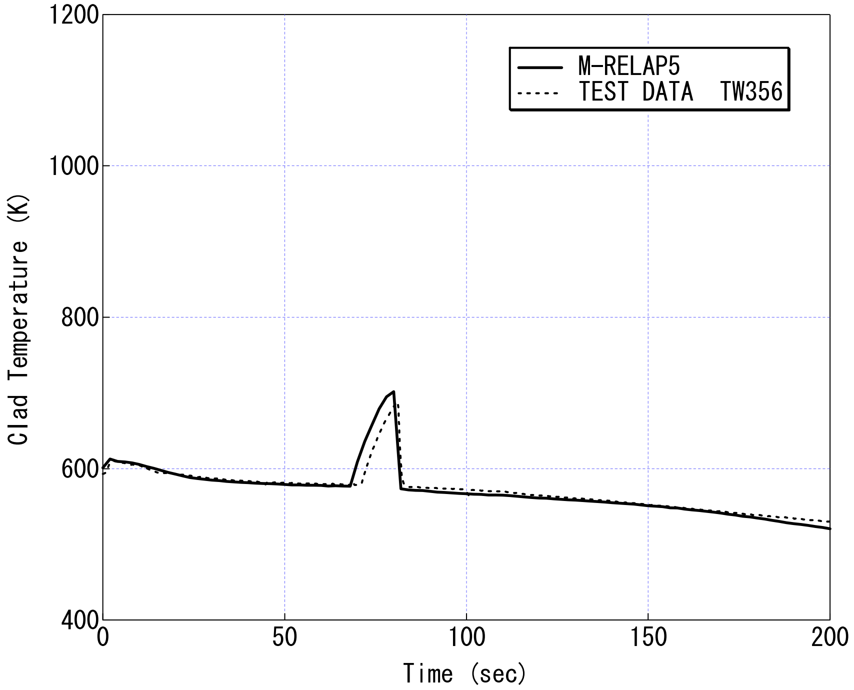

Figure RAI-8.2.1-3.11 Heater Rod Surface Temperature at 1.02m (Test Data) and at 1.11m (M-RELAP5) (10% break)

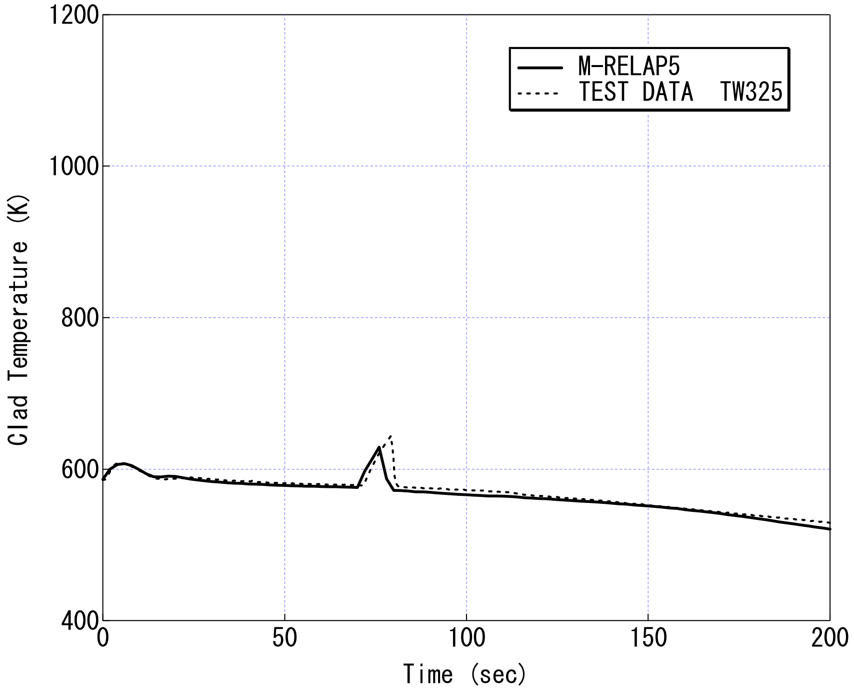

Figure RAI-8.2.1-3.12 Heater Rod Surface Temperature at 0.61m (Test Data) and at 0.64m (M-RELAP5) (10% break)

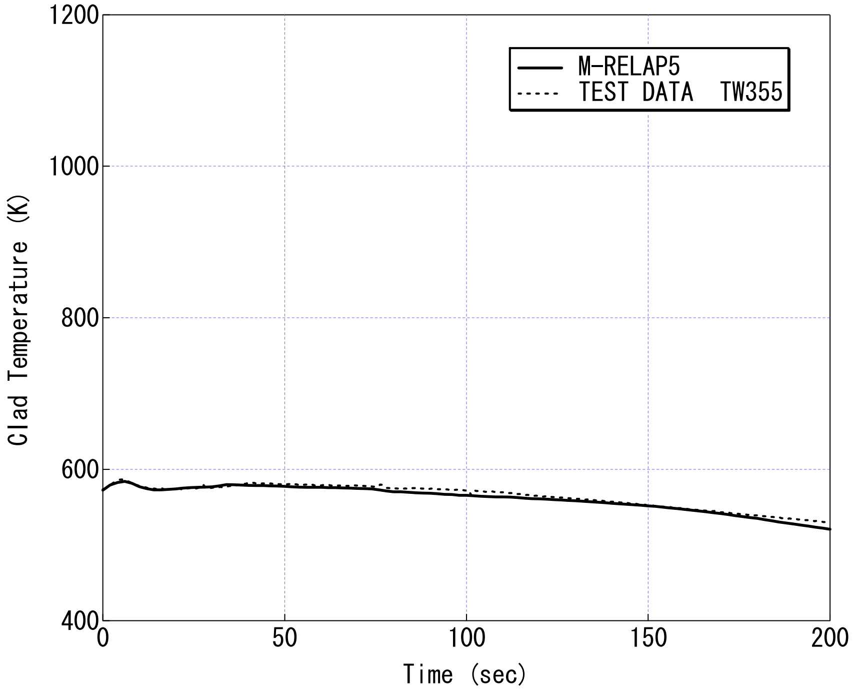

Figure RAI-8.2.1-3.13 Heater Rod Surface Temperature at 0.05m (Test Data) and at 0.07m (M-RELAP5) (10% break)

REQUEST 8.2.1-4

What is the timing of 10 MW in the decay heat curve (120% of ANS curve) in terms of scaling with respect to the US-APWR?

RESPONSE

The power curve of ROSA-IV assumes that the initial power is 71.3MW (see Footnote 2 of Table RAI-8.2.1-1.1). 10MW is about 14% of 71.3MW, which exceeds 120% of the initial value of decay heat from the ANS curve. The ROSA-IV power curve is higher because it simulates delayed neutron fission power following reactor trip. The time after initiation of control rod insertion that the core power reaches 14% of the initial power follows for the US-APWR analysis:

1-ft^2 break : about 4 seconds
7.5-inch break : about 9 seconds
2-inch break : about 11 seconds

The time depends on the break size because of the reactivity feedback.

References

1. MHI, Small Break LOCA Sensitivity Analyses for US-APWR, MUAP-07025-P (R0), December 2007.

REQUEST 8.2.1-5

[

]

RESPONSE

[

]

REQUEST 8.2.1-5

[

]

RESPONSE (Revision 1)

[

]

REQUEST 8.2.1-6

Figure 8.2.1-17 shows that M-RELAP5 core water level drops earlier than test (300 sec for the analysis vs. 400 sec for the test.) during the boil off period. Section 8.2.1.5 (d) (1) attributes it to more liquid remaining in the cross-over legs for the analysis (Figures 8.2.1-32 and -33). However, the figures show that water holdup is larger during the period preceding this difference, and the difference is decreasing at 300 seconds. This observation seems contradictory to the above explanation. Provide an explanation for the observed inconsistency.

RESPONSE

[

]

[

]

REQUEST 8.2.1-7

[

]

RESPONSE

[

]

REQUEST 8.2.1-8

[

]

RESPONSE

[

]

REQUEST 8.2.1-8-1
(Related RAI 8.2.1-8)
[

]

RESPONSE
[

]

REQUEST 8.2.1-9

(Related RAI 8.1.4-7)

[

]

RESPONSE

[

]

REQUEST 8.2.1-10

On page 8.2.1-7 MHI defines the time period from 50 s to 95 s as the natural circulation period. According to the pump coastdown curves (Figure 8.2.1-11 and 8.2.1-12), however, the pump speed is still high during that period (about 5/8 of the initial speed at 50 s and about 5/16 of the initial speed at 95 s). So the flow rate seems to be still primarily determined by the pumps. Please justify quantitatively that the time period of 50 s to 95 s can be defined as the natural circulation period.

RESPONSE

As described previously in the response to REQUEST 4-1 (Ref. 1), the natural circulation period starts (the blowdown period ends) when the primary system pressure has decreased to nearly that of the secondary system. The natural circulation period ends when the liquid flow rate at the top of SG U-tubes decreases to zero. During this period, the RCP pump head is expected to be zero or negative, since the RCP trips concurrently with the reactor trip in the accident scenario for the US-APWR LOCAs.

Figure RAI-8.2.1-10.1 shows temporal changes of the primary and secondary pressures. The period from 50 to 95 seconds is identified as the natural circulation phase based on the definition described above. During this period, the RCP head stayed below zero, as shown in Figures RAI-8.2.1-10.2 and 3, which indicates that the primary mass flowrate was not determined by the pumps, but instead was determined by natural circulation.

Reference:

1. Mitsubishi Heavy Industries, Ltd., MHI's Partial Responses to the NRC's Requests for Additional Information on Topical Report MUAP-07013-P (R0) "Small Break LOCA Methodology for US-APWR", UAP-HF-09002-P (R0), January 16, 2009.

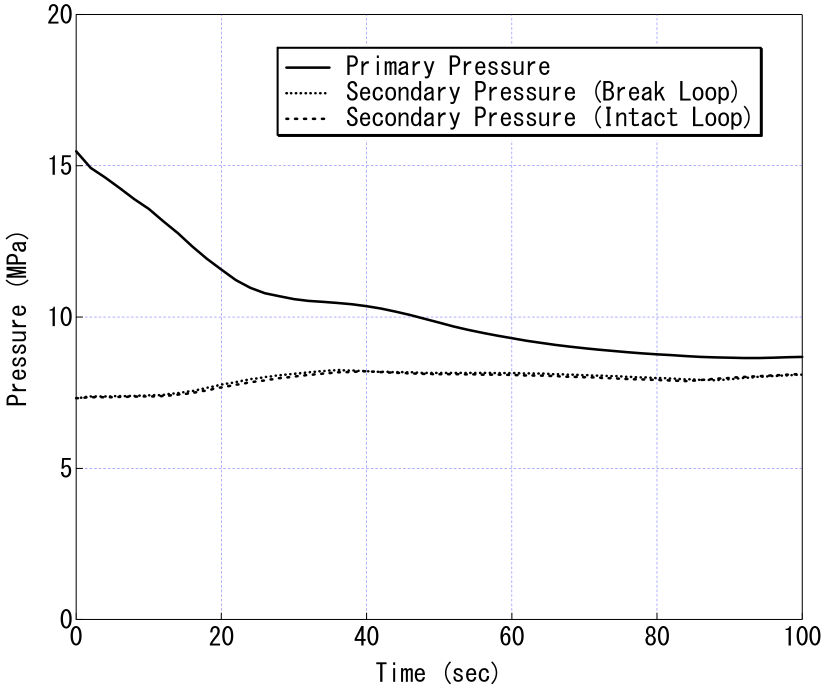

Figure 8.2.1-10.1 Primary and Secondary Pressures

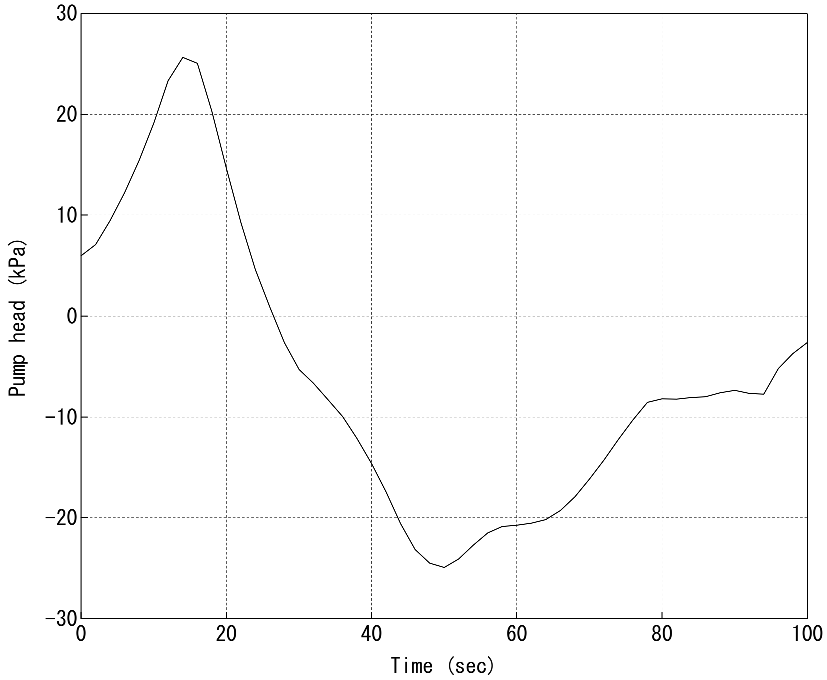

Figure 8.2.1-10.2 Pump Head (Broken Loop)

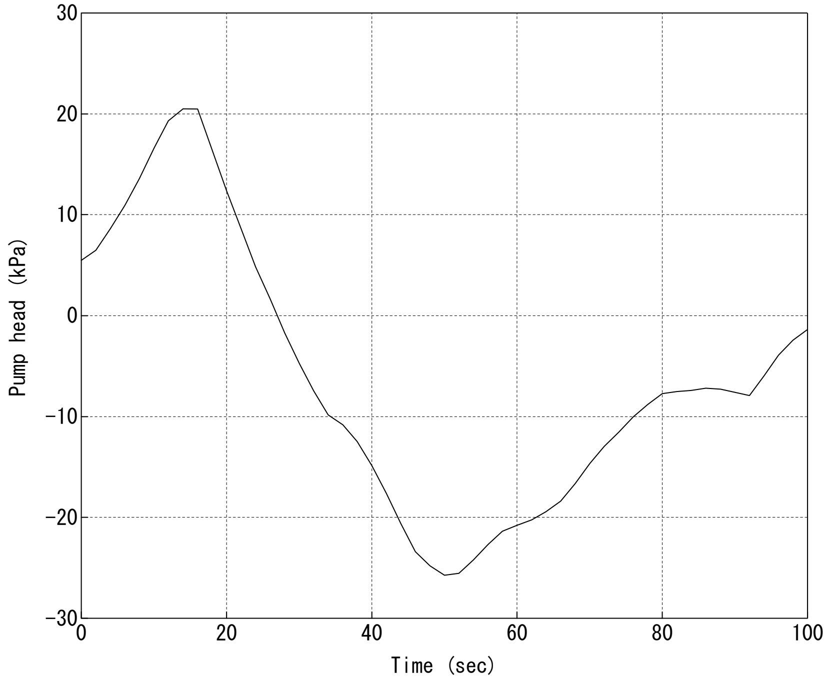

Figure 8.2.1-10.3 Pump Head (Intact Loop)

REQUEST 8.2.1-11

On page 8.2.1-7 MHI states, “Both loops flowrate at cross-over leg of M-RELAP5 calculation agree with these of the test data during natural circulation period (Figure 8.2.1-18 and 19). As a result, M-RELAP5 capability to predict SG primary and secondary heat transfer is good.”

As discussed in RAI 8.2.1-10, the loop flowrate seems to be mostly determined by the pump speed during that time period. And the pump coastdown curve was given as an input. As a result, it is obvious that the predicted loop flowrate agrees well with the test data. MHI’s conclusion above regarding the heat transfer prediction being good is based on an essentially specified flow rate, a major determinant of the heat transfer coefficients. Please explain how this assessment is useful for assessing M-RELAP5 for application to the US-APWR SBLOCA where the flow rate must be predicted by the code.

RESPONSE

The response to REQUEST 8.2.1-10 showed that the primary coolant flowed under the natural circulation condition. The primary flowrate was primarily dependent on the coolant vaporization in the core and steam condensation in the SG during the identified time period (50-95 seconds). Heat removal to the secondary system is modeled to simulate the steam condensation in the present code assessment. The capability of M-RELAP5 to predict the heat transfer in the SG is discussed in the response to REQUEST 8.2.1-12.

REQUEST 8.2.1-12

The 2nd last paragraph on page 8.2.1-7 states, "Break flowrate of M-RELAP5 calculation is adjusted to test data (Figure 8.2.1-15), as a result, primary pressure drop behavior agrees with test data excellently (Figure 8.2.1-16). Signal timings agree with test data (Table 8.2.1-6). Secondary pressures are also adjusted to test data (Figure 8.2.1-13 and 8.2.1-14). Primary pressure and secondary pressures of M-RELAP5 calculation agree with test data, as a result, M-RELAP5 capability to predict SG primary and secondary heat transfer is good."

It is obvious that the primary and secondary system pressures show good agreements between the prediction and the measurement because the primary system pressure was predicted with the adjusted break flow and the secondary system pressure was also adjusted to the test data. Since this is not the manner in which the plant calculations will be performed, i.e. break flow and secondary pressure will not be specified as boundary conditions, please explain how this assessment establishes the ability of M-RELAP5 to predict the plant response for SBLOCA events.

RESPONSE

The break flow and secondary pressures were input as boundary conditions so that the validation could focus on the code's ability to calculate important RCS phenomena such as natural circulation, liquid holdup in the U-tubes, loop seal clearing, core uncovery, and core heat-up without the influence of errors caused by peculiarities of experimental systems, such as break geometry, steam generator heat loss, steam generator valve leakage, and so forth.

Although the break flow model of M-RELAP5 has not been explicitly validated, the uncertainty of break flow and/or its impact to US-APWR SBLOCAs is adequately addressed via the break spectrum sensitivity calculations that were performed to support the DCD (Ref. 1). In addition, M-RELAP5 uses the Moody critical flow model for the plant calculations in conformance to the Appendix K requirement. Thus, MHI validated to use the adjusted break flow rate for the present code validation calculation.

As pointed out by the reviewer, on the other hand, the SG heat transfer predicted by M-RELAP5 was not validated using the ROSA/LSTF SB-CL-18 test calculation (Ref. 2). Therefore, MHI will provide additional sensitivity calculations where the mechanical motion of the main steam isolation and relief valves is explicitly modeled to validate the capability of M-RELAP5 to predict the SG secondary-side pressure as well as the SG heat transfer. Results of the additional sensitivity calculations will be provided to complete MHI response to the present REQUEST in the second response of the 3rd set of NRC's RAI for the M-RELAP5 topical report, scheduled to be submitted to the NRC on November 6, 2009.

References:

1. Mitsubishi Heavy Industries, Ltd., SBLOCA Sensitivity Analysis for US-APWR Technical Report MUAP-07025-P (R0), December 2007.
2. Mitsubishi Heavy Industries, Ltd., Small Break LOCA Methodology for US-APWR, MUAP-07013-P (R0), July 2007.

REQUEST 8.2.1-12

The 2nd last paragraph on page 8.2.1-7 states, “Break flowrate of M-RELAP5 calculation is adjusted to test data (Figure 8.2.1-15), as a result, primary pressure drop behavior agrees with test data excellently (Figure 8.2.1-16). Signal timings agree with test data (Table 8.2.1-6). Secondary pressures are also adjusted to test data (Figure 8.2.1-13 and 8.2.1-14). Primary pressure and secondary pressures of M-RELAP5 calculation agree with test data, as a result, M-RELAP5 capability to predict SG primary and secondary heat transfer is good.”

It is obvious that the primary and secondary system pressures show good agreements between the prediction and the measurement because the primary system pressure was predicted with the adjusted break flow and the secondary system pressure was also adjusted to the test data. Since this is not the manner in which the plant calculations will be performed, i.e. break flow and secondary pressure will not be specified as boundary conditions, please explain how this assessment establishes the ability of M-RELAP5 to predict the plant response for SBLOCA events.

RESPONSE (Revision 1)

Followings are the quantitative evaluation result that MHI stated in the previous response to this REQUEST (Ref. 1).

MHI has performed an additional sensitivity analysis where mechanical motions of the main steam isolation and relief valves are modeled with the VALVE components. SG secondary pressure transients are shown in Figures RAI-8.2.1-12.1 and 2. The heat transfer through the SG U-tubes is validated by comparing the integral of steam mass discharged out the main steam isolation and relief valves between the calculation and measurement. It is noted that SG primary and secondary side heat transfers are identified as high-ranked phenomena during the blowdown, natural circulation, and loop seal clearance phases in the US-APWR SBLOCA PIRT (Ref. 2).

Although M-RELAP5 overestimates the steam released from the SGs as shown in Figures RAI-8.2.1-12.3, the difference between the calculation and measurement of the total discharge is less than 10%. This overestimation is negligibly small from the impact to the primary system pressure response as confirmed in Figure RAI-8.2.1-12.4. In addition, Figure RAI-8.2.1-12.5 shows that the core liquid level (differential pressure) in the sensitivity calculation agrees with that obtained by the base model described in the topical report (Ref. 1). This fact suggests that the code assessment results presented in the topical report are sufficiently meaningful, even though the secondary system pressure is imposed by the boundary condition there.

References:

1. Mitsubishi Heavy Industries, Ltd., MHI's 1st Response to the NRC's Request for Additional Information on Topical Report MUAP-07013-P (R0) “Small Break LOCA Methodology for US-APWR” on 09/08/2009, UAP-HF-09492-P (R0), October 23, 2009.
2. Mitsubishi Heavy Industries, Ltd., Small Break LOCA Methodology for US-APWR, MUAP-07013-P (R0), July 2007.

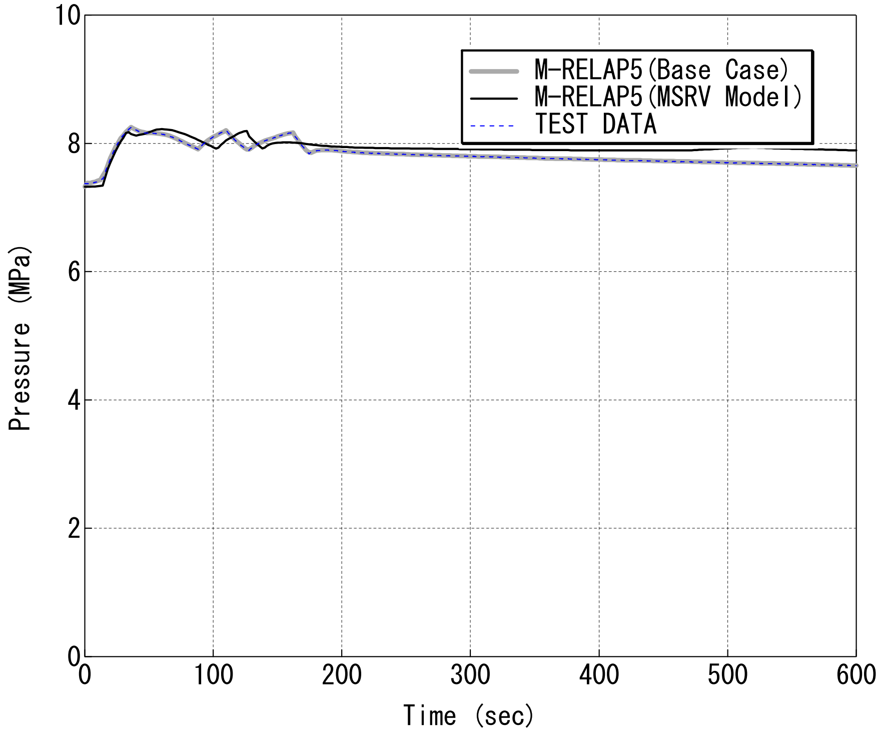

Figure 8.2.1-12.1 Broken Loop Secondary Pressure

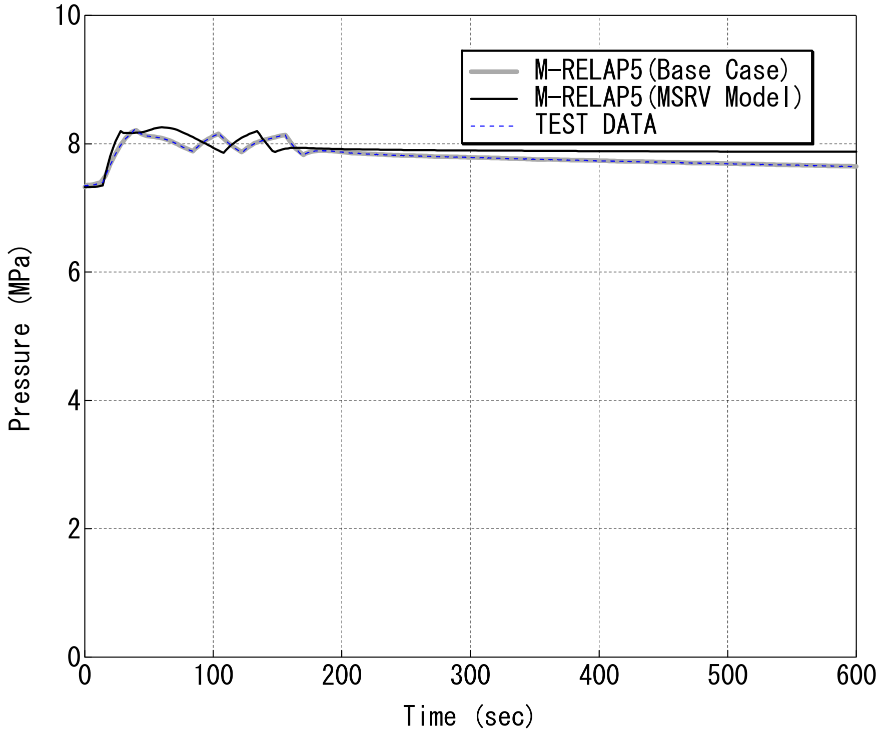

Figure 8.2.1-12.2 Intact Loop Secondary Pressure

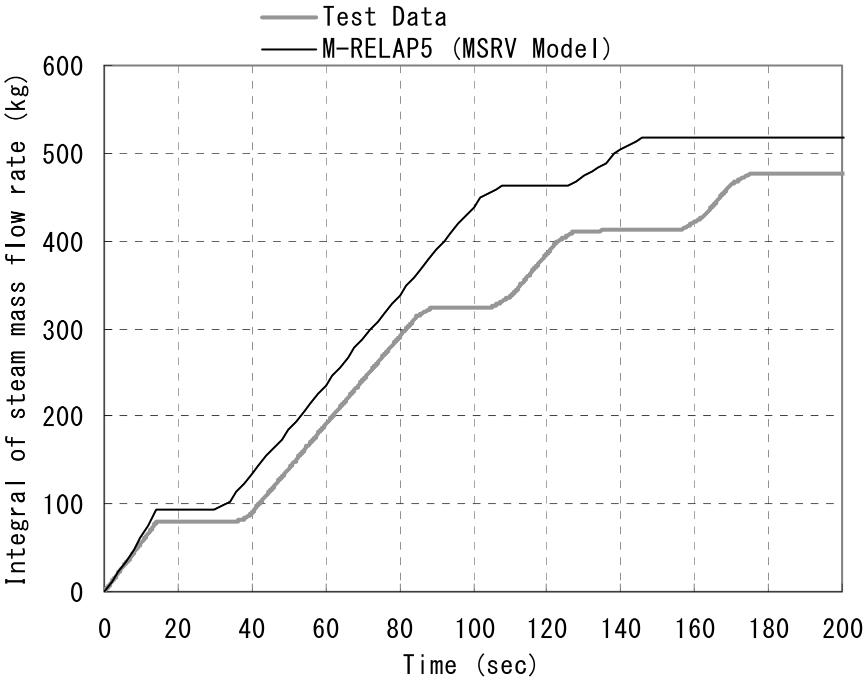

Figure 8.2.1-12.3 Integral of SG Secondary Outlet Steam Mass

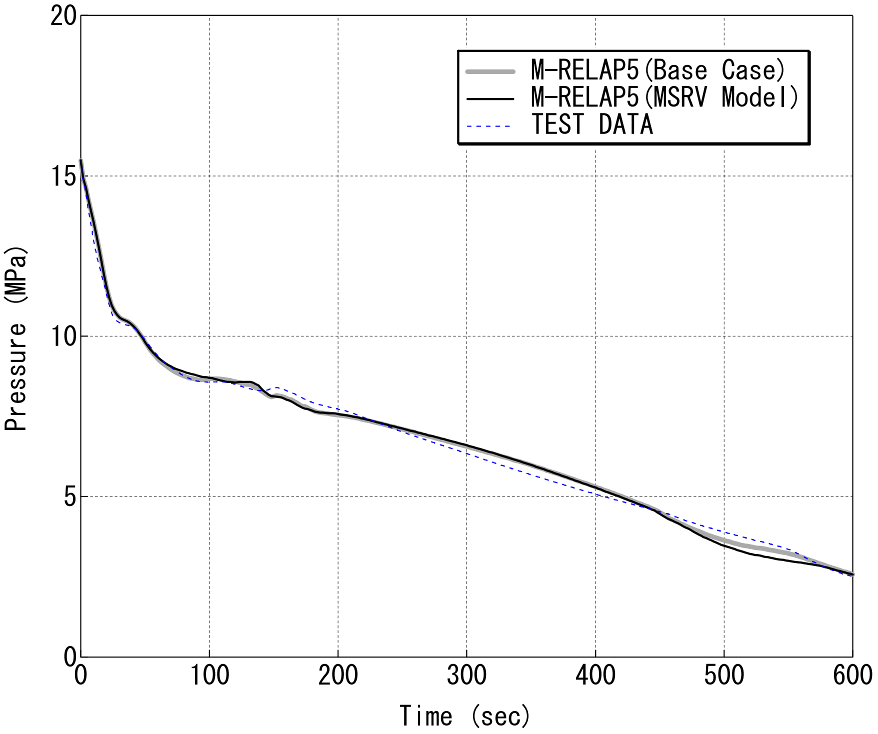

Figure 8.2.1-12.4 Pressurizer pressure

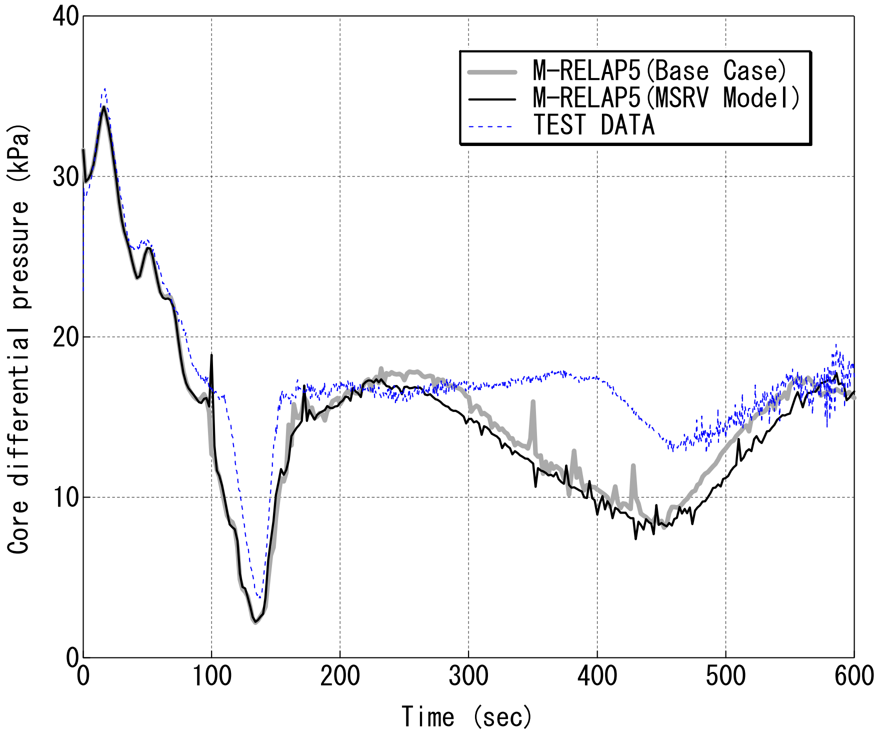

Figure 8.2.1-12.5 Core Differential Pressure

REQUEST 8.2.1-12-1

(Related RAI 8.2.1-12)

MHI mentioned that errors may arise by not specifying some important parameters as boundary conditions. However, if that is the case then one might expect that similar errors can arise in the US-APWR SBLOCA simulations. That is why M-RELAP5 needs to be assessed against IETs' data and the errors need to be identified and considered in establishing the capability of M-RELAP5 to predict the plant response for SBLOCA events.

The approach that MHI used in this case makes this a SET and not an IET. MHI has performed other tests in an IET manner. The documentation should reflect the limitations of the conclusions that can be drawn from this assessment. Either modify the discussion to accurately portray what can be concluded from this assessment or explain how the assessment of ROSA-IV/LSTF Small Break (5%) LOCA test in Section 8.2.1 establishes the ability of M-RELAP5 to predict the US-APWR response for SBLOCA events in light of specifying important parameters as boundary conditions.

RESPONSE

As the Moody critical flow model incorporated in M-RELAP5 generally predicts an excessive break flowrate, it is not expected that the break flowrate of an experiment can be matched when the Moody model is applied. Break flowrate significantly affects the thermal hydraulic behavior in the primary system. Therefore, break flowrate is specified as the boundary condition to validate important phenomena during SBLOCA transients in the ROSA-IV/LSTF test analysis presented in MUAP-07013-P (Ref. 1). The secondary pressure is also specified as the boundary condition to focus on the code's ability to predict primary system behavior. **[**

]

NRC pointed out that the SG primary to secondary heat transfer is not validated by the calculation in which the primary and secondary pressures are specified as boundary conditions (Ref. 2). **[**

]

Therefore, an additional calculation was performed to respond to REQUEST 8.2.1-12 (Ref. 3). The secondary system mechanical motions, like the main steam isolation valve closing and relief valve opening and closing, are simulated in the calculation. And it is confirmed that M-RELAP5 predicts excellently the SG primary to secondary heat transfer.

NRC also pointed out in REQUST 8.2.1-22 that the integral applicability of M-RELAP5 to US-APWR SBLOCA analysis has not been validated because the break flowrate was specified as the boundary condition and the assessment was not performed in the same manner as the plant analysis was performed (Ref. 2). MHI responded that the Moody critical flow model required by Appendix K is used in the US-APWR SBLOCA analysis, the uncertainty in the calculation of break flow is adequately considered in the break spectrum sensitivity calculations, and that the accuracy of the Moody model compared to ROSA-IV/LSTF test data is not relevant (Ref. 4). However, it is meaningful to perform the assessment with the break flow model in the same manner as the plant analysis and confirm an absolute conservatism of M-RELAP5.

Therefore, an additional assessment with the break flow model is performed for the ROSA-IV/LSTF. In this calculation, the secondary system behaviors are also simulated. **[**

] Obtained results are shown in the Appendix to this response. The predicted PCTs are higher than the measured values during both loop seal clearance and boil-off periods. It is confirmed that M-RELAP5 can be conservatively applied to US-APWR SBLOCA analysis by this assessment. In addition, both the primary and secondary pressure responses agree well with the measured values from the break initiation through the loop seal clearance, indicating that M-RELAP5 is able to predict the SG primary to secondary heat transfer **[**

].

MHI intends to modify Chapter 8.2.1 of MUAP-07013-P (Ref. 1) to reflect the NRC's comments about the primary and secondary boundary conditions and to include the additional calculations performed to respond to the NRC's requests. The structure of the section will be changed as shown in Table RAI-8.2.1-12-1.1. The sensitivity calculations performed to investigate the core water level predictions during the boil-off phase are included in section 8.2.1.8. Contents of the revised or added description for each section are shown in Table RAI-8.2.1-12-1.2.

[

] Finally, the conservatism of M-RELAP5 for US-APWR SBLOCA analysis is confirmed by the ROSA-IV/LSTF calculation performed in the same manner as the plant analysis. The conclusions obtained from these calculations will be described in Section 8.2.1.10 of MUAP-07013-P.

References:

1. Mitsubishi Heavy Industries, Ltd., Small Break LOCA Methodology for US-APWR, MUAP-07013-P (R0), July 2007.
2. NRC, "Request for Additional Information on Topical Report MUAP-07013-P, 'Small Break LOCA Methodology for US-APWR'," dated on September 8, 2009.
3. Mitsubishi Heavy Industries, Ltd., MHI's 2nd Response to the NRC's Request for Additional Information on Topical Report MUAP-07013-P (R0), "Small Break LOCA Methodology for US-APWR" on 09/08/2009, UAP-HF-09512, November 2009.
4. Mitsubishi Heavy Industries, Ltd., MHI's 1st Response to the NRC's Request for Additional Information on Topical Report MUAP-07013-P (R0), "Small Break LOCA Methodology for US-APWR" on 09/08/2009, UAP-HF-09492, Octorber 2009.

Table RAI-8.2.1-12-1.1 Revision of the Content Table of Chapter 8.2

Table RAI-8.2.1-12-1.2 Description Revision of Chapter 8.2

Appendix to Response to REQUEST 8.2.1-12-1

[

]

[

]

REQUEST 8.2.1-12-2
(Related RAIs 8.2.1-10, 8.2.1-11, 8.2.1-12)
[

]

RESPONSE
[

]

[

]

REQUEST 8.2.1-13

The 2nd paragraph on page 8.2.1-8 states, “Downcomer water level of M-RELAP5 result agrees with that of test data at about 150 sec (Figure 8.2.1-34). As a result, M-RELAP5 capability to predict downcomer mixture level is good during loop seal period.”

Figure 8.2.1-34 shows that the predicted behavior of the downcomer water level (in terms of differential pressure) is different from the measured data until around 150 s. Explain this difference.

The initial differential pressure is higher in the simulation than in the experiment by around 3 kPa. Does this mean that the measurement points of the differential pressure are different between the simulation and the test? Explain why there is approximately a 3 kPa difference in the differential pressure at time zero.

RESPONSE

The M-RELAP5 noding diagram for the ROSA-IV/LSTF calculation and the axial locations for the downcomer differential pressure measurement are shown in Figure RAI-8.2.1-13.1. The predicted differential pressure between Location 1 and Location 2 was used in the Figure 8.2.1-34 of MUAP-07013-P (Ref. 1). Location 1 is the center of component 100, and Location 2 is the middle of the centers of components 112 and 116. These axial locations are different from those for the measurement as shown in Figure RAI-8.2.1-13.1. The differential pressure for the measurement locations is obtained from the calculation results and is compared with the measurement data in Figure RAI-8.2.1-13.2. The calculated initial differential pressure agrees with the measurement data.

The initial coolant temperature in the upper downcomer above the cold leg **[** **]** is not adequately calculated in the steady state initialization because the coolant temperature of **[** **]** is not accurately calculated by the one-dimensional nodalization and then the heat transfer from **[** **]** through the wall is not accurately calculated. As the initial core power of the ROSA-IV/LSTF is 14% of the scaled power, the initial loop flow rate is also reduced to 14% of the scaled flow rate (Ref. 2). And the bypass flow between the downcomer and the upper head is 0.3% of the rated core flow **[** **]**. As the flow rate into the upper downcomer is small, the coolant stays there for a long time. The heat transferred from the coolant having the hot leg temperature that occurred in the upper plenum and the upper head through the wall cannot be neglected. It is estimated that the initial coolant temperature in the upper downcomer is higher than the cold leg temperature and is near the primary coolant system average temperature. The obtained temperature in the original steady state initialization is slightly higher than the cold leg temperature.

The sensitivity calculation was performed to investigate the effect of the initial coolant temperature in the upper downcomer on the differential pressure of the downcomer. In this calculation, the initial coolant temperature in the upper downcomer region is set to the primary coolant average temperature, and also the temperatures in thermal equilibrium with the adjacent coolant are applied for the heat structures in the upper downcomer and also the upper head. In the original calculation, the measured temperature near the hot leg temperature is already applied to the coolant in the upper head, but the cold leg temperature is still applied to the heat structures in the upper head. **[** **]**

[

]

The calculated result is shown in Figure RAI-8.2.1-13.3. The predicted differential pressure decreases more before 150 seconds and agrees better with the measurement than the original calculation. As the initial coolant temperature in the upper downcomer is higher and the coolant warmed by the heat transfer from the heat structure in the upper head comes through the spray nozzle in the present calculation, the coolant in the upper downcomer begins to flash earlier as the primary coolant system depressurizes and this flashing pushes out hotter coolant to the lower downcomer. The flashing in the upper downcomer and the coolant temperature increase in the lower downcomer decrease the differential pressure in the downcomer. The predicted core differential pressure is shown in Figure RAI-8.2.1-13.4 compared with the original calculation. The changes of the initial coolant temperature in the upper downcomer, the initial heat structure temperature in the upper part of the reactor vessel **[** **]** hardly affect the other parameters rather than the differential pressure in the downcomer.

The over-prediction of the differential pressure of the downcomer until around 150 seconds in MUAP-07013-P is considered to be caused by the initial coolant temperature in the upper downcomer, the initial heat structure temperature in the upper part of the reactor vessel **[** **]**.

References:
1. Mitsubishi Heavy Industries, Ltd., Small Break LOCA Methodology for US-APWR, MUAP-07013-P (R0), July 2007.
2. “ROSA-IV/LSTF 5% Clod Leg Break LOCA Experiment Run SB-CL-18 Data Report,” JAERI-M89-027, March 1989.

Figure RAI-8.2.1-13.1 The M-RELAP5 Noding Diagram and Differential Pressure Measurement Location

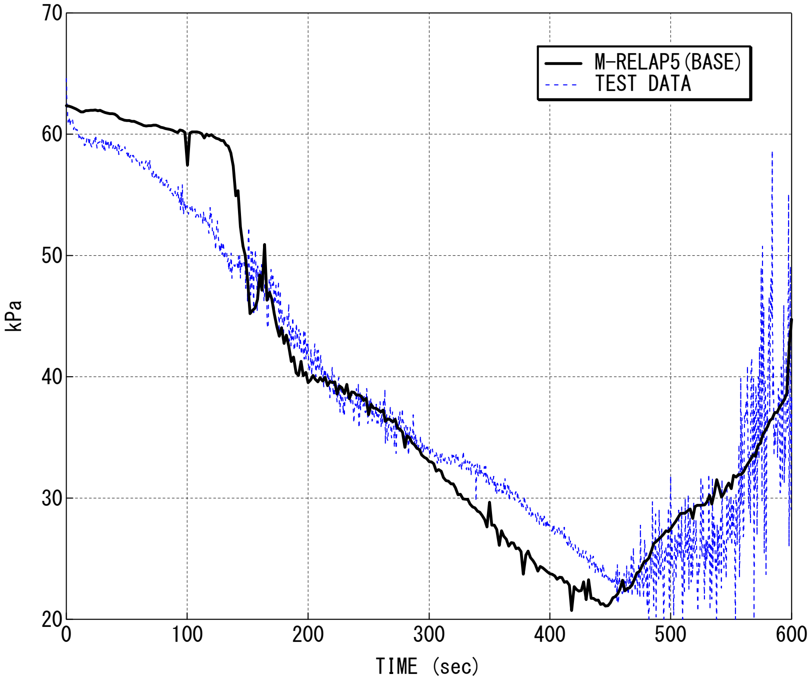

Figure RAI-8.2.1-13.2 Downcomer Differential Pressure (Locations are adjusted)

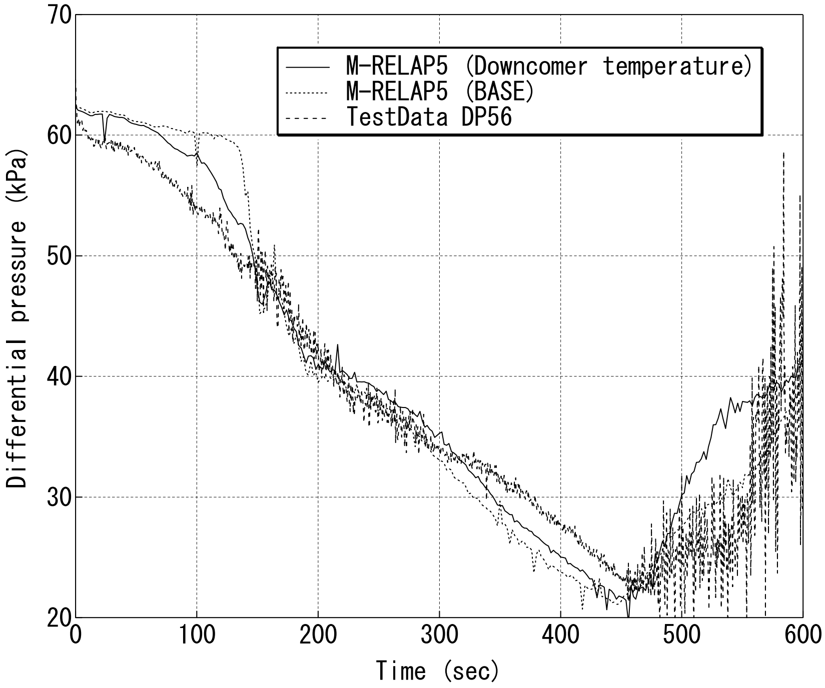

Figure RAI-8.2.1-13.3 Downcomer Differential Pressure (Revised Models are applied)

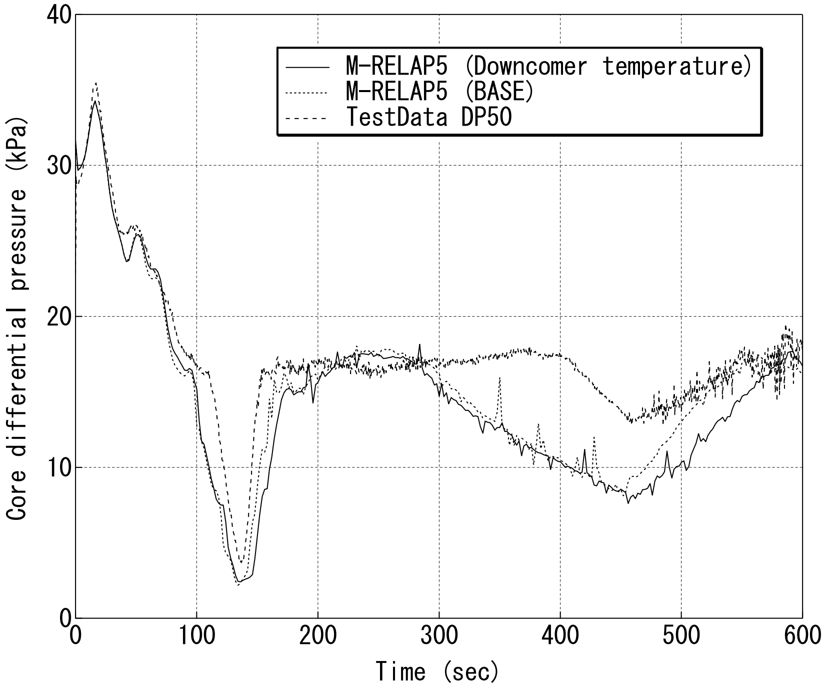

Figure RAI-8.2.1-13.4 Core Differential Pressure

REQUEST 8.2.1-14

Figures 8.2.1-37 and 8.2.1-38 show the measured and predicted rod surface temperatures, respectively. However, it is very difficult to distinguish the temperatures given at several elevations. Please provide figures which show the temperatures clearly.

RESPONSE

Figures RAI-8.2.1-14.1 and 2 provide the correspondence of each temperature history with the axial elevation. Comparisons between M-RELAP5 and measurement at each axial elevation are given in Figures 8.2.1-39 to -44 in the topical report (Ref. 1).

Reference:

1. Mitsubishi Heavy Industries, Ltd., Small Break LOCA Methodology for US-APWR, MUAP-07013-P (R0), July 2007.

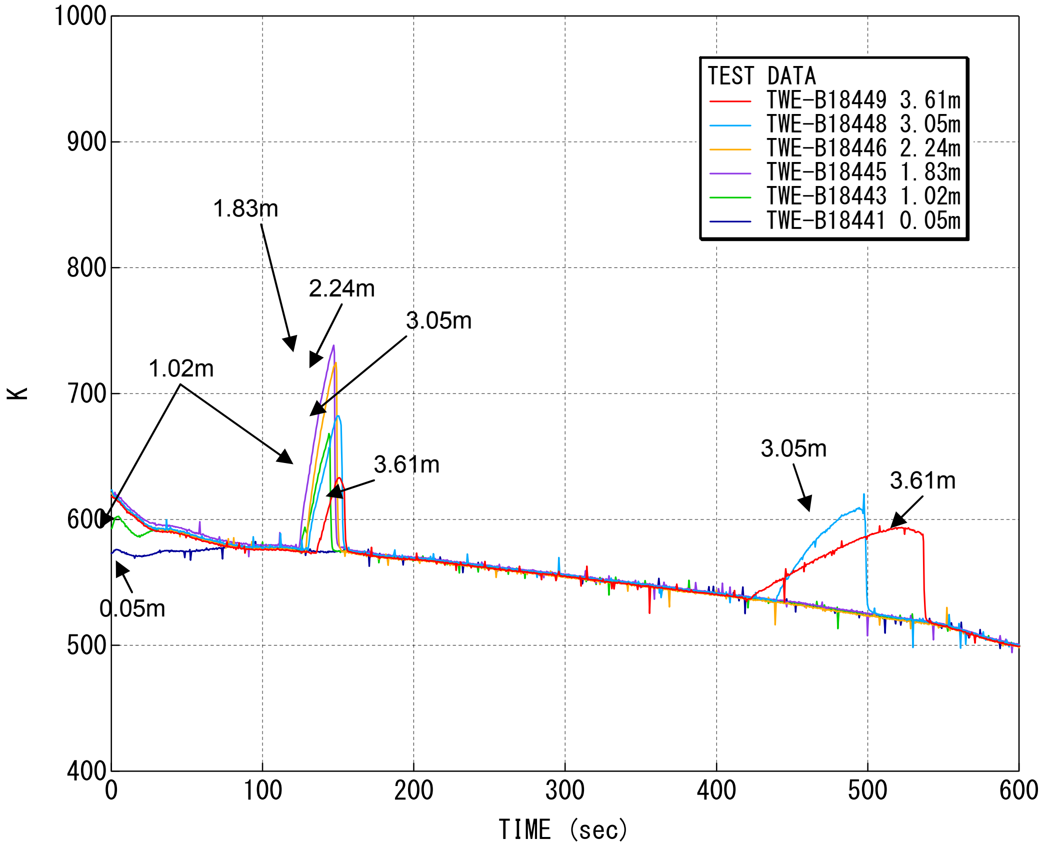

Figure RAI-8.2.1-14.1 Heater Rod Surface Temperature (Test Data)

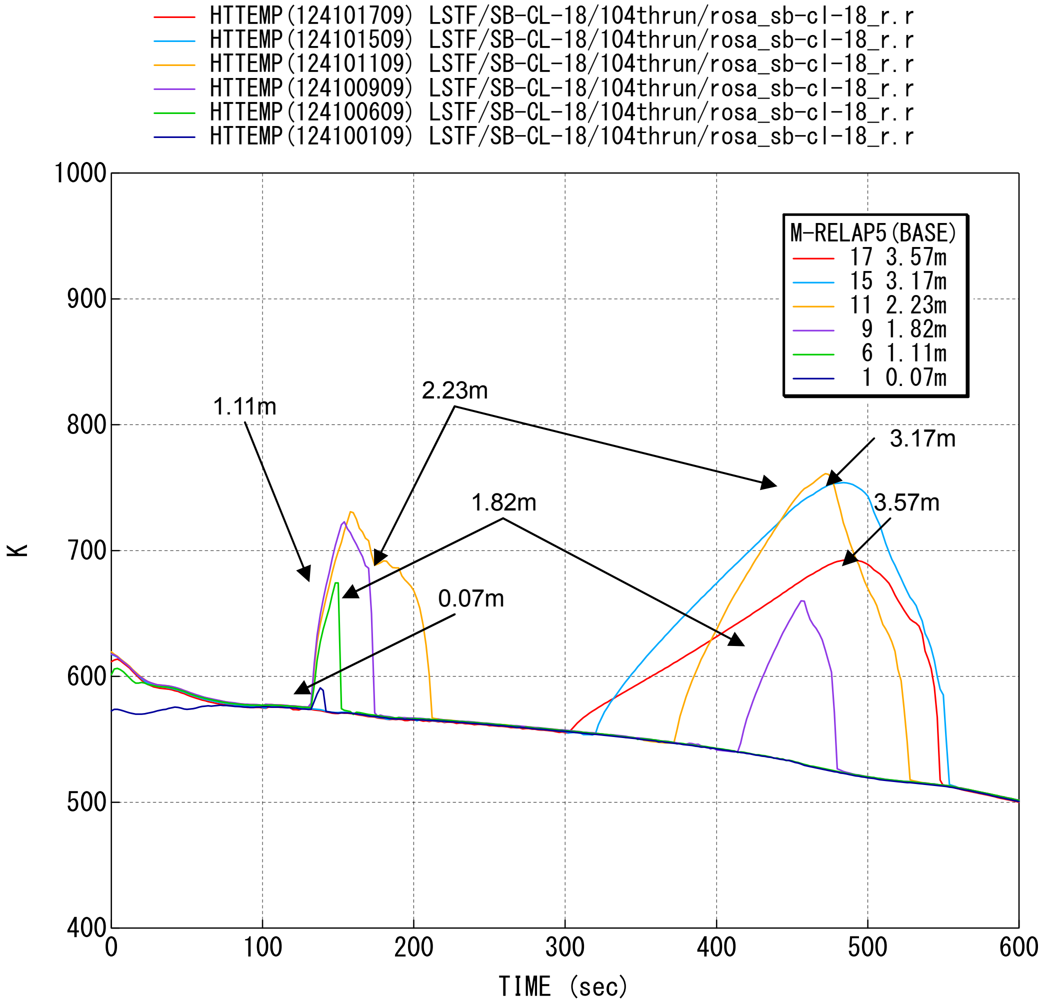

Figure RAI-8.2.1-14.2 Heater Rod Surface Temperature (M-RELAP5, Base Case)

REQUEST 8.2.1-14-1

(Related RAI 8.2.1-14)

Please confirm that the figures provided in the RAI response 8.2.1-14 will be incorporated into MUAP-07013-P.

RESPONSE

MHI will incorporate Figures RAI-8.2.1-14.1 and 2 into the revised topical report MUAP-07013-P (R1), which is scheduled to submit to the NRC at the end of March, 2010, as agreed between the NRC and MHI.

REQUEST 8.2.1-15

Figures 8.2.1-39 and 8.2.1-40 show comparisons of the predicted and measured rod surface temperatures in the upper part of the core. From these figures it can be seen that M-RELAP5 does not predict the rod temperature increase at around 130 s while there are the temperature increases in the test data at that time. Please explain.

RESPONSE

The rod temperature increase at around 130 seconds is caused by the core uncovery during the loop seal clearance phase. The vapor generated in the core by the decay heat flows into the steam generator and condenses therein, during the loop seal clearance period. The condensate produced by the condensation heat transfer in the uphill side steam generator flows back into the core via hot leg and upper plenum. Then, the counter-current flow exits in the core uncovered region. The void fraction in the core uncovered region is in the range of 0.94 to 0.97, as shown in Figures 8.2.1-45, 46 of MUAP-07013-P (Ref. 1).

In RELAP-3D, CHF at these low flow conditions is predicted by the Zuber pool boiling CHF correlation and the vertical flow factor k7 multiplier is applied to account for the void fraction effect on CHF. **[**

]

M-RELAP5 can predict the rod temperature increase at the upper core region during the loop seal clearance phase **[** **]** as shown in Figures 8.2.1-47, 48 of MUAP-07013-P.

References:

1. Mitsubishi Heavy Industries, Ltd., Small Break LOCA Methodology for US-APWR, MUAP-07013-P (R0), July 2007.

REQUEST 8.2.1-16

(Related RAI 8.2.1-6)

[

]

RESPONSE

[

]

REQUEST 8.2.1-17

The 1st sentence of the 2nd last paragraph on page 8.2.1-10 states, “ACC flow was initiated at 455 sec (test data) or 480 sec (M-RELAP5), and then core water level started to recover (Figure 8.2.1-35 and 36).” Table 8.2.1-6 also shows that the accumulation injection time is 480 s in the prediction.

However, Figures 8.2.1-35 and 8.2.1-36 show that M-RELAP5 predicts earlier ACC flow injection than the test data and the injection time is around 440 s. Do the figures show the results of a different case? If not, explain the discrepancy between the figures and the description in the text.

RESPONSE

The accumulator injection timing written in page 8.2.1-10 and Table 8.2.1-35 of the topical report (Ref. 1) is incorrect (typo). As pointed out by the reviewer, M-RELAP5 predicts accumulator injection around 445 seconds. MHI will correct the accumulator injection timing in page 8.2.1-10 and Table 8.2.1-35.

Reference:

1. Mitsubishi Heavy Industries, Ltd., Small Break LOCA Methodology for US-APWR, MUAP-07013-P (R0), July 2007.

REQUEST 8.2.1-18

Figures 8.2.1-39 and 8.2.1-40 show that M-RELAP5 predicts the heater rod rewetting occurred slightly earlier at 3.57 m at around 550 s than at 3.17 m at around 560 s while the heater rod is rewetted first at 3.17 m at around 500 s and then at 3.57 m at around 540 s in the test. Explain why the heater rod rewetting occurs later at the lower section (at 3.17 m) than the upper section (at 3.57 m) in the simulation whereas the test data shows that the rewetting occurs later at the upper section.

RESPONSE

The rewetting phenomenon during the core recovery phase is discussed here. During the core recovery and the preceding boil-off phases, the core is covered almost by single-phase vapor in the region above the mixture level. The predicted heater rod temperature transients at various elevations are shown in Figure RAI-8.2.1-18.1. The heater rod heat-up occurs systematically from the upper elevation to the lower elevation during the boil-off phase as the core mixture level decreases. Also, the heater rod rewetting occurs systematically from the lower elevation to the upper elevation during the core recovery phase as the core mixture level increases until the rewetting elevation reaches 3.17m. However, the heater rod rewetting occurs earlier at the upper elevation of 3.57m compared to that at 3.17m.

[

] The void fractions at the elevation of 3.17m and 3.57m are shown in Figure RAI-8.2.1-18.2. The upper elevation of 3.57m has a larger void fraction and poorer heat transfer to the fluid near the rewetting time. As the axial rod power distribution used in the ROSA-IV/LSTF experiments is cosine, the power generation rate at the upper section is small and the heater rod temperature rise during the core uncovery is also small as shown in Figure RAI-8.2.1-18.1. It is considered that the heater rod temperature is dominant for the rewetting phenomena compared to the fluid condition at the upper section and the upper section rewets earlier. Even so, the rewetting at 3.57m elevation is conservatively predicted compared to the experimental data as shown Figure 8.2.1-39 of MUAP-07013-P (Ref. 1).

Reference

1. Mitsubishi Heavy Industries, Ltd., Small Break LOCA Methodology for US-APWR, MUAP-07013-P (R0), July 2007.

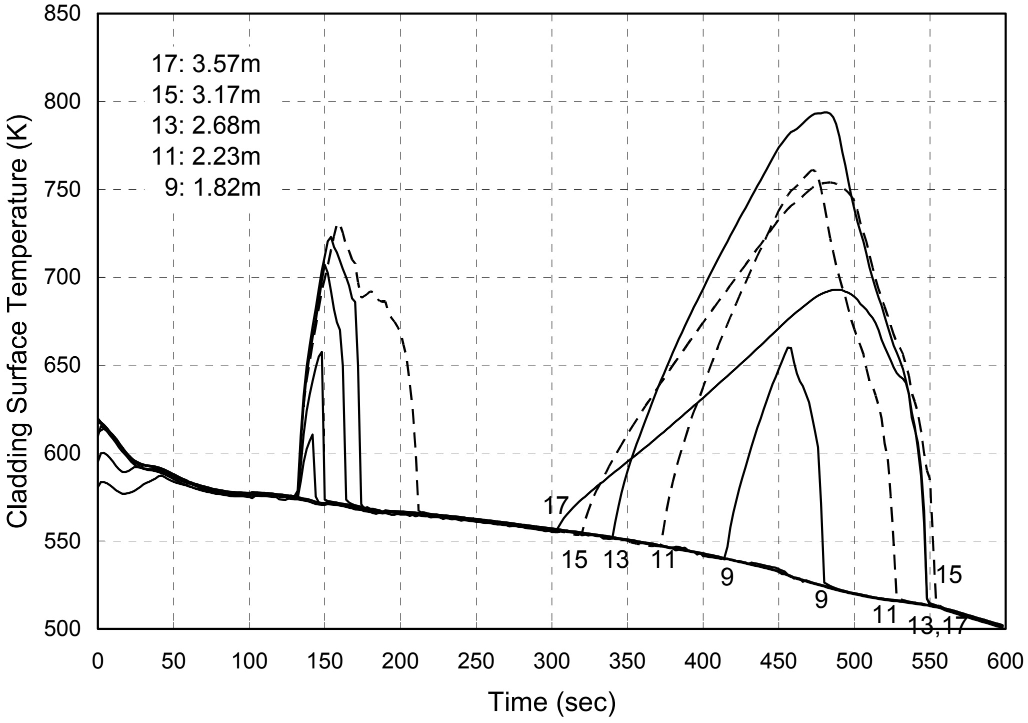

Figure RAI-8.2.1-18.1 Heater Rod Surface Temperature

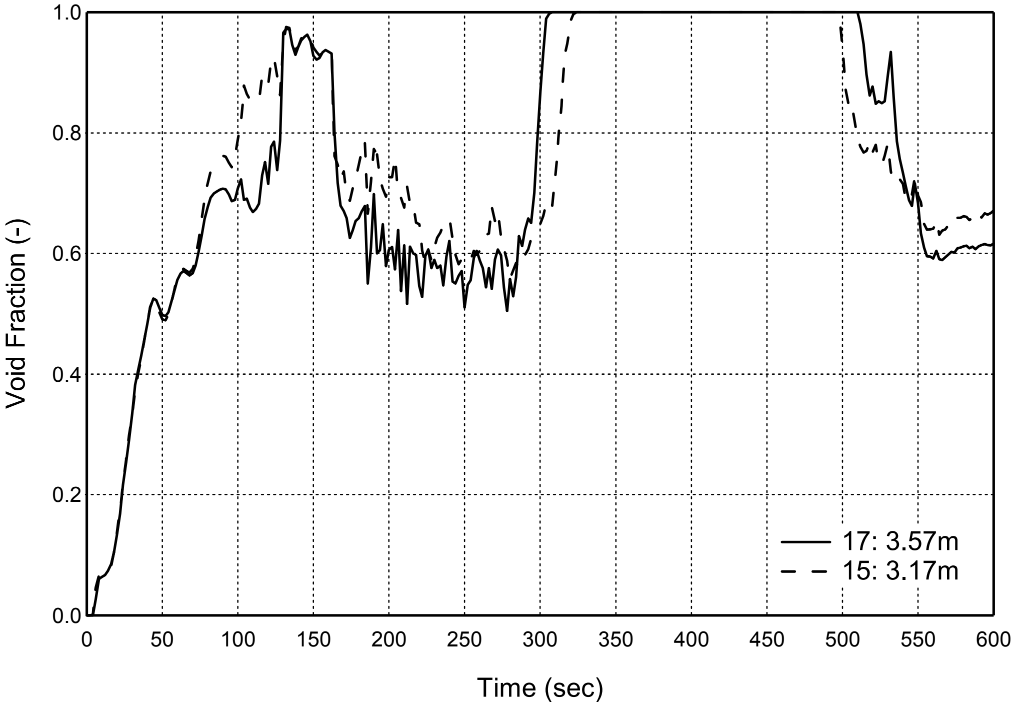

Figure RAI-8.2.1-18.2 Void Fraction at Upper Elevations

REQUEST 8.2.1-19

The 2nd paragraph on page 8.2.1-11 says, "There are some heater rods heated up at such a upper portion in the experimental data. It indicates that the accumulated water on the upper plenum region partly flow down to the core region. This is consistent with the view that a spatially non-uniform liquid distribution exists in the core region. Such liquid distribution effects are already modeled as CHF multiplier in M-RELAP5. But this base case results indicate that this CHF multiplier is not enough for ROSA-IV/LSTF SBLOCA analysis."

The meaning of the above quotation is not clear. Explain how the flowing down of the accumulated water from the upper plenum region is related to the heater rods heating up in the upper portion of the core region in the experimental data. Explain how the liquid distribution effects are modeled in M-RELAP5 with the CHF multiplier. Describe the specific multiplier that is referred to and why it is not enough for ROSA-IV/LSTF SBLOCA analysis.

RESPONSE

The vapor generated by the core decay heat flows into the steam generator and condenses there during the loop seal clearance phase. The liquid-condensate due to the condensation heat transfer in the uphill side of steam generator flows back into the upper plenum via hot leg and the accumulated liquid in the upper plenum drains into the core. The drained liquid flows down on the fuel rod surface as the liquid film. CHF occurs when the liquid film on the fuel rod surface disappears. The liquid flow rate into the core is expected to non-uniformly distribute in the radial and azimuthal directions by complex multi-dimensional two-phase flow phenomena. Then, CHF initially occurs at less rod surface heat flux compared with the situation in which the liquid flows down uniformly into the core.

The rod surface temperatures were measured in many heater rods which are radially and azimuthally distributed and at several axial locations in the ROSA-IV/LSTF SB-CL-18 experiment. The heater rod surface temperatures in the high power region in the upper core during the loop seal clearance period are shown in Figure RAI-8.2.1-19.1 and Figure RAI-8.2.1-19.2. The locations of these heater rods are shown in Figure RAI-8.2.1-19.3. Most heater rods experience CHF, but several heater rods do not experience CHF at both elevation. The CHF occurrence time varies for each rod and is not closely correlated with elevations. The rod surface temperature transients during the boil-off and core recovery phases of the same heater rods are shown in Figure RAI-8.2.1-19.4 and Figure RAI-8.2.1-19.5. As the liquid does not flow down into the core from the upper plenum during these periods, all heater rods experience CHF and the CHF proceeds from the lower elevations to the higher ones. So, the non-uniform flow effect in the bundle described here is required only for the loop seal clearance phase.

The radial flow and enthalpy imbalance effects in the bundle on CHF are already accounted in the bundle factor in the 1986 AECL-UO CHF lookup table. **[**

]

Reference:
1. Mitsubishi Heavy Industries, Ltd., Small Break LOCA Methodology for US-APWR, MUAP-07013-P (R0), July 2007.

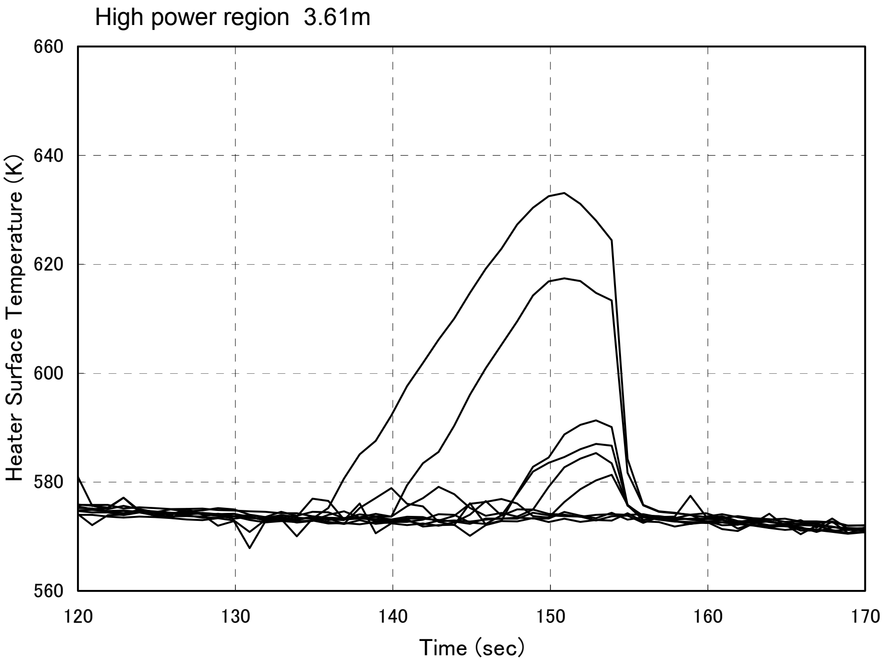

Figure RAI-8.2.1-19.1 Heater Rod Surface Temperature during Loop Seal Clearance Period at 3.61m

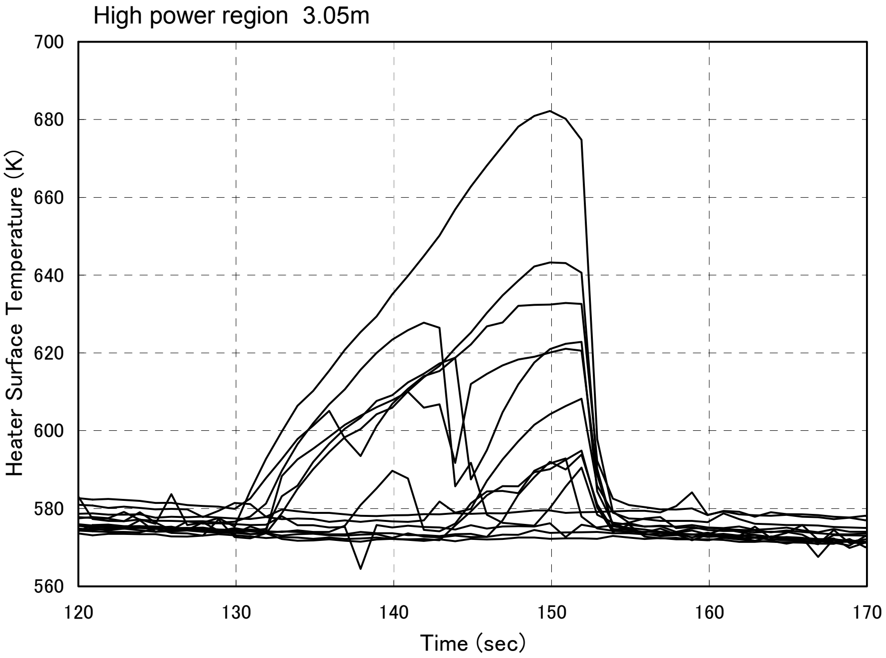

Figure RAI-8.2.1-19.2 Heater Rod Surface Temperature during Loop Seal Clearance Period at 3.05m

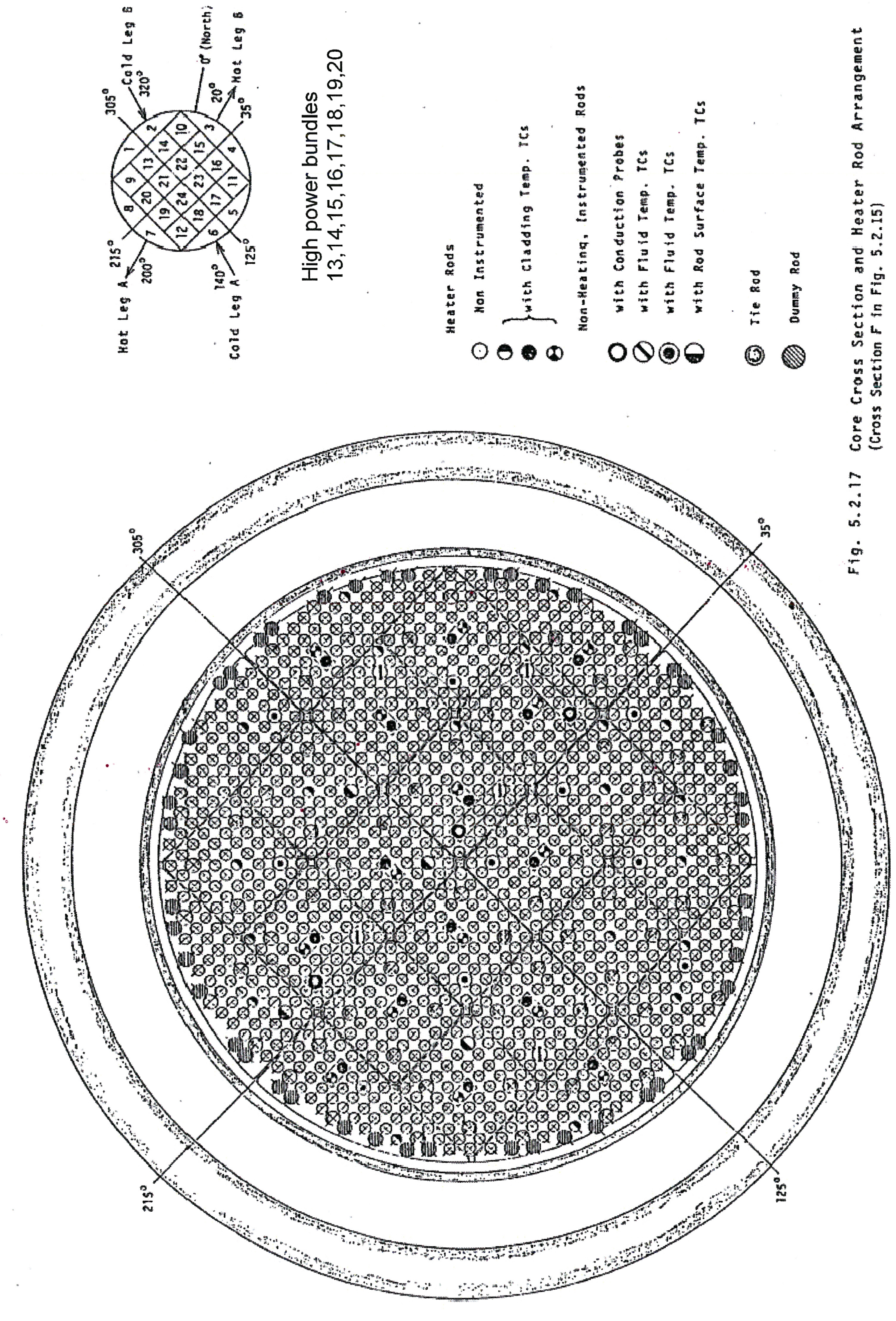
Hot Leg A
215°
200°
305°
Cold Leg B
320°
0° (North)
20°
Hot Leg B
35°
140°
Cold Leg A
125°
1 2 3 4 5 6 7 8 9 10 11 12 13 14 15 16 17 18 19 20 21 22 23 24
High power bundles
13,14,15,16,17,18,19,20
Heater Rods
Non Instrumented
with Cladding Temp. TCs
Non-Heating, Instrumented Rods
with Conduction Probes
with Fluid Temp. TCs
with Fluid Temp. TCs
with Rod Surface Temp. TCs
Tie Rod
Dummy Rod
305°
35°
215°
125°

Fig. 5.2.17 Core Cross Section and Heater Rod Arrangement (Cross Section F in Fig. 5.2.15)

Figure RAI-8.2.1-19.3 Surface Temperature Measured Heater Rod location in the Bundle

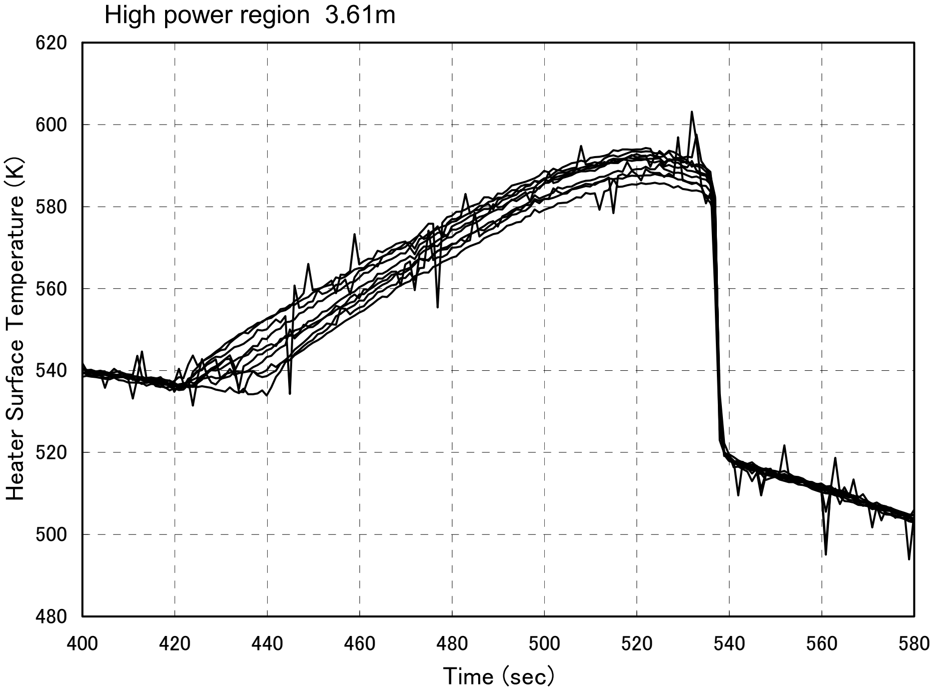

Figure RAI-8.2.1-19.4 Heater Rod Surface Temperature during Boil-off/Core-recovery Period at 3.61m

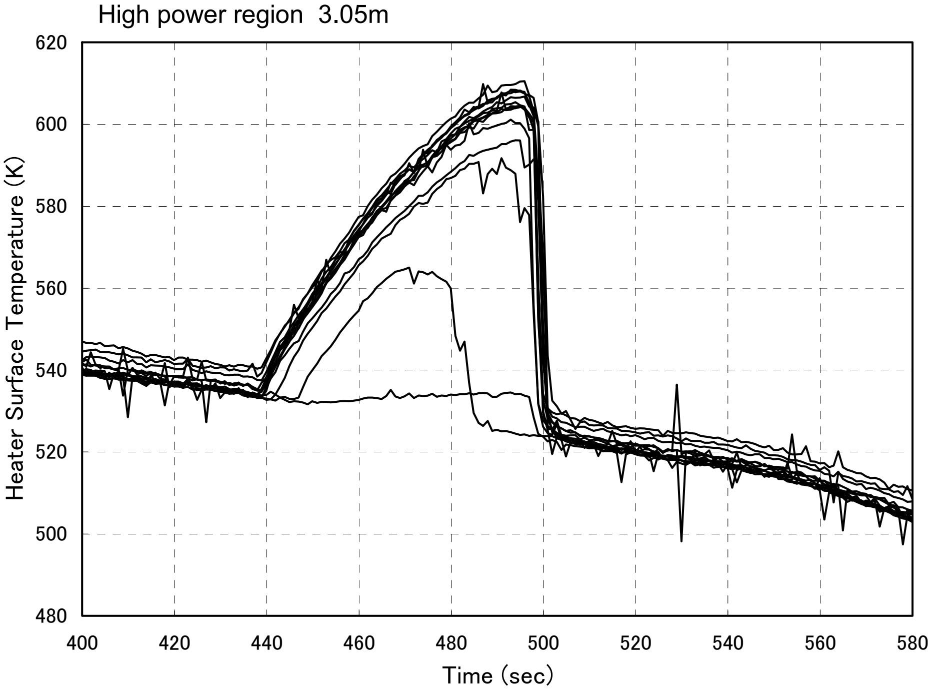

Figure RAI-8.2.1-19.5 Heater Rod Surface Temperature during Boil-off/Core-recovery Period at 3.05m

REQUEST 8.2.1-20

[

]

RESPONSE

[

]

[

]

REQUEST 8.2.1-21

The 2nd sentence of the 1st paragraph on page 8.2.1-12 says, “The rod surface temperatures are also shown in Figure 8.2.1-55 through 70.” The figure number Figure 8.2.1-70 needs to be changed to Figure 8.2.1-60.

RESPONSE

MHI will correct the second sentence in the first paragraph on page 8.2.1-12 of the topical report (Ref. 1) by ‘The rod surface temperatures are also shown in Figure 8.2.1-55 through 60.’

Reference:

1. Mitsubishi Heavy Industries, Ltd., Small Break LOCA Methodology for US-APWR, MUAP-07013-P (R0), July 2007.

REQUEST 8.2.1-22

The conclusion section needs to be re-written in light of adjusting some important parameters such as the break flow, and as a consequence primary system pressure, etc., and specifying them as boundary conditions (user inputs). In effect the way the assessment was performed makes it a SET and not an IET. While it shows that some aspects of the M-RELAP5 model can predict the test data, the assessment was not performed in the same manner as the plant analysis was performed and hence it doesn't demonstrate the M-RELAP5 is capable of predicting plant SBLOCA responses.

RESPONSE

The break flow and the steam generator secondary pressure from the experimental data were supplied so that the validation could focus on the code's ability to calculate important RCS phenomena for the SBLOCA analysis such as natural circulation, liquid holdup in the U-tubes, loop seal clearing, core uncovery, and core heatup without the influence of errors caused by peculiarities of experimental systems, such as break geometry, steam generator heat loss, steam generator relief valve leakage, etc.

A separate effect test is used to assess an empirical correlation or closure model for representing the important phenomena described in the PIRT. An integral effect test is used to assess the code capability to predict global system behavior and interactions between systems, components, and processes and to quantify accuracy to predict various parameters of interest described in the PIRT. Although the assessment using the ROSA-IV/LSTF was not performed in the same manner as the plant analysis, the important parameters besides break flow rate and steam generator heat transfer are confirmed as accurately predicted. These assessed parameters are the consequences of global system behavior and the interactions between systems, components, and processes. Therefore, the assessment performed in MUAP-07013-P can still be classified as an IET assessment.

As Moody critical flow model required by the Appendix K is used in the US-APWR SBLOCA analyses using M-RELAP5, the accuracy of the Moody model compared to ROSA-IV/LSTF test data is not relevant. Furthermore, the uncertainty in the calculation of break flow is adequately considered in the break spectrum sensitivity calculations in the DCD analysis.

However, the steam generator primarily and secondary heat transfer models have not been validated in the assessment using the ROSA-IV/LSTF experiment which closely matched the primary pressure and exactly matched the SG secondary pressure by specification of the boundary conditions as pointed out in REQUEAST 8.2.1-12. As the steam generator primary and secondary heat transfers are ranked as high-level phenomenon for blowdown, natural circulation, and loop seal clearance phases in the US-APWR SBLOCA PIRT (Ref. 1), an assessment for the related models is required. MHI intends to perform the additional assessment using the ROSA-IV/LSTF SB-CL-18 experiment. In the analysis, the secondary system will be simulated in detail rather than using the boundary condition.

The conclusion section will be rewritten to reflect the NRC comment about specifying the break flow and the SG secondary pressure as boundary conditions. Also, the current statement about the steam generator heat transfer will be deleted and the additional statement about the new results concerning the steam generator heat transfer will be added in the conclusion section.

Reference:

1. Mitsubishi Heavy Industries, Ltd., Small Break LOCA Methodology for US-APWR, MUAP-07013-P (R0), July 2007.

REQUEST 8.2.1-23

In the 2nd last paragraph on page 8.2.1-9 of MUAP-070130P (R0) MHI says, “Core water level was dropping at about 300 sec in M-RELAP5, while core water level did not drop until 400 sec in test data (Figure 8.2.1-17). Downcomer water level drop timing is also earlier than the test data (Figure 8.2.1-34). As a result, the water mass inventory in the vessel of M-RELAP5 was smaller than that of the test data.”

Please clarify the time period for the downcomer water level drop and the smaller vessel mass inventory. How do you establish that the total vessel mass inventory is lower since there is no data for some regions like the upper head?

RESPONSE

The downcomer water level calculated by M-RELAP5 falls below the test data after about 300 seconds (Figure RAI-8.2.1-23.1). In terms of the upper plenum and core barrel region, M-RELAP5 predicts smaller water level than the measurement after about 150 seconds (Figure RAI-8.2.1-23.2). Figure RAI-8.2.1-23.1 is not the same graph as that in Figure 8.2.1-34 of Reference 2. To compare the downcomer differential pressure with the test data at the exact axial location as the test data, the method of estimating the downcomer differential pressure was properly modified.

There remains an uncertainty in predicting the liquid mass for the upper head region, since no measurement data is provided in the test report, as pointed by Reviewer. **[**

] Consequently, MHI judged that M-RELAP5 predicts the total vessel mass inventory lower than the measurement, in spite of the uncertainty caused from the upper head mass.

To this end, MHI will modify the corresponding conclusion stated in the topical report such that Reviewer is able to recognize the remaining uncertainty.

References:
1. Mitsubishi Heavy Industries, Ltd., MHI's 2nd Response to the NRC's Request for Additional Information on Topical Report MUAP-07013-P (R0) “Small Break LOCA Methodology for US-APWR”, UAP-HF-08041-P(R0), February 2009.
2. Mitsubishi Heavy Industries, Ltd., Small Break LOCA Methodology for US-APWR, MUAP-07013-P (R0), July 2007.

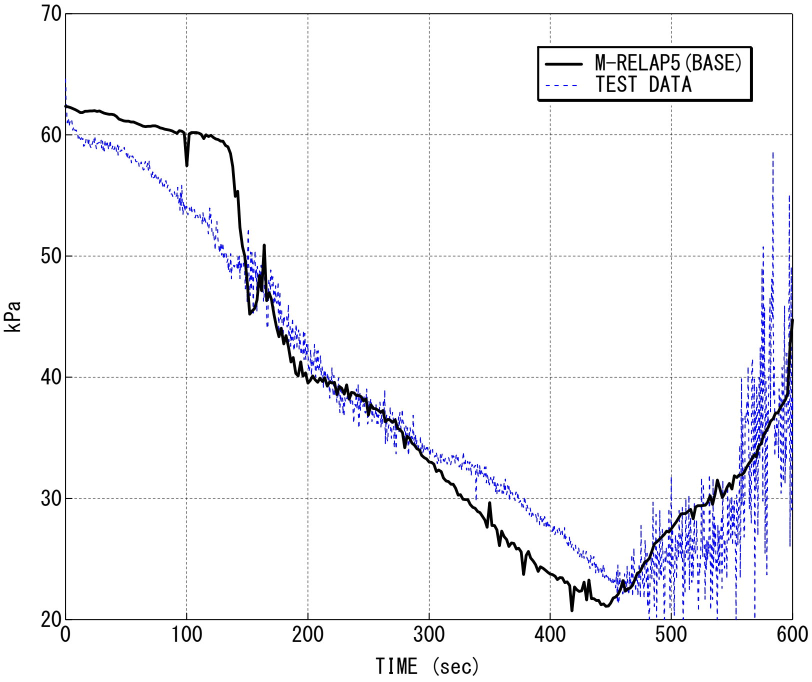

Figure RAI-8.2.1-23.1 Downcomer Differential Pressure

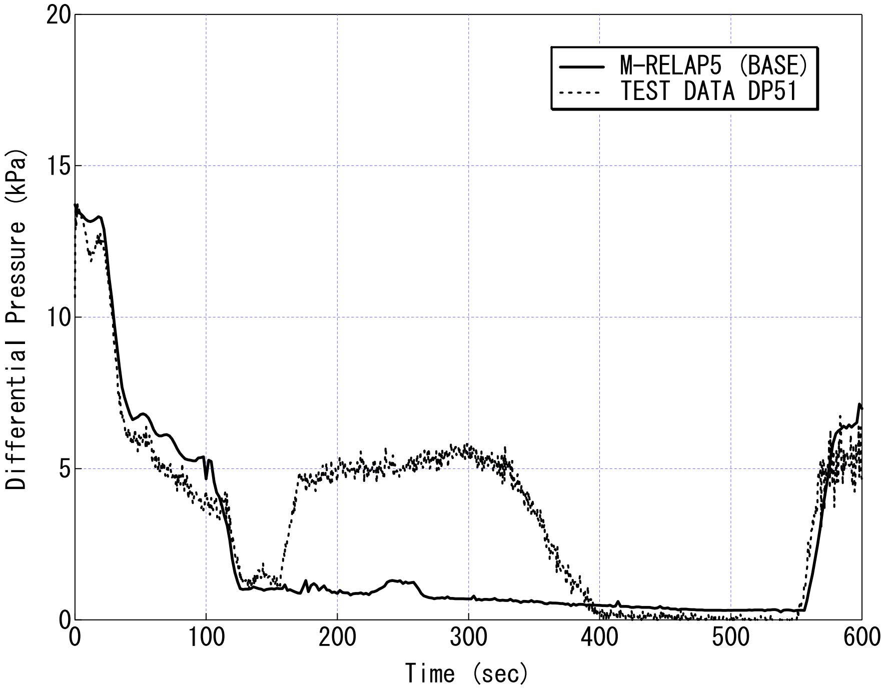

Figure RAI-8.2.1-23.2 Upper Plenum Differential Pressure

REQUEST 8.2.1-23-1

(Related RAI 8.2.1-23)

In the response to RAI 8.2.1-23, MHI committed to modifying the conclusions in the subject report section to such that the reviewer is able to recognize the remaining uncertainty. In revising the conclusion, please address the following concern.

MHI states that M-RELAP5 predicts the total vessel mass inventory lower than the measurement, in spite of the uncertainty resulting from the upper head mass inventory. The reviewer understands the MHI's believes that there is a distortion of the initial total vessel mass inventory. However, Figures 8.2.1-15 and -16 show good agreements of the break flowrate and the pressurizer pressure between the prediction and the measurement. This means that if the geometry of the facility was modeled accurately, the mass inventory in the primary system is similar in the analysis and the test during the transient period.

As shown in Figure RAI 8.2.1-23-2, the mass was accumulated in the upper plenum in the experiment from around 150 s to 320 s and then started decreasing and the water level reached the upper elevation of the core region at around 400 s while M-RELAP5 does not predict the mass accumulation in the upper plenum during that time period. Figure 8.2.1-17 shows that the water started decreasing from around 400 s in the core region of the test facility. Therefore, the difference in the core water level dropping time appears to be caused by the accumulation of water in the upper plenum in the test, while it is not accumulated in the analysis. The source of the water being accumulated in the upper plenum in the test seems to be the upper head water.

RESPONSE

MHI's response to RAI 8.2.1-6 describes the water being accumulated in the upper plenum in the test as a possible cause of the earlier decrease in the core liquid level in the calculation than in the test. A draft of the additional explanations for the calculated downcomer and core liquid level behaviors including sensitivity calculations is attached below. The draft is to be incorporated into the revised topical report as Chapter 8.2.1.8.

Appendix to Response to REQUEST 8.2.1-23-1

[

]

[

]

[

]

REQUEST 8.2.1-24

Figures 8.2.1-41 and 8.2.1-42 show that the predicted rod surface temperatures have the 2nd peaks at around 450 s while the measured data do not have them. Please explain what phenomena in the RELAP5 prediction causes these peaks which do not occur in the experimental data.

RESPONSE

M-RELAP5 tends to predict more core level depression than measured in the experiment, during the boil-off phase, as shown in Figure 8.2.1-17 of the topical report (Ref. 1). This results in the predicted heat-up at the lower elevations in the core compared to the measurement. The relevant description is given in the first and second paragraphs on page 8.2.1-10 of the topical report.

Possible sources of the larger core liquid level depression predicted by M-RELAP5 are addressed in the response to REQUEST 8.2.1-6 (Ref. 2).

References:

1. Mitsubishi Heavy Industries, Ltd., Small Break LOCA Methodology for US-APWR, MUAP-07013-P (R0), July 2007.
2. Mitsubishi Heavy Industries, Ltd., MHI’s 2nd Part Responses to the NRC’s Requests for Additional Information on Topical Report MUAP-07013-P (R0) “Small Break LOCA Methodology for US-APWR”, UAP-HF-09041, February 13, 2009.

REQUEST 8.2.1-25

The 1st paragraph on page 8.2.1-10 says, “Heater rod surface temperature heat up timing is earlier than test data (Figure 8.2.1-37 and 38) because onset of core collapsed liquid level depression is earlier than test data (Figure 8.2.1-17). In M-RELAP5, heater rod surface temperature heated up when core collapsed liquid level was about 15kPa, while in test data, heater rod surface temperature heated up when core collapsed liquid level was about 16kPa, equivalent to M-RELAP5. As a result, M-RELAP5 capability to predict core dryout in boil off transient is good.”

The core collapsed liquid levels are not equivalent. The above statements should be modified to recognize the differences between predictions and tests and realistically evaluate possible implications of any differences.

RESPONSE

MHI believes that the difference of 1kPa (=16kPa-15kPa) causes negligible impact to the liquid collapsed level. **[**

]

To this end, MHI will modify the second sentence of the first paragraph on page 8.2.1-10 (Ref. 1) as follows:

> “In M-RELAP5, heater rod surface temperature heated up when core collapsed liquid level was about 15kPa, while in test data, heater rod surface temperature heated up when core collapsed liquid level was about 16kPa. This difference in pressure drop is negligibly small, after converting to the collapsed liquid level and comparing with the node height employed for the core nodalization.”

Reference:

1. Mitsubishi Heavy Industries, Ltd., Small Break LOCA Methodology for US-APWR, MUAP-07013-P (R0), July 2007.

REQUEST 8.3.1-1

In Section 8.3.1-4 it is stated that “The bypass path between the downcomer and upper head becomes an alternative steam flow path connecting the cold leg and the hot leg during the loop seal clearing period. Thus, the flow resistance of the path affects the core mixture level depression.”

Also in Section 8.3.1-5 it is stated that “A leak path between hot leg nozzles and the downcomer upper region becomes a steam flow path connecting the cold leg and the hot leg during the loop seal clearing period. Thus, the flow resistance of the path affects the core mixture level depression.”

As both of these flow paths can act to release steam from above the core during the loop seal clearing period, please explain how the uncertainty in the flow path area and the subsequent steam flow are treated in the SBLOCA methodology.

RESPONSE

The bypass path between the downcomer and upper head, which is called the spray nozzle, is explicitly modeled in the US-APWR SBLOCA methodology. On the other hand, a leak path between the hot leg nozzles and downcomer upper region is not modeled, because that the flowrate through the path is negligibly small. In addition, ignoring the bypass path between the hot leg nozzles and downcomer causes more steam flow into the hot legs, leading to a larger core level depression and to a higher PCT during the loop clearing seal phase.

[

] The steam bypassing through the spray nozzle primarily affects the core liquid level depression during the loop seal phase. In the US-APWR SBLOCAs, however, the top of the spray nozzle is covered with sufficient coolant during the loop seal phase, which impedes steam flowing from the upper head to the downcomer as described in MHI’s response to REQUEST 7-1 (Ref. 1). Therefore, the steam flow resistance at the spray nozzle is not sensitive to the PCT occurring during the loop seal phase, and then, an additional conservatism is not necessary for the steam flow resistance at the spray nozzle.

Reference:

1. Mitsubishi Heavy Industries, Ltd., MHI's Partial Responses to the NRC's Requests for Additional Information on Topical Report MUAP-07013-P (R0) “Small Break LOCA Methodology for US-APWR”, UAP-HF-09002, January 2009.

REQUEST 8.3.1-2

[

]

RESPONSE

[

]

[

]

REQUEST 8.3.1-3

Section 8.3.1.2 of MUAP-07013-P states that counter current liquid flow against the upward in-vessel flow of vapor is simulated in the M-RELAP5 model field equations, and cites the ORNL/THTF reflood separate effects test and the ROSA-IV/LSTF 5% SBLOCA integrated effects test as validation of the M-RELAP5 rewet simulation.

Discuss whether the ORNL/THTF reflood separate effects test and the ROSA-IV/LSTF 5% SBLOCA integrated effects test provide validation of the in-vessel counter current flow component of the rewet simulation in M-RELAP5. Also, explain the relative contribution of liquid counter current flow heat transfer during rewet, and discuss the occurrence of counter current flow limitation during rewet.

RESPONSE

(1) Counter-Current flow in ORNL/THTF and ROSA/SBLOCA Tests

The liquid and vapor counter-current flow condition is not expected in the ORNL/THTF high-pressure reflood tests. The test started from the steam cooling condition by injecting the coolant from the test section inlet. Coolant forcedly injected was vaporized in the heated region, and the single-phase vapor or two-phase flow were removed from the test section.

In contrast, the liquid and vapor counter-current flow probably occurred at the core exit location during the loop seal phase in the ROSA-IV/LSTF SB-CL-18 test, from an observation of the measurements. As described in Section 8.2.1.6 of Reference 1, a limited number of the heater rod shows heat-up in the upper portion of the core. This indicates that the accumulated water in the upper plenum region partly flows down to the core against the vapor upward flow, which facilitates rewetting in a part of the core upper region.

In M-RELAP5, effects of the liquid downward flow on the heat transfer is taken into account for **[**

] The dryout (uncovered) heat transfer model, which primarily consists of the Dittus-Boelter, Dougall-Rohsenow (vapor convection), and Bromley (film boiling) heat transfer correlations, is not affected by the flow orientation, upward or downward. The CHF and uncovered heat transfer models in M-RELAP5 have been assessed using the separate effects and integral effects tests as described above.

(2) Contribution of Liquid Counter-Current Flow Heat Transfer during Rewet

[

]

[

]

(3) Occurrence of Counter-Current Flow Limitation during Rewet

[

]

Reference:

1. Mitsubishi Heavy Industries, Ltd., Small Break LOCA Methodology for US-APWR, MUAP-07013-P (R0), July 2007.

REQUEST 8.3.1-4

Section 8.3.1.1 states that the local power is modeled as the power distribution of the fuel rod in the axial and radial directions, and that it is defined by the input to the heat structure model.

Describe how the 10CFR50 Appendix K requirements of maximum peaking factor allowed by Technical Specifications and worst combination of power distribution shape and peaking factor are implemented in the US APWR SBLOCA Evaluation Model, including a summary of the power distribution studies performed to arrive at the selected combination of peaking factor and power distribution shape that results in the most severe calculated consequences of the SBLOCA.

RESPONSE

SBLOCAs result in higher PCT when the fuel rod power is higher and its axial power distribution is top-skewed because the upper portion of the fuel rod is dried out for a longer period of time as shown in Figure RAI-8.3.1-4.1. The figure shows the temporal change of the core two-phase mixture level during the limiting US-APWR SBLOCA (1-ft^2 cold leg break), which is identical to Figure RAI-7-14.23 in MHI response to REQUEST 7-14 (Ref.1).

Therefore, a core power distribution satisfying the following conservative conditions is used in the safety analysis for the US-APWR SBLOCAs.

Heat flux hot channel factor (F_Q)	: Design limit (=2.6)
Enthalpy rise hot channel factor ($F_{\Delta H}$)	: Design limit (=1.78)
Axial power shape	: Conservatively top-skewed profile*

*Figure 15.6.5-13 of US-APWR DCD (Ref.2)

Technical Specifications of the US-APWR regulate F_Q and $F_{\Delta H}$ below the design limits. Therefore, the power peaking factors applied to the SBLOCA analysis satisfy the conservative requirement specified in Appendix K to 10 CFR 50.

Regarding the axial power profile, the following features are taken into account in determining the safety analysis conditions.

[

]

In order to validate the procedure in determining the hottest rod's axial power distribution, the following sensitivity calculations have been performed by MHI. The hottest rod's axial power distributions were made based on some representative core states **[** **]** according to the procedure described above. The developed power distributions are compared in Figure RAI-8.3.1-4.2. It should be noted that **[** **]** is identical to the case used in the safety analysis for US-APWR SBLOCAs. In the present SBLOCA sensitivity calculations, the 1-ft^2 cold leg break (top orientation) is postulated with LOOP (loss of off-site power), which is the most severe analysis condition for the US-APWR SBLOCA (Ref.4).

PCTs obtained by M-RELAP5 using the axial power profile, shown in Figure RAI-8.3.1-4.2, without changing other input conditions are compared in Table RAI-8.3.1-4.1 to confirm the effects of the axial power profile on the PCTs. As shown in the table, **[** **]** top-skewed shape (DCD case) provides the highest PCT, although the sensitivity is relatively small because all the power profiles used here are conservatively top skewed and have the same F_Q and $F_{\Delta H}$.

References:

1. Mitsubishi Heavy Industries, Ltd., MHI's 1st Response to the NRC's Request for Additional Information on Topical Report MUAP-07013-P (R0) "Small Break LOCA Methodology for US-APWR" on 06/11/2009, UAP-HF-09362, July 2009.
2. Mitsubishi Heavy Industries, Ltd., Design Control Document for the US-APWR, Chapter 15 Transient and Accident Analyses, MUAP-DC015 Revision 2, November 2009.
3. Mitsubishi Heavy Industries, Ltd., Design Control Document for the US-APWR, Chapter 4 Reactor, MUAP-DC004 Revision 2, November 2009.
4. Mitsubishi Heavy Industries, Ltd., Small Break LOCA Sensitivity Analyses for US-APWR, MUAP-07025-P (R0), December 2007.

Table RAI-8.3.1-4.1 PCT Results for Axial Power Distribution Sensitivity Study

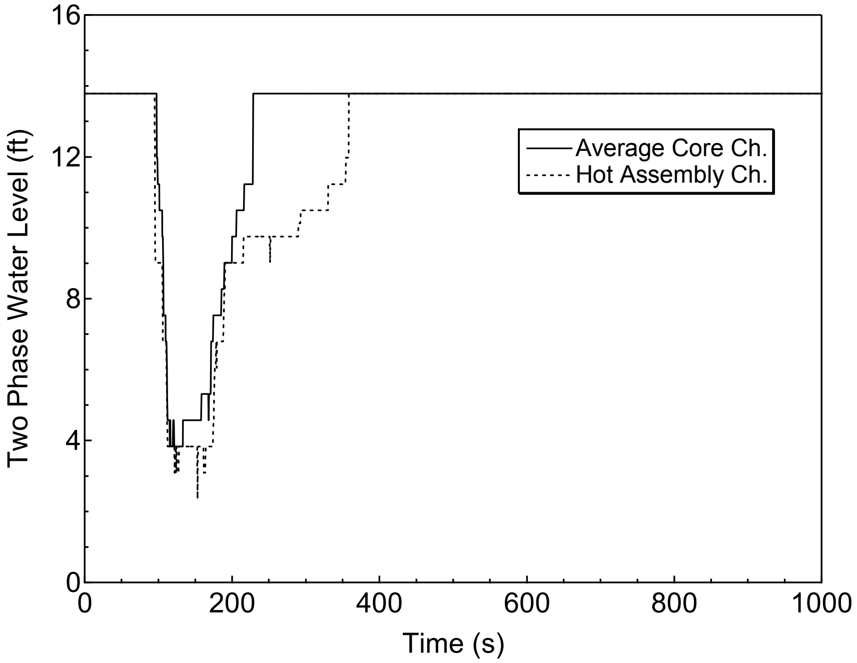

Figure RAI-8.3.1-4.1 Core Two-Phase Level for 1-ft^2 Break

Figure RAI-8.3.1-4.2 Postulated Hottest Rod Axial Power Distribution for Sensitivity Calculations

REQUEST 8.3.1-5

Section 8.3.1.2 states that the 3-D flow distribution can be determined by simulating the 3-D flow and heat transfer. US APWR DCD FSAR Section 15.6.5.3.1 describes the SBLOCA Evaluation Model as being one-dimensional.

Clarify the application of 3-D modeling in the SBLOCA Evaluation Model.

RESPONSE

[

]

REQUEST 8.3.1-6

Section 8.3.1.5 states that the M-RELAP5 mixture level tracking model can be used to refine the calculated mixture level in the upper plenum. Table 6.2.1-4 indicates that the mixture level tracking model is not utilized in the upper head and plenum regions of the SBLOCA Evaluation Model.

Clarify whether the mixture level tracking model is used in the calculation of reactor vessel upper plenum mixture level in the SBLOCA Evaluation Model.

RESPONSE

The mixture level tracking model is not used in calculating the reactor vessel upper plenum mixture level for the US-APWR SBLOCA safety analysis. The corresponding description is just an introduction for one of the M-RELAP5 functions and capabilities. MHI judged that the description probably confuses the exact status in the US-APWR SBLOCA evaluation model, and therefore, MHI will revise the corresponding portion from Section 8.3.1.5 of the topical report as follows:

25. Mixture Level:
The M-RELAP5 two-fluid nonequilibrium field equations track the liquid and vapor separately, allowing the formation of the appropriate liquid and mixture levels in the upper plenum. Although M-RELAP5 has a level tracking model that can determine the location of a mixture level within a control volume, the model is not used in the US-APWR SBLOCA calculations because an adequate representation of the void fraction distribution can be obtained using an appropriate number of control volumes. ~~The two phase regions, and thus the height of the mixture level in the upper plenum, are determined from the interface and wall mass, momentum, and energy transfer constitutive models. The resulting mixture level can be refined using the M-RELAP5 mixture level tracking model. The mixture level tracking model is applied through user input when a water level is formed by gravity.~~

REQUEST 8.3.1-7

Section 8.3.1.7 states that the M-RELAP5 mixture level tracking model can be used to refine the calculated mixture level in the pressurizer. Table 6.2.1-4 indicates that the mixture level tracking model is not utilized in the pressurizer component of the SBLOCA Evaluation Model.

Clarify the application of the M-RELAP5 mixture level tracking model to the pressurizer and pressurizer surge line volumes, including, if applicable, the conditions under which the model is applied and its effect on the calculated pressurizer mixture level.

RESPONSE

Similarly to the response to REQUEST 8.3.1-6, the mixture level tracking model is not used in the calculation of the pressurizer and pressurizer surge line volumes. The mixture level tracking model is not necessary to calculate the mixture level of the pressurizer because the two-fluid field equations provide a reasonable representation of the mixture level during the pressurizer out surge, particularly for the limiting SBLOCA cases with 7.5-in and 1-ft^2 break sizes.

MHI will revise Section 8.3.1.7 of the topical report as follows:

33. Mixture Level:
The M-RELAP5 two-fluid nonequilibrium field equations track the liquid and vapor separately, allowing the formation of the appropriate liquid and mixture levels in the pressurizer. Although M-RELAP5 has a level tracking model that can determine the location of a mixture level within a control volume, the model is not used in the US-APWR SBLOCA calculations because an adequate representation of the void fraction distribution can be obtained using an appropriate number of control volumes. ~~The two phase regions, and thus the height of the mixture level in the pressurizer, are determined from the interface and wall mass, momentum, and energy transfer constitutive models. The resulting mixture level can be refined using the M-RELAP5 mixture level tracking model. The mixture level tracking model is applied through user input when a water level is formed by gravity.~~

REQUEST 8.3.1-8

[

]

RESPONSE

[

]

REQUEST 8.3.1-9

Section 8.3.1.9 states that the calculated loop seal mixture level can be refined using the M-RELAP5 mixture level tracking model. Table 6.2.1-4, however, does not indicate that the mixture level tracking model is used in the crossover leg.

Clarify whether the mixture level tracking model is used in the calculation of loop seal mixture level in the SBLOCA Evaluation Model. Explain why the mixture level tracking model is / is not used to refine the loop seal mixture level calculation.

RESPONSE

Similarly to the response to REQUEST 8.3.1-6, the mixture level tracking model is not used in calculating the loop seal mixture level. The water head in the loop seal is important rather than the mixture level in evaluating the core liquid depression during the loop seal phase, which affects the PCT behavior.

MHI will revise Section 8.3.1.9 of the topical report as follows.

45. Loop Seal Formation and Clearance (Entrainment/Flow regime/Interfacial drag/Flow resistance):

A loop seal forms when the two phase natural circulation loop flow is not sufficient to carry the steam down through the pump suction piping. The M-RELAP5 two-fluid nonequilibrium field equations track the liquid and vapor separately, allowing the formation of the appropriate liquid and mixture levels in the loop seal. Accurate predictions of the water head and the void distribution are required in evaluating the loop seal behavior. Accurate predictions of both can be accomplished by dividing the region into an appropriate of control volumes. ~~The two phase regions, and thus the height of the mixture level in the loop seal, are determined from the interface and wall mass, momentum, and energy transfer constitutive models. The resulting mixture level can be refined using the M-RELAP5 mixture level tracking model. The mixture level tracking model is applied through user input when a water level is formed by gravity.~~

After the loop seal forms, the core mixture level depression is calculated according to the pressure balance between the head in the crossover leg and the head in the downcomer mixture. The loop seal clears when the liquid level in the crossover leg becomes lower, because the vapor flows into the lowermost part of the crossover leg and the liquid is carried by vapor to the pump side. The field equations of M-RELAP5 consider the momentum exchange between liquid and vapor phases based on interfacial friction and describe the carry over of liquid by high velocity vapor flow. In addition, interfacial friction is calculated appropriately for horizontal stratified flow regime or annular mist flow regime, which is determined by flow regime map. Therefore, the field equations are capable to simulate the loop seal clearing. After the loop seal clearing, the head in the crossover leg is lost and the core mixture level increased through the pressure adjustment described by the field equations.

The loop seal formation and clearance is ranked as high in the PIRT. The modeling capability of M-RELAP5 has been validated by analyzing ROSA-IV/LSTF small break (5%) LOCA test as an IET.

REQUEST 8.3.1-10

Section 8.3.1.13 states that the calculated vessel downcomer and lower plenum mixture level can be refined using the M-RELAP5 mixture level tracking model. Table 6.2.1-4, however, does not indicate that the mixture level tracking model is used in the downcomer and lower plenum vessel components.

Clarify whether the mixture level tracking model is used in the calculation of downcomer and lower plenum mixture level in the SBLOCA Evaluation Model.

RESPONSE

Similarly to the response to REQUEST 8.3.1-6, the mixture level tracking model is not used in calculating the downcomer and lower plenum mixture level. MHI will revise Section 8.3.1.13 of the topical report as follows.

60. Mixture Level/Void Distribution:

The M-RELAP5 two-fluid nonequilibrium field equations track the liquid and vapor separately, allowing the formation of the appropriate liquid and mixture levels in the downcomer and lower plenum. Although M-RELAP5 has a level tracking model that can determine the location of a mixture level within a control volume, the model is not used in the US-APWR SBLOCA calculations because an adequate representation of the void fraction distribution can be obtained using an appropriate number of control volumes. ~~The two phase regions, and thus the height of the mixture level in the downcomer and lower plenum, are determined from the interface and wall mass, momentum, and energy transfer constitutive models. The resulting mixture level can be refined using the M-RELAP5 mixture level tracking model. The mixture level tracking model is applied through user input when a water level is formed by gravity.~~

The flashing or condensation in the downcomer region is determined from the interface and wall heat and mass transfer models. Even if flashing does not occur in the downcomer or lower plenum, void generated in the hot legs is carried to the downcomer by convective or natural circulation.

The mixture level is ranked as high in the PIRT. The applicability of M-RELAP5 has been validated by analyzing ROSA-IV/LSTF small break (5%) LOCA test as an IET.

REQUEST 8.3.1-11

In Section 8.3.1.13, item 63, it is stated that the 1-D model is considered to give a conservative evaluation compared to the 3-D model because the liquid in the downcomer easily flows out to the break in the model.

Justify this statement based on the code assessment results or other published materials.

RESPONSE

The 1-D downcomer model is considered to provide a conservative calculation because it neglects the turning losses associated with flow in the azimuthal direction. Therefore, liquid is expected to get to the break easier in a 1-D downcomer model than in a 3-D model.

The appropriateness of the modeling of the US-APWR has been validated through the code assessment analysis using Integral Effects Test data. The downcomer modeling was specifically validated in the ROSA/LSTF SB-CL-18 test analysis, where the one-dimensional hydraulic model was employed similar to that used in modeling the US-APWR.

MHI will revise Section 8.3.1.13 of the topical report as follows.

63. 3-D Flow:

~~Because the field equations of M-RELAP5 have multidimensional fluid models besides 1-D models, 3-D flow can be simulate. In addition, a~~ M-RELAP5 has a multidimensional component that can simulate 3-D flow. In addition, a pseudo 3-D effect can be simulated using parallel 1-D channels that are connected by cross-flow junctions. However, the 1-D model is adopted for the downcomer in the US-APWR SBLOCA analyses because the experimental validation using the ROSA/LSTF test data showed that the 1-D modeling is well suited to the SBLOCA analysis, including an ability to predict the downcomer liquid level.

REQUEST 8.4.1-1

[

]

RESPONSE

[

]

[

]

REQUEST C-1

[

]

RESPONSE

[

]

REQUEST C-2

Appendix C
What is the impact of the discontinuity exhibited by the right end points of the curves in Figure C-4?

RESPONSE

As described in the response to REQUEST 7-8, the under-relaxation method relaxes the magnitude or level of the discontinuity of the critical flow rate. Therefore, no impact is anticipated in the small-break-LOCA analyses for the US-APWR.

REQUEST D-1

Appendix D also describes uncertainty in Cv. A set of questions were asked in Topical report on Adv Accumulator (MUAP-07001) and LBLOCA Methodology report (MUAP-07011), and will not be repeated here.

RESPONSE

MHI understands that NRC does not expect a specific response from MHI to this particular REQUEST, as a set of questions were raised in the Topical Reports for Advanced Accumulator and will be raised in the Topical Report for LBLOCA Methodology.
MHI response to NRC's questions for the uncertainty in the flow rate coefficients is already presented in UAP-HF-07086-P(R0) (Ref.1). And, when additional questions are raised in the Topical Report for LBLOCA Methodology, MHI will response to them.

References

1. Response to NRC's Questions for Topical Report MUAP-07001-P(R1) The ADVANCED ACCUMLATOR, UAP-HF-07086-P(R0), Mitsubishi Heavy Industries, Ltd., July 2007.

REQUEST D-2

(Related RAI D-1)

Appendix D describes the model and uncertainty in the correlations. The model description is for regular accumulator and there is description of spherical accumulator that is not representative of the advanced accumulator in the US-APWR. The model does not explicitly provide expressions for calculating level in tank (“H”). Also, how does the code calculate L_{fL}? The definitions of A_g and A_f (top of page D-5) are not clear.

RESPONSE

The above request is decomposed into the following 4 (four) questions.

(1) The model description is for regular accumulator and there is description of spherical accumulator that is not representative of the advanced accumulator in the US-APWR.

(2) The model does not explicitly provide expressions for calculating level in tank (“H”).

(3) Also, how does the code calculate L_{fL}?

(4) The definitions of A_g and A_f (top of page D-5) are not clear.

The corresponding answers are discussed below.

(1) The US-APWR advanced accumulator is cylindrical in the vertical direction. For the cylindrical type accumulator, the equations D-16 to D-19 and D-34 to D-35 are not used.

(2) The head of accumulator tank is calculated by the equation D-23. Therefore, the equation D-1, which calculates the cavitation factor σ_v, can be obtained as follows:

$$\sigma_v = \frac{P_D + P_{at} - P_v}{\left(P_A + \rho g H\right) - \left(P_D + \dfrac{\rho V_D^2}{2} + \rho g H'\right)} = \frac{P_{exit} - P_v}{P - P_{exit} + \Delta P_Z - \dfrac{\rho v^2}{2}}$$

P : vapor/gas dome pressure (abs)
P_v : Vapor pressure (abs)
P_{exit} : pressure at exit of surge line (abs)
ΔP_Z : elevation pressure differential between discharge line entrance and liquid surface
v : velocity at the accumulator tank outlet
ρ : Density of water

Therefore, it is not necessary to explicitly express the liquid level in tank is not necessary for calculating the cavitation factor.

[

]

(4) A_g and A_f are same as the tank flow area A_{TK}, because the advanced accumulator is cylindrical in the vertical direction.

REQUEST E-1

[

]

RESPONSE

[

]

REQUEST CA-1

In Section 15.6.5 of the DCD, MHI identifies two small break LOCAs as being limiting for peak clad temperature: 1) a 7.5 inch break diameter SBLOCA (PCT = 774°F) which is the limiting case during the period of loop seal clearing and 2) a 1 ft^2 SBLOCA (13.5 inch break diameter) which is limiting during the boil-off phase (PCT = 1,317°F).

In comparison with other PWR designs that employ four coolant loops, the break size associated with SBLOCA most limiting case for the US-APWR (i.e., 13.5 in) is significantly larger. Typically the SBLOCA limiting break diameter for conventional Westinghouse-designed four-loop PWRs is on the order of 2 to 4 inches. The issue is the reason why the limiting break size is so much larger for the US-APWR.

Provide a discussion, substantiated by analysis, of the reasons why the US-APWR system design has such a different small-break LOCA response relative to conventional Westinghouse-designed four-loop PWR plants. Include a discussion of the design philosophy used in the US-APWR that may account for this difference.

RESPONSE

The following sensitivity calculations support to understand the characteristic of break spectrum for US-APWR SBLOCAs.

1) Enhanced Capacity of HHIS
   The flowrate capacity of the high-head injection system (HHIS) is greatly enhanced in the US-APWR to suppress the consequences of SBLOCAs, particularly for smaller break sizes. The injected flowrate of HHIS is a factor of **[ ]** times higher compared with that of the existent high-pressure injection system employed in typical 4-Loop PWRs. The HHIS provides the RCS with sufficient safety coolant to prevent the core from significant uncovery, resulting in lower PCT in comparison with the 4-Loop PWRs when smaller break sizes are assumed. In the case of larger break sizes, depressurization of the RCS becomes faster due to larger break flowrate, and thus the accumulator plays a primary role to suppress the fuel cladding heat-up.

   Table RAI-CA-1.1 compares calculated PCT results at the various break sizes when the HHIS capacity is reduced to **[ ]** of the nominal US-APWR specification with those results obtained for the US-APWR DCD Revision 2 (Ref. 1). This sensitivity study shows that the limiting PCT (1587 ˚F) appears at the 4-in break, which is smaller than the limiting break sizes for the US-APWR DCD calculations (7.5-in for the loop seal PCT 773 ˚F, and 1-ft^2 for the boil-off PCT 1323 ˚F). Transient evolutions under the 4-in break case are shown in Figures RAI-CA-1.1 through 13. The reduced HHIS is not able to provide the RCS with sufficient safety coolant to recover the coolant discharged out the break until the accumulator starts injecting the additional safety coolant at the low reactor pressure level. Consequently, the core uncovery continues for a long duration of the boil-off phase, resulting in higher PCT. This behavior is similar to that observed during a smaller break in the existent 4-Loop PWR.

2) Delay Time for Safety Coolant Injection
   One of the unique features in US-APWR is employing the gas turbine generator (GTG) for

the emergency electric source instead of the existent diesel generator (DG). The HHIS starts injecting safety coolant after generation of the ECCS actuation signal with a longer delay time of **[ ]**, versus **[ ]** for the DG. A sensitivity result when the delay time is shortened **[ ]** is listed in the fourth line of Table RAI CA-1.1. This indicates that the PCT does not significantly increase by employing the GTG for US-APWR.

3) CCFL in Steam Generator

CCFL phenomenon at the SG inlet plenum and U-tubes plays an important role to form and clear the loop seal in the piping, which affects the PCT during loop seal period. As shown in Table RAI-CA-1.2, the SG primary-side flow area of US-APWR is remarkably larger than that of the existent 4-Loop PWR. The smaller flow area of the 4-loop PWR results in more severe liquid flooding (less liquid flow) compared to the US-APWR assuming that the same amount of steam flows into each SG and that the U-tubes have the same diameter.

[

]

The fifth line of Table RAI-CA-1.1 shows sensitivity results, where the analysis model is changed to cause more severe liquid flooding in the SG as mentioned above. Although the sensitivity calculation shows meaningful increase in PCT for the 7.5-in break case, no heat-up occurs for breaks smaller than 7.5-in. Therefore, the effect of CCFL in the SG does not significantly change the break size spectrum results in US-APWR SBLOCAs.

The US-APWR is designed such that consequence of SBLOCAs with smaller break sizes are sufficiently suppressed by its engineered safety features, particularly by the HHIS with the enhanced capacity. Although adoption of the GTG system for emergency electric sources requires a longer delay time to start the safety injection in the US-APWR, the PCT increase from cases with the shorter delay time is negligibly small in comparison with the PCT reduction accomplished by employing the HHIS. In addition, sensitivity calculations with the model that intentionally induces more severe flooding in the SG result in no significant heat-up during the SBLOCA with smaller break sizes less than 7.5-in.

To this end, the limiting PCT tends to occur in the SBLOCAs with larger break sizes in the break spectrum analysis for the US-APWR (Ref. 2).

References:

1. Mitsubishi Heavy Industries, Ltd., Design Control Document for the US-APWR, Chapter 15 Safety Analyses, MUAP-DC015, Revision 2, October 2009.
2. Mitsubishi Heavy Industries, Ltd., Small Break LOCA Sensitivity Analyses for US-APWR, MUAP-07025-P (R0), December 2007.

Table RAI-CA-1.1 Sensitivity Calculations Results (PCT)

Break Size	2-in	4-in	7.5-in
DCD Rev.2	No PCT*	No PCT	773˚F (136s)**
SI Flow **[ ]**	No PCT	1587˚F (1455s)	778˚F (136s)
SI Delay (GTG -> DG)	-	-	733˚F (130s)
CCFL (4-Loop PWR)	-	No PCT	843˚F (144s)

*No PCT: Less than initial cladding temperature
**: PCT occurrence time

Table RAI CA-1.2 US-APWR Primary Reactor Design Specifications

Characteristics	PWR*	US-APWR	US-APWR/ PWR
Pressure (MPa)	15.5	15.5	1.00
Fluid temp. at hot leg (K)	598	601	1.01
Fluid temp. at cold leg (K)	562	564	1.00
Core			
Core power (MW)	3423	4540	1.33
Number of fuel rods	50952	67848	1.33
Number of unheated rods	4825	6425	1.33
Diameter of fuel rod (mm)	9.5	9.5	1.00
Diameter of unheated rod (mm)	12.2	9.7	0.80
Rod pitch (mm)	12.6	12.6	1.00
Hydraulic diameter of core (mm)	10.9		
Core height (m)	3.66		
Power density (MW/m^3)	9.9		
Core flow area (m^2)	4.75		
Core inlet flow rate (ton/s)	16.7		
Pressurizer			
Volume (m^3)	51		
Downcomer			
Downcomer flow area (m^2)	3.38		
Downcomer gap (m)	0.26		
Hot leg			
Diameter (m)	0.737		
Flow area (m^2)	0.427		
Cold leg			
Diameter (m)	0.699		
Flow area (m^2)	0.384		
Steam Generator (SG)			
Number of Tubes per one SG	3382		
Tube inner diameter (mm)	19.6		
Flow area per one SG (m^2)	1.02		
Length of SG tube (average) (m)	20.2		
Height from the top of heated part of core to the top of SG U-tube (m)	14.92		

* W-type 4-loop PWR in JAERI-M84-237 (ROSA-IV System description)

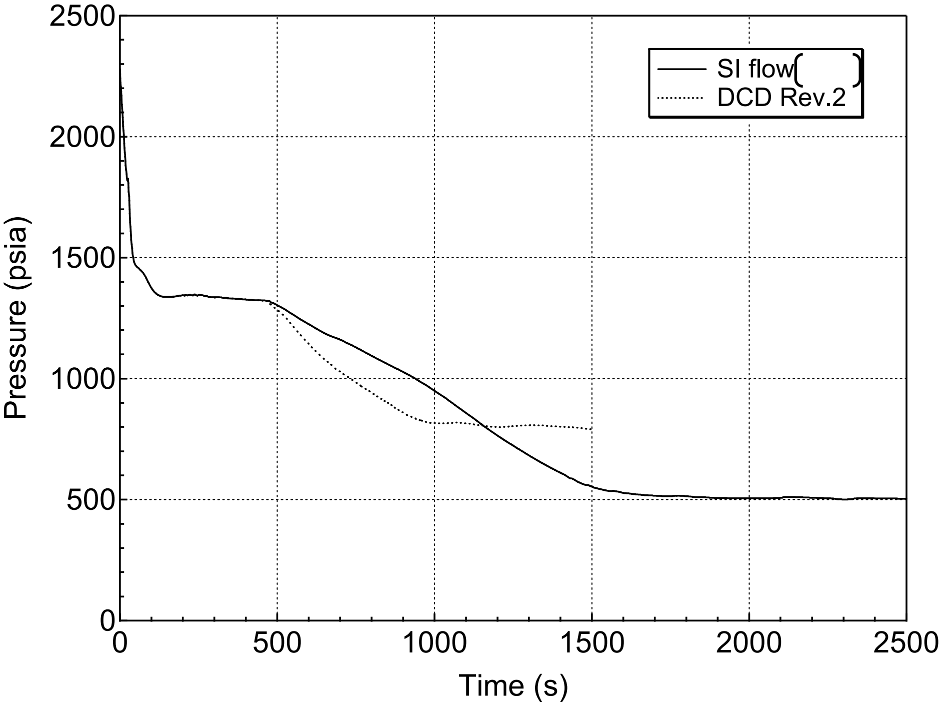

Figure RAI-CA-1.1 RCS Pressure Transient for 4-inch Break (Reduced HHIS Capacity)

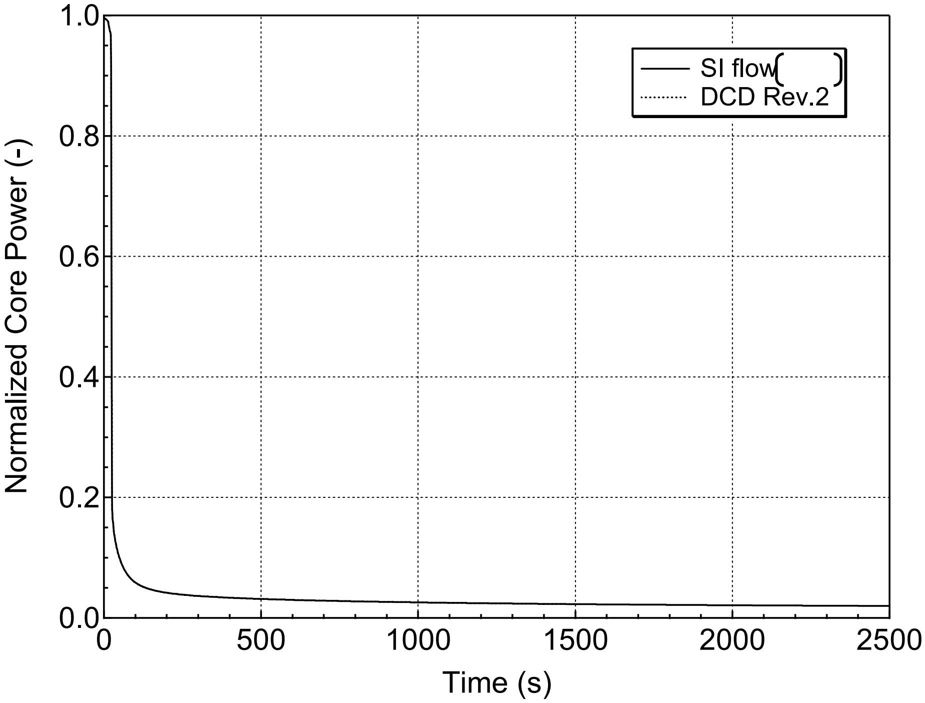

Figure RAI-CA-1.2 Normalized Core Power for 4-inch Break (Reduced HHIS Capacity)

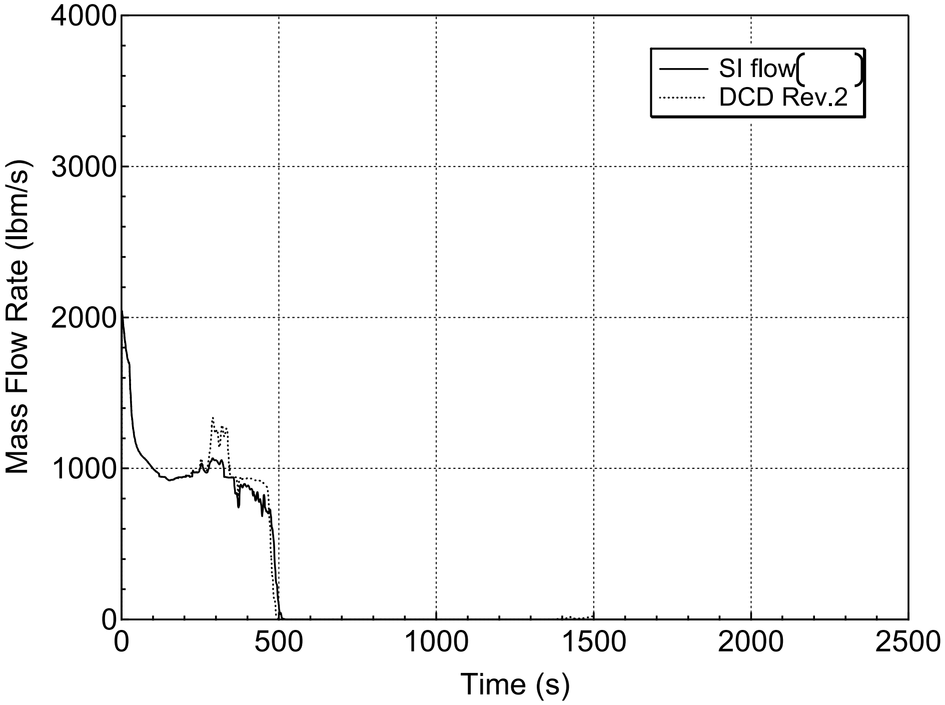

Figure RAI-CA-1.3 Liquid Discharge through the Break for 4-inch Break (Reduced HHIS Capacity)

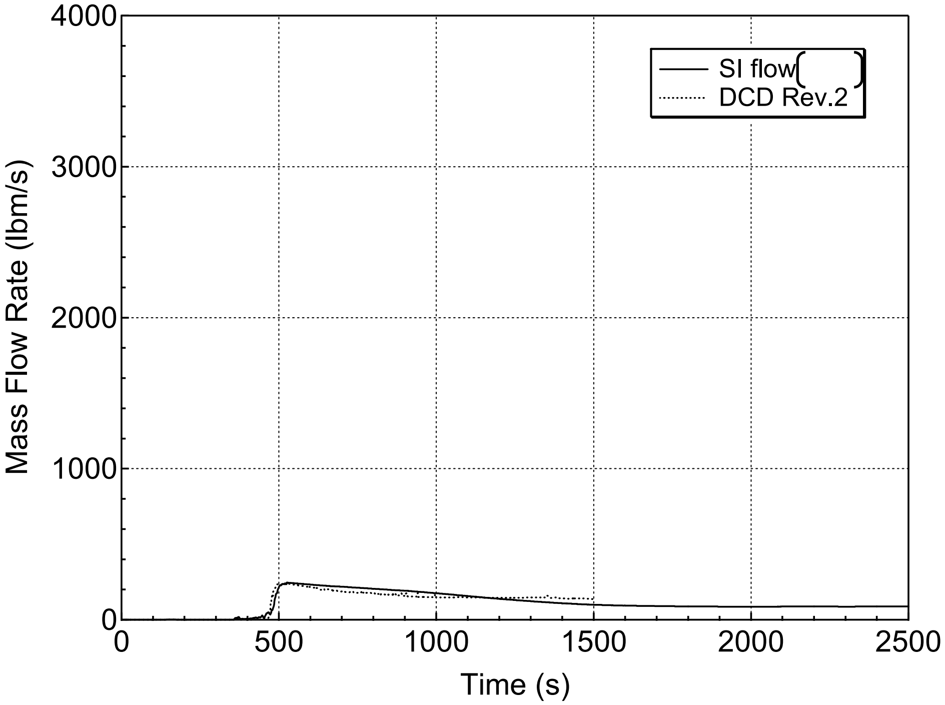

Figure RAI-CA-1.4 Vapor Discharge through the Break for 4-inch Break (Reduced HHIS Capacity)

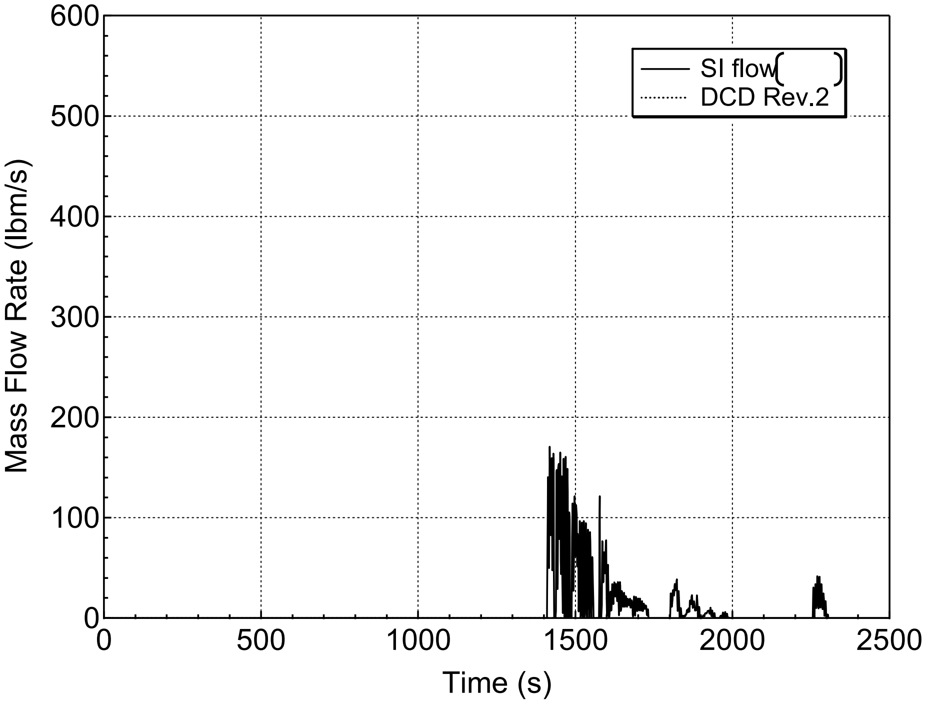

Figure RAI-CA-1.5 Accumulator Injection Mass Flowrate for 4-inch Break (Reduced HHIS Capacity)

Figure RAI-CA-1.6 Safety Injection Mass Flowrate for 4-inch Break (Reduced HHIS Capacity)

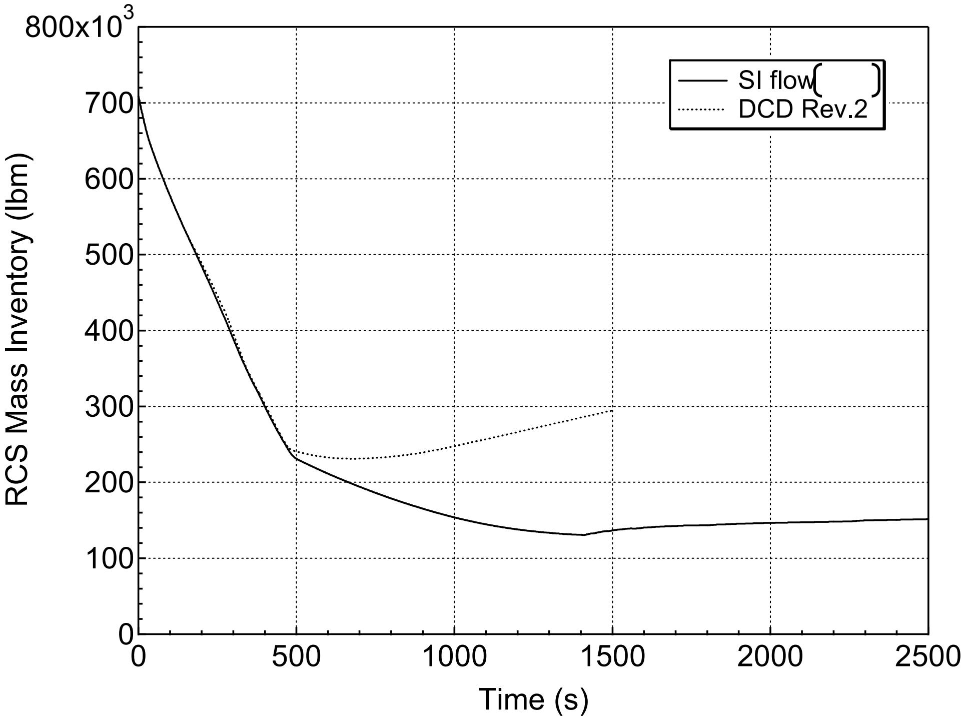

Figure RAI-CA-1.7 RCS Mass Inventory for 4-inch Break (Reduced HHIS Capacity)

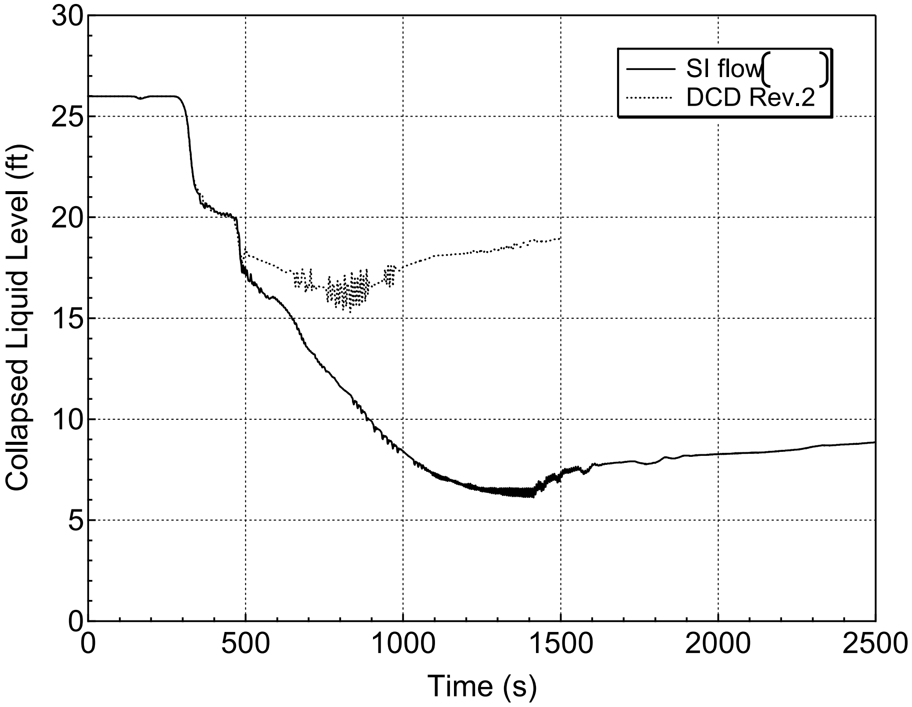

Figure RAI-CA-1.8 Downcomer Collapsed Level for 4-inch Break (Reduced HHIS Capacity)

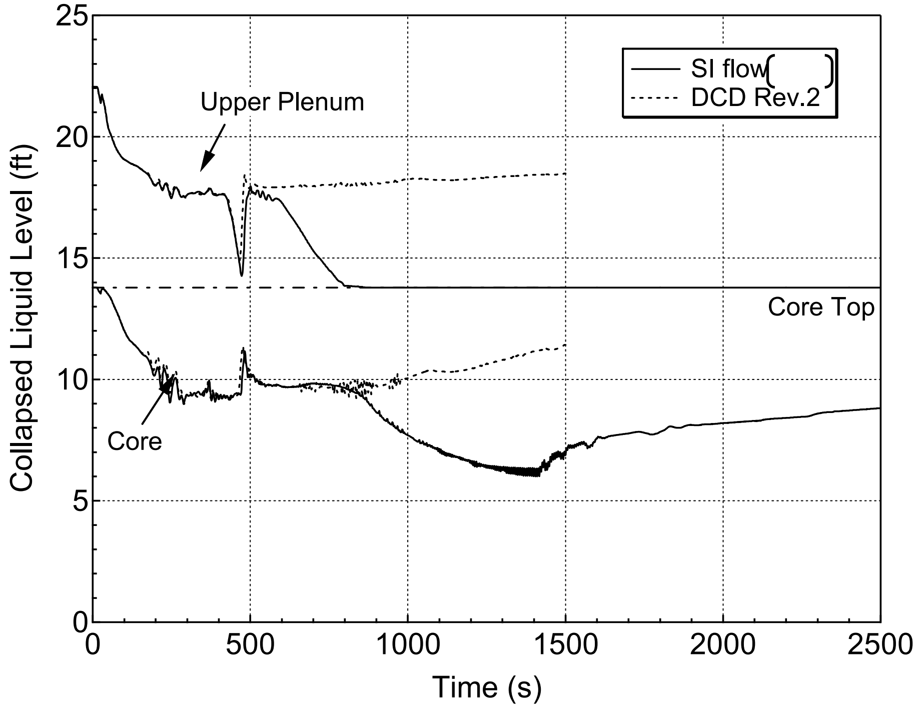

Figure RAI-CA-1.9 Average Core and Upper Plenum Collapsed Levels for 4-inch Break (Reduced HHIS Capacity)

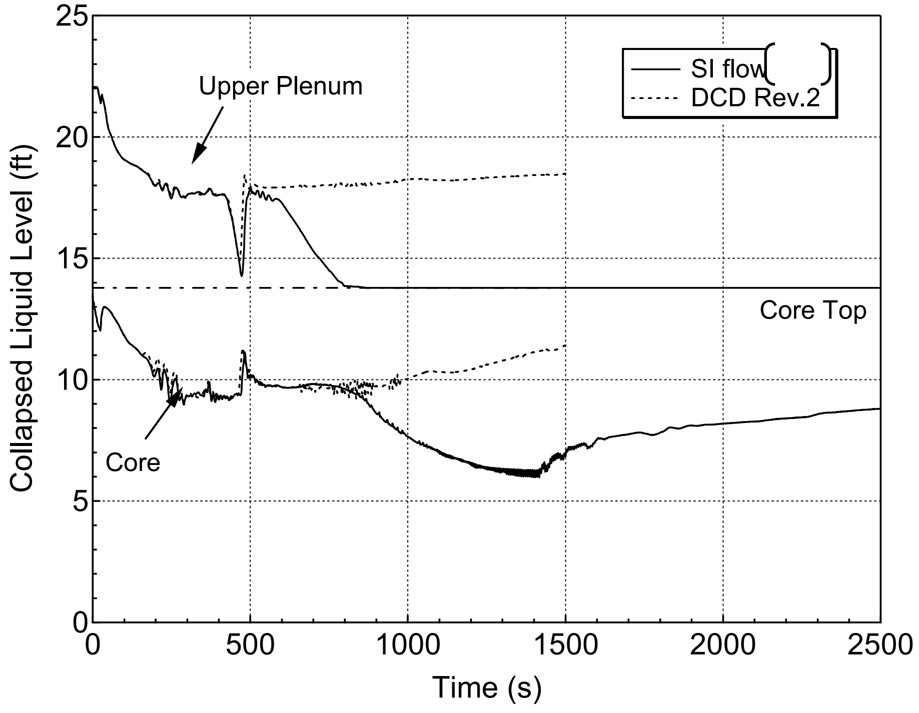

Figure RAI-CA-1.10 Hot Assembly and Upper Plenum Collapsed Levels for 4-inch Break (Reduced HHIS Capacity)

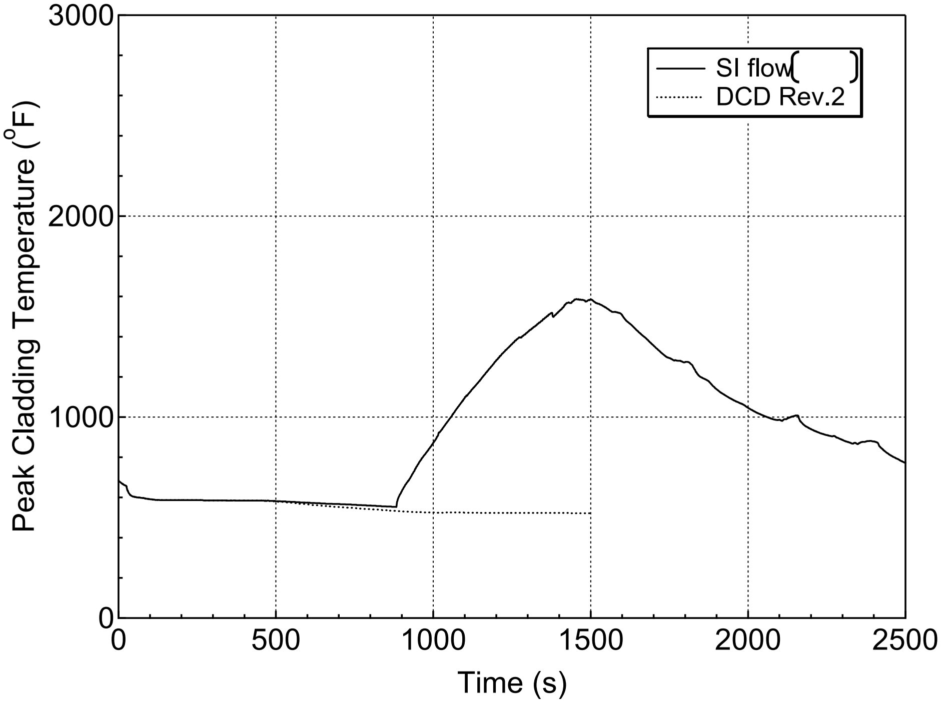

Figure RAI-CA-1.11 PCT at All Elevations for Hot Rod in Hot Assembly for 4-inch Break (Reduced HHIS Capacity)

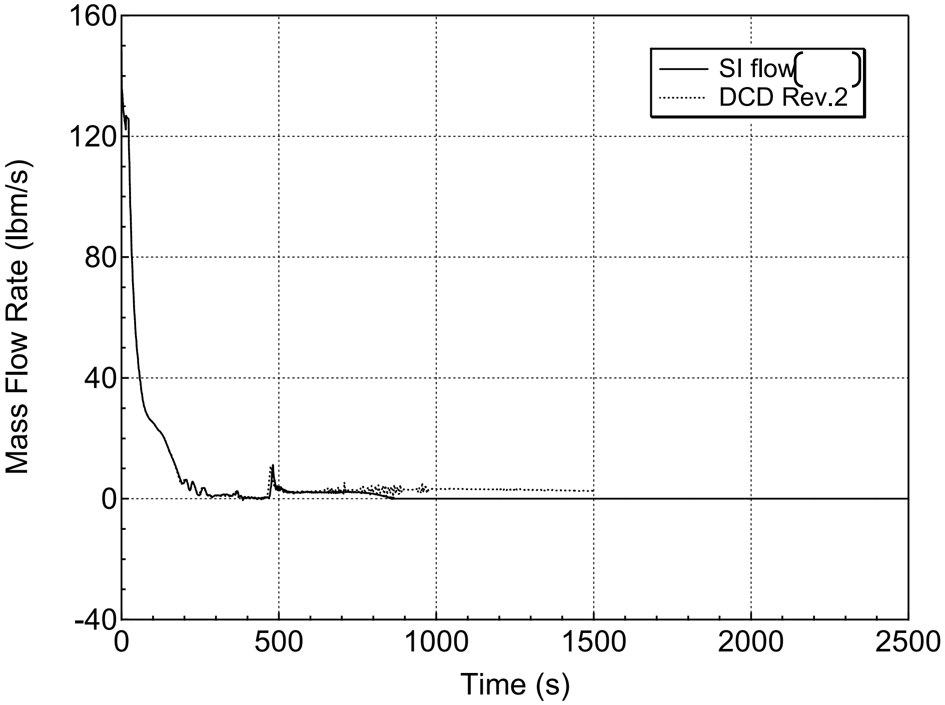

Figure RAI-CA-1.12 Hot Assembly Exit Liquid Mass Flowrate for 4-inch Break (Reduced HHIS Capacity)

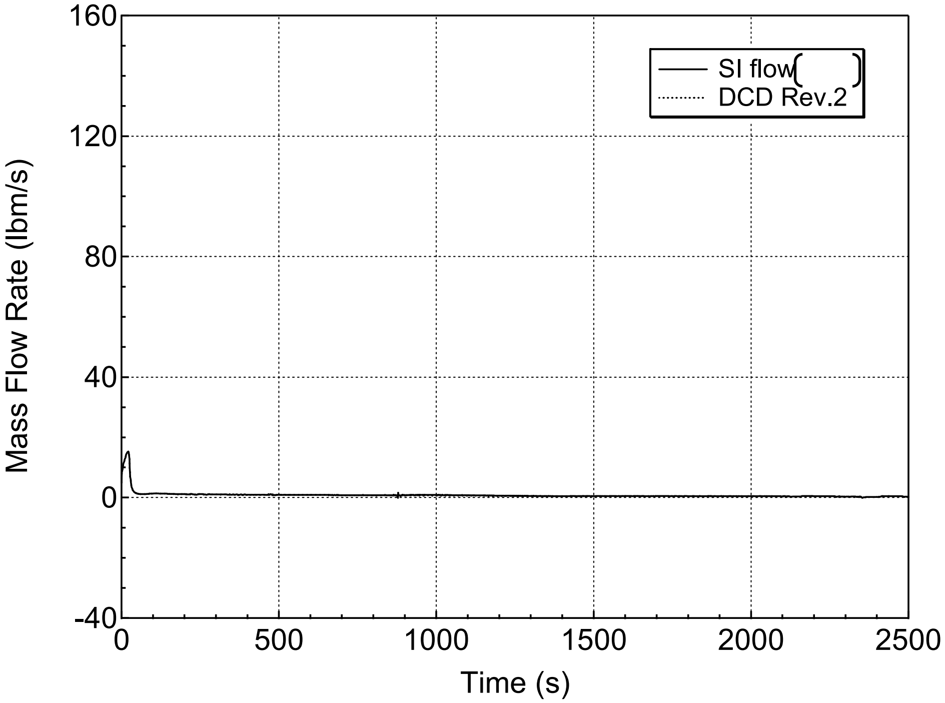

Figure RAI-CA-1.13 Hot Assembly Exit Vapor Mass Flowrate for 4-inch Break (Reduced HHIS Capacity)

REQUEST CA-2

(Related RAI 8-4)

[

]

RESPONSE

[

]

REQUEST CA-3

In Section 4.4.4.2 of the DCD (Revision 1), MHI lists several components of core bypass flow including flow through the control rod guide tubes and instrument guide tubes. No mention is made of a flow path between the upper head and upper plenum. Provide confirmation and supporting documentation that there are no leakage paths or bypass flows between the upper head and upper plenum besides through the guide tubes.

RESPONSE

[

]

REQUEST CA-4

Figure 3-2 of MUAP-0725-P (R0), which presents the nodalization scheme for the reactor vessel, shows that there is no connection between the upper plenum and upper head except through the guide tubes. A consequence of this noding approach is that the fluid temperature in the upper head region (~554.6° F – MHI 6AS-1E-UAP-090036(R0)) is approximately equal to the cold leg temperature. In contrast, the water temperature in the core upper plenum region is ~621.5° F (based on the reactor vessel outlet temperature - MHI 6AS-1E-UAP-090036(R0)). The upper head temperature appears to be overly influenced by the cold leg temperature and is thermally isolated from the rest of the system. As a result, the temperature in the core region may be underpredicted during SBLOCA depressurization when water flashes and flows through the guide tubes.

Provide further information on the expected vessel temperature distribution in the reactor vessel (perhaps from a reactor heat balance) during steady state operation and a comparison to the M-RELAP5 predicted conditions in the vessel. If changes need to be made to the M-RELAP5 model, then determine and document the effect of any model changes on the SBLOCA results.

RESPONSE

The upper head region and the upper plenum region are mainly connected by the guide tubes that have only small pressure loss coefficients. When the bypass flow rate is small, the pressure drop through the guide tubes becomes comparably small with the static pressures distribution in the upper plenum. In consequence, the upward flow can occur in several guide tubes where the static pressure at the upper plenum is relatively high, which increase coolant temperature in the upper head.

In the US-APWR, the pressure loss coefficient at the splay nozzle, which is dominant for the bypass flow rate, is designed to be small so that the bypass flow rate and the pressure drop through the guide tube are sufficiently large to suppress the upward flow from the upper plenum. Therefore, the upper head coolant temperature is kept at the cold leg temperature during normal operation. Due to the above reasons, in the M-RELAP5 analysis, it is appropriate to apply the cold leg temperature at the upper head region as an initial condition.

The thermal-hydraulic design specification in terms of vessel temperature distribution is listed in Reference 1, where the converged vessel temperature distribution obtained by M-RELAP5 steady-state calculation for the US-APWR SBLOCAs is compared and agrees with the design specification.

Reference:

1. Mitsubishi Heavy Industries, Ltd., ‘Initial Condition for US-APWR’s SBLOCA Analysis using M-RELAP5, 6AS-1E-UAP-090036 (R0), April 2009 (Proprietary).

REQUEST CA-5

[

]

RESPONSE

[

]

[

]

REQUEST CA-6

[

]

RESPONSE

[

]

REQUEST CA-7

[

]

RESPONSE

[

]

[

]

[

]

[

]

REQUEST LS-1

Please include both of these assessments in MUAP-07013P.

RESPONSE

MHI will include the code assessment results using both of the LOFT L3-1 and Semiscale S-LH-1 test data in Revision 1 to MUAP-07013-P, which is scheduled to submit to the NRC at the end of May, 2010.

REQUEST LS-2

In the last sentence of the first paragraph of the INTRODUCTION, the ROSA/LSTF SB-CL-18 test is stated to be "sufficiently scalable" to the US-APWR SBLOCAs. Either eliminate this remark or give a definition of what the term "sufficiently scalable" means.

RESPONSE

The description intends to explain that the ROSA/LSTF SB-CL-18 test is being examined to demonstrate its scalability to US-APWR SBLOCAs in the scaling analysis report (Ref. 1). However, MHI will eliminate the description.

Reference:

1. Mitsubishi Heavy Industries, Ltd., Scaling Analysis Report for US-APWR Small Break LOCAs, UAP-HF-09568, December 25, 2009.

REQUEST LS-3

[

]

RESPONSE

[

]

REQUEST LS-4

[

]

RESPONSE

[

]

Appendix A:
Draft Scripts of M-RELAP5 LOFT L3-1 Calculation for MUAP-07013-P (R1)

This appendix explains M-RELAP5 code assessment using the LOFT L3-1 experimental data. Scripts in the present appendix will be inserted as Sections 5.2.2.4 and 8.2.4 in the upcoming revision 1 to the M-RELAP5 topical report MUAP-07013-P.

Appendix B:
Draft Scripts of M-RELAP5 Semiscale S-LH-1 Calculation for MUAP-07013-P (R1)

This appendix explains M-RELAP5 code assessment using the Semiscale SL-H-1 experimental data. Scripts in the present appendix will be inserted as Sections 5.2.2.5 and 8.2.5 in the upcoming revision 1 to the M-RELAP5 topical report MUAP-07013-P.

REQUEST LS-5

[

]

RESPONSE

[

]

REQUEST LS-6

[

]

RESPONSE

[

]

REQUEST LS-7

In the plant analysis it is necessary to predict the secondary side pressures from a description of the system characteristics. For both the LOFT and Semiscale assessments, MHI input the secondary pressures as boundary conditions. Explain why MHI performed all of the assessments of integral effects tests by predicting only the primary system response and not the complete system response.

RESPONSE

Please refer to MHI's response to REQUEST LS-4 in the present report.

REQUEST S-1

Section 1.2 of the report states "In this report, quantitative scaling analyses based on the hierarchical two-tiered scaling (H2TS) methodology[1-7] were performed to complete the M-RELAP5 development and assessment which is required in the EMDAP." It further states that both top down and bottom up analyses are performed. One purpose of the top down analysis is to address system interactions. Yet, on the one hand the report contains arguments concerning US-APWR likeness to a traditional 4-loop Westinghouse PWR and at the same time, the report does not mention any specific system interactions whose scalability is of particular interest.

What specific new and/or unique system interactions is the top down scaling analysis intending to address?

RESPONSE

No known new responses or interactions are being investigated. The primary focus is on whether the new US-APWR specific design features cause significant changes in response relative to ROSA/LSTF which was scaled to a standard 4-loop Westinghouse plant.

Important phenomena and processes expected to take place in the US-APWR during SBLOCAs are similar to those expected in the conventional Westinghouse 4-loop PWRs. The accident progression can be divided into five phases: 1) blowdown, 2) natural circulation, 3) loop seal clearance, 4) boil-off, and 5) core recovery phases.

The new and improved features adopted in the US-APWR design, related to LOCA are as follows:

a) Advanced Accumulator
b) HHIS/DVI
c) Neutron Reflector
d) Gas Turbine Generator

a) Advanced Accumulator (Reference S-1-1)
The advanced accumulator primarily contributes to suppressing the PCT for cases with larger break sizes. The advanced accumulator is designed to start injecting emergency coolant passively when the RCS pressure falls below the set point pressure. The set point pressure is the same as that for the 4-loop PWR. For cases with larger break sizes, the RCS sufficiently depressurizes below the set point pressure. Therefore, there is no significant concern on the interaction between the RCS and the advanced accumulator operating behavior. In this regard, the advanced accumulator does not contribute to suppressing the PCT for cases with smaller break sizes, in which the HHIS suppresses the fuel cladding heat-up during the loop seal phase.

b) HHIS/DVI
The High Head Injection System (HHIS) injects emergency coolant through a Direct Vessel Injection (DVI). In the case of US-APWR SBLOCAs, PCT occurs in the 1 ft^2 break and the accumulator governs the core thermal-hydraulics. The effect of system interaction between the RCS and HHIS behaviors on the PCT is negligible.

c) Neutron Reflector
In comparison with large break LOCAs, the effect of the neutron reflector on the phenomena and processes during reflood phase is smaller, because core liquid level depression is not as large during an SBLOCA transient.

d) Gas Turbine Generator
The gas turbine generator has no direct interaction with the reactor responses.

Therefore, due to the inherent similarity of the US-APWR design to the 4-loop Westinghouse design as described above, the top-down scaling analysis is limited to a confirmatory approach. The scope is limited to the SBLOCA scenarios resulting in the highest peak cladding temperatures (PCT). The objective of the top-down scaling analysis is to show that the same phenomena and mechanism are active and dominant in the US-APWR and IET responses.

Reference:

S-1-1 Mitsubishi Heavy Industries, Ltd., The Advanced Accumulator, MUAP-07001 (R2), September 2008.

REQUEST S-2

In reference to the repeated argument of “similarity” between US-APWR and traditional PWRs, which in the past were analyzed, for purposes of scaling, as a simple loop with emphasis on local phenomena ranges and traditional non-dimensional parameters, such as Re, Nu, Bi, etc.

- What is new and different about the systems of US-APWR that requires a top down scaling analysis to ensure that the code can predict the new system interactions?
- What sequence of events and conditions are expected to vary from that of conventional PWRs due to US-APWR larger dimensions?
- Is it not possible to evaluate the sufficiency of the data base and the applicability of the code through a bottom up (local component and phenomena ranges) scaling analysis? What exactly does the top-down approach, based on a single IET, contribute to this goal?

RESPONSE

There are several new features in the US-APWR design (14 foot core, advanced accumulator, HHIS flow with DVI). While no significant changes in LOCA response are expected relative to the reference 4-loop Westinghouse plant, that outcome cannot be assumed a priori. The present scaling analysis was performed to conform to the requirements specified in Steps 6, 8, and 15 of the EMDAP as described in Regulatory Guide 1.203. In the corresponding sections of the Regulatory Guide there are references to reports INEL-96/0400 and INEL-96/0040. Where possible the methodologies in those reports were used as templates for this scaling analysis.

No expected changes to the sequence of events or specific changes in mechanisms have been identified.

(1) *What is new and different about the systems of US-APWR that requires a top down scaling analysis to ensure that the code can predict the new system interactions?*

As described in the Response to REQUEST S-1, the top down scaling analysis was performed as a confirmatory analysis limited to the SBLOCA scenarios resulting in the highest PCT. It clarifies that there are no new system interactions in the US-APWR during an SBLOCA transient relative to the 4-loop Westinghouse plant used as the reference design for the ROSA facility.

(2) *What sequence of events and conditions are expected to vary from that of conventional PWRs due to US-APWR larger dimensions?*

The accident progression, observed phenomena and processes during the US-APWR SBLOCAs are similar to those in the conventional Westinghouse 4-Loop PWRs. Effects due to the US-APWR larger dimensions are addressed in previous MHI RAI responses(S-2-1, S-2-2) and in the scaling analysis report(S-2-3), which indicates that there are no significant effects caused by the larger dimensions in the US-APWR design.

(3) *Is it not possible to evaluate the sufficiency of the data base and the applicability of the code through a bottom up (local component and phenomena ranges) scaling analysis? What exactly does the top-down approach, based on a single IET, contribute to this goal?*

The applicability and scale-up capability of the thermal-hydraulic models in M-RELAP5 and RELAP5-3D have been well assessed and validated in various studies using experimental test data obtained in SET and IET facilities scalable to the 4-Loop PWRs. In the present scaling analysis, MHI demonstrated that the SBLOCA experiments in ROSA are sufficiently scaled to the representative US-APWR SBLOCA. In other words, even though the ROSA facility was originally scaled to the conventional 4-Loop PWRs, the test data and code validation using the test data are applicable to the US-APWR SBLOCAs. RELAP5-3D, the basis of M-RELAP5 has been established based on the past various code validations, and these past works show that the code is applicable also to the US-APWR SBLOCAs.

Using the bottom-up scaling, each response mechanism is studied separately and it is not possible to assess the relative importance of the mechanisms. In the top-down scaling, all the relevant processes during a phase are assessed together and through numerical magnitude ranking of the ψ groups the relative importance of each mechanism is clarified. Comparing the numerical ranking of the ψ groups between the test facility and the plant provides a better understanding of how well the system level processes are represented in the test facility. In the top-down scaling two IETs from the ROSA facility were studied to see how well the system level processes were represented over a range of break sizes.

References:

S-2-1 Mitsubishi Heavy Industries, Ltd., MHI’s Partial Responses to the NRC’s Requests for Additional Information on Topical Report MUAP-07013-P (R0) “Small Break LOCA Methodology for US-APWR”, UAP-HF-09002-P (R0), January 2009.

S-2-2 Mitsubishi Heavy Industries, Ltd., MHI’s 2nd Response to the NRC’s Request for Additional Information on Topical Report MUAP-07013-P (R0) “Small Break LOCA Methodology for US-APWR” on 09/08/2009, UAP-HF-09512-P (R0), November 2009.

S-2-3 Mitsubishi Heavy Industries, Ltd., Scaling Analysis for US-APWR Small Break LOCAs, UAP-HF-10152, June 2010.

REQUEST S-3

In section 1.2 of the scaling report it is stated that *"Specifically, the IET and SET facilities and experimental data are evaluated by the top-down and bottom-up approaches to respond to Step 6 in Element 2 of EMDAP 'Perform Scaling Analysis and Identify Similarity Criteria', which demonstrates whether similar thermal-hydraulic behaviors expected in the US-APWR are also observed in the scaled test facilities."*

This implies that multiple facilities are included in the scaling analysis. The Regulatory Guide 1.203 (on page 13) also refers to multiple facilities. However, the text of this scaling report seems to imply that the SBLOCA "scaling analysis" is limited to a single facility and a single test.

If that is the case, what demonstrates that the data base is sufficient, being that a single test does not contain all of the ranges of phenomena expected in the prototype?

RESPONSE

The top down scaling analysis for SBLOCA is looking at data from two break sizes from tests in the ROSA/LSTF facility. The top-down scaling analysis results show that for the two break sizes studied, in general the same thermal-hydruaulic mechanisms are occurring with the same phenomena dominant for important responses. Based on the results of the top-down scaling analysis, the responses in the ROSA/LSTF tests appear to be in the correct range for simulating the US-APWR response (Reference S-3-1). This is determined by comparing the individual evaluated dimensionless groups from the two facilities and the numerical rankings of the dimensionless groups.

In the bottom-up scaling analysis, data from several test facilities are being used. In each case the applicability of the test data to the US-APWR conditions is assessed and found to cover the range of conditions expected in the US-APWR.

Reference:

S-3-1 Mitsubishi Heavy Industries, Ltd., Scaling Analysis for US-APWR Small Break LOCAs, UAP-HF-10152, June 2010.

REQUEST S-4

In Section 6.1.2.3 it states *"…the governing conservation equations, (6.1-1) and (6.1-2), is nondimensionalized by dividing by the reference quantity of the parameter, e.g. the initial value …"* The text further states that the reference time is chosen to make a particular nondimensional coefficient (Φ_6) equal to unity.

Please provide the criterion for the selection of each of the other "reference quantities".

RESPONSE

The top-down scaling analysis of the blowdown phase reported in Reference S-4-1 was a direct implementation of the approach used in INEL-96/0040, including the assumption that there was no saturated fluid outside the pressurizer. This assumption did not apply during the duration of the blowdown phase in the larger break sizes investigated for the US-APWR. The analysis of the blowdown phase has been redone using equations consistent with saturated fluid outside the pressurizer.

The overall approach to selecting reference parameters is based on making the individual dimensionless variable terms of order unity. For the SBLOCA analysis the RCS inventory is generally the metric of highest interest because it strongly affects core cooling and ultimately PCT. When the accident scenario is broken into phenomenologically based phases the reference mass or in some cases reference time can be selected to highlight the mass inventory response to the initial system mass or a component mass. In the analysis referred to in the request the reference parameters were selected such that Φ_6 would be equal to unity at the time the pressurizer emptied. In this case $\phi_6 = \frac{\dot{m}_0 t_0}{M_0}$ where $\dot{m}_0$ is the average surge line flow during the phase, t_0 is the phase duration, and M_0 was the initial liquid inventory in the pressurizer. With these definitions, making Φ_6 equal to unity provided a direct comparison of the times for the pressurizer to empty in ROSA and the US-APWR.

Reference:

S-4-1 Mitsubishi Heavy Industries, Ltd., Scaling Analysis for US-APWR Small Break LOCAs, UAP-HF-09568, December 2009.

REQUEST S-5

Equation (6.1-9) defines the coefficient Φ6 and the reference time.

- How was the pressurizer mass flow used as the reference chosen?
- How was the reference pressurizer mass flow calculated?
- Since the rest of the system is apparently subcooled, the break flow might serve as a better reference value. Please address the merits of using the pressurizer mass flow as a reference as opposed to the break flow.

RESPONSE

The parameters are addressed as follows in Reference S-5-1:

(1) How was the pressurizer mass flow used as the reference chosen?

The use of pressurizer mass flow was based on directly implementing the methodology used in INEL-96/0040 used to analyze the 1-inch break in the AP600 design.

(2) How was the reference pressurizer mass flow calculated?

The reference pressurizer mass flow was calculated as the average surgeline mass flow while the pressurizer was draining.

(3) Since the rest of the system is apparently subcooled, the break flow might serve as a better reference value. Please address the merits of using the pressurizer mass flow as a reference as opposed to the break flow.

If the remainder of the RCS was subcooled the pressurizer and break volumetric flows would be essentially equal and the mass flows would be related by the ratio of the densities in the pressurizer and the cold leg.

Subsequently it was determined that the remainder of the RCS was not subcooled during the blowdown phase for the larger break sizes studied in the US-APWR. In the hot leg and upper plenum flashing was decoupling the break flow from the pressurizer surge line flow. The analysis of the blowdown phase has been updated to account for flashing outside the pressurizer in the revised version of the scaling report (Reference S-5-2).

References:
S-5-1 Mitsubishi Heavy Industries, Ltd., Scaling Analysis for US-APWR Small Break LOCAs, UAP-HF-09568, December 2009.
S-5-2 Mitsubishi Heavy Industries, Ltd., Scaling Analysis for US-APWR Small Break LOCAs, UAP-HF-10152, June 2010.

REQUEST S-6

Table 6.1-2 defines Φ_6 as a *"Ratio of integrated mass flow to a reference mass."*

Does this mean that the reference pressurizer mass flow is an average of some sort?
How is the reference mass flow defined for the plant?

RESPONSE

In Reference S-6-1, the reference mass flow rate is the average surge line mass flow rate from the time of break initiation to the time when the pressurizer was empty. For the plant this was evaluated by determining the time when the pressurizer was empty and averaging the surge line mass flow from break initiation up to that time.

Reference:

S-6-1 Mitsubishi Heavy Industries, Ltd., Scaling Analysis for US-APWR Small Break LOCAs, UAP-HF-09568, December 2009.

REQUEST S-7

Table 6.1-1 has a column named *"Reference Parameters"* If one calculates the reference time so that Φ_6 = 1.0, one gets different values than those in the table.

Please describe how the reference values were determined and provide their values as used in the scaling analysis.

RESPONSE

In Table 6.1-1 there was a numerical error. The process for selecting reference values is discussed in the responses to REQUEST S-4. The equations used to analyze the blowdown phase have been updated to account for saturated fluid outside the pressurizer. The results are described in the updated version of the scaling report (Reference S-7-1).

Reference:

S-7-1 Mitsubishi Heavy Industries, Ltd., Scaling Analysis for US-APWR Small Break LOCAs, UAP-HF-10152, June 2010.

REQUEST S-8

[

]

RESPONSE

[

]

REQUEST S-9

At the end of Section 6.2.4, the following statements are made: *"… ROSA/LSTF was designed so that the test facility is scalable to the reference plant (Westinghouse-designed 4-loop PWR) which is also scalable to the US-APWR"* and *"Consequently, it can be judged that the ROSA/LSTF is sufficiently scalable to the US-APWR …"*

- What is the definition of "scalable" in this context?
- What is the definition of "sufficient" as used here?

RESPONSE

The description of "scalable" is discussed in the responses to S-14 and S-18. In the revised scaling report (Reference S-9-1), the "sufficiently" was removed.

Reference:

S-9-1 Mitsubishi Heavy Industries, Ltd., Scaling Analysis for US-APWR Small Break LOCAs, UAP-HF-10152, June 2010.

REQUEST S-10

Section 6.3.2.3 states, *"Each of the physical parameters in the governing conservation equations, (6.3-16) and (6.3-17), is nondimensionalized' by dividing by a reference quantity of the parameter, e.g. the initial value."*

- Please define and discuss the criterion used to select these reference values?

RESPONSE

In Reference S-10-1, **[**

]

Following a more detailed internal review, the equations were simplified to account for the fact that the downcomer remained full during the phase. When these equations were nondimensionalized individual reference values were selected for each variable to ensure that each term was of order unity. The updated equations are in the updated version of the report (Reference S-10-2).

References:
S-10-1 Mitsubishi Heavy Industries, Ltd., Scaling Analysis for US-APWR Small Break LOCAs, UAP-HF-09568, December 2009.
S-10-2 Mitsubishi Heavy Industries, Ltd., Scaling Analysis for US-APWR Small Break LOCAs, UAP-HF-10152, June 2010.

REQUEST S-11

Section 6.3.2.3 states *"the equations are mathematically solved to obtain the temporal derivatives of the core and upper plenum liquid levels and the liquid level at the loop seal clearing"*

- Does this mean that an analytical solution was obtained? Please provide the "solution" referred to in this statement.

RESPONSE

The equations were solved by combining each term in the right hand side of the equations in time series analysis, each term was evaluated using the calculated or measured results (References S-11-1 and S-11-2).

References:

S-11-1 Mitsubishi Heavy Industries, Ltd., Scaling Analysis for US-APWR Small Break LOCAs, UAP-HF-09568, December 2009.
S-11-2 Mitsubishi Heavy Industries, Ltd., Scaling Analysis for US-APWR Small Break LOCAs, UAP-HF-10152, June 2010.

REQUEST S-12

Equation 6.3-18 contains numerous non-dimensional mass flow terms, and various non-dimensional level terms. The definitions of starred variables just below this equation suggest that all of these mass flows are normalized with respect to one reference flow (same for all), and all of the levels are normalized with respect to one reference level, and the same is true of the non-dimensional areas.

- Is this interpretation correct? Are the reference mass flow, reference level, and reference area the same for all like-variables? What is the rationale for this approach?
- Is this also true of the other non-dimensional parameters of other governing equations and in other phases of the transient?

RESPONSE

(1) Is this interpretation correct? Are the reference mass flow, reference level, and reference area the same for all like-variables? What is the rationale for this approach?

In this case the same reference values were used. The reference mass flow was the break flow since that is the only flow changing the liquid inventory in the RCS. The sum of the individual mass flows was normalized since the sum represented the net reactor vessel mass change. The formulation of the equations has been updated to account for the fact that the downcomer remains full during the phase. In the updated equations separate reference values were used for each variable.

(2) Is this also true of the other non-dimensional parameters of other governing equations and in other phases of the transient?

No, in general we used separate reference values for each variable in each equation.

REQUEST S-13

In Section 6.3.2.3, the reference time is defined as the difference between the timing of two events, neither of which is determined by a simple calculation. This reference time itself is not identified with any one specific process, but rather the result of competing processes.

- If it is necessary to know a priori, t_1 and t_2, in order to do the quantification of the nondimensional coefficients required for the analysis, how are the plant numbers evaluated?
- How sensitive are the analysis results to the reference time?

RESPONSE

(1) If it is necessary to know a priori, t_1 and t_2, in order to do the quantification of the nondimensional coefficients required for the analysis, how are the plant numbers evaluated?

[

]

(2) How sensitive are the analysis results to the reference time?

The reference time appears in the ψ_1 term as $\psi_1 = \frac{\dot{m}_{0a} t_0}{\rho_0 L_{0a} A_{0a}}$. This makes the ψ_1 group directly proportional to the reference time. Since the reference times agree within 2.5% it does not have a significant impact on the calculated ψ values.

[

]

REQUEST S-14

Section 6.3.2.4 states “In the scaling analysis for AP1000, it is shown that an acceptable range for the facility/plant scaling ratios is from 0.5 to 2.0.” The specific document cited is NUREG-1793, Section 21.5.7, 2004.

NUREG-1793, Section 21.5.7 suggests that for the relationship between AP600 and AP1000 there is a range for which the AP600 test data base is applicable to AP1000 scaling analysis. It does not demonstrate (as implied by the word “shown” in the US-APWR scaling report) or offer any explanation for why the range was chosen. We can easily demonstrate (attached draft reference) that this overly simplified criterion does not ensure similarity at all.

References cited in S-14 and S-15:

1. Ortiz, M. G. “On Top-Down Scalability Criteria” Draft manuscript attached
2. Ortiz, M.G. and Gavrilas, M. “PUMA Scaling Distortion Analysis: A Method” Presented at the NRC 19th Annual Regulatory Information Conference (RIC)
3. Banerjee, S., M. G. Ortiz, T. K. Larson, D. L. Reeder. "Scaling in the safety of next generation reactors," Nuclear Engineering and Design, vol186, 1998, pp 111-133.
4. Banerjee, S., M. G. Ortiz, T. K. Larson, D. L. Reeder. "Scaling In The Safety Of Next Generation Reactors," Eighth International Topical Meeting on Nuclear Reactor Thermal-Hydraulics, Kyoto, Japan, September 30 -October 4, 1997, Proceedings Volume 1 pp 508-527
5. Ortiz, M. G., S. Banerjee, T. K. Larson. ``A Systems Approach To The Scaling Analysis Of Integral Test Results," Presented at The Fifth International Topical Meeting on Nuclear Thermohydraulics, Operations & Safety (NUTHOS-5), Beijing, China, April 13-18, 1997. Published in the Conference Proceedings, pp Q1-Q7

RESPONSE

The issue of when is scaling good enough has not been addressed in a definitive way for reactor safety experiments investigating LOCA response. There is no regulatory guidance for assessing the applicability of scaled facility experimental data to a plant design. In recent years during the licensing process for the Westinghouse AP1000 and the General Electric ESBWR, several criteria were used by the vendors and NRC staff and presented to the ACRS. For the AP1000, the acceptability criteria used were that the ratio of ψ groups for the plant and experimental facility, for a specific mechanism should be between ½ and 2 (Reference S-14-1). This range was used by Westinghouse and the USNRC and presented to the ACRS. For the ESBWR, General Electric used a range of 1/3 to 3. In a July 2003 meeting of the ACRS Subcommittee on Thermal Hydraulic Phenomena, it was stated by one of the members that the use of the ½ to 2 criteria for the AP1000 established a tradition. Other members noted that the ranking of the ψ groups was more important than the numerical value of the ratios (Reference S-14-2).

For the US-APWR scaling study, we are using the ranking of ψ groups in ROSA and US-APWR as the primary metric for scalability. We are using the ½ to 2 range for the ratio of ψ groups between facilities metric as a heuristic guideline. The range provides a convenient way to assess the scalability of individual phenomena. Applying the range criterion also helps ensure that the individual mechanisms are reasonably similar between the facilities (Reference S-14-3).

References:

S-14-1 U.S. Nuclear Regulatory Committee, ‘Final Safety Evaluation Report Related to Certification of the AP1000 Standard Design,’ NUREG-1793, Section 21.5.7, September 2004.

S-14-2 U.S. Nuclear Regulatory Commission Advisory Committee on Reactor Safeguards, Thermal-Hydraulic Phenomena Subcommittee, July 8, 2003, Transcript ACRST-3243.

S-14-3 Mitsubishi Heavy Industries, Ltd., Scaling Analysis for US-APWR Small Break LOCAs, UAP-HF-10152, June 2010.

REQUEST S-15

The documents suggest that the nondimensional coefficients of US-APWR appear to have been derived in a fundamentally different fashion than how it was done for AP600 and AP1000 scaling analysis. The US-APWR analysis appears to use a single reference variable to create the starred variables of several like variables (one mass-flow, one mass, one area are reference to several flows, masses and areas of the system); for the AP600 analysis, an individual reference value is chosen for each variable, so as to make all the starred variables of order one. The only common reference is the reference time, which is chosen according to the timing of the process of interest. These are the qualities that allow, in AP600, the ranking of processes based on the magnitude of their π values, and the direct comparison between facilities based on these π values. Moreover, the identification of potential distortions is made not only by comparing magnitudes of π s but how they stack against each other in the same equation and different facilities. There are several public domain references that describe these methods in some detail (attached is a presentation given at the NRC 19th Annual Regulatory Information Conference (RIC) and available online, the first 3 references at the end of that presentation are also available without proprietary restrictions)

- Since the approach in the scaling analysis of US-APWR seems to depart significantly from the AP-1000 scaling in the various aspects described above, please explain in more specific detail, how the single ROSA SB-CL-18 facility and test case demonstrates that the experimental database is sufficiently diverse that the expected plant-specific response is bounded and the EM calculations are comparable to the corresponding tests in non-dimensional space.

References cited in S-14 and S-15:

1. Ortiz, M. G. “On Top-Down Scalability Criteria” Draft manuscript attached
2. Ortiz, M.G. and Gavrilas, M. “PUMA Scaling Distortion Analysis: A Method” Presented at the NRC 19th Annual Regulatory Information Conference (RIC)
3. Banerjee, S., M. G. Ortiz, T. K. Larson, D. L. Reeder. "Scaling in the safety of next generation reactors," Nuclear Engineering and Design, vol186, 1998, pp 111-133.
4. Banerjee, S., M. G. Ortiz, T. K. Larson, D. L. Reeder. "Scaling In The Safety Of Next Generation Reactors," Eighth International Topical Meeting on Nuclear Reactor Thermal-Hydraulics, Kyoto, Japan, September 30 -October 4, 1997, Proceedings Volume 1 pp 508-527
5. Ortiz, M. G., S. Banerjee, T. K. Larson. “A Systems Approach To The Scaling Analysis Of Integral Test Results," Presented at The Fifth International Topical Meeting on Nuclear Thermohydraulics, Operations & Safety (NUTHOS-5), Beijing, China, April 13-18, 1997. Published in the Conference Proceedings, pp Q1-Q7

RESPONSE

The top-down scaling analysis approach used for US-APWR does not depart significantly from the methodology used for the AP600 and AP1000. In fact the methodology developed for the AP600, as described in INEL-96/0040, was used as the template for US-APWR analysis. The perception that the methodology was different appears to result from a few instances where a single reference parameter was used for more than one variable. In those instances, the analyses have been redone with unique reference values for each variable.

Two ROSA tests are being used in the top-down scaling study (Reference S-15-1). The tests correspond to the two break sizes resulting in the highest PCT in the US-APWR SBLOCAs. In the 7.5-in break (Reference S-15-2), the PCT occurs at high pressure (~9 MPa) during the loop seal clearing phase, before the ECCS are activated. In the 1-ft^2 break (Reference S-15-3), the PCT occurs at low pressure (< 1 MPa) during the boil-off phase, after the ECCS are activated. These experiments cover a wide range of rewet conditions and include all the expected processes and mechanisms occurring in small break LOCAs.

References:
S-15-1 Mitsubishi Heavy Industries, Ltd., Scaling Analysis for US-APWR Small Break LOCAs, UAP-HF-10152, June 2010.
S-15-2 H. Kumamaru et al., 'ROSA-IV/LSTF 5% Cold Leg Break LOCA Experiment Run SB-CL-18 Data Report,' JAERI-M 89-027, March 1989.
S-15-3 JAEA, "Experimental Report on Simulated Intermediate Break Loss-of-Coolant Accident using ROSA/LSTF," March 2010 (*in Japanese, proprietary*).

REQUEST S-16

Section 6.1.3, Bottom-up Scaling Analysis, states:
“From the viewpoint of the bottom-up approach, the discharge flow characteristic out the break is important in determining the initial plant response. Since the US-APWR SBLOCA methodology employs a break flow model approved in Appendix K to 10 CFR 50 for its application to the licensing safety analysis, the break flow model in M-RELAP5 was not explicitly assessed using experimental test data. In addition, occurrence of dryout (DNB) is not expected during the blowdown phase which was confirmed in the spectrum analyses of US-APWR SBLOCAs. 6-' Therefore, there is no need to evaluate the breakflow model and relevant experimental data by using the bottom-up scaling approach.”

- A conservative model implies an intended distortion in the plant model. How will this distorted behavior impact other phenomena and processes in its proximity?
- We still need to verify that the range of available data contains the expected response of the code calculation in nondimensional space. If it is not done, what makes the calculation believable?

RESPONSE

(1) A conservative model implies an intended distortion in the plant model. How will this distorted behavior impact other phenomena and processes in its proximity?

The break flow model used in M-RELAP5 is compliant with the Appendix K requirements, which means it is expected to over-predict the break flow for any RCS conditions upstream of the break during a LOCA. By over-predicting the break flow the calculated RCS inventory will be lower at any given pressure than the expected plant inventory would be. This artificially low RCS inventory will result in higher cladding temperatures due to less mass being available for core cooling. This conservative estimate of core thermal response is one of the expected and intended results of using the Appendix K model for break flow. Furthermore, spectral analyses for the break size are performed in order to cover an uncertainty of break mass flow rate prediction.

As shown in the bottom-up scaling study Section 6.1.3 in the updated Scaling Report, the tendency of M-RELAP5 over-prediction was attained for the ROSA/LSTF IB-CL-02 17% cold leg break test (Reference S-16-1). The over-prediction gives lower RCS inventory but the accumulator injection starts earlier due to the faster depressurization. From the safety analysis viewpoint, we used the IET data to verify the code applicability.

(2) We still need to verify that the range of available data contains the expected response of the code calculation in nondimensional space. If it is not done, what makes the calculation believable?

The updated Scaling Report discusses the range of available data in Chapter 8 using Figure 8-1. And the applicability of M-RELAP5 break flow model was verified using two ROSA/LSTF tests in Section 6.1.3 as mentioned above.

Reference:
S-16-1 Mitsubishi Heavy Industries, Ltd., Scaling Analysis for US-APWR Small Break LOCAs, UAP-HF-10152, June 2010.

REQUEST S-17

Also in page 6-18, the report states: “The heat transfer between the primary and secondary sides of the SG can also be an important phenomenon during the blowdown phase. In the top-down scaling analysis, however, the steam generator heat transfer was not explicitly addressed because the outflow from the pressurizer was adopted as the dominant factor including the effect of the steam generator heat transfer implicitly, as discussed in Section 6.1.2. Therefore, the heat transfer in the SG is not directly addressed by the bottom-up approach for the present study”

- The statement implies that the scaling analysis of one “important” phenomenon is discarded based on a subjective decision that chooses another phenomenon to be the focus of attention. Please, either demonstrate that the steam generator heat transfer is indeed irrelevant and requires no scaling analysis, or show that the experimental data covers the range of conditions expected to occur in the plant.

RESPONSE

[

]

REQUEST S-18

[

]

RESPONSE

[

]

[

]

REQUEST M-1

[

]

RESPONSE

[

]

REQUEST M-2

For the US-APWR 1 ft^2 SBLOCA, please provide the (Option 1) results of a run with a best estimate critical flow model.

RESPONSE

In general, the Ransom-Trapp critical flow model is known to provide a higher accuracy for the two-phase break flow calculation. Therefore, results by the Ransom-Trapp model are compared with the results by the Moody critical flow model in Figures RAI-M-2.1 to 4.

[

]

Figures RAI-M-2.1 and 2 show the liquid and vapor mass flow rate, respectively. Figure RAI-M-2.3 shows the integral of break flow. Figure RAI-M-2.4 shows the core and upper plenum collapsed liquid level. Figure RAI-M-2.5 shows the peak cladding temperature. The PCT is **[ ]** with the Ransom-Trapp model, which is smaller than the PCT with the Moody model (**[ ]**). The Ransom-Trapp model generally gives the smaller break flow rate and higher core liquid level, resulting in the lower PCT. The sensitivity calculation indicates that the critical flow model for the licensing analysis (the Moody two-phase critical flow model) tends to provide a conservative PCT.

Figure RAI-M-2.1 Liquid Break Flow Rate

Figure RAI-M-2.2 Vapor Break Flow Rate

Figure RAI-M-2.3 Integral of Break Flow

Figure RAI-M-2.4 Core and Upper Plenum Collapsed Liquid Level

Figure RAI-M-2.5 Peak Cladding Temperature

REQUEST M-3

For the ROSA test with the 1 ft^2 equivalent break, please provide the experimental data and the M-RELAP5 input deck.

RESPONSE

The requested ROSA/LSTF IB-CL-02 experimental data and the M-RELAP5 input deck used for the code assessment are provided in Enclosure 6 (Optical Storage Medium) concurrently submitted with the present RAI response.

[

]

REQUEST M-4

[

]

RESPONSE

[

]

REQUEST 1

Confirmatory calculations performed by the staff with version 1.5 of MRELAP5 showed that the Henry-Fauske critical flow correlation is sometimes being used to calculate the break flow when the upstream conditions are two-phase. For most of the time when the Henry-Fauske correlation is used, the calculated critical flow is lower than what would be calculated using the Moody correlation. 10-CFR-50, Appendix K, Section I.C.1.b, Discharge Model, states "For all times after the discharge fluid has been calculated to be two-phase in composition, the discharge rate shall be calculated by use of the Moody model (F. J. Moody, "Maximum Flow Rate of a Single Component, Two-Phase Mixture", Journal of Heat Transfer, Trans American Society of Mechanical Engineers, 87 No. 1, February 1965). The discharge model in version 1.5 of M-RELAP5 does not meet this requirement.

MHI modified the M-RELAP5 code and produced a new version 1.6 that modifies the break flow model to conform to the Appendix K requirement cited above.

Provide a description of the code changes made to the break flow model, the source code for version 1.6, the PC Windows executable for version 1.6 and plots of break flow and PCT versus time for the limiting SBLOCA case. Confirm that version 1.6 includes an edit that identifies which critical flow model is being used at any time to facilitate confirmation that the Moody model is being used as required by Appendix K. In addition to adding a minor edit/plot variable, a good way to display this information in a major edit would be to print out a count of how many times each critical flow correlation was used since the last major edit.

RESPONSE

The following modifications have been made for M-RELAP5 M1.6:
[

]

Details of the code modification are described in Enclosure 4 of this document. The source code and PC-windows executable for M-RELAP5 M1.6 are in Enclosure 6 (OSM). The plots of break flow and PCT versus time for the limiting SBLOCA case (bottom of cold leg1-ft^2 break) are shown in Figure RAI-1.1 and 1.2, respectively. The edit of the critical flow model flag is shown in Figure RAI-1.3. **[**

]

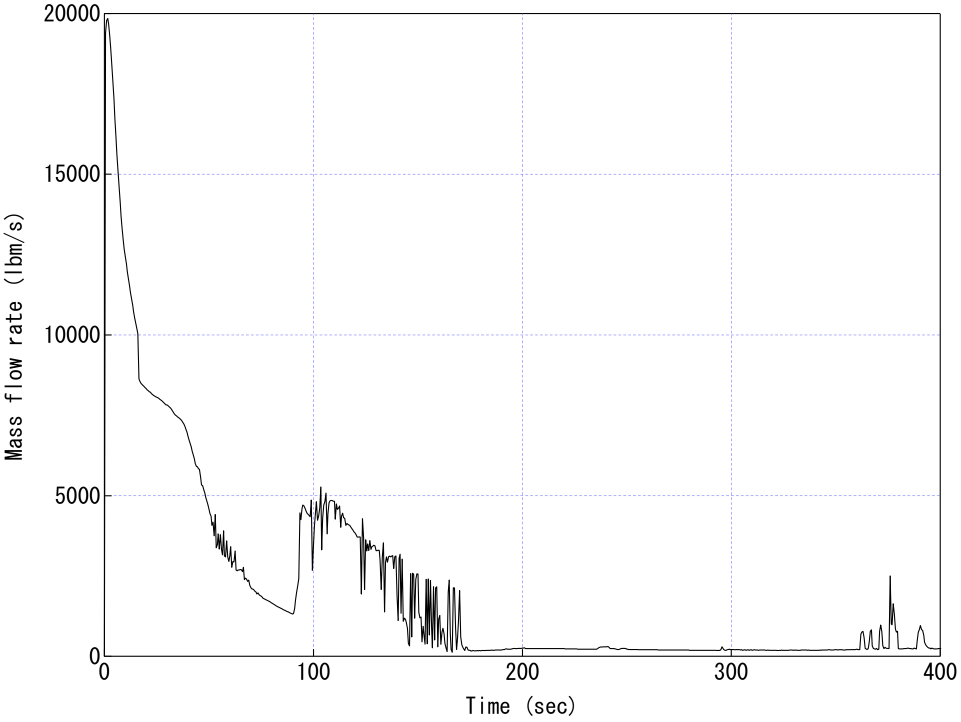

Figure RAI-1.1 Break Flow Rate

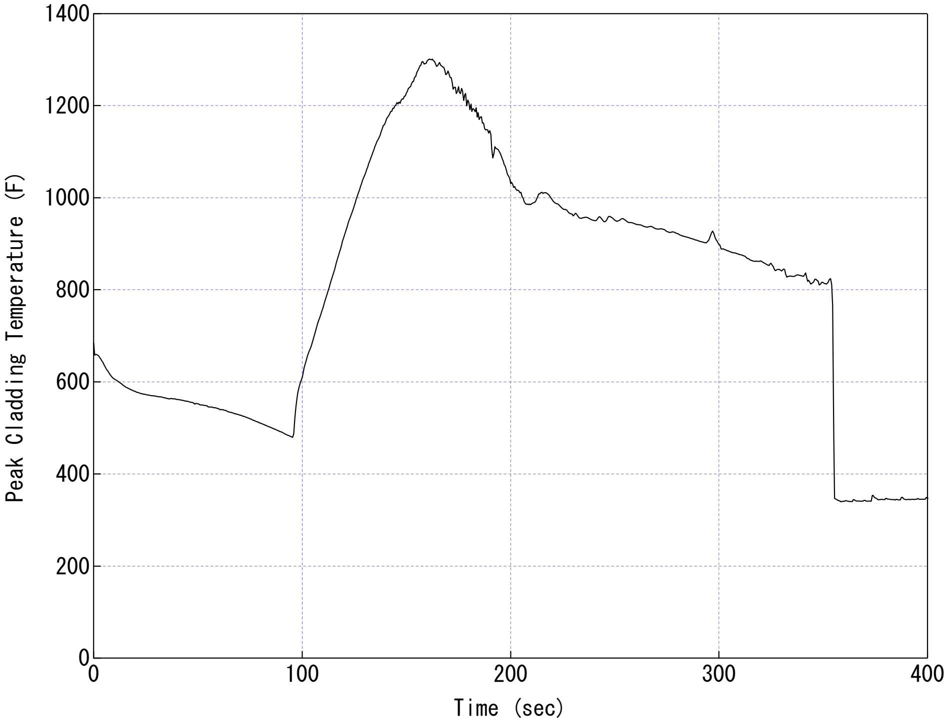

Figure RAI-1.2 Peak Cladding Temperature

Figure RAI-1.3 Choking Flag

REQUEST 2

The staff modified version 1.5 of the M-RELAP5 code by implementing a critical flow model selection criterion based upon void fraction rather than quality. With this selection criterion the code used the Moody model to calculate break flow during the time when the conditions upstream of the break were predicted to be two-phase. Confirmatory calculations performed by the staff with this modified code version showed that the bottom of cold leg break became limiting. MHI's calculations with version 1.5 of M-RELAP5 showed the top of cold leg break to be limiting.

Provide the results of calculations with version 1.6 of M-RELAP5 that identify the limiting break location with respect to PCT.

RESPONSE

The PCTs with M-RELAP5 M1.6 are shown in Table RAI-2.1, and the limiting break location is the bottom of the cold leg 1-ft^2 break.

Table RAI-2.1 The Lists of Peak Cladding Temperature

Break Orientation / Break Size & Location	Bottom	Top	Side	Homogeneous
1-ft^2 at cold leg	1302 (°F)	1298 (°F)	1292 (°F)	1213 (°F)

REQUEST 3

MHI identified one code improvement for the mass conservation in the accumulator component, and one error related to the CHF model.

Provide a description of them and the code changes made in M-RELAP5 version 1.6. Include an evaluation of the effect on PCT for the limiting SBLOCA case.

RESPONSE

The details of the code modification are described in Enclosure 4 of this document. The effect of these code modifications on PCT for the limiting case of M-RELAP5 M1.5 is -11 ˚F.